IAEA-TECDOC-844

Characteristics and use of urania–gadolinia fuels

INTERNATIONAL ATOMIC ENERGY AGENCY IAEA

The IAEA does not normally maintain stocks of reports in this series. However, microfiche copies of these reports can be obtained from

INIS Clearinghouse
International Atomic Energy Agency
Wagramerstrasse 5
P.O. Box 100
A-1400 Vienna, Austria

Orders should be accompanied by prepayment of Austrian Schillings 100,— in the form of a cheque or in the form of IAEA microfiche service coupons which may be ordered separately from the INIS Clearinghouse.

The originating Section of this publication in the IAEA was:

Nuclear Materials and Fuel Cycle Technology Section
International Atomic Energy Agency
Wagramerstrasse 5
P.O. Box 100
A-1400 Vienna, Austria

CHARACTERISTICS AND USE OF URANIA–GADOLINIA FUELS
IAEA, VIENNA, 1995
IAEA-TECDOC-844
ISSN 1011–4289

Printed by the IAEA in Austria
November 1995

PLEASE BE AWARE THAT
ALL OF THE MISSING PAGES IN THIS DOCUMENT
WERE ORIGINALLY BLANK

FOREWORD

In BWRs, the issue of power mismatch between fresh fuel assemblies and partially burned fuel assemblies causing the power in the former to be depressed was recognized at an early stage. Since the earlier absorbers used to address this issue presented inconveniences, the use of gadolinium in urania-gadolinia fuel became routine in all BWRs soon after the decision of General Electric to implement it in Dresden 2 in the mid-1960s. All the BWR fuel vendors have since progressively adopted gadolinia. Out of the total of 420 reactors around the world with an installed capacity of 330 GW(e), approximately 90, with an installed capacity of 70 GW(e), are BWRs. Experience with gadolinia over the past twenty years has become statistically significant, providing confidence in the concept.

When advanced duty conditions (i.e. extended burnup, increased reactor cycle lengths and/or in-out core refuelling schemes) were considered and implemented in PWRs, the use of burnable absorbers for that reactor type also came into consideration. There is an obvious advantage in not sacrificing the fuel rod positions for burnable absorbers, so integral burnable absorber fuel was an attractive choice. The good experience accumulated with gadolinia fuel and the fact that some fuel vendors were fabricating both BWR and PWR fuel made gadolinia the prime choice to meet the needs.

In the recent past, the extended duties considered both for BWR and for PWR fuel, and the perceived advantages in using burnable absorbers in WWERs for the same reasons as in PWRs increased the prospects for gadolinia utilization and hastened the need for higher gadolinia contents. Against this background, the IAEA considered it appropriate to launch in 1990 a Co-ordinated Research Programme on Technology and Performance of Integrated Burnable Absorbers for Water Reactor Fuel (in short "BAF"). The aim was to issue a report summarizing the various aspects of burnable absorber utilization. The participation was on a voluntary basis. This report is the result of the inputs of the participants to the Co-ordinated Research Programme.

The IAEA would like to express its appreciation for the work performed by the participants and, in particular, to acknowledge the contributions of H. Bairiot (Belgium), D. Farrant (United Kingdom) and V. Onufriev (Russian Federation) in the drafting and review of this report.

The scientific secretaries of the programme were successively P. Chantoin and G. Sukhanov of the IAEA, Division of Nuclear Fuel Cycle and Waste Management.

EDITORIAL NOTE

In preparing this publication for press, staff of the IAEA have made up the pages from the original manuscript(s). The views expressed do not necessarily reflect those of the governments of the nominating Member States or of the nominating organizations.

Throughout the text names of Member States are retained as they were when the text was compiled.

The use of particular designations of countries or territories does not imply any judgement by the publisher, the IAEA, as to the legal status of such countries or territories, of their authorities and institutions or of the delimitation of their boundaries.

The mention of names of specific companies or products (whether or not indicated as registered) does not imply any intention to infringe proprietary rights, nor should it be construed as an endorsement or recommendation on the part of the IAEA.

CONTENTS

INTRODUCTION

Burnable absorber fuels (BAF) are utilized, or are being considered for utilization, in all BWRs, in most PWRs and more recently in WWERs. The topic is therefore relevant to approximately 330 out of the 420 operating reactors in the world, representing 280 of the 330 GW(e) installed capacity worldwide. In the light of this importance, the IAEA has decided to issue this report providing an overall view of the various aspects of BAF. With the exception of Chapter 1, the whole report is devoted to urania-gadolinia fuel ("Gd fuel")[1], the most commonly used BAF, and a comprehensive technical review of this topic is provided, although the report does not include a complete survey of all examples of Gd utilization throughout the industry. The report is organized in the following way:

Chapter 1. Strategic considerations: describes the reasons for application of BAFs, their advantages and disadvantages and the various absorbers being utilized.

The underlying success of Gd fuel is due to a large extent to almost 30 years industrial utilization in BWRs. The application to PWRs is more recent, as more challenging conditions have to be met in PWR cores. In addition to Gd fuel, two alternative BAF types have been developed and are utilized in commercial PWRs. They present advantages and disadvantages which are compared in this chapter.

Chapter 2. Unirradiated gadolinia fuel properties: outlines the differences between Gd fuel properties and U fuel properties.

Even if Gd is homogeneously dispersed in the uranium oxide matrix, it would normally be expected to affect the properties of the fuel for three reasons. Firstly, the natural structure of Gd oxide is a body-centered cubic lattice, while U oxide is a face-centered cubic lattice. Secondly, Gd is a trivalent atom, unlike U, which is tetravalent in nuclear fuel. Thirdly, the absorption cross sections of the various Gd isotopes interfere with the resonances of the U isotopes. Both of the first two differences influence or are likely to influence the physical and mechanical properties of BAF in "as-fabricated" conditions. Moreover, the fabrication technique influences the dispersion of Gd within the fuel.

Chapter 3. Fuel manufacturing: deals with the specific fabrication processes and quality control techniques for Gd fuel.

Although fabrication techniques to produce perfectly homogenous Gd fuels have been developed, all industrial fabrication processes are based on a mechanical blending of the two ingredients. Specific quality controls are implemented to verify the proper dispersion of Gd within the BAF fuel and the specified positioning of the BAF fuel rods in the fuel assembly.

Chapter 4. Design and modelling considerations: describes how the specific properties of Gd fuel and the manufacturing constraints are taken into account for utilization of Gd in BWRs, PWRs and WWERs and how the modelling codes incorporate Gd fuel properties.

---

[1] urania-gadolinia fuel is usually called "gadolinia fuel" within the nuclear industry. In this report, for convenience, the abbreviation "Gd fuel" is being used.

Design flexibility is afforded by the use of Gd: the location of the Gd fuel rods within the fuel assembly and the axial shaping of the Gd along the Gd fuel rods, can be tuned to various design objectives (e.g. reduced fabrication cost, improved design margins, improved reactivity evolution and so on). As Gd fuel is a more complicated fuel than standard U fuel, the design code incorporates a number of modifications to address the use of Gd fuel and its licensing.

Chapter 5. Experience with gadolinia fuel: presents typical examples of Gd fuel utilization and results from fuel and core surveillance and from experimental programmes.

Extensive experience with Gd fuel acquired by several fuel vendors and utilities has led to Gd fuel meeting high performance standards. A few examples illustrate extent of this experience.

Chapter 6. Fuel cycle back end: considers the implications of the presence of Gd in spent fuel.

An obvious consequence of additions of Gd to the fuel is to increase the quantity of material to be incorporated into high level waste in the reprocessing option.

1. STRATEGIC CONSIDERATIONS FOR THE USE OF BURNABLE ABSORBERS

1.1. INTRODUCTION

The need to improve reactor performance through longer cycle lengths or improved fuel utilization has been apparent since the beginning of commercial nuclear power generation. Among several modifications introduced as a consequence, the fuel initial enrichment has been increased, which has meant that the additional amount of fissile material in the core has had to be compensated for by the introduction of additional absorber material in the core. This was initially achieved by lumped absorbers located between the assemblies (control rods or removable steel curtains) or by soluble absorber (boric acid) in the coolant.

In BWRs, the use of soluble absorber in the coolant/ moderator was prohibited for technological reasons. Therefore, lumped absorbers were the only solution. Since the earlier lumped absorbers (steel curtains) were causing not only the power in the fresh fuel assemblies (FA) to be depressed, but also the power in the adjacent assemblies, the advantage of locating the absorber within the FA became obvious. Due to the high rating of the fuel rods (FR), withdrawing a FR to replace it with an unfuelled absorber rod was not possible. This is the reason why integral burnable absorbers were introduced in 1967 in Dresden 2. This particular burnable absorber was gadolinium oxide mixed in the fuel. Since then, this type of absorber has been routinely used in this type of reactor. It is routinely called "gadolinia fuel" and will be abbreviated to "Gd fuel" in this report.

In PWRs, the use of soluble absorber in the coolant was acceptable. Boric acid in the coolant/moderator has therefore been used routinely to meet the needs of increased reactivity compensation. However, the increase in initial fuel enrichment cannot be indefinitely compensated for by increasing boric acid concentration, as beyond a certain concentration, thermal expansion of water at startup reduces the quantity of boron (B) in the core, resulting ultimately in a positive moderator temperature reactivity coefficient (MTC). To avoid this unacceptable situation the introduction of solid burnable absorbers in the fuel was considered. Two alternative solutions have been successively developed:

- Introduction into the FAs of unfuelled rods containing burnable absorber (borosilicate glass, boron carbide dispersed in alumina and others) in so-called Rod Cluster Control Assemblies which are withdrawn from the FA after its first irradiation cycle.

- Addition of an absorber within the fuel rods themselves.

1.2. APPLICATIONS OF BURNABLE ABSORBERS

1.2.1. Cycle length extension

To minimize the fuel cost, the amount of spent fuel and the amount of waste after reprocessing, increased fuel discharge burnup is considered as one of the most important goals by utilities. This has been confirmed by the results of the IAEA's programme WREBUS [1.1].

Two different approaches can be used to increase burn up depending on the relative proportion of nuclear generation in the total installed electrical capacity of the country. The first is typically the type of management used in France where more than 70% of the electricity produced is of nuclear origin. The higher burnup is achieved by an increased

fractioning of the reload, keeping reactor cycle length unchanged (annual refuelling scheme). The power mismatch between FAs of successive reloads can be kept under control without the need to add burnable absorber to the fresh fuel.

For most other countries, where the proportion of installed nuclear capacity is low, increasing burnup and increasing cycle length are joint goals. In order to achieve these, burnable absorbers have to be used since the power mismatch between the assemblies of successive reloads becomes too great to be compensated through in-core fuel management only.

1.2.2. Low leakage fuel management and vessel fluence reduction

The traditional PWR and WWER fuel management scheme (without burnable absorber) is to load fresh fuel assemblies at the core periphery and move them toward the centre of the core after the 1st cycle (out-in management).

To minimize irradiation damage to the vessel, an alternative fuel management scheme is now usually adopted consisting of fresh FAs loaded in the centre of the core which are then shifted to the core periphery for their last cycle (in-out management). This type of fuel management scheme is called a "low leakage loading pattern" (LLLP) and requires that the power of the fresh FAs be depressed: i.e. burnable absorbers must be introduced in those FAs.

It is worth noting that, with the utilization of MOX fuel, higher fast neutron doses are produced compared with U fuel, and therefore loading fresh MOX FAs in outer positions has to be avoided, giving an additional incentive for the in-out reload strategy.

1.3. ADVANTAGES AND DISADVANTAGES OF BURNABLE ABSORBER FUEL

1.3.1. Power distribution control

The consequence of introducing new fuel assemblies into a core which has reached equilibrium is to induce mismatches in the power distribution.

In a reload without burnable absorbers, the core configuration is determined so as to be within the maximum permissible power peaking factor at the beginning of cycle. This peaking factor decreases with burnup.

For a reload incorporating BAF, the maximum power peaking no longer occurs at the beginning of life in a fresh subassembly, but rather after consumption of the burnable absorber. This effect is shown in Fig.1.1 which presents the situation for Gd fuelled WWERs. The figure shows the coefficient of power density non-uniformity within the FA (K_q, called assembly-wise peaking factor in PWRs), the same coefficient for the core volume (K_v, called total peaking factor for PWRs) and the evaluation of the axial offset (AO). This figure shows that meeting the design limits at the beginning of life (max $K_q = 1.35$ and max $K_v = 1.56$) does not imply that the criteria are met over the whole cycle. In fact, the situation deteriorates after 200 EFPD. Both FA design and core management are more complicated if burnable absorbers are utilized.

1.3.2. Waste volume reduction

As mentioned earlier, the BAF option replaces the use of lumped absorbers, consisting either, for BWRs, of stainless steel curtains withdrawn after one cycle or, for PWRs, burnable control rod assemblies inserted in the fresh RCC FAs and extracted after their first irradiation cycle.

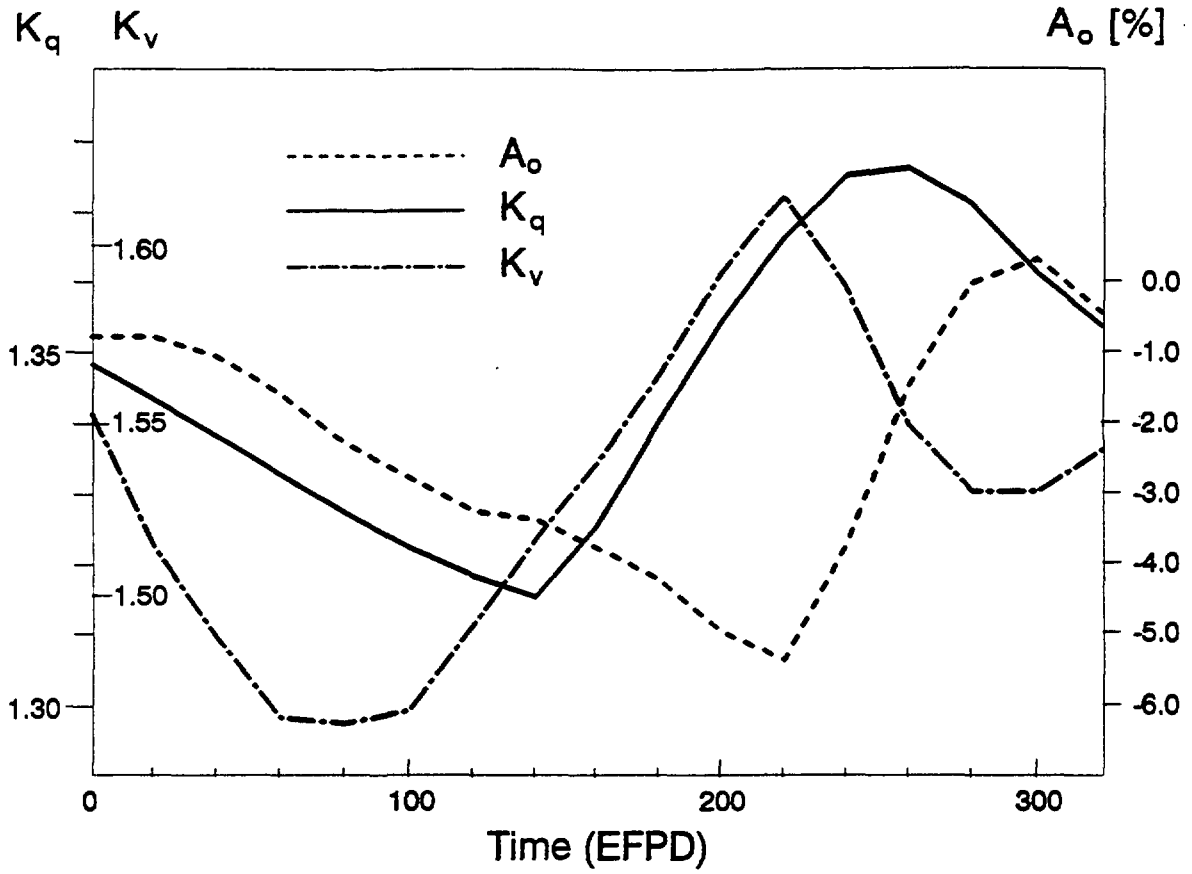

Fig. 1.1. Typical time dependence of the variation of the power density non-uniformity coefficients (K_q and K_v) and of the axial offset (A_o) in a WWER designed for the use of Gd [1.2].

Today, with increasing emphasis being placed on reducing wastes, the reduction of structural core material by discontinuing the stainless steel curtain option in BWRs, and the abandonment of the burnable control rod assemblies in a PWR, are points in favour of the use of BAF.

For PWRs, these arguments are not valid for countries having taken an irreversible decision on the final disposal of spent FAs as a waste. In this case, the spent burnable control rod assemblies can be inserted in the spent FAs, which act as a final repository for them and thereby do not increase the total volume of waste.

1.3.3. Uranium / Water ratio

Lumped burnable absorber can be introduced in a reactor either by occupying control rod positions within a FA (PWRs and WWERs) or the water gap between FAs (BWRs) or by replacing a FR within a FA. In both cases, the moderation ratio is modified from what was originally designed to be an optimum.

In the first case, the positioning of the lumped burnable absorbers is restricted to core positions not located on control rod drive mechanism locations.

In the latter case, the heat transfer surface between fuel and coolant is reduced due to the replacement of an active rod by an absorbing rod. This leads to higher heat flux hot-spot-factors.

These disadvantages of lumped burnable absorbers are not apparent, or are minimized, if burnable absorbers are incorporated within FRs.

1.3.4. Residual absorption penalty

Neutron capture in absorber isotopes results in new isotopes, the macroscopic cross-sections of which should be as small as possible if the absorber is to be left in the FA up to end of life.

1.4. CHOICES OF INTEGRATED BURNABLE ABSORBERS

1.4.1. Gadolinia (Gd_2O_3)

The progressive development of Gd as a burnable absorber from 1w/o Gd* or even a fraction of a percent in the early utilizations in BWRs, to the present 6 to 10 w/o Gd level for PWRs, has enabled a good data base to be built up. This large data base and the good performance of Gd FRs were reasons for its progressive utilization by most fuel suppliers.

However, with increasing Gd content, the complexity of nuclear design increases significantly and the fuel properties (in particular thermal conductivity and melting point) are affected to a significant extent. As a result, to maintain adequate safety margins, the design power of the Gd FRs must be reduced and the power sharing between Gd FRs and standard uranium FRs becomes altered. In extreme cases, depleted U was utilized in early PWR applications of high Gd content BAF to prevent the erosion of any uncertainty margins in the design and licensing phases. With the development of data bases up to higher Gd contents, such conservative approaches are not necessary and the potential benefits of Gd fuel can be used to their full extent.

Burnable absorbers work by neutron capture on a large cross section isotope (eg.Gd^{155} and Gd^{157}). The isotopes produced by this nuclear reaction (eg. Gd^{156} and Gd^{158}) have a small absorption cross section, which is undesirable since this induces a reactivity penalty over the life time of the fuel.

These difficulties in implementing high Gd content fuel have resulted in two other alternative absorbers being applied commercially: ZrB_2 and Er.

1.4.2. Zirconium diboride (ZrB_2)

Developed by Westinghouse under the name of IFBA (Integral Fuel Burnable Absorber), this fuel consists of a thin layer of ZrB_2 (0.02 mm) deposited by sputtering on the surface of the UO_2 pellets. The resulting B^{10} loading is 1.7 mg B^{10}/cm and the layer adheres perfectly to the UO_2 substrate. The material properties (including thermal conductivity) of the substrate are not affected by this layer.

IFBA presents all the advantages of a BAF and a lower residual absorption penalty than the other BAFs, since it can be designed for complete depletion of the B^{10} at the end of the first irradiation cycle. Technical details on IFBA are given in [1.3 - 1.5]

Although apparently more complicated, the fabrication techniques have been incorporated into a large scale manufacturing facility by Westinghouse. Issues such as the

---

* In this report, all the Gd contents are expressed in weight percent Gd_2O_3 in the fuel, but noted w/o Gd, for simplification (see all abbreviations and symbols)

hygroscopic nature of the ZrB_2 coating are simply addressed and the manufacturing and quality control complexity are not substantially different from those for Gd fuel manufacture.

Additionally, although there is a higher tritium content of the IFBA fuel (resulting from the interaction of fast neutrons with B^{10}), this has a negligible impact of the reprocessing option. There is almost no environmental impact or Intermediate Level Waste impact and the High Level Waste impact is roughly the same as that from an equivalent mass of gadolinia.

The consumption of B generated He which results in a need to reduce the pre-pressurization level of the fuel rod (FR). It implies an increased creep down rate of the cladding early in life and, consequently, potentially affects PCI propensity. Although the production of He during B depletion presents no operational limitations, the He release must be explicitly treated in fuel rod design. This analysis is readily performed with a properly benchmarked fuel rod design code.

The FA design is based on a radial and axial shaping of the absorber. The radial positioning of the IFBA FRs in the FA, typically 30-40 % of the FA, is designed to minimize the radial power peaking within the FAs. The axial zoning is designed to reduce the axial shape factor by avoiding the presence of B^{10} at the FR ends, thus suppressing the power in the centre of the FR. The borated length in the pellet stack is typically 2.3 m over an active fuel length of 3.7 m.

Since the layer is thin and the absorber quite weak, the depression of the thermal neutron flux within the absorber is low and the nuclear design is less complicated than for other BAFs. Unlike other BAF FRs, the IFBA FRs need not systematically be derated to account for lower thermal conductivity, lower melting point and increased nuclear design uncertainty margins.

Following irradiation of test segments in Turkey Point 3 and of test FRs in BR3 since 1981, IFBA fuel has now been commercially utilized by Westinghouse since 1987. In 1990, a total of 34 reload batches incorporating 165 000 IFBA FRs were being irradiated in 20 PWRs, most of them operating on 18 month reactor cycles.

Further developments being considered are the use of enriched B^{10} instead of natural B and an increase in the B^{10} content of the IFBA FRs, resulting in a reduction of the proportion of IFBA FRs in a 17 X 17 FA from 18-48 % to 12-30 %. The within-FA power peaking factors could thus be reduced to the level of a FA without IFBA e.g.:

- peaking factors for FA with no IFBA: 1.05 - 1.04
- peaking factors for FA with current design IFBA: 1.10 - 1.04
- peaking factors for FA with enriched boron IFBA: 1.05 - 1.04

It should be noted that local peaking factors can be lower with IFBA than for an assembly without IFBA depending on the specific burnable absorber placement, U enrichment and lattice etc.

A comparison of IFBA and Gd BAF by Westinghouse for a particular scenario indicates that:

- the cycle length is increased by 1 % with IFBAs due to the lower residual absorption penalty

- the radial power peaking factor is reduced by 2.2 % when using IFBAs

- the BOC HFP critical B concentration is increased by 80 ppm (i.e. 6%) when using IFBAs, leading potentially to a positive MTC. This is the only disadvantage stated by Westinghouse, although a number of plants are operating well with appropriate MTC control using only IFBAs.

1.4.3. Erbium (Er)

The effective capture cross sections of Er are well known and the double resonance peak at 0.5 eV plays an important role in managing the MTC. This is the major advantage of Er over ZrB_2. Otherwise, it has most of the advantages of the latter, such as a cross section similar to B. The difficulties typical of Gd, i.e. neutron spectrum hardening and wide neutron flux variations with Gd depletion, are thereby avoided [1.6].

Er has been utilized in TRIGA research reactors since 1974 and has been demonstrated to be predictable and reliable. For PWRs, Er_2O_3 is directly blended with UO_2 as for Gd BAFs, but only in a proportion of 1 to 2 w/o. The number of Er FRs required is typically 20 - 30 % of the FA although more recent verbal presentations quote higher percentages.

The advantages of Er are, besides those common to Gd and IFBA:

- a smaller impact on the fuel properties (thermal conductivity, melting point) due to the lower rare earth contents compared with Gd fuel and the absence of a thermal barrier at the FR surface (unlike the IFBA).

- excellent control of the MTC and the FA power sharing.

The main disadvantage is a high residual poisoning effect due to the slow consumption of Er.

The adoption of Er by CE (now ABB/CE) was preceded by an experimental programme demonstrating that the properties of Er fuel are close to the properties of Gd fuel and can benefit from the Gd database. Four demonstration FAs fabricated in 1989 have been loaded in Calvert Cliffs 2 and four others in 1991 in San Onofre 2 to confirm the validity of the design package and the fuel performance. The first full reload with Er is scheduled to be loaded in 1994. More recent brochures from ABB suggest that Gd fuel is more appropriate for the routine cycle lengths in PWRs and Er fuel more appropriate for the very long cycle lengths, e.g. 24 months.

It should also be mentioned that Dysprosium (Dy) was initially contemplated as a burnable absorber in Belgium [1.7], before Gd was chosen due to its general commercial implementation which provided greater confidence. These early R & D and irradiations in Belgium have proved that Dy behaves, from fabrication and fuel properties viewpoints, similarly to Gd (and consequently Er).

1.4.4. Comparison of BAFs

Based on an evaluation of relevant publications, a comparison of the three types of BAF is summarized in Table 1.1 taking into account the most common specifications for PWR fuel.

The availability of raw materials to meet the increased demand that would result from the wide - spread utilization of any of these three solutions in nuclear power plants (NPP) is not a criterion to select one of them preferentially. Not only is there an ample

TABLE 1.1. *COMPARISON OF BAF TYPES*

BAF Type	Gd	IFBA	Er
Fuel fabricators	(a)	Wh (USA)	ABB / CE (USA)
BAF concentrations in fuel pellet	6 - 10 w / o	----	1 - 2.5 w / o [1.8]
Thermal conductivity decrease	significant	negligible	small
Melting point reduction	significant	negligible	small
Proportion of BAF FRs per FA	3 - 6 %	30 - 40 %	20 - 30 %
Reduction of U^{235} quantity in the FA	small	negligible	small
Depletion rate	high	high	medium
Residual reactivity	low	negligible	significant
FA power distribution	good	fair (b)	good
Local power peaking	significant (c)	low	low
MTC control	good	fair	best
Fabrication facility	parallel small throughput line	additional large throughput equipment	parallel throughput line
Fuel reprocessability	good	questionable	no problems anticipated

(a) FBFC (Belgium), SIEMENS (Germany), Fabricazione Nucleari (Italy), JNF, MNF and NFI (Japan), KNFC (Korea), ENUSA (Spain), ABB Atom (Sweden) BNFL (United Kingdom), TENEX/Novosibirsk/Ulbinskij (Russia/Kazakhstan), BWFC, GE and SPC (USA).

(b) due to fast depletion

(c) due to design challenges resulting from self-shielding and neutron spectrum effects

supply of B, but Er and Gd resources are also plentiful (App I). Taking Gd as an example, upper bounds of Gd requirements can be calculated as:

160 kg Gd_2O_3 / a. GWe	for BWRs
50 " "	for WWERs and
33 " "	for PWRs (assumed to operate on an 18 month cycle)

The total requirements to refuel all the world LWRs with Gd fuel would be 12 + 1 + 6 = 19 t Gd_2O_3 / a, which represents only 1 to 3% of the annual production of Gd (App.I). If Er were to be the absorber used in refuelling all LWRs world - wide, however, this would represent an increase of 20 to 50 % of the present annual production of Er.

REFERENCES TO CHAPTER 1

[1.1] INTERNATIONAL ATOMIC ENERGY AGENCY, Technical Report Series No. 343, Water Reactor Fuel Extended Burnup Study (WREBUS), 1992

[1.2] ONUFRIEV, V.D., PROSELKOV, V.N., "Issues of safety ensurance and economic indices of the USSR water-cooled reactor using U-Gd fuel", presented at the IAEA BAF Research Coordination Meeting, 22-25 October 1990, Vienna, Austria

[1.3] SIMMONS, R.L. et al., Integral Fuel Burnable Absorbers with ZrB_2 in PWRs, Nuclear Technology, Vol. 80, March 1988

[1.4] PRITCHETT, J.E. et al., Operational Experience with ZrB_2 Integral Fuel Burnable Absorbers, ANS 1987 Winter Meeting Proc., pp. 117 - 118

[1.5] SRINILTA, S. et al., A comparison of Gd and ZrB_2 as Integral Fuel Burnable Absorbers in PWRs, ANS 1987 Winter Meeting Proc., pp. 124 - 126.

[1.6] JONSSON, A., Initial Physics Evaluation of Er as BA in a PWR, ANS Annual Meeting, Nashville, June 1990

[1.7] MESTDACH, G., FLIPOT, A.J., Control autoradiographique de la répartition de Dy_2O_3 dispersé dans une matrice en UO_2, Energie Nucléaire, mars - avril 1968.

[1.8] FIERO, I.B. et al., Status of erbium burnable absorber development at ABB Combustion Engineering Nuclear Fuel, International Topical Meeting on Light Water Reactor Fuel Performance, West Palm Beach, Florida , USA, April 1994

2. UNIRRADIATED GADOLINIA FUEL PROPERTIES

2.1. STRUCTURE AND CHEMISTRY OF THE (U, Gd)O_2 SOLID SOLUTIONS

2.1.1. Principal properties of Gd_2O_3

Goldschmidt and co-workers recognized three crystallographic structures of the rare-earth oxides [2.1]. As temperature increases, C cubic (b.c.c. with 16 molecules to the unit cell - $TlCl_2$ type) transforms into B monoclinic, and finally into A hexagonal. Shafer and Roy [2.2] indicated that only the C-type structure exists for rare earths with an atomic number greater than 65, that only the A-type exists for lanthana and ceria and that the B-form is stable for samaria and gadolinia. They indicate the probable existence of the A-type structure for gadolinia and samaria at elevated temperatures. Its existence probably depends on the purity of the starting materials and duration of heat treatment according to Guentert and Mozzi [2.3].

Roth and Schneider [2.4] and others, (e.g. [2.5]), observed that the C to B transformation is not truly reversible and occurs at approximately 1250°C or, according to Warshaw and Roy, at approximately 1200°C [2.6]. Thus, it could be concluded that depending on the previous heat treatment, gadolinia oxide could exist either in C cubic form (for heat treatments at temperatures below 1200-1250°C, depending on time of exposure) or in B monoclinic form (for heat treatments at temperatures higher than 1250°C, depending on heat exposure).

Table 2.1 compares some characteristics of Gd_2O_3, UO_2 and ZrB_2: lattice type and parameters, theoretical density (TD), mean linear expansion coefficient for 20-1200°C region (a), elastic Young's modulus (E), shear modulus (G) and Poisson's ratio (ν) calculated for zero porosity materials.

Unit cell dimensions of the three forms of Gd_2O_3 are given by Roth and Schneider [2.4] as follows:

A-type: $a = 3.76$ Å, $c = 5.89$ Å (hexagonal);

B-type: $a = 14.06$ Å, $b = 3.572$ Å, $c = 8.75$ Å, $\beta = 100'10''$ (monoclinic);

C-type: $a = 10.8122$ Å (cubic, b.c.c., $TlCl_2$ type).

More detailed information on elastic properties and microcracking of Gd_2O_3 and compositions Gd_2O_3-HfO_2 is given by Dole and Hunter [2.8] and Case, Smyth and Hunter [2.11].

2.1.2. Types of (U, Gd)O_2 solid solution

Gd_2O_3 can be considered as having a cubic fluorite-type structure with one-quarter of the O^{2-} ions in the anion sub-lattice vacancy. Therefore, and due to the nearness of the cation radii, solid solutions of cubic fluorite-type structure are easily formed in the UO_2-Gd_2O_3 system (as well as in the ZrO_2-Gd_2O_3 system). Charge compensation in the UO_2-Gd_2O_3 system can be realized through vacancy formation in the anion (oxygen) sublattice, oxidation of U^{4+} to U^{5+} or U^{6+}, interstitial formation or a combination of these defect types, depending on the sintering atmosphere.

This aspect was considered in detail by Ho and Radford [2.12]. They classified nine models: for very reducing (dry H_2) atmosphere (models 1-3); for normal (H_2 bubbled through a water bath) atmosphere (models 4-5); and for more oxidizing (CO_2/CO or H_2 bubbled through a heater water bath) conditions (models 6-9). Formulae, defect types and O/U and O/M ratios for these models are given in Table 2.2.

TABLE 2.1. SOME CHARACTERISTICS OF Gd_2O_3, UO_2 AND ZrB_2

Oxide	Lattice type	Parameters (Å)	TD (g cm^{-3})	T_m (°C)	a 10^{-6} (K^{-1})	E (kbars)	G (kbars)	ν
Gd_2O_3 [2.5, 2.7] [2.8, 2.9]	monoclinic	a = 14.06 b = 3.572 c = 8.75 ß = 100'10"	7.403	2330		1502	588	0.2771
	or cubic $Tl Cl_2$	a = 10.81221						
$U O_2$ [2.10]	cubic $Ca F_2$	a = 5.4686	10.96	2860	12.0	2300	874	0.316
$Zr B_2$ [2.10]	hexagonal, $Al B_2$	a = 3.17 c = 3.533	6.092	3040	7.7	4200		

2.1.3. Lattice Parameter

For the near-stoichiometric $(U,Gd)O_2$ solid solutions, lattice parameter decreases with increase of Gd_2O_3 content at least up to Gd content of 40 mol.%.

The variation in the lattice parameter (a) with Gd content X, expressed as mole fraction, is given by the formula:

a = 5.474 - 0.190 X [2.5]
(for mechanically mixed Gd fuel; sintered in H_2, 1700°C,4h; 0-40%mol.Gd_2O_3);

a = 5.470 - 0.162 X [2.5]
(for mechanically mixed Gd fuel; sintered in Ar, 1700°C,4h; 0-40%mol.Gd_2O_3);

a = 5.4704 - 0.237 X [2.13]
(for coprecipitated Gd fuel; sintered in H_2, 1600°C, 2h; 0-30 w/o Gd_2O_3);

a = 5.4725 - 0.185 X [2.14]
(for mechanically mixed Gd fuel; sintered in H_2, 1800°C, 2h; 0-15 w/o Gd_2O_3);

a = 5.4725 - 0.185 X [2.14])
(for mechanically mixed Gd fuel; sintered in humidified H_2, 1700°C, 4h; 0-12 w/o Gd_2O_3).

Summarizing these results it is concluded that for near-stoichiometric (U, Gd)O_2, the solid solution lattice parameter decreases with the increase of Gd_2O_3 content (=0.002Å per 1 mol % Gd_2O_3) independently of the pellet fabrication route (mechanical mixing or coprecipitation).

TABLE 2.2. *O / U AND O / M RATIOS FOR THE DIFFERENT STRUCTURAL MODELS [2.12]*

Model	Formula	$x \approx y$ $y \approx z$	Cation Lattice	Anion Lattice	Interstices	O / U	O / M
1. Oxygen vacancy	$(U^{4+}_{1-x}\,Gd^{3+}_{x})\,O_{2-(x/2)}$	$y = 0$	Full	Defect	None	$= 2$	< 2
2. Cation interstitial	$(U^{4+}_{1-(3/4)x}\,Gd^{3+}_{x})\,O_{2}$	$y = 0$	Full	Full	$(x/4)Gd^{3+}$	$= 2$	< 2
3. U^{5+} and oxygen vacancies	$(U^{4+}_{1-x-y}\,U^{5+}_{y}\,Gd^{3+}_{x})\,O_{2-(x-y)/2}$	$x > y$	Full	Defect	None	> 2	< 2
4. U^{5+}	$(U^{4+}_{1-x-y}\,U^{5+}_{y}\,Gd^{3+}_{x})\,O_{2}$	$x = y$	Full	Full	None	> 2	$= 2$
5. U^{6+} and anion interstitial	$(U^{4+}_{1-x-y}\,U^{5+}_{y}\,Gd^{3+}_{x})\,O_{2+(y-x)/2}$	$x < y$	Full	Full	$[(y-x)/2]O^{2-}$	> 2	> 2
6. U^{6+}	$(U^{4+}_{1-(3/2)x}\,U^{6+}_{z}\,Gd^{3+}_{x})\,O_{2}$	$z = x/2$	Full	Full	None	> 2	$= 2$
7. U^{6+} and anion interstitial	$(U^{4+}_{1-x-z}\,U^{6+}_{z}\,Gd^{3+}_{x})\,O_{2+z-(x/2)}$	$z > x/2$	Full	Full	$[z-(x/2)]O^{2-}$	> 2	> 2
8. U^{5+} and U^{6+}	$(U^{4+}_{1-x-y-z}\,U^{6+}_{z}\,U^{5+}_{y}\,Gd^{3+}_{x})\,O_{2}$	$x = y + 2z$ $y = 2z$	Full	Full	None	> 2	$= 2$
9. U^{5+}, U^{6+} and oxygen vacancies	$(U^{4+}_{1-x-y-z}\,U^{6+}_{z}\,U^{5+}_{y}\,Gd^{3+}_{x})\,O_{2-(x-y-2z)/2}$	$x > y + 2z$ $y \geq 2z$	Full	Defect	None	> 2	< 2

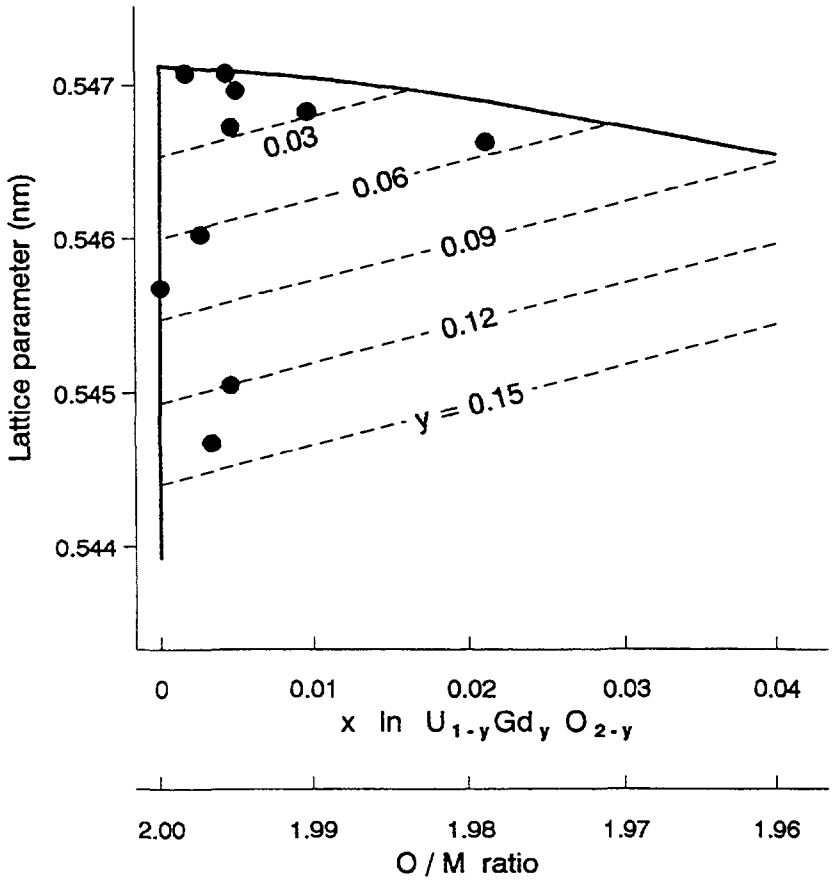

Fig. 2.1. *The relation between lattice parameter and the degree of oxygen deficiency, or O / M ratio, for $U_{1-y}Gd_yO_{2-y}$ solid solution. The gradient of parallel straight lines represents da / dx at constant concentrations of gadolinium [2.14].*

TABLE 2.3. *RELATION BETWEEN O / U RATIO AND U^{5+} CONCENTRATION [2.12]*

O / U ratio	Gd_2O_3		U^{5+}/U	$U^{5+}/U+Gd$
	(mole fraction)	(w/o)	(mole fraction)	
2.01	0.10	6.94	0.02	0.018
2.01	0.20	14.37	0.02	0.016
2.01	0.30	22.34	0.02	0.014
2.03	0.10	6.94	0.06	0.054
2.03	0.20	14.37	0.06	0.048
2.03	0.30	22.34	0.06	0.042
2.05	0.10	6.94	0.10	0.090
2.05	0.20	14.37	0.10	0.080
2.05	0.30	22.34	0.10	0.070

As mentioned before for the stoichiometric (U, Gd)O_2 solid solution, a mixed model of "U^{5+}" and "oxygen vacancy" (Table 2.2) looks more suitable, in which U^{5+} (0.88Å) is smaller than U^{4+} (1.001Å), and the lattice parameter decreases even though relatively large Gd^{3+} (1.053Å) ions are introduced (ion radii were taken from [2.13]). This dependence was deduced by Ohmichi et al. [2.14] who gives the derivative of lattice parameter (a) with Gd content (X) as:

$$\frac{da}{dX} = \frac{4}{\sqrt{3}}(r_{Gd^{3+}} + r_{U^{5+}} - 2r_{U^{4+}}) = -0.16$$

For hypostoichiometric (U, Gd)O_2 solid solutions of $(U^{4+}_{1-2x+2y}U^{5+}_{x-2y}Gd^{3+}_{x})O_{2-y}$ type it was shown [2.14] that the lattice parameter increases with a decrease in the O/M ratio or an increase of oxygen vacancy concentration at constant concentration of gadolinium (Fig. 2.1).

Omichi et al. [2.14] explained that this increase in the lattice parameter was due to the size of the oxygen vacancy, which is 10% larger than that of the O^{2-} ion. However, Ho and Radford [2.12] connected this dependence with a fewer number of small U^{5+} ions being developed as the number of vacancies increases at constant Gd content.

For the partial non-equilibrium (U, Gd)O_2 solid solutions (due to insufficient time and /or temperature of sintering) two or three types of solid solutions with different Gd content can be observed with markedly different lattice parameters.

2.1.4. O/U and O/M ratios and oxygen potentials in the (U,Gd)O_2 solid solutions

Diffusion-controlled phenomena of constituent ions in UO_2 and (U, Gd)O_2 such as sintering, creep, grain growth and fission gas release depend principally on their composition [2.14, 2.15]. This is because these phenomena are rate-controlled by the slower cation diffusivity.

Theoretically, the O/U ratio of the solid solution is controlled only by the number of uranium cations in valency states other than U^{4+}. Proceeding from this assumption Ho and Radford estimated O/U and O/M ratios for the (U, Gd)O_2 solid solutions (see Table 2.3) and the relationship between O/U and the U^{5+}/U ratio [2.12].

Their results showed that the smaller the U^{5+}/U ratio, the closer to 2.000 the O/U ratio will be. Thus, in order to obtain the optimum properties of Gd fuel, it is essential to minimize the amount of U^{5+} and U^{6+} ions. Although the O/U ratio can be adjusted by sintering in a controlled CO_2 atmosphere, this has the effect of increasing the U^{5+} and U^{6+} content. Ho and Radford proposed that the addition of a doping agent such as Nb_2O_5 would be more beneficial [2.12].

The relation between oxygen potential ΔG_{O_2} and O/M ratio was measured by a thermogravimetric (TGA) technique for UO_{2+x} and $(U_{1-y}Gd_y)O_{2\pm x}$, where $0.02 < x < 0.08$ and $y = 0.04$, 0.14 and 0.27 mole fractions [2.16, 2.17]. Samples were obtained by mechanical blending, pressing and sintering in an H_2 atmosphere at 1700°C for 2h. Results of these measurements at 1000 and 1300°C are given in Figs 2.2 and 2.3.

The stable hypostoichiometric phase is seen for the $U_{1-y}Gd_yO_2$ solid solutions at oxygen potentials above -400 kJ/mol, even though such a phase is not seen for UO_2. The stabilization trend in the hypostoichiometric $U_{1-y}Gd_yO_2$ fuel is explained by an increase in the oxidation state of the uranium ions, thereby producing more positive oxygen potentials.

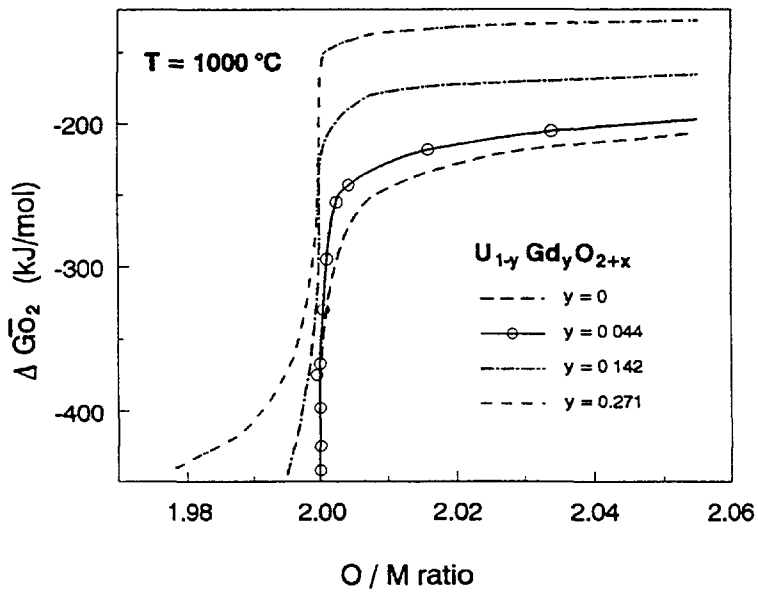

Fig. 2.2. *Oxygen potentials for $U_{0.96}Gd_{0.04}O_{2+x}$ plotted as a function of O / M ratio at 1000 °C [2.17]*

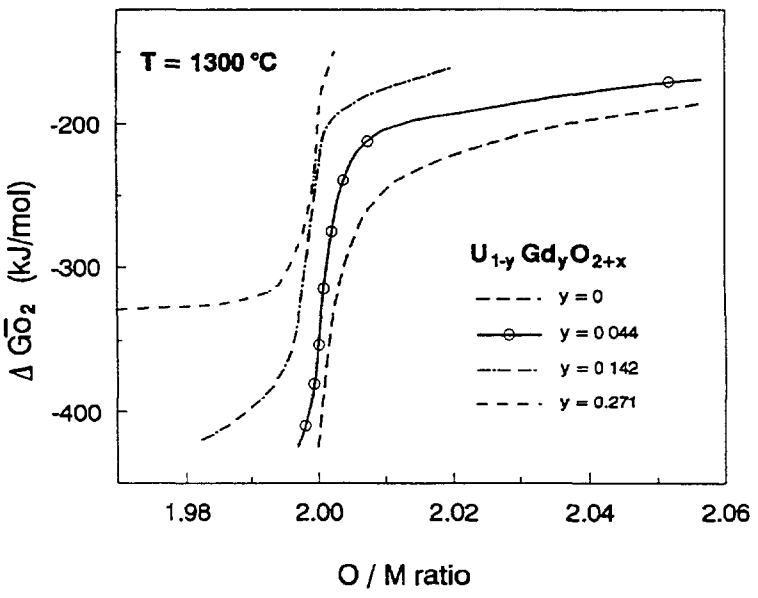

Fig. 2.3. *Oxygen potentials for $U_{0.96}Gd_{0.04}O_{2+x}$ plotted as a function of O / M ratio at 1300 °C [2.17]*

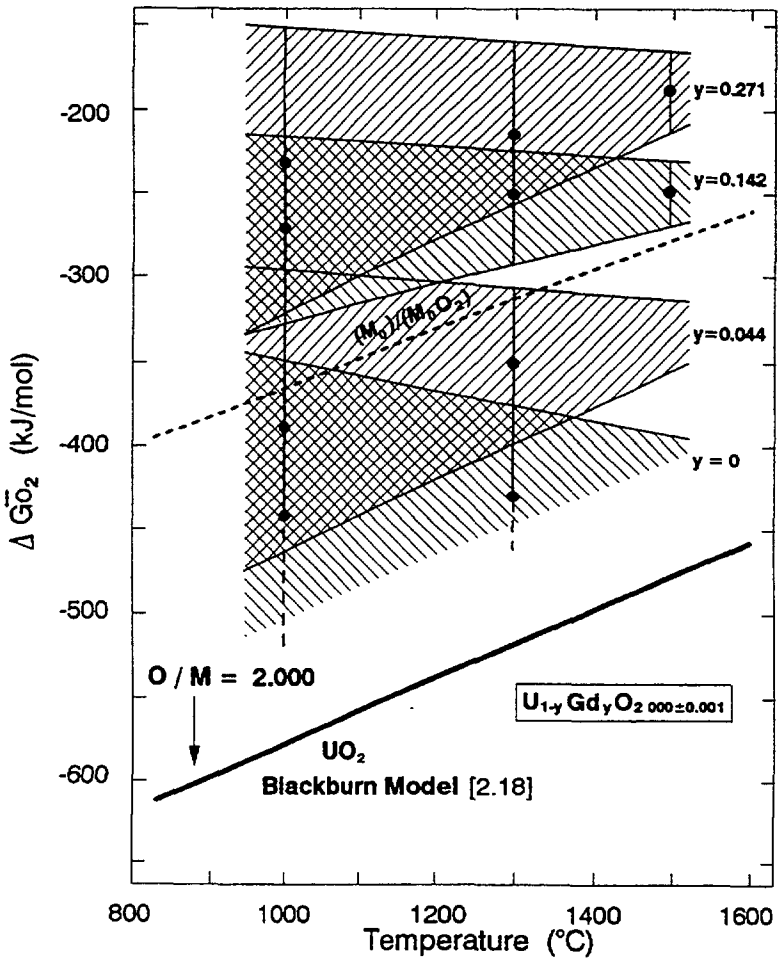

Fig. 2.4. *Oxygen potentials for exactly stoichiometric $U_{1-y}Gd_yO_2$ solid solutions [2.17]*

The oxygen potentials for near-stoichiometric (O/M = 2.000±0.001) UO_2 and $U_{1-y}Gd_yO_2$ solid solutions are given in **Figs. 2.2.; 2.3. and 2.4.** [17]. The solid circles represent the ΔG_{O_2} values at O/M=2.000. The hatched area represents the ΔG_{O_2} values within the O/M region from 1.999 to 2.001. The values of pure stoichiometric composition, calculated from the Blackburn model [18], are 90 to 140 kJ lower than the data obtained by K.Une et al. [16, 17]

These results suggest that further experimental work is needed to obtain more data both in the low temperature range (1000°C - 1500°C) and in the high range (1600°C - 1100°C) in order to improve the oxygen potential assessment of the $(U_{1-y}Gd_y)\ O_{2-x}$ solid solution for low Gd content fuel (y < = 0.1).

2.2. Physical properties

2.2.1. Theoretical and sintered density of (U, Gd)O_2 system

Calculations of the theoretical (or X-ray) density (TD) of the (U, Gd)O_2 solid solution require knowledge of the chemical composition, lattice parameter and structural model.

For example, the density of a solid solution with X mole fraction of Gd_2O_3 (adopting the "oxygen vacancy" model item 1 in table 2.1.) is given by

$$\rho = 4\,\frac{238(1-x) + 157x + 16\,(2-x/2)}{0.6023\,a^3\,10^{24}} \qquad (1)$$

Anion exchange, the EDTA titration method [19] and spectro-photometric methods [20] are usually used for the determination of Gd content and U^{6+}/U^{4+} ratio. The O/(U+Gd) ratios can be calculated using the following equation

$$6\,\frac{W_{U^{6+}}}{M_U} = +\,4\,\frac{W_{U^{4+}}}{M_U} + 3\,\frac{W_{Gd^{3+}}}{M_{Gd}} = 2\frac{W_{O^{2-}}}{M_o} \qquad (2)$$

where W is a weight fraction and M is an atomic weight.

Ho and Radford [12] used the experimental data (Gd content, U^{6+}/U^{4+} ratios, O/(U+Gd) ratios, lattice parameters) obtained by Fukushima et al.[21] for coprecipitated UO_2-Gd_2O_3 solid solutions with Gd contents up to 15 mol% and calculated the TD using different structural models (Fig. 2.5.). The line plotted above Fukushima's is from the "U^{5+}" model showing higher TD, and the lower line is from the "oxygen vacancy" model.

The analysis of Fukushima et al. implied that U^{5+} ions were more likely than U^{6+} ions, especially taking into account that the pellets were sintered in an Ar/H_2 mixture [21]. It is considered that an adequate representation of the expected TD of the Gd fuel pellets is attained when using the models developed by Ho and Radford.

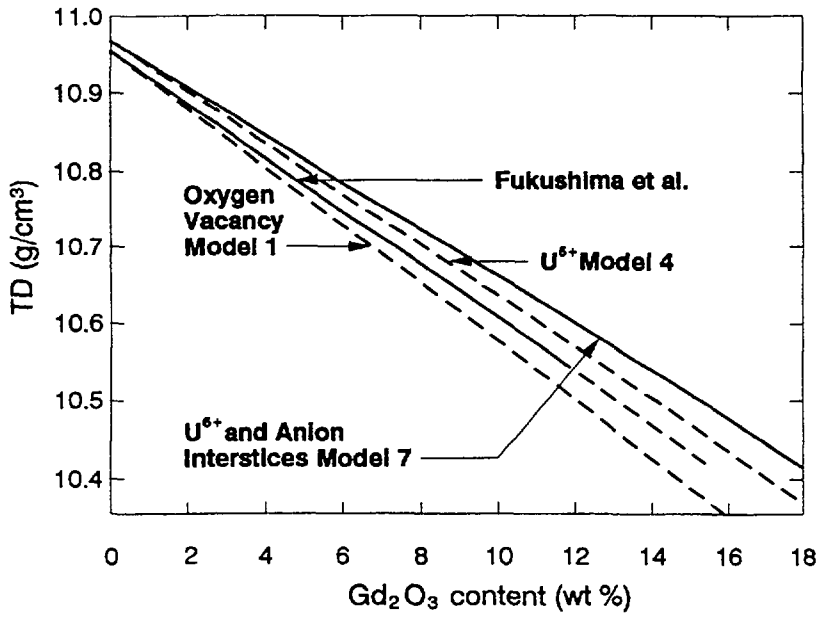

Fig. 2.5. *Comparison of UO_2 - Gd_2O_3 densities based on the data of Fukushima et al. [2.21] in relation to theoretical models [2.12]*

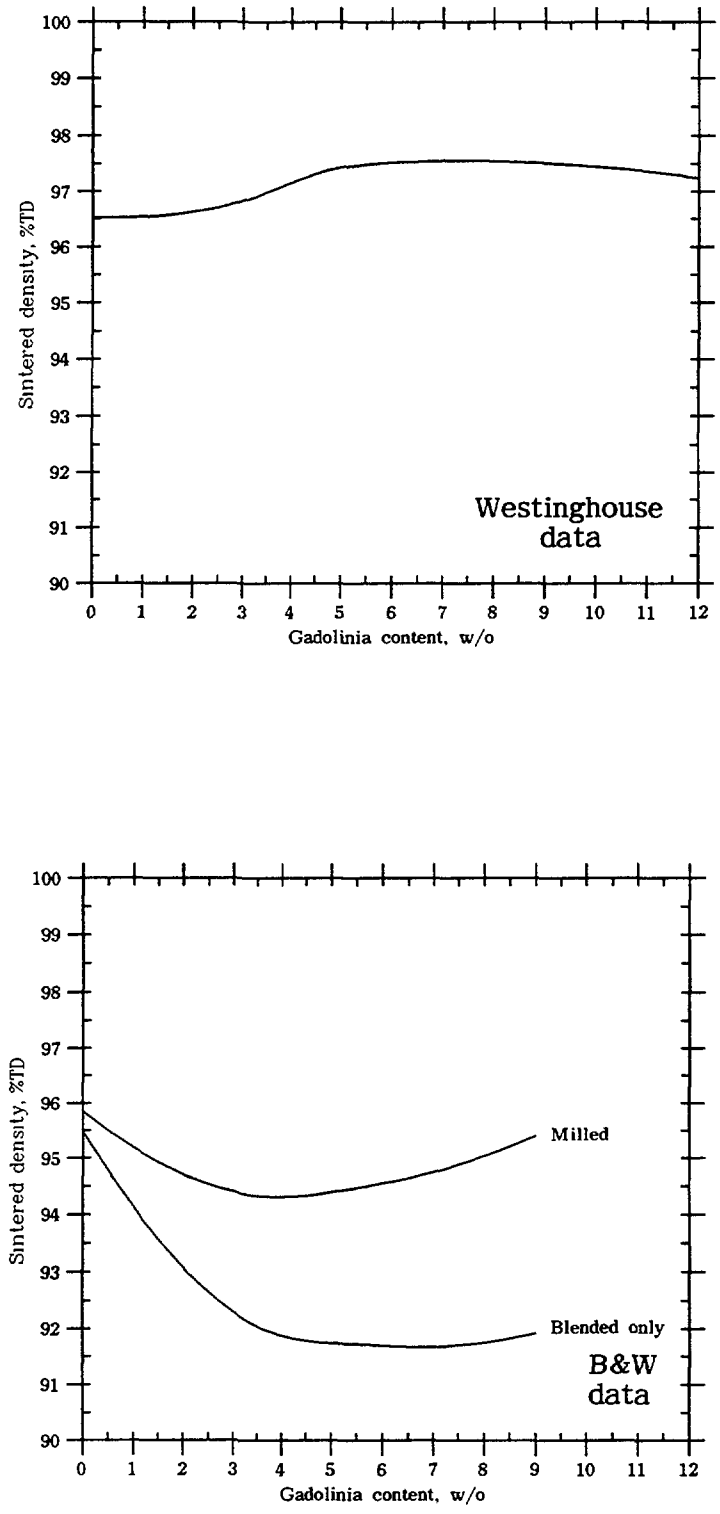

Fig. 2.6. *Effect of gadolinia content on sintered density [2.12, 2.13].*

Three equations describing the TD are listed below:

$$\rho = 10.962 - 0.0348x \qquad [2.21]$$

$$\rho = 10.960 - 0.033x \qquad [2.13]$$

$$\rho = 10.960 - 0.02x - 0.0027x^2 + 0.00015x^3 \qquad [2.22]$$

where ρ is the TD in g/cm^3 and x is the Gd_2O_3 content (w/o), valid for $0 < x < 12$.

It was shown that up to 10 w/o of Gd_2O_3 content, the quantity of the UO_2 phase in a $(U,Gd)O_2$ solid solution has no significant effect on the TD [2.21]. In comparison with the diminishing TD with increasing Gd_2O_3 the dependence of sintered density (as a percentage of the TD) is more complicated, for the simple reason that the solution type and its nature can undergo changes with increasing Gd_2O_3 content.

Fig. 2.6 shows the effect of Gd_2O_3 content on the sintered density of material as observed by two different sources [2.12, 2.23]. The Westinghouse specimens (data by Ho and Radford) were sintered for six hours in wet H_2 at 1750°C, but no details of the B & W sintering conditions are given. Similar data were obtained by Une and Oguma [2.17] where samples were sintered in a flowing dry H_2 atmosphere for 2 hours at 1700°C. It can be seen that there is considerable disagreement as to the effect that Gd content has on the sintered density.

It has been shown that Gd reduces cation diffusivities and sinterability, especially for a dry H_2 sintering atmosphere. Sintering in a wet H_2 atmosphere could result in enhanced oxidation of U^{4+} to smaller U^{5+} and U^{6+} ions and correspondingly quicker cation diffusion (for 4-8 w/o Gd_2O_3, Ho and Radford [2,12]). In the case of the B & W experiments, increased sinterability was achieved by implementing a powder milling process (Newman et al [2.23]).

2.2.2. Thermal conductivity

Of all the properties of Gd fuel, thermal conductivity has probably received the most attention over the past 10 years. This is because as gadolinia is added to UO_2 its thermal conductivity reduces significantly, which, in reactor, leads to higher fuel temperatures all other conditions being equal.

However, the experimenters disagree on the magnitude of the reduction in thermal conductivity as Fig. 2.7 shows. This presents results from four different out-of-pile sources [2.21, 2.22, 2.24, 2.25] and shows the ratio of the thermal conductivity of gadolinia-doped UO_2 to undoped UO_2 for various gadolinia contents (w/o) as a function of temperature. All show that the effect of gadolinia is to reduce the thermal conductivity and that this effect becomes less important at higher temperatures, but the graphs show marked difference in absolute levels.

No details of the measurement techniques used for the Exxon data are available, but the other experiments used the laser-flash technique to determine the thermal diffusivities of samples. This technique involves applying a short duration pulse of energy on one face of a sample and measuring the temperature rise on the opposite face as a function of time. The thermal conductivity is then calculated from the thermal diffusivity, specific heat capacity and density of the samples, the density being corrected for thermal expansion in most cases. The French experimenters also performed a second method involving the direct measurement of thermal conductivity by steady state radial heat flow which showed reasonable agreement with their laser-flash results.

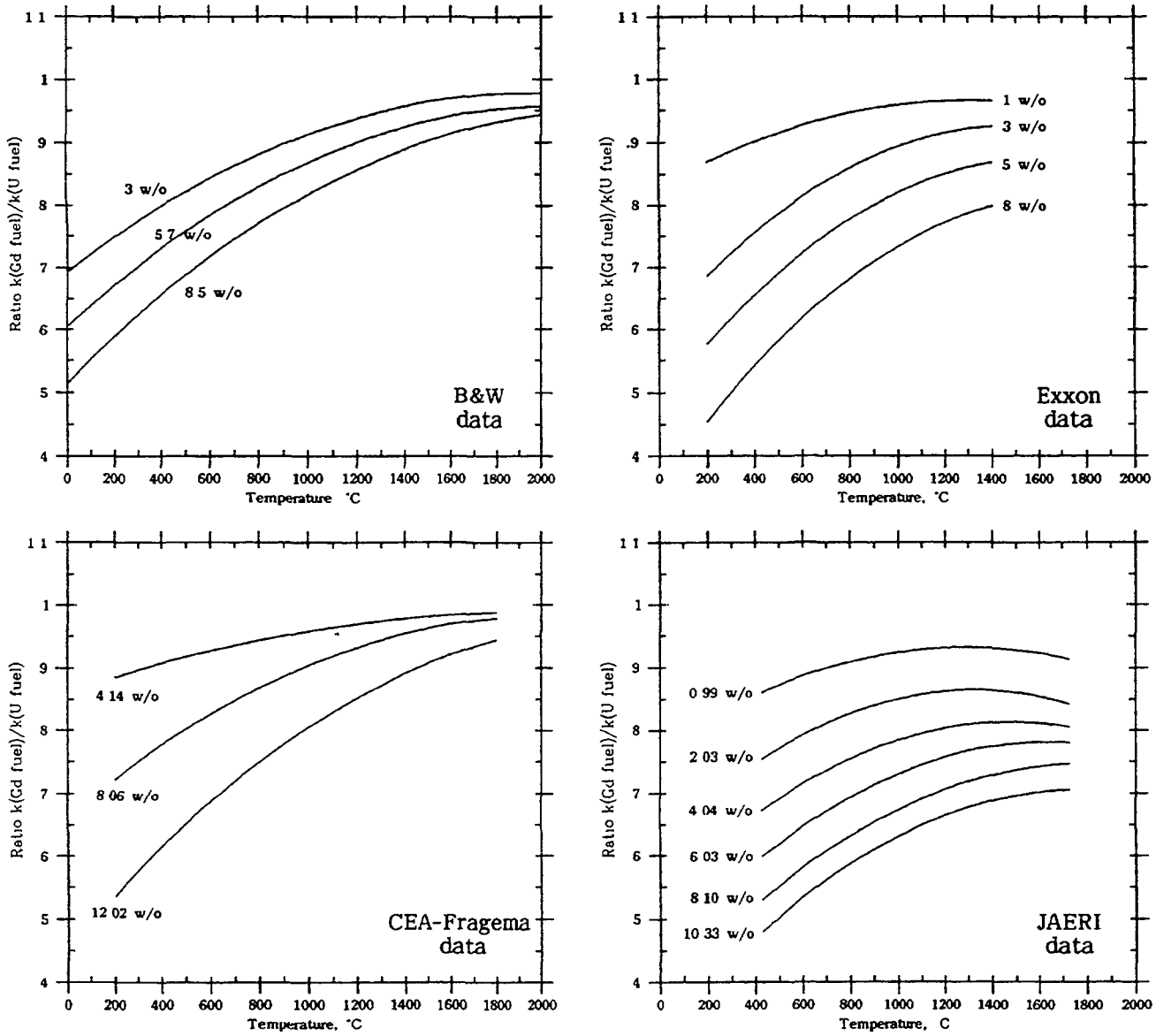

Fig. 2.7. *Thermal conductivity measurements as a function of gadolinia content and temperature [2.21, 2.22, 2.24, 2.25].*

Individual experimenter's calculations were as follows:

a. **B & W data [2.24]**

The expression used to calculate thermal conductivity was

$k = a_d C_P \rho_o (1 + 3a_e)-1$

where a_d : - thermal diffusivity

C_P: - specific heat capacity

ρ_o: - room temperature density

a_e: - thermal expansion coefficient

The specific heat was derived from measured enthalpy data using a Bunsen-type ice-drop calorimeter. Thermal expansion was measured by a recording quartz dilatometer over the range O to 900°C and by optical dilatometry over the range 900 to 2000°C. The thermal conductivity data were correlated for each gadolinia concentration as a function of temperature T(K) using expressions of the form:

$$k = (A + BT)^{-1}$$

where A and B are constants normalized to 95% theoretical density. Values for A and B are not given.

b. Exxon data [2.25]

No details are available.

c. CEA-FRAGEMA data [2.22]

The expression used to calculate thermal conductivity was

$$k = a_d C_P \rho$$

where a_d: - thermal diffusivity

C_P: - specific heat capacity

ρ: - density

Specific heat capacity was derived from enthalpy measurements using differential microcalorimetry. It is not clear whether thermal expansion effects were considered but if they were, pure UO_2 values would have been used.

No details on the correlation of thermal conductivity data with temperature are provided, although an $(A+BT)^{-1}$ relationship is again likely.

d. JAERI data [2.21]

The expression used to calculate thermal conductivity was

$$k = a_d C_P \rho$$

where a_d: - thermal diffusivity

C_P: - specific heat capacity

ρ: - density

Specific heat capacity was estimated from a weighted average of previously published data for specific heats of UO_2 and gadolinia, which had, in any case, to be extrapolated to temperatures outside the ranges for which they were originally intended. Thermal expansion effects were included in the density term, but values for pure UO_2 were used.

The thermal conductivity data were correlated for each gadolinia concentration as a function of temperature T K up to around 1300°C using expressions of the form

$$k = (A + BT)^{-1}$$

TABLE 2.4. *VALUES OF CONSTANTS A AND B IN THE EXPRESSION FOR THERMAL CONDUCTIVITY* $k = (A + BT)^{-1}$ *AS DETERMINED BY JAERI [2.21]*

Gadolinia content (w/o)	A (10^{-2} mK/W)	B (10^{-2} m/W)
0.00	3.29	0.0236
0.99	6.53	0.0235
2.03	10.18	0.0233
4.04	13.37	0.0234
6.03	17.29	0.0229
8.10	22.41	0.0220
10.33	27.19	0.0210

Note: *temperatures T must be in K*

where A and B are constants normalized to 95% theoretical density. Values for A and B are given in Table 2.4.

e. ARSRIIM and RCC KI (Russian Federation) data

The results of calculations of k values (by an indirect measurement method) for near-stoichiometric (U, Gd)O_2 pellets with Gd_2O_3 contents of 5 and 6 w/o [2.26] are similar to JAERI (Fukushima et al [2.21]) data.

In assessing these data, it is clear that apparently similar experimental techniques have yielded dissimilar results. More credibility could be attached to the B&W results, since all parameters used in the calculation of thermal conductivity were obtained from the samples used in the test program. The JAERI results used extrapolated hybrid specific heat data employing the rule of mixtures. JAERI and FRAGEMA used thermal expansion data pertaining to pure UO_2, but the effect of this should be negligible. There are no details available for the Exxon data.

2.2.3. Specific heat capacity

This is an important characteristic, especially as it is used by most experimenters to derive thermal conductivity. For simplicity's sake, the specific heat capacity of pure UO_2 is often used for gadolinia-doped UO_2 and Fig. 2.8 shows that this is a reasonably good approximation for most doping levels up to temperatures of around 700°C. Fig.2.8 presents specific heat capacity data for gadolinia-doped UO_2 from two different sources [2.22, 2.27] and compares each with standard data for UO_2. The heat capacity is seen to be weakly dependent on doping level up to around 700°C (with the exception of the 10 w/o Japanese data), the maximum deviation from the pure UO_2 data being around 5%. Above this temperature, however, Japanese data show a significant increase over the pure UO_2 data, which is temperature and Gd content dependent.

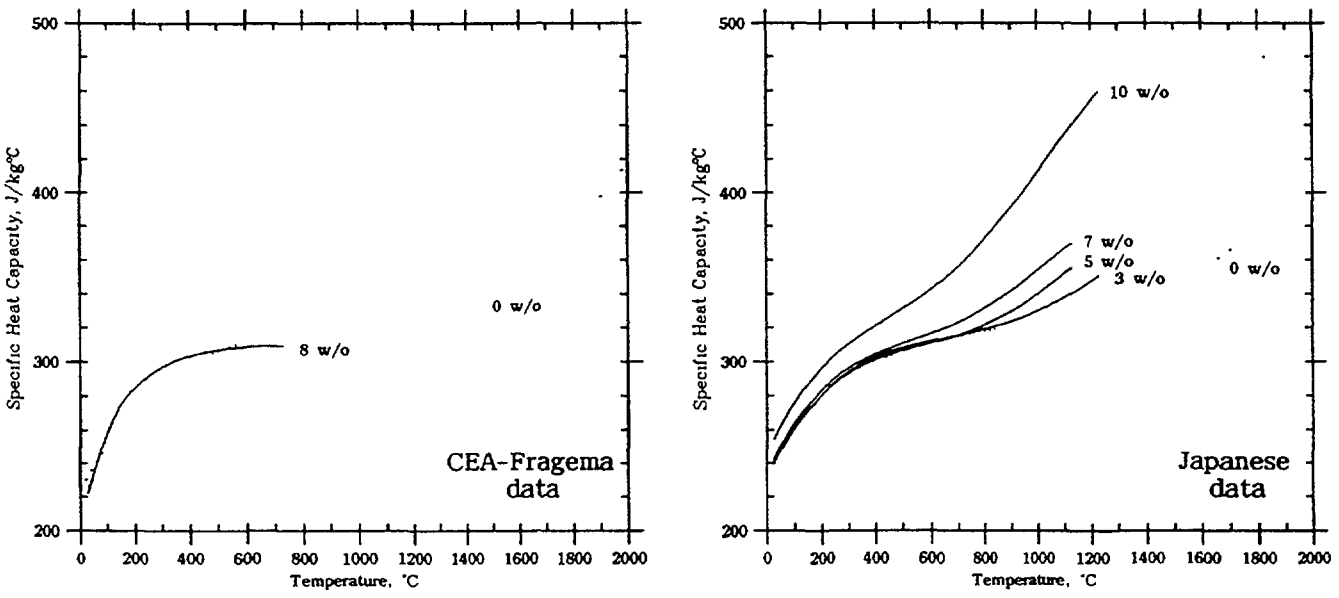

Fig. 2.8. *Specific heat capacity measurements as a function of gadolinia content and temperature [2.22, 2.27].*

Individual experimenter's calculations were as follows:

a. CEA-FRAGEMA data [2.22]

Specific heat capacity was obtained by differential microcalorimetry by measuring the enthalpy variation during thermal cycling of the samples. The expression used to calculate specific heat capacity was:

$$C_P = 337.7 - (1.823 \cdot 10^{-2}\, T) - (0.997 \cdot 10^{-7}\, T);$$

where T is temperature in K and C_P is given in J/kg K. Data were obtained for 8 w/o gadolinia only.

b. Japanese data [2.27]

Specific heat capacity data were obtained for a number of different Gd content levels of the form $U_{1-y}Gd_yO_2$ up to 1500 K by means of direct heating pulse calorimetry. The data were fitted to equations of the form

$$C_p = A + BT + CT^{-1} + DT^{-2} + ET^{-3} + dC_p$$

where A, B, C, D and E are constants given in Table 2.5, T is temperature in K and dC, the excess heat capacity, is given by

$$dC_p = \{ (\Delta H)^2 / RT^2 \} \exp(\Delta S/R) \exp(-\Delta H/RT)$$

where ΔH and ΔS are the enthalpy and entropy of activation respectively, R is the universal gas constant 8.314 J/mol·K. and C_p is given in J/mol·K.

It is clear that both experimenters have found that the specific heat capacity of gadolinia-UO_2 is very close to that of pure UO_2 for any Gd content, up to around 700°C. The

TABLE 2.5. *VALUES OF CONSTANTS A, B, C, D AND E, AND ENTHALPY AND ENTROPY OF ACTIVATION (ΔH, ΔS) IN THE EXPRESSION FOR SPECIFIC HEAT CAPACITY AS DETERMINED BY JAPANESE [2.27].*

Gadolinia content (w / o)	A (J / mol K^2)	B 10^{-2} (J / mol K)	C 10^4 (J / mol)	D 10^7 (J K / mol)	E 10^9 (J K^2 / mol)	ΔH 10^3 (J / mol)	ΔS (J / mol K)
3	45.905	1.7805	3.5171	-1.6717	2.1997	106.6	29.5
5	55.330	1.4582	2.3691	-1.1677	1.4657	90.9	28.9
7	61.215	1.2100	1.9362	-1.0336	1.3170	71.2	22.1
10	38.596	2.2130	4.0941	-1.7856	2.2220	53.3	21.2

Note: *temperatures T must be in K*

data beyond this temperature shows a clear deviation from the standard UO_2 data and from the values that the rule of mixtures would predict. Inaba et al. [2.27] postulates the formation of oxygen clusters as being the reason for the excess heat capacity, but experimental error effects and scatter of results could equally account for a large part of it. It is clear that further investigations at these higher temperatures are desirable. Also, where experimenters have used pure-UO_2 values for specific heat capacity, this may have unduly pessimised their calculations of thermal conductivity.

2.2.4. Thermal diffusivity

Thermal diffusivity of (U, Gd)O_2, from which thermal conductivity is usually derived, is another important property for estimating the fuel behaviour.

Generally, the factors affecting the measured values of thermal diffusivity are roughly classified into chemical factors such as displaced Gd^{3+} ions and consequently oxidized U^{5+}, and geometrical factors such as microcracks, pores and cracks.

TABLE 2.6. *THERMAL DIFFUSIVITY SAMPLE CHARACTERISTICS*

Reference	Gd_2O_3 content (w / o)	Fabrication route	Sample thickness (mm)	Density (% TD)	Presence of microcracks
[2.28]	0, 10	mechanical blend and co-precipitation	0.5 - 1.2	93.6 - 98.5	in several samples
[2.26]	0, 6, 8, 10	mechanical blend	0.8 - 0.9	~ 95	no

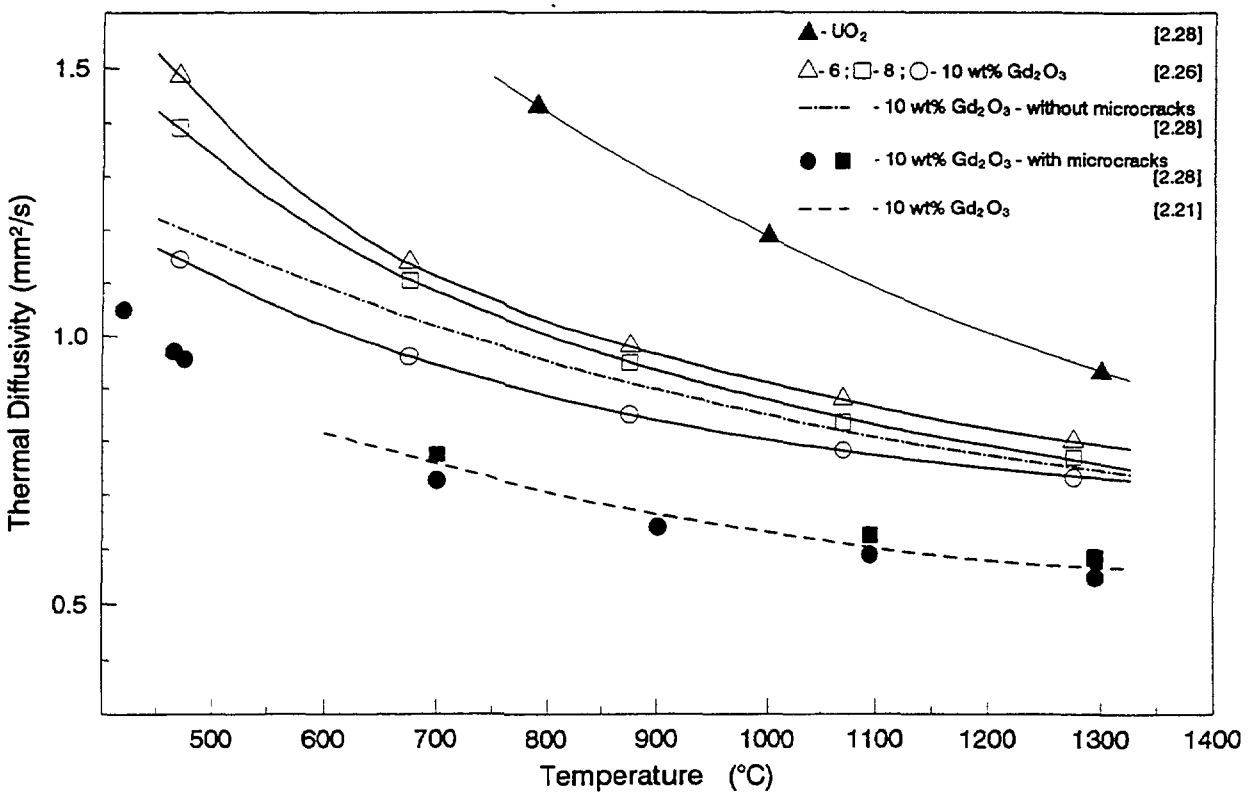

Fig. 2.9. *Thermal Diffusivity of UO_2 and (U, Gd) O_2 samples (normalized to 95 % TD)*

The thermal diffusivity of UO_2 and $(U,Gd)O_2$ samples was measured by the laser pulse method over a temperature range of 473-1273 K [2.26] and 300-2000 K [2.28]. Principal characteristics of samples are given in Table 2.6 and measurements results in Fig.2.9. Data obtained by Fukushima et al. [2.21] are also given in Fig.2.9.

The principal results of the thermal diffusivity measurements [2.21,2.26,2.28] can be summarized as follows:

- the data are independent of sample thickness and fabrication route;
- thermal diffusivity of $(U,Gd)O_2$ fuel is lower than that of UO_2 fuel at low ($\leq$ 1200 K) temperatures, the magnitude of the difference depending on Gd concentration;
- at higher temperatures (near 2000 K), the diffusivities of the $(U,Gd)O_2$ solid solution and UO_2 are almost the same;
- below 1200 K the diffusivities of the $(U,Gd)O_2$ samples with microcracks are about 30% lower than the microcrack-free pellets and agree with the data of Fukushima et al. [2.21].

2.2.5. Thermal expansion

Wada et al. [2.13] measured the thermal expansion coefficient of Gd fuel (coprecipitated, sintered in H_2 atmosphere at 1600°C, 24h) in the composition range 0-30 w/o Gd up to a temperature of 1223 K using a dilatometer. They found that the addition of Gd_2O_3 up to 12 w/o in UO_2 had little effect on the thermal expansion coefficient (= $10.5 \cdot 10^{-6} K^{-1}$). Beyond 12 w/o, it increased slightly with Gd_2O_3 content to $11.7 \cdot 10^{-6} K$ at 30 w/o Gd_2O_3.

Chotard et al. [2.22] (for mechanically blended samples, sintered in a humidified H_2 atmosphere at 1700°C, 4h) obtained results consistent with those of Wada et al. [2.13]. They showed that over the temperature range 300 to 2000 K and a concentration range 0 to 12 w/o Gd_2O_3, the thermal expansion coefficient is the same as for pure UO_2.

Une [2.29] measured the linear thermal expansion of Gd fuel (mechanically blended, sintered in a flowing H_2 atmosphere at 1720 or 1750°C) in the composition range of 0,5,8,10 w/o Gd_2O_3 over the temperature range of 298 to 1973 K using a dilatometer. Results indicate that the linear thermal expansion coefficient becomes larger with increasing Gd_2O_3 content. At 1973 K the linear thermal expansions for UO_2- 5 w/o Gd_2O_3, UO_2 - 8 w/o Gd_2O_3 and UO_2 - 10 w/o Gd_2O_3 were about 2.7, 5.4 and 6.2% larger than the values for UO_2 pellets, respectively.

The linear thermal expansion can be expressed by the following least-square fitted equation:

$$dL/L_0 = A + BT + CT^2;$$

where T is the temperature in K and L_o is the specimen length at 298 K. Table 2.7 gives the regression constants A,B and C obtained by Une for the temperature range 298 to 1973 K [2.29].

B & W data by Newman [2.23] were obtained by quartz and optical dilatometry for $(U,Gd)O_2$ pellets with Gd_2O_3 contents of 0, 5.66 and 8.50 w/o (Fig. 2.10). They are similar to the data of Chotard [2.22] and Une [2.29].

Summarizing all the above-mentioned results, it is considered that the mean coefficient of linear thermal expansion shows negligible variation from values for pure UO_2.

TABLE 2.7. *REGRESSION CONSTANTS FOR EQUATION OF LINEAR THERMAL EXPANSION OF UO_2 - Gd_2O_3 FUEL ($dL/L_o = A + BT + CT^2$) [2.29]*

Gd_2O_3 content (w / o)	A 10^{-3}	B 10^{-6}	C 10^{-9}	Standard deviation 10^{-5}
0	-2.238	7.165	2.095	5.2
5	-2.314	7.358	2.156	7.1
8	-2.391	7.433	2.278	9.4
10	-2.284	7.162	2.430	7.4

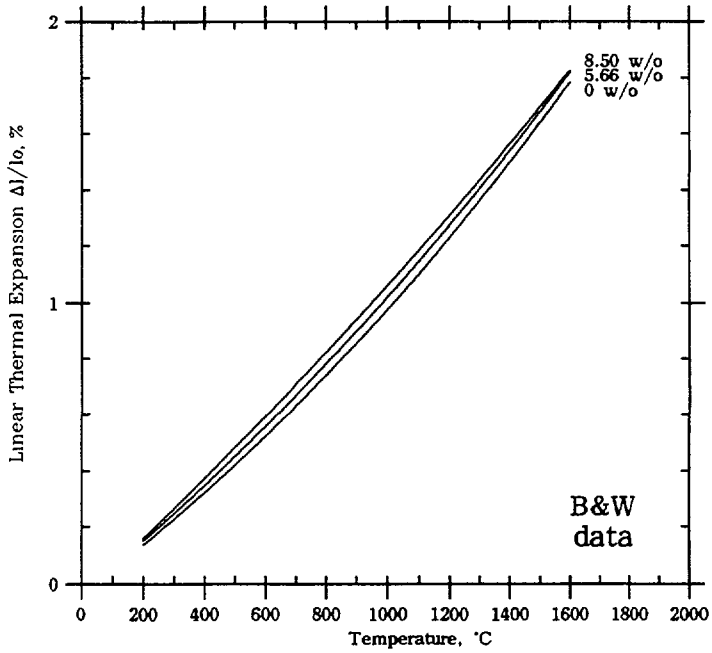

Fig. 2.10. *Linear thermal expansion measurements as a function of gadolinia content and temperature [2.23].*

2.2.6. UO_2 - Gd_2O_3 phase diagram and melting temperature

Two factors should be taken into account before analysing the UO_2 - Gd_2O_3 phase diagram:

1) Solid solutions of the rare earth oxides and urania form readily. Materials whose ionic radii are within 20% of the ionic radii of the rare earths form solid solutions [2.30]. The ionic radii of urania and gadolinia cations are: U^{4+} 0.97 A, U^{6+} 0.8 A and Gd^{3+}0.97 A.

2) Rare earth oxides are stabilizers of urania in an oxidizing and reducing environment [2.15].

Phase diagrams of $(U,Gd)O_2$ solid solutions obtained by two different methods (mechanical blending [2.15] and coprecipitation [2.13]) are shown in Fig. 2.11 and 2.12 respectively. X-ray diffraction analysis indicated in both cases the presence of only one f.c.c. solid solution at gadolinia contents up to 30-40 mol.% and a linear decrease of the solid solution lattice parameter with increasing gadolinia content.

Specimens (pieces of crushed pellets) were put directly on a tungsten (W) heater and heated in an inert gas atmosphere (He [2.15] and Ar + 5%H_2 [2.13]). Liquidus temperatures represent the complete melting of the composite.

Liquidus temperatures from both studies decrease practically linearly with increasing gadolinia content (from 2800 to 2760°C [2.5] or 2800 to 2700°C [2.13] for Gd content up to 30 w/o). However, the solidus line, reported by Beals et al. [2.15] to be at 2250°C, was not found by Wada et al. [2.13]. Liquid phases sometimes observed at grain boundaries were identified [2.13] as W-U-Gd-O or Mo-U-Gd (when a molybdenum, Mo, heater was used) but not as U-Gd-O. Therefore it was assumed [2.13] that the solidus line would probably lie very close to the liquidus and that the phase relationship of the $(U,Gd)O_2$ system could be similar to that of the $(U,Gd)O_2$ system reported by Grossman et al. [2.31] and Chotard et al [2.22].

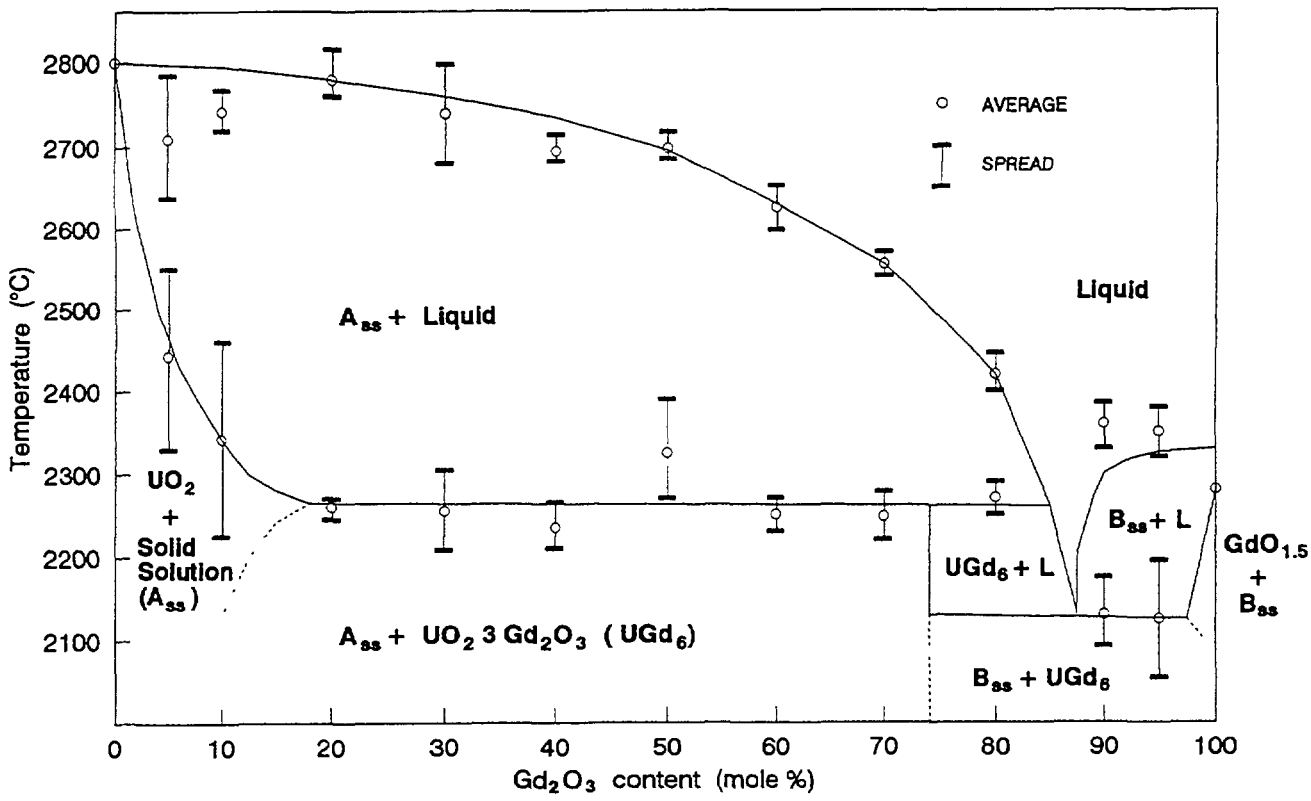

Fig. 2.11. *(U, Gd) O_2 phase diagram [2.15]*

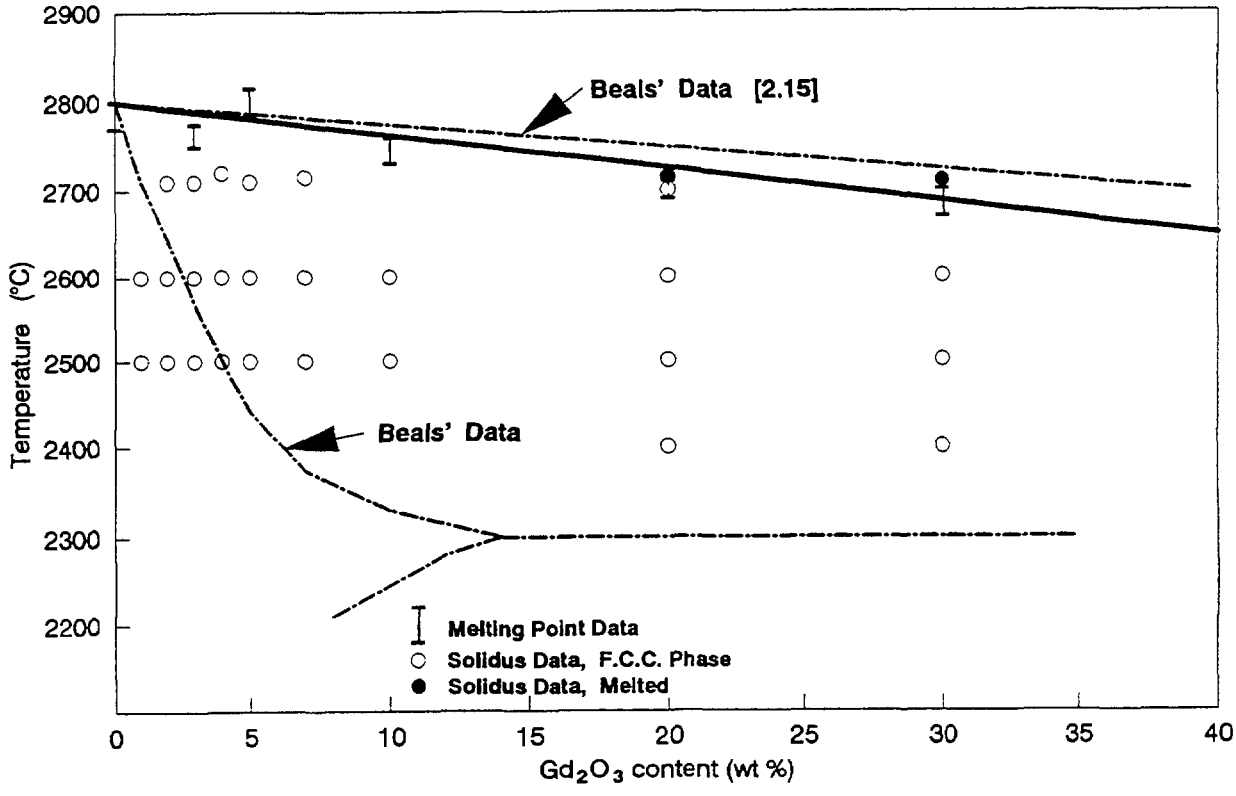

Fig. 2.12. *(U, Gd) O_2 phase diagram [2.13]*

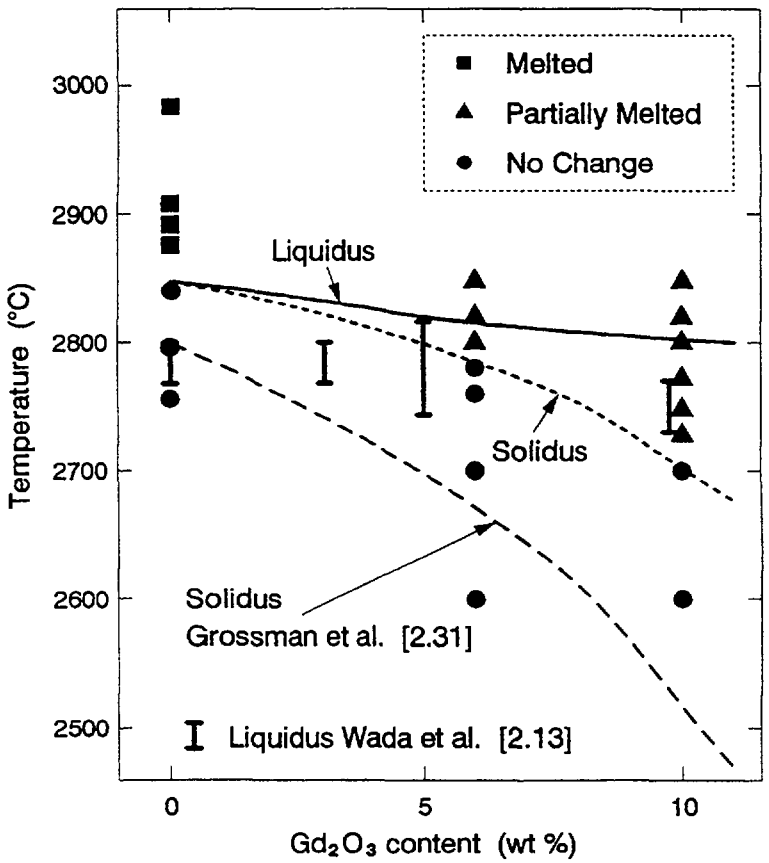

Fig. 2.13. *(U, Gd) O_2 phase diagram [2.32]*

The left corner of the $(U,Gd)O_2$ phase diagram was recently investigated by Matsuoka [2.32]. Gd_2O_3 contents of the pellets were 0.6 and 10 w/o. The pellets were heated up to the specified temperature in an Ar gas atmosphere, held there for a specified duration and then cooled rapidly. The specified temperature was selected at 20-30°C intervals around 2800°C. The liquidus and solidus were determined by visual and ceramographic observation of the heated specimens.

The results of [2.32] are shown in Fig. 2.13 together with those presented by Wada [2.13] and Grossman [2.31] for comparison. In these experiments, the solidus line can be observed separately from the liquidus for 10 w/o Gd_2O_3 pellets, the solidus temperature being 2700-2725$\pm$18°C.

Summarizing the above data, it is concluded that the solidus line lies close to the liquidus although it is difficult to specify the exact temperature difference between these lines.

Although many reports have been published concerning the melting point of $(U,Gd)O_2$, the melting point is still not yet finally established, due principally to the instability of samples over 2800°C and the difficulty of measuring the temperature at such a high level. Data by Beals [2.5], Wada [2.13], Jamanouchi [2.33], Matsuoka [2.32] and Hanson [2.34] showed a slight decrease in melting temperature with increasing gadolinia content (Figs. 2.11-13). In contrast with these results Chotard [2.22] showed (Fig. 2.14) that the melting temperature was largely independent of gadolinia content up to 12 w/o (pellets were obtained by mechanical milling, blending, granulation and sintering in a humidified H_2 atmosphere at 1700°C for 4 hours).

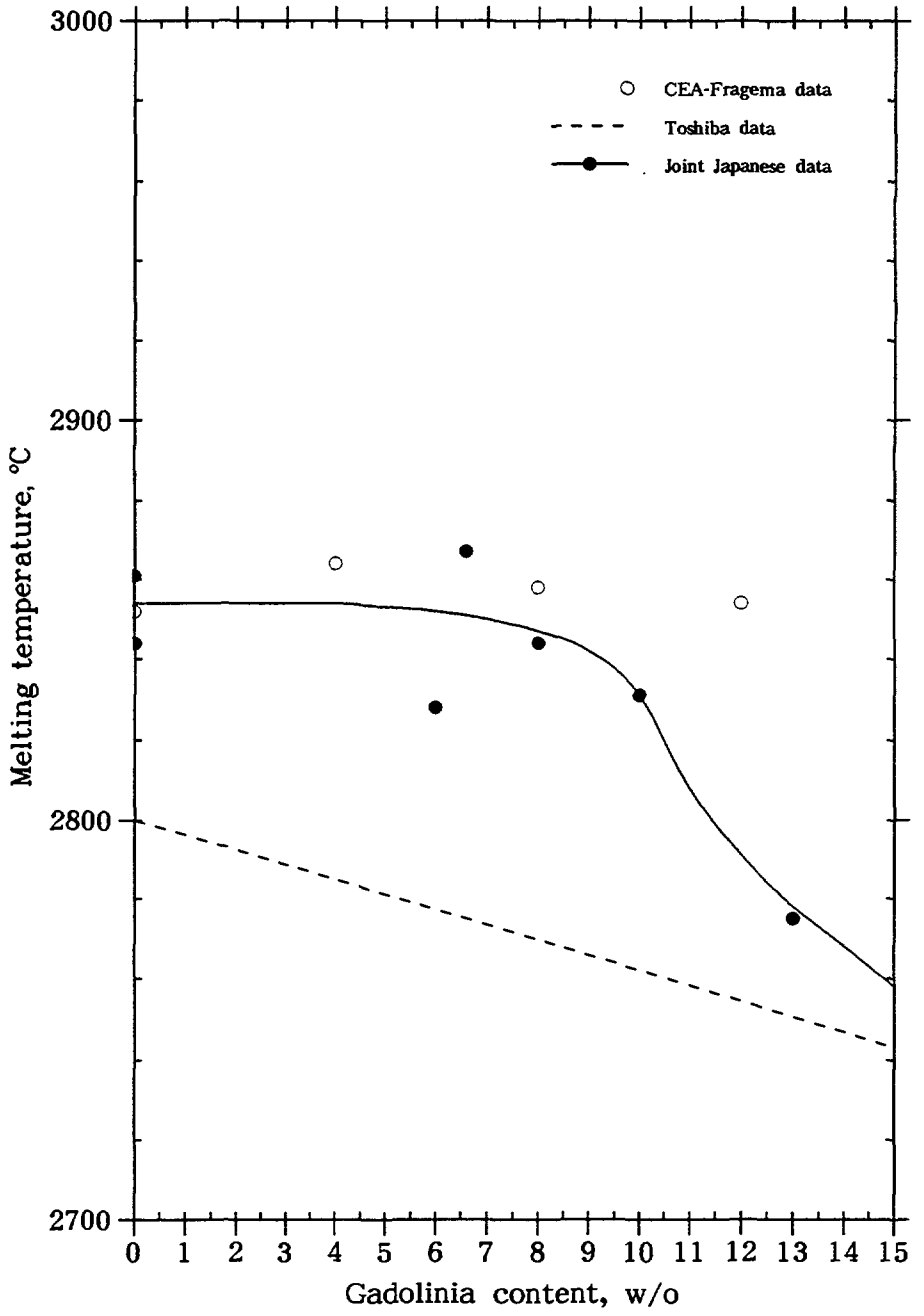

Fig. 2.14. *Melting temperature as a function of gadolinia content [2.13, 2.22, 2.35].*

In a recent joint study of five Japanese utilities [2.35] the melting temperature of fragments of pellets obtained by a master blending technique and sintered in cracked ammonium with steam at 1700°C for 4 hours was studied using a tungsten ribbon heater method. The results of this study are also shown in Fig. 2.14 for two groups of specimens (the quantity of UO_2 phase of type 1 was 5% while that of type 2 was 20-25%). The maximum difference in the melting temperature was 40°C but it was confirmed that there was no significant decrease of melting temperature up to 8 w/o Gd_2O_3. From 10 to 15 w/o Gd_2O_3, a 50-60°C decrease was observed but no change was observed from 15 to 25 w/o Gd_2O_3. The same dependence of melting temperature on additive concentration was obtained for UO_2-Sm_2O_3 and UO_2-Dy_2O_3 systems.

2.2.7. Grain growth

Grain growth behaviour at 1700-2000°C of UO_2 and $(U,Gd)O_2$ fuel pellets prepared by the coprecipitation method and mechanical blending was investigated in [2.36]. The contents of Gd_2O_3 in the $(U,Gd)O_2$ pellets prepared by mechanical blending were 3,5,8 and 10 w/o and those by coprecipitation were 5 and 10 w/o.

Powder of UO_2 and $(U,Gd)O_2$ was pressed at 340-390 MPa, and the green pellets were sintered at 1600°C in hydrogen for 2 hours (95-97% TD). As expected the coprecipitation method provided better homogeneity of the $(U,Gd)O_2$ solid solution than the mechanical blending, where small amounts of free UO_2 and Gd_2O_3 were observed.

The prepared specimens were heated in a reducing atmosphere of He-8%H_2 at 1700-2000°C for 1-30 hours with no significant change in O/M ratio. Grain diameters were measured by the linear intercept method. The data scatter in the Gd due to the differences in pellets between mechanical blending and coprecipitation was not too large. Data were best fitted by fourth power rate equations:

for UO_2: $D^4 - D^4_0 = 3.79 \times 10^{18} \exp(-142{,}000/RT)\ t\ (\mu m^4)$,

for $(U,Gd)O_2$: $D^4 - D^4_0 = 4.98 \times 10^{17} \exp(-140{,}000/RT)t\ (\mu m^4)$

where R is the gas constant (1.987 cal/mol K), T - temperature (K), and t - time (hours).

It is clear that the grain growth rate of the $(U,Gd)O_2$ pellet is approximately one order of magnitude smaller that the UO_2 growth rate.

The authors of [2.36] explained the difference in grain growth rate between UO_2 and $(U,Gd)O_2$ through suppression of U atom diffusion in the $(U,Gd)O_2$ pellets. They explained the absence of this difference for pellets with different Gd contents through keeping the O/M ratio well below 2.0 and an unchanged vacancy concentration.

Littlechild et al. [2.37] also observed that the addition of small amounts of gadolinia (0-6 w/o) caused a decrease in grain size, but that, as gadolinia content was increased above 6 w/o, grain size increased again.

2.2.8. Diffusion coefficient of U -> Gd and Gd -> U

The data described above show that for Gd fuel sintered in a typical atmosphere, cation diffusion is slower than in pure UO_2.

The kinetics of cation interdiffusion was studied with the help of alpha and neutron autoradiography [2.38] and SEM and EDX techniques [2.39] (see App.V). The diffusion couples were prepared by placing Gd_2O_3 green pellets into UO_2 powder, and compacting and sintering in a hydrogen atmosphere in the temperature range of 1600 to 1900°C for 4, 16 and 64 hours [2.38] and at 1700 and 1800°C for 100 hours [2.39] respectively. The temperature dependence of cation interdiffusions is given by the equations

$D = 3.3 \cdot 10^{-6} \exp(-200000/RT)\ cm^2/s$ [2.38]

$D = 1.0 \cdot 10^{-5} \exp(-260000/RT)\ cm^2/s$ [2.39]

where R is the gas constant (8,314 J/mol·K) and T - temperature (K).

Numerical values for typical sintering temperature (1750°C) are:

$2.26 \cdot 10^{-11}$ cm^2/s [2.38]

$1.93 \cdot 10^{-12}$ cm^2/s [2.39]

Based on these results, it was estimated that the distance between Gd_2O_3 grains should be less than 4-5 μm [2.39] and ~15μm [2.38] at powder blending in order to obtain a homogeneous pellet by sintering at 1750°C for 4 hours.

2.2.9. Electrical conductivity

Only one investigation of electrical conductivity of gadolinia-doped UO_2 has been found [2.40]. Samples with gadolinia contents ranging from 2 to 10 w/o have been investigated using the four-probe DC technique to avoid the high resistance problem at the contacts between probe and sample. Data were obtained during both the heating and cooling process, and no real differences were noticed between the two sets of data. Fig. 2.15 shows the

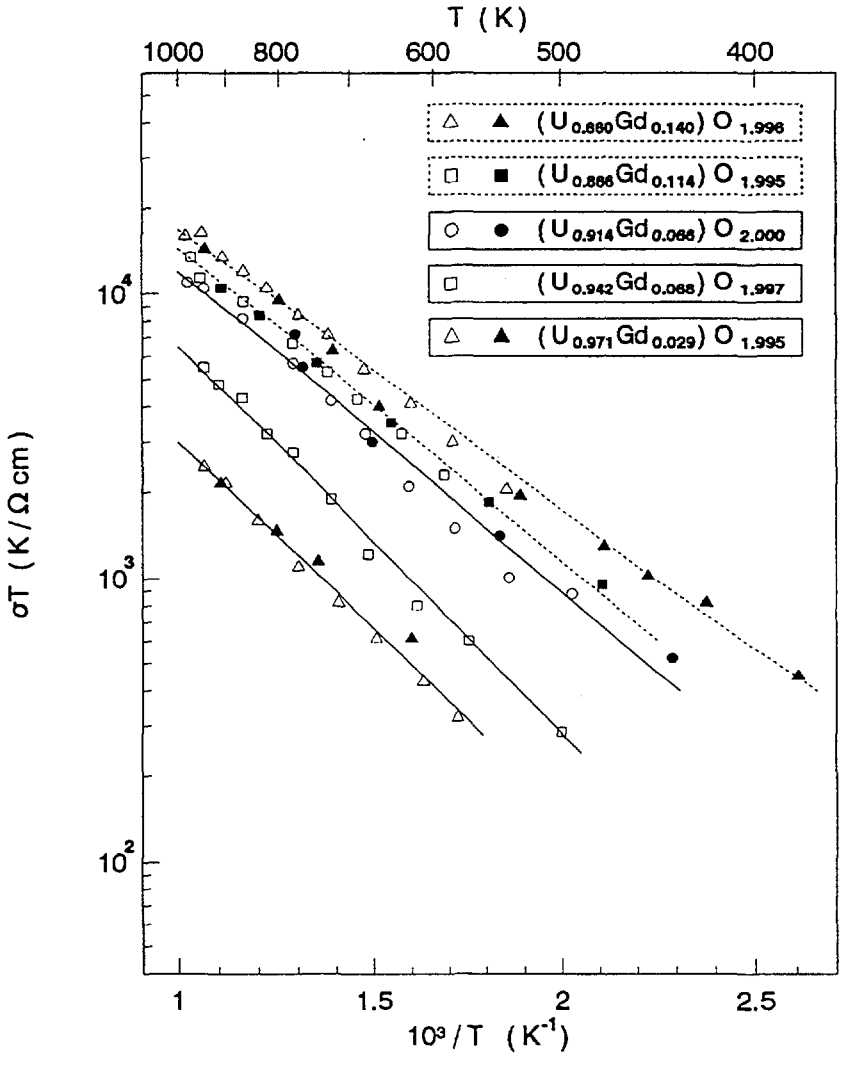

Fig. 2.15. *Electrical conductivity of near stoichiometric (U, Gd) O_2 solid solutions plotted as σT versus 1/T. Open and solid marks are the data measured on the heating and cooling process, respectively [2.40].*

results in the form of the product of electrical conductivity σ and absolute temperature, T, plotted against 1/T. The electrical conductivity was seen to increase with temperature for all samples and to increase with gadolinia content. The values of electrical conductivity of the gadolinia-doped samples were about two or three orders of magnitude higher than those of pure UO_2.

2.3 MECHANICAL PROPERTIES

2.3.1 Elastic modulus

The data on elastic constants are limited only to one publication [2.41]. In this paper the elastic constants of UO_2 - Gd_2O_3 , UO_2 - Nb_2O_5 and UO_2 - TiO_2 pellets were measured at room temperature using the pulse echo overlap method to determine the additive content dependency.

Specimens of UO_2 with Gd_2O_3 content ranging from 0 to 20 w/o, with Nb_2O_5 content ranging from 0 to 0.8 w/o and TiO_2 content ranging from 0 to 0.2 w/o were prepared using the mechanical blending method and the coprecipitation method. The specimens were of cylindrical configuration of 10 ~ 15 mm diameter and 7 ~ 13 mm length, both ends of which were cut by a slicing machine to generate a high degree of parallelism. The natual frequency of the oscillator was 5 MHz.

Fig. 2.16 presents the results of the Young's modulus measurements for UO_2 - Gd_2O_3 pellets. The data were normalized to 100% TD using the density correction expression obtained from the experiment and are presented relative to the Young's modulus of pure UO_2. The Gd_2O_3 content dependency expressions of the Young's modulus and Poisson's ratio of UO_2 - Gd_2O_3 pellets at room temperature were obtained by fitting a linear regression expression to the data as follows:

$$E/E_o = 1 - 5.686.10^{-3}\, C_{Gd}$$

$$v/v_0 = 1 - 6.59.10^{-3}\, C_{Gd}$$

where E_o and v_o are Young's modulus and the Poisson's ratio of pure UO_2, C_{Gd} is Gd_2O_3 content (w/o).

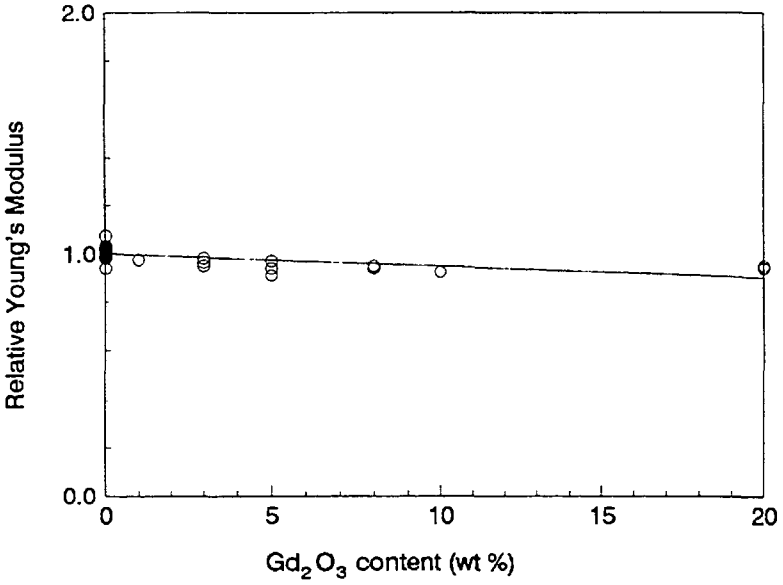

Fig. 2.16. *Young's modulus of Gd_2O_3- UO_2 pellet vs. Gd_2O_3 content [2.41]*

TABLE 2.8. PARAMETERS OF THERMAL CREEP TESTS OF (U, Gd) O_2 PELLETS

Reference	Gd_2O_3 content (w / o)	σ (MPa)	t (°C)
Peehs et al [2.42]	0; 6.5	100	1500
Hirai et al [2.43]	0; 3; 5	8 - 75	1200 - 1520
Watarumi et al [2.44]	3 - 15	30 - 60	1300 - 1500
Godin et al [2.45]	0 - 10	10 - 50	1200 - 1400

The Young's modulus and Poisson's ratio of UO_2 - Nb_2O_5 and UO_2 - TiO_2 pellets remained constant within the range of the experiment.

2.3.2. Creep

There are only a few publications describing thermal creep of Gd pellets [2.42-2.45]. In all cases pellets were obtained by a mechanical blending method followed by sintering under conditions providing a solid solution. A rated load compression method in vacuum [2.42, 2.44, 2.45] or in N_2 - 8% H_2 atmosphere [2.43] was used to obtain the data. Gd_2O_3 content, compression stresses and test temperatures are given in Table 2.8.

Some results of the above-mentioned thermal creep test for (U, Gd)O_2 pellets are presented in Fig 2.17 [2.45] and 2.18 [2.43]. The difference in absolute values of creep rate between [2.43] and [2.45] can be explained by a significant difference in stress values (12 and 30 MPa respectively). A strong dependence of UO_2 and (U,Gd)O_2 sample creep stress was confirmed in [2.45]. In both cases sample density was ~95% TD and grain size ~ 10 μm.

These studies as well as [2.43,2.44] concluded that:

1. There is a tendency for a slight decrease of (U, Gd)O_2 pellet creep rate with increasing Gd_2O_3 content . This agrees with other cation intergranular diffusion rate-determining phenomena such as grain growth in which the creep behaviour was shown to be determined by the intergranular diffusion of cations. The following equation showing the Gd_2O_3 concentration x (w/o) dependency of (U, Gd)O_2 pellet creep rate ϵ was suggested by Hirai et al [2.43].

   $\log \epsilon = \log \epsilon\, UO_2 - 0.2\, x.$

   It was suggested [2.45] that the effect could probably be due to the higher cation diffusion rates in less stable (U, Gd)O_2 solid solutions.

2. Creep rate of (U, Gd)O_2 pellets within the low stresses regime ($\leq$ 50-60 MPa) is almost proportional to stress [2.43-2.45].

3. As with the creep rate of UO_2 pellets, the creep rate of Gd_2O_3 doped UO_2 pellets is inversely proportional to the second power of the grain size [2.43, 2.44].

Data on irradiation creep and power law creep as a function of Gd_2O_3 content have not been published, and hence the standard UO_2 equations should be used in the absence of any other information.

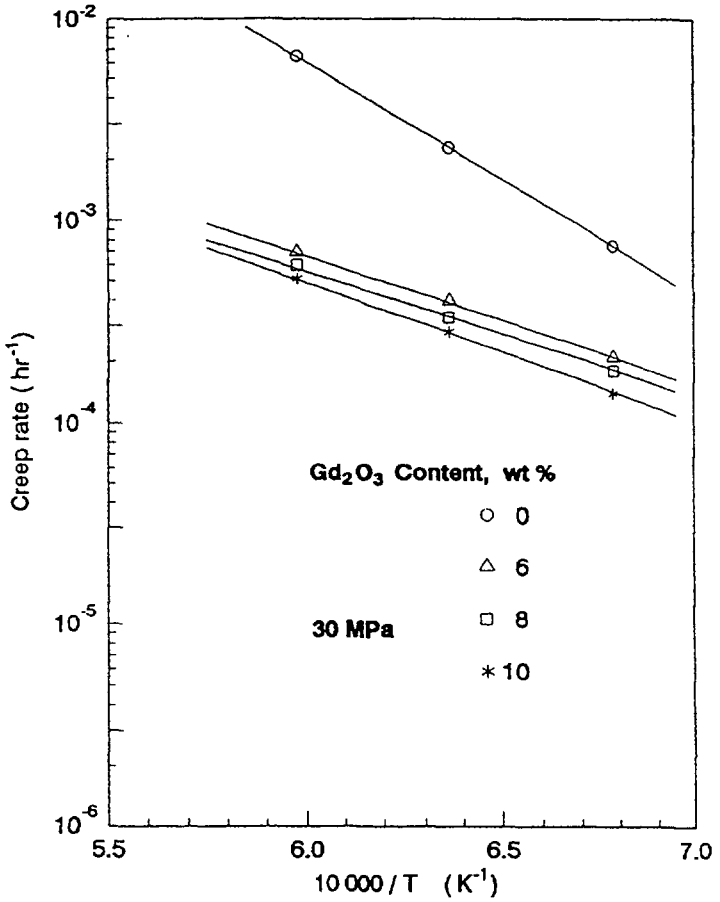

Fig. 2.17. *Temperature dependence of (U, Gd)O_2 sample creep rate [2.45]*

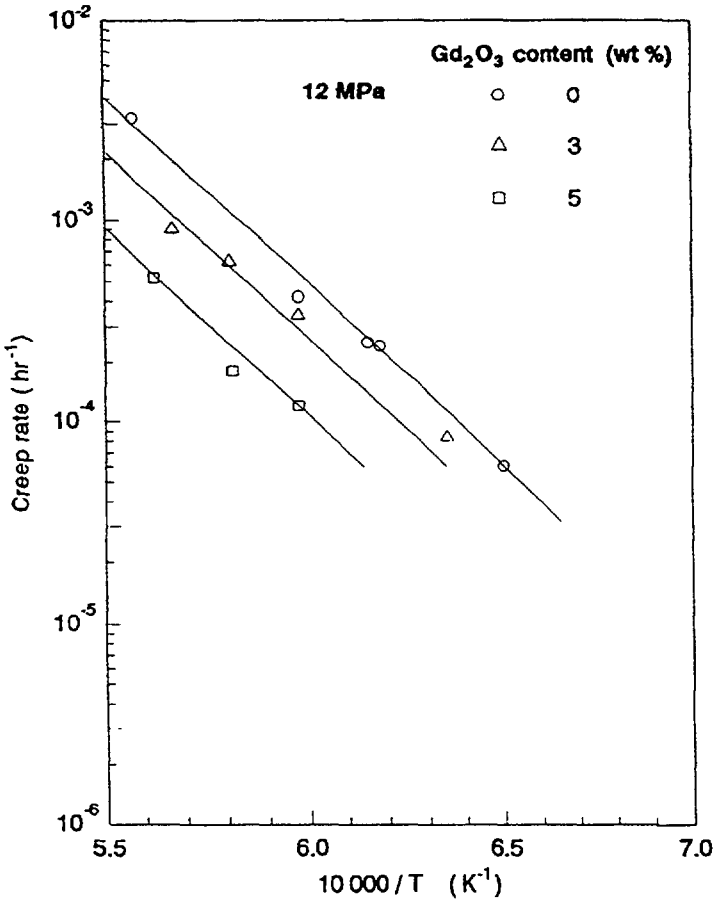

Fig. 2.18. *Temperature dependence of (U, Gd)O_2 pellet creep rate [2.43]*

TABLE 2.9. *THERMAL CROSS SECTIONS OF NEUTRON ABSORPTION, WESTCOTT FACTORS AND RESONANCE INTEGRALS OF GADOLINIUM [2.46]*

Gadolinium isotopes	Content of isotope in natural mixture (%)	Thermal cross section (barn)	Westcott factor	Resonance integral (barn)
Gd (Nat. mixture)	-	48890± 104	0.8467	390± 10
Gd^{152}	0.2	735± 20	0.9784	2020± 160
Gd^{154}	2.1	85± 12	0.9967	230± 26
Gd^{155}	14.8	60900± 500	0.8425	1447± 100
Gd^{156}	20.6	1.5± 1.2	1.0006	104± 15
Gd^{157}	15.7	254000± 815	0.8510	700± 20
Gd^{158}	24.8	2.2± 0.2	1.0009	73± 7
Gd^{160}	21.8	0.77± 0.2	0.9997	7.2± 1

TABLE 2.10. *EXPERIMENTAL VALUES OF SPECTRAL INDICES IN Gd FUEL WITH LATTICE PITCH 15.00 ± 0.03 mm, TRIANGULAR ARRAY AND Gd_2O_3 CONTENT 3.0 w/o [2.47].*

Type of lattice and absorber in central cell	Lu^{176} s-------- Dy^{164}	Pu^{239} s-------- Dy^{164}	U^{235} s-------- Dy^{164}	Pu^{239} s-------- U^{235}	Eu^{151} s-------- Dy^{164}	In^{115} s-------- Dy^{164}	Mn^{55} s-------- Dy^{164}
Regular *	1.597 ±0.026	1.650 ±0.027	1.113 ±0.017	1.483 ±0.023	1.143 ±0.018	5.568 ±0.086	1.363 ±0.022
(U, Gd) O_2 ** Gd / U = 3.0 % O / U = 2.00 ^{235}U = 6.50 %	1.811 ±0.033	2.733 ±0.046	1.368 ±0.023	1.998 ±0.033	1.934 ±6.032	16.67 ±6.268	2.227 ±0.037

* rod is in a central cell

** (U, Gd) O_2 absorber is in a central cell

2.4. NEUTRONIC PROPERTIES

2.4.1. Cross sections

Natural gadolinium has the following isotopes: Gd^{152}, Gd^{154}, Gd^{155}, Gd^{156}, Gd^{157}, Gd^{158} and Gd^{160}. Two of these, Gd^{155} and Gd^{157}, are characterized by large cross sections of neutron absorption in the thermal energy region, which is due to the presence of resonances (Table 2.9).

The energy dependence of the total neutron absorption of natural gadolinium decreases much more rapidly than is suggested by the law 1/v within the neutron energy range 0.08-0.18 eV.

2.4.2. Spectral effects

The spectral indices are functions of many parameters such as lattice pitch, lattice type and gadolinium concentration (Table 2.10).

2.4.3. Self shielding effects

Estimates of the Gd^{155} and Gd^{157} resonance self shielding influence on k_{inf} have been performed using the TVS code (RRC KI, Russian Federation) [2.48]. Calculations have shown that the effect of Gd^{155} and Gd^{157} resonance self shielding is practically negligible at all

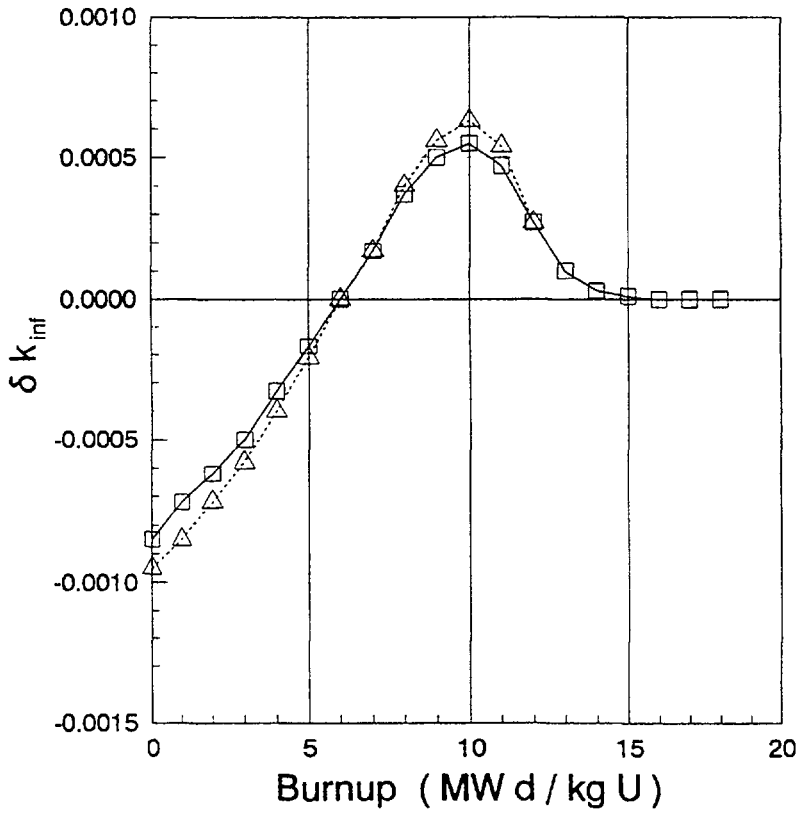

Fig. 2.19. *Influence of Gd^{155}, Gd^{157} resonance self shielding and Gd^{155} resonance integral variations on k_{inf} for a supercell case [2.48].*

□ *without taking into account of self shielding*

TABLE 2.11. BASIC CHARACTERISTICS OF Gd ISOTOPE GENERATION BY U^{235} THERMAL NEUTRON FISSION AND OTHER FISSION PRODUCT DECAY (TOTAL SUM OF FISSION YIELDS 2.0) [2.48]

Isotope Gd	Yields of Gd from		Total Yield	Half-Life of FP	Half-Life of Gd
	Fission Process	Decay of Fiss. Prod.			
155		$3.10\ 10^{-4}$	$3.10\ 10^{-4}$	4.96 a	stable
156		$9.00\ 10^{-5}$	$9.00\ 10^{-5}$	15.20 d	stable
157		$2.76\ 10^{-5}$	$2.76\ 10^{-5}$	15.15 h	stable
158	$2.86\ 10^{-8}$	$2.00\ 10^{-5}$	$2.00\ 10^{-5}$	46.00 m	stable
159	$1.00\ 10^{-7}$	$1.52\ 10^{-8}$	$1.62\ 10^{-8}$	18.70 m	18.56h
160	$1.52\ 10^{-7}$	$9.40\ 10^{-7}$	$1.09\ 10^{-8}$	42.00 s	stable

burnups (Fig. 2.19). This figure also shows the influence of Gd^{155} resonance integral variation on k_{inf}. It is seen that a 3% deviation of the Gd^{155} infinite dilution resonance integral from the nominal value, which characterizes the uncertainty of nuclear data in the resonance energy region, does not markedly influence the results of the calculations.

The neutron absorption cross section is not the only characteristic affecting the Gd depletion rate. The particle sizes in the Gd fuel are also important. Due to a large capture cross section, the Gd burnup in the fuel pellets proceeds from the periphery to the pellet interior, i.e. at the beginning of the fuel cycle, Gd^{155} and Gd^{157} burning in the peripheral layer, shields neutron penetration deeper into the fuel [2.49].

Taking into account the isotopic composition and the presence of isotopes with resonance neutron absorption cross sections, the development and use of spectral codes for calculation of the burnup of odd isotopes and their generation from even isotopes is important. These problems were discussed at length at the conference on "In-Core Fuel Management" in Pinehurst, USA, 1986 [2.50]. Firstly, the fact that the capture of a neutron in the nucleus of either Gd^{154} or Gd^{156} transforms these nuclei into the nuclei of Gd^{155} or Gd^{157} respectively, means that all other gadolinium isotopes (at least the chain from Gd^{154} to Gd^{157}) need to be considered in time dependent problem calculations. Besides this, some gadolinium isotopes can originate directly from the fission process and some can be formed by the decay of other fission products. The basic characteristics (yields, half-lives) of Gd isotope generation by these processes (for U^{235} fission by thermal neutrons), are summarised in Table 2.11 (based on the ENDF/B-IV library).

Comparing the data describing the contributions to gadolinium isotope concentration directly from fission and through the decay of some other fission products the following conclusions are reached:

(i) Gd^{158} and successive heavier isotopes can originate directly from fission of U^{235} but with relatively low yields.

(ii) Gd^{155} and heavier isotopes can be formed by the decay of other fission products.

(iii) The accumulated yield of Gd^{155} is rather high (in relation to the other gadolinium isotopes). However, as Gd^{155} originates from the decay of Eu^{155} with a half-life of nearly 5 years, this contribution to Gd^{155} concentration probably need not be considered in reactor calculations.

(iv) In spite of the facts that, for the other gadolinium isotopes, the contributions from the decay of other fission products are greater than the direct yields from fission, the corresponding half-lives are quite short and the accumulated yields are comparable, only Gd^{157} is normally considered to be formed as a result of the fission process. This is explained through the difference of their thermal cross sections; that of Gd^{157} is several orders of magnitude higher than that of the other isotopes.

It is worth noting that all the Gd isotopes are stable except for Gd^{159}, and that the yield of Gd^{157} given in Table 2.11 due to fission products of the U^{235} fission by thermal neutrons is 6.26E-05, and the yield from the fission of U^{238} is 1.7E-04.

The effect of Gd depletion in the pellets must also be taken into account in the thermal-mechanical calculations of the FRs (see Section 4.2).

REFERENCES TO CHAPTER 2

[2.1] GOLDSCHMIDT, V.M., ULRICH, F., BARTH, T., Geochemical Distribution of the Elements: IV Crystal Structure of Oxides of the Rare Earth Metals, Skrifter Norske Videnskaps - Akad., Oslo, I: Mat. Naturv. Kl., 5, 1925, pp.5-25.

[2.2] SHAFER, M.W., ROY, R., Rare earth polymorphism and phase equilibria in rare earth oxide-water systems", J. Am. Ceram. Soc., 42(11) (1959) 563-570.

[2.3] GUENTERT, O.J., MOZZI, R.L., Monoclinic modification of gadolinia sesquioxide, Acta Cryst., 11(10) (1958) 746.

[2.4] ROTH, R.S., SCHNEIDER, S.J., Phase equilibria in systems involving the rare earth oxides. Part 1. Polymorphism of the oxides of the trivalent rare earth ions, J. Res. Ntl. Bur. Std., 64A(4) (1960) 309-316.

[2.5] BEALS, R.S., HANDWERK, J.H., Solid solutions in the system urania - rare earth oxides: I, UO_2 -$GdO_{1.5}$, J. Am. Ceram. Soc., 48(5) (1965) 271-274.

[2.6] WARSHAW, I., ROY, R., Polymorphism of the rare earth sesquioxides, J. Phys. Chem., 65(11) (1961) 2048-2051.

[2.7] HAGLUND, J.A., HUNTER, O., Elastic properties of polycrystalline monoclinic Gd_2O_3, J. Am. Ceram. Soc., 56(6) (1973) 327-330.

[2.8] DOLE, S.L., HUNTER, O., Elastic properties of some Gd_2O_3-HfO_2 compositions, J. Nucl. Mat., 59(1956) 207-214.

[2.9] Handbook of chemistry physics, 56th Edition, CRC, 1975.

[2.10] Handbook on special refractory elements and compositions, Metallurgia, Moscow (1969).

[2.11] CASE, E., SMYTH, J., HUNTER, O., Microcracking behaviour of monoclinic Gd_2O_3, J. Nucl. Mat., 102 (1981) 132-142.

[2.12] HO, S.M., RADFORD, K.C., Structural chemistry of solid solutions in the UO_2-Gd_2O_3 systems, Nucl. Techn., 73 (1986) 350-360.

[2.13] WADA T., NORO, K., TSUKUI, K., "Behaviour of UO_2 - Gd_2O_3 fuel", Proc. Int. Conf. BNES on Nuclear Fuel Performance, 15-19 Oct. 1973, London, UK, 63.1-63.3.

[2.14] OHMICHI, T. et al., On the relation between lattice parameter and O/M ratio for uranium dioxide-trivalent rare earth oxide solid solution, J. Nucl. Mat., 102 (1981) 40-46.

[2.15] BEALS, R.Y., HANDWERK, J.H., WRONA, B.Y., Behaviour of urania - rare earth oxides at high temperature, J. Am. Ceram. Soc., 52(11) (1969) 578-581.

[2.16] UNE, K., OGUMA, M., Oxygen potentials of $(U,Gd)O_2$ solid solutions in the temperature range 1000-1500°C, J. Nucl. Mat., 115 (1983) 84-90.

[2.17] UNE, K., OGUMA, M., Oxygen potential of $U_{0.96}Gd_{0.04}(UO_2$-3 wt%$Gd_3)$ solid solution", J. Nucl. Mat., 131 (1985) 88-91.

[2.18] BLACKBURN, P.E., J. Nucl. Mat., 46 (1973) 244.

[2.19] The Committee on Analytical Chemistry of Nuclear Fuels and Reactor Materials, Japan Atomic Energy Research Institute, JAERI 4053, 57 (1971).

[2.20] KIHARA, S. et al., Z. Anal. Chem. 303 (1980) 28.

[2.21] FUKUSHIMA et al., The effect of gadolinium content on the thermal conductivity of near-stoichiometric $(U,Gd)O_2$ solid solutions, J. Nucl. Mat., 105 (1982) 201-210.

[2.22] CHOTARD, A. et al., "Out-of-Pile physical properties and In-Pile thermal conductivity of $(U,Gd)O_2$", IWGFPT 26, Vienna (1986) 77-86.

[2.23] NEWMAN, L.W. et al., Burnable Poisons for Extended Burnup Fuel Management - Present and Future, 7-25 to 7-37.

[2.24] THORNTON, T.A. et al., "Thermal conductivity of sintered urania-gadolinia", ANS Winter Meeting, Washington DC, Nov. 14-18, 1982, 348-349.

[2.25] SKOGEN, R.B. KILLGORE, M.R., "Performance of Exxon nuclear gadolinia-bearing fuel in pressurized water reactors", ANS Topical Meeting LWR Fuel Performance, Orlando, Florida, April 21-24 1985, 5-43 to 5-49.

[2.26] MILOVANOV, O.A.,PROSELKOV, V.N. ET AL., Mechanical, physical and thermophysical properties of U-Gd fuel. Preprint RRC KI, Moscow, 1994.

[2.27] INABA, H. et al., Heat capacity measurement of $U_{1-y}Gd_yO_2$ ($0.00<y<0.142$) from 330 to 1500K, J. Nucl. Mat., 149 (1987) 341-348.

[2.28] HIRAI, M., Thermal diffusivity of UO_2-Gd_2O_3 pellets, J. Nucl. Mat., 173 (1990) 247-252.

[2.29] UNE, K., Thermal expansion of UO_2-Gd_2O_3 fuel pellets, J. Nucl. Sci. Tech., 23(11) (1986) 1020-1022.

[2.30] CURTIS, C.E., JOHNSON, J.R., Ceramic properties of samarium oxide and gadolinium oxide: X-ray studies of other rare earth oxides and some compounds, J. Am. Ceram. Soc., 40(1) (1957) 15-19.

[2.31] GROSSMAN, L.N. et al., $(U,Gd)O^2$ phase equilibria at high temperatures, Colloques Int., CNRS 205 (1972) 453.

[2.32] MATSUOKA et al., "Out-of-pile testing on the properties of the high content gadolinia bearing fuel", 1990 Fall Meeting of the Atomic Energy Society of Japan.

[2.33] JAMANOUCHI, S., TACHIBANA, T., Melting temperature of irradiated UO_2 and UO_2-2wt% Gd_2O_3 fuel pellets up to burnup of about 30 GWd/tU, J. Nucl. Sci. and Tech., 25(6) (1988) 528-533.

[2.34] HANSON, L., Use of UO_2-Gd_2O_3 fuel in pressurized water reactors, Technical Research Centre of Finland, Report 630 (1986) p. 39.

[2.35] Presented in part at the Spring Meeting of the Atomic Energy Society of Japan, April 1992. The work was done as a joint venture of 5 utilities (Kansai, Kyushu, Shikoku, Hokkaido and JAPCO) and NFI.

[2.36] KOGAI, T. et al., In-pile and out-of-pile grain growth behaviour of sintered UO_2 and $(U,Gd)O_2$ pellets, J. Nucl. Sci. Techn., 28(6) (1989) 744-751.

[2.37] LITTLECHILD, J.E., BUTLER, G.G., LESTER, G.W. "The production of burnable poison oxide fuel", Proc. Int. Conf. BNES on Nuclear Fuel Performance, 15-19 Oct. 1973, London, UK, 65.1-65.4.

[2.38] LOOSE, A. et al., "Diffusion measurement in UO_2-Gd_2O_3", Proc. IAEA Symp. on Improvements in Water Reactor Fuel Technology and Utilization, 15-19 Sept. 1986, STI/PUB/721 (1987) 578-584.

[2.39] YUDA, R., et al., "UO_2-Gd_2O_3" Solid State Reacton", Fall Meeting of the Japan Atomic Energy Society, Oct. 1991, L47, 733

[2.40] ARAI, Y. et al., Electrical conductivity of near-stoichiometric $(U,Gd)O_2$ solid solutions, J. Nucl. Mat., 150 (1987) 233-237.

[2.41] HIRAI, M. et al., "Young's modulus of Gd_2O_3 - UO_2, Nb_2O_5 - UO_2 and TiO_2 - UO_2 pellets", Fall Meeting of Japan Atomic Energy Society, Oct. 1991, F58, p20

[2.42] PEEHS, M., Zur Warmeleitfahigkeit und Plastizitat von UO_2 mit Gd-Zusatsen, J. Nucl. Mat., 106 (1982) 221-230

[2.43] HIRAI, M. et al., "Creep Property of UO_2-Gd_2O_3 pellet", Annual Meeting of Japan Atomic Energy Society, Apr. 1988, L34, p262

[2.44] WATARUMI, K., et al., "Thermal properties of Gd_2O_3 doped UO_2 pellet (I)", Fall Meeting of Japan Atomic Energy Society, Oct. 1988, G36, p36

[2.45] GODIN, J.G., et al., "Mechanical properties of Uranium-Gadolinium pellets", International Conference on Atomic Power in Space Podolsk, Russian Federation, 21-23 October 1993, p.19

[2.46] MUGHABHAB, S.F., Neutron Cross Sections, v.1, part 8, New York - London, Academic Press (1984).

[2.47] POLJAKOV, A.A. et al., "Investigation of neutronic parameters of uranium-water lattice with Gd absorber" in Modelling and investigation of neutronic processes in nuclear power reactors, Moscow, Energoatomizdat, 118-121.

[2.48] PSHENIN, V. et al., "Comparison of calculations for WWER-1000 lattice containing BA rods with gadolinium", USSR contribution to the IAEA CRP on Safe Core Management with Burnable Absorbers in WWERs (1990)

[2.49] HARTLEY, K., et al., Trans. ANS, 44 (1983) 526-527.

[2.50] ANS Conference on "In-Core Fuel Management", Pinehurst, North Carolina, USA, 1986.

3. FUEL MANUFACTURING

3.1. FABRICATION PROCESSES

Fabrication can be done mainly by two different methods:

(i) mixing of Gd and U oxides at a molecular level

(ii) mixing of Gd and U oxides as fine powders.

The former is achieved by the sol-gel and coprecipitation processes [3.1-3.13] while the latter is achieved by dry blending [3.14-3.21].

3.1.1. Sol-gel and coprecipitation

In the early stages of development a method of sintered UO_2 pellet impregnated with gadolinium nitrate solution and subsequent reduction to oxides was tested. However, using this method it was difficult to obtain high (>0.5%) concentrations of Gd_2O_3 in UO_2, and to ensure uniform Gd distribution in the pellet volume.

About three decades ago the sol-gel method was introduced. In this method uranium and gadolinium nitrate solution is gelled in ammonia. This provides a homogeneous mixture of uranium and gadolinium. The structure of pellets obtained by this method is a solid solution and the grain size is determined by the regime of high temperature treatment. The flow sheet of fuel production is given in Fig. 3.1.

There are two routes for the sol-gel process. One is internal and the other is external gelation. In both cases gadolinium nitrate, $Gd(NO_3)_3$, and uranyl nitrate $UO_2(NO_3)_2$, are dissolved in water to achieve the correct gadolinium oxide (Gd_2O_3) to uranium dioxide (UO_2) ratio. The Gd_2O_3 content should not exceed 10% in the product otherwise new phase formation can take place.

Powder preparation

For the internal gelation route, hexamethylene tetramine (hexa, $C_4N_4H_{12}$) is added at a temperature below 10°C. The solution is forced by an inert gas through a nozzle into hot silicon oil at around 90°C. Hexa decomposes at this temperature and gives off ammonia (NH_3) which gelates the purged solution droplets within seconds. The gelled microspheres are washed first with carbon tetrachloride to remove the silicon oil and then with ammonia solution.

For the external gelation route, urea and ammonium nitrate are added to the nitrate solution mixture of uranium and gadolinium. Urea makes a complex with uranyl ions (UO_2^{+2}), and ammonium nitrate provides stability. To improve the physical properties of the fuel, titanium trichloride ($TiCl_3$) can be added to yield about 0.1% titanium dioxide (TiO_2) in the sintered fuel.

Sintering behaviour

Sintering is carried out under a "nitrogen + hydrogen", or "argon +hydrogen" atmosphere at 1600 to 1700°C for 3 hrs. Densification is improved by sintering under a wet atmosphere.

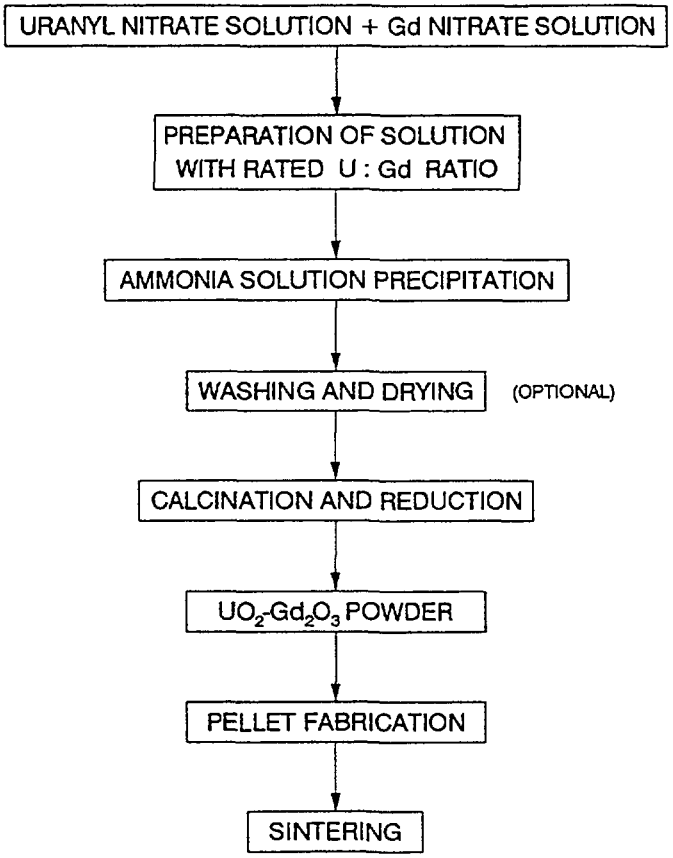

Fig. 3.1. *Example flow-sheet of Gd pellet preparation by the sol-gel technique*

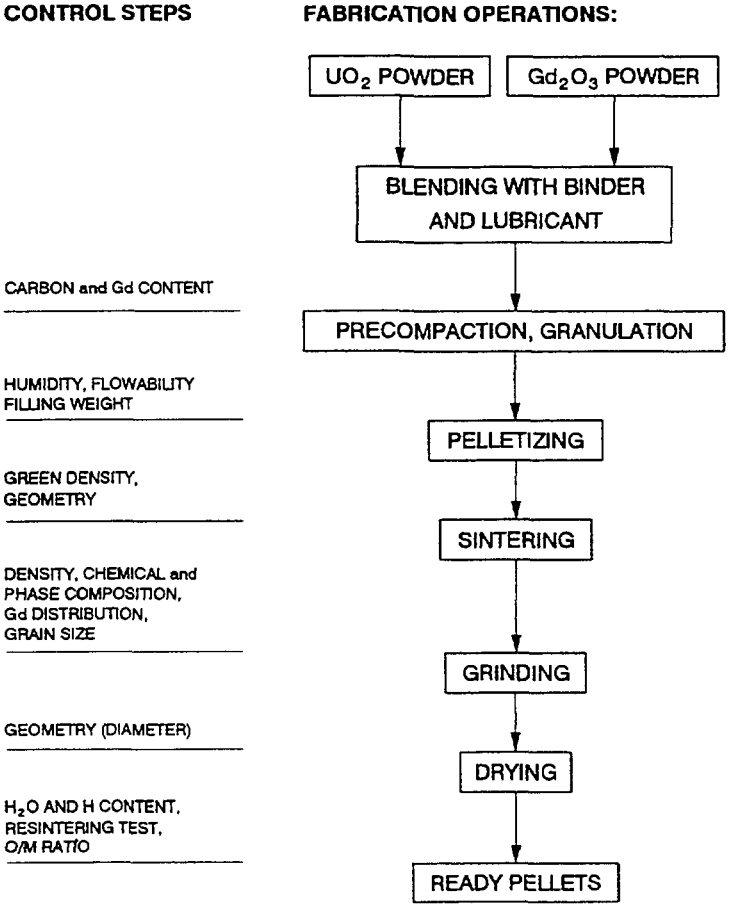

Fig. 3.2. *Example flow-sheet of QC and Gd fuel preparation by dry blending*

Resulting product

Uranium dioxide, gadolinium oxide and titanium dioxide all form a homogeneous phase upon sintering. The presence of gadolinium oxide tends to increase the porosity and the lattice parameter. The presence of titanium dioxide tends to decrease both of them.

The sol-gel method is not used in industrial production because of the large amounts of liquid wastes.

3.1.2. Dispersion of gadolinium oxide in uranium dioxide matrix by dry blending

Dry mixing of UO_2 and Gd_2O_3 powders mechanically is a much simpler process and is therefore used industrially in all plants. The flow sheet of fuel production is given in Fig. 3.2.

Powder preparation

Uranium dioxide powder is prepared from reduction of either ammonium diuranate or ammonium uranyl carbonate (wet routes) or by a dry route, e.g.Integrated Dry Route (IDR). The physical morphology of dry route UO_2 powder is very beneficial to the manufacture of non-segregating blends containing gadolinia powder. The powder has a very low pour density of about 0.7 g/cm^3 and consists of an open structure of interlocking platelet type crystallites which prevent segregation of the mixture with gadolinia.

Blending can be achieved by means of local high shear mixing using an orbital screw blender. Batches up to a few tonnes can be fully homogenised with no segregation on discharge. For laboratory work on the 1 kg scale, the two powders may be physically stirred together and passed through a 100 micron sieve three or four times to ensure homogenisation.

The addition of TiO_2 or aluminium oxide (Al_2O_3) in small quantities improves the density, grain size and thermal conductivity of the final product. Stearic acid or zinc stearate is usually added as a lubricant.

Granulation is performed first by isostatic compression followed by crushing and sieving. A granulate size of less than 1 mm is produced. The granulate is lubricated with additional zinc stearate and pellets are produced by uniaxial compression. The green density is about 50% of theoretical density.

Sintering behaviour

A two-step sintering process, first in an oxidizing atmosphere at 1100 °C and then in a reducing atmosphere at 1700°C, leads to the best interdiffusion of Gd and U oxides. This however cannot be achieved in a continuous type furnace as used in an industrial fabrication plant. To achieve the same result, sintering is performed in a humidified hydrogen atmosphere at 1700°C for 3-4 hrs producing a slightly oxidizing atmosphere to enhance grain growth and to achieve good interdiffusion of the Gd and U oxides.

Resulting product

The addition of gadolinium oxide retards sintering and imparts a higher porosity. The O/U ratio also increases with Gd_2O_3 content. The sintering conditions, like temperature, duration and nature of atmosphere, all affect the physical and mechanical properties of the product. At 4, 8 and 12 w/o Gd_2O_3 contents, the O/U ratio is 2.03,

2.06, and 2.09, and the O/M ratio is 2.00, 2.00, and 1.99 respectively. The density achieved is 94.5 - 95% of theoretical density.

By slightly changing the technological regimes, it is possible to obtain a dispersion type structure in which Gd rich regions with a fine-grain solid solution of high Gd_2O_3 content (4.5 - 25 w/o) are dispersed in a matrix of reduced Gd_2O_3 content and normal grain size (7 - 13 μm). Studies of the thermal-physical properties have shown that pellets with such dispersed-type structure possess higher thermal conductivity.

When using IDR powder with a pore former, the pore size distribution is binomial with 1 μm and 13 μm sizes. Resintering at 1700°C for 24 hrs increases the density by 0.6%. The ratio of open to closed porosity is affected to a large extent by the sintering atmosphere.

3.1.3. Dispersion of gadolinium oxide microspheres in a UO_2 matrix

Another method of introducing Gd_2O_3 into UO_2 is to prepare Gd_2O_3 microspheres of about 100 μm by the sol-gel technique and disperse them in a UO_2 matrix. The fuel thus obtained contains separate Gd_2O_3 and UO_2 zones. This fuel is appealing because the matrix is pure UO_2, so the melting point and the thermal conductivity are not significantly changed. Moreover, since the gadolinia microspheres have well defined shapes, neutronic calculations are more precise. However, it is almost impossible to achieve a homogeneous distribution of Gd_2O_3 microsphere in a UO_2 matrix, which is undesirable, and, with the additional calculational complications, this method is not used on an industrial scale.

3.2. QUALITY CONTROL

The IAEA has recently published a "Guidebook on QC of MOX and Gd bearing fuels" [3.22], with the contribution of BELGONUCLEAIRE, FRAGEMA, PNC and SIEMENS/KWU. Since it still represents the best material on the subject, excerpts of it will be utilized hereafter.

3.2.1. Specifications

The main problems in Gd fuel manufacture and assembly fabrication are to prevent mixing of pellets and mixing of rods and to ensure that rod locations in the fuel assemblies are correct. Specific Quality Assurance measures, including specific inspection methods and techniques, are established to control this. Otherwise the specification is basically the same as for standard U fuel with some Gd-specific extensions which will be outlined below.

3.2.1.1. Gadolinium oxide

Typical specifications imposed by the manufacturer are [3.22].

- Loss of weight on ignition: less than 1.2 w/o

- Impurities (max ppm related to Gd):

B:	6 ppm	F:	40 ppm
Cs:	1000 ppm	Fe:	300 ppm
Ca:	400 ppm	N:	600 ppm
Cd:	12 ppm	Ni:	200 ppm
Cl:	40 ppm	Si:	300 ppm

other rare earths (Dy, Eu, Sm, Tb, Yb): 300 ppm

TABLE 3.1. *EXAMPLES OF Gd INFLUENCED REQUIREMENTS TO BE INCORPORATED IN THE SPECIFICATION*

	Oxygen-to-uranium ratio:		***Ref.***
either	$O/U = (2.000 + 0.008 \times \% Gd_2O_3) + 0.015$	*up to 12 w/o* Gd_2O_3	[3.22]
or	$O/(U + Gd) = 2.00 + 0.02$		[3.22]
or	$O/U = 2.020 + 0.045$	*for 5 w/o* Gd_2O_3	[3.23]

	Density		***Ref.***
either	$\rho = \rho_o - 0.04 \% Gd_2O_3 \, {}^{+0.15}_{-0.20}$ (g/cm³)	*up to 12 w/o* Gd_2O_3	[3.22]
	where ρ *is the specified density of the gadolinia-doped* UO_2 ρ_o *is the theoretical density of pure* UO_2		
or	$\frac{\rho}{\rho_{th}} = 95 \, {}^{+1.0\,\%}_{-1.5\,\%}$		[3.22]
	where $\rho_{th} = \frac{100}{\frac{\% Gd_2O_3}{\rho_{th} Gd_2O_3} + \frac{\% UO_2}{\rho_{th} UO_2}}$		
or	$\rho = 10.25 - 10.55$ (g/m³)	*for 5 w/o* Gd_2O_3	[3.23]

Table 3.1. *(CONT.)*

Gd Distribution	***Ref.***
- relative areas (on optical micrograph):	
either high Gd_2O_3 content < 15 w/o	[3.22]
pure UO_2 < 40 %	[3.22, 3.23, 3.24, 3.25]
UO_2 - Gd_2O_3 mixed oxide solid solution 60 - 94 %	[3.22, 3.23, 3.25, 3.26]
or Gd_2O_3 - rich particles with d > 10 μm shall contain less than 2.5 % of the Gd_2O_3 mass	[3.22]
or Gd_2O_3 - rich agglomerates 40 - 100 μm shall be less than 2 % of the area	[3.23]
- local concentrations:	
average size of Gd_2O_3 - rich agglomerates < 10 to 200 μm (to be defined in the specification)	[3.22, 3.23, 3.25, 3.26]
maximum size of Gd_2O_3 rich zone < 15 μm	[3.24]
average size of UO_2 rich zones < 30 to 1000 μm (to be defined in the specification)	[3.22, 3.23, 3.24, 3.25]
Gd_2O_3 - rich zone volume fraction < 6 to 15 %	[3.24, 3.26]

- Gd 155: 14.9 ± 0.6 w/o

  Gd 157: 15.7 ± 0.6 w/o

- Particle size: 95 w/o below 10 μm

  99 w/o below 20 μm

3.2.1.2. Pellets

Over and above the requirements for UO_2 pellets, some Gd-specific requirements have also to be met and controlled: e.g. O/U ratio depends on the Gd_2O_3 content. The definition of the UO_2 equivalent pellet density has to be related to the theoretical density and the allowable range of distribution of oxide phases (UO_2, Gd_2O_3 and U-Gd-O solid solution) must also be specified, as illustrated in Table 3.1.

3.2.1.3. Fuel rods

The additional controls specified are to ensure that no mixing of pellets or confusion of length and position of different zones of the pellet stack occurs.

3.2.1.4. Fuel assemblies

The only difference from U FAs is encountered at the final stage of manufacturing, and quality control when it is necessary to ensure proper positioning of the BAF fuel rods.

Two types of verification are usually performed. One is through the traceability system, the other is through the permanent marking of the FRs. Since both are very simple and fast, one is performed just after insertion of the fuel rods in the loading magazine and the second after loading the fuel assembly just before securing the nozzles.

3.2.2. Control techniques

The control techniques common to U fuel will not be described here. The following are those specific to Gd fuel:

3.2.2.1. Pellets

The Gd distribution is determined by ceramography with adequate colour etching and measured by optical control or image analysis.

The Gd_2O_3 content is analysed by mass spectrometry, gamma spectrometry or X-ray fluorescence.

3.2.2.2. Fuel rods

The correct positioning of the Gd pellets within the pellet stack and the absence of rogue U pellets therein are controlled by:

- activated gamma radiography of the U pellets
- high field magnetometry of Gd pellets
- low field magnetic examination

- visual (or image analysis) examination of the pellet stack, if the different pellet types have specific characteristics (e.g. length)

- a combination of the above.

3.2.2.3. Fuel assemblies

The first verification is performed by bar code or other marking identification (preferably automatic) relative to the position in the magazine (usually computer recorded).

The final verification, after loading of the fuel assembly, is performed either by a template or by camera recording to cross-check the position of the Gd fuel rods in the fuel assembly.

REFERENCES TO CHAPTER 3

[3.1] FERGUSON, D.E., DEAN, O.C. HASS, P.A., CEND-153 (vol. 1) pp. 23-38, 1961.

[3.2] FERGUSON, D.E., Progress in Nuclear Energy, Series III, Vol. 4, Process. Chemistry, pp. 37-78, 1970.

[3.3] HAAS, P.A., KITTS, F.G., BEUTLER, H., Chemical Engineering Progress Symposium Series. Nuclear Engineering-Part XVIII. No. 80, Vol. 63, pp. 16-27.

[3.4] FERGUSON, D.E., DEAN, O.C., DOUGLAS, D.A., Third Conference on Peaceful Uses of Atomic Energy, P/237, USA, pp. 307-313, 1964.

[3.5] HAAS, P.A., CLINTON, S.D., KLEINSTEUBER, I and EC. Prod. Res. Dev. 5(3), pp. 236-244, 1964.

[3.6] HAAS, P.A., CLINTON, S.D., KLEINSTEUBER, Can. J. Eng., Dec., pp. 348-353, 1966.

[3.7] ZIMMER, E., NAEFE, P., RINGEL, H., Trans. Am. Nucl. Soc., Vol. 20, pp. 591-593, 1975.

[3.8] ZIMMER, E., RINGEL, H.D., Nucl. Tech. 45(1979) 287-298.

[3.9] ZIMMER, E., NAEFE, P., Nucl. Tech., 42(1979) 163-171.

[3.10] YAMAGISHI, S., YOSHIHISA, T., J. Nucl., Sci., 22(1985) 995-1000.

[3.11] MATHEWS, R.B., HAT P.E., J. Nucl. Mater., 92(1980) 207-216.

[3.12] GÜNDÜZ, G., ÖNAL, I., DURMAZUCAR, H.H. J. Nucl. Mater., 178(1991) 212-216

[3.13] GANGULY, C., BASAK, U., J. Nucl. Mater., 178(1991) 179-183.

[3.14] LITTLECHILD, J.E., BUTLER, G.G., LESTER, G.W., Proc. Int. Conf. on Nuclear Fuel Performance, London (BNES, 1973) paper 65.

[3.15] DAVIS, H.H., POTTER, R.A., Mater. Sci. Res. 11(1978) 515.

[3.16] MANZEL, R., DOERR, W.O., Am. ceram. Soc. Bull. 59(1980) 601.

[3.17] UNE, K., OGUMA, M., J. Nucl. Mater., 131(1985) 88.

[3.18] HO, S.M., PADFORT, K.C., Nucl. Technol. 73(1986) 350.

[3.19] UNE, K., J. Nucl. Mater., 158(1988) 210.

[3.20] YUDA, R., UNE, K., J. Nucl. Mater., 178(1991) 195.

[3.21] RIELLA, H.G., DURAZZO, M., HIRATA, M., NUGUEIRA, R.A., J. Nucl. Mater., 178(1991) 204.

[3.22] IAEA-TECDOC-584, Guidebook on QC of MOX and Gd Bearing Fuels, International Atomic Energy Agency, February 1991.

[3.23] GODIN, J.G., et al., "Mechanical properties of Uranium-Gadolinium pellets", International Conference on Atomic Power in Space, Podolsk, Russian Federation, 21-23 October 1993, p.19

[3.24] NEWMAN, L., Thermal and Physical Properties of Urania-Gadolinia, Babcock & Wilcox Utility Power Generation, Rep. RAW-1759 (1984).

[3.25] ASSMANN, H., PEEHS, M., ROEPENACK, H., J. Nucl. Mater., 153 (1988) 115.

[3.26] HAELDAHL, L., ERIKSON, S., J. Nucl. Mater., 153 (1988) 66.

4. DESIGN AND MODELLING CONSIDERATIONS

4.1. PRINCIPLES OF GADOLINIA FUEL ROD, ASSEMBLY AND REACTOR CORE DESIGN

4.1.1. General considerations

The purpose of Section 4.1.2. - 4.1.4. is to describe the factors influencing the choice of Gd fuel design as seen by a number of different countries, and the reasons for their eventual decisions.

The design of a first core or reload with Gd fuel requires consideration of a number of parameters:

a. Distribution of the gadolinia in the pellet (large or small grain size, annular or solid pellet)
b. Gadolinia content (weight percent)
c. U-235 enrichment of UO_2-Gd_2O_3
d. Axial grading of gadolinia in the rod
e. Number of Gd FRs in the assembly
f. Location of Gd FRs in the assembly
g. Number of FAs in the core
h. Location of fresh FAs in the core (loading pattern)

Points b, e, g, h are linked to the loading pattern and are optimized during a reload safety analysis with the constant aim of maximizing core operating margins (DNB, LOCA, etc.). Points a, c, d, f are specific to a particular burnable absorber design.

4.1.2. BWR fuel design

Several companies in the world supply Gd fuel for BWRs including Siemens/ KWU in Germany, GE and SPC in the USA, ABB in Sweden and Hitachi, Toshiba and NFI in Japan. Design features of Gd fuel produced in Japan are taken from the Japanese contribution to the BAF CRP and those of GE and ABB from open literature.

Gd fuel has been used in Japanese BWRs from the early 1970s with the adoption of an advanced 7 × 7 type fuel. Since that time, the fuel design has been changed several times in order to increase reliability as well as to adapt to changes in reactor design and operation methods. Gd has been used continously in spite of the design changes - see Table III.1 (App. III).

Since the early 1980s Axially Zoned Reactivity Fuel (AZR fuel) has been used [4.1]. In this type of fuel assembly, the U-235 enrichment and Gd_2O_3 content are divided axially into two parts (Fig. 4.1). In the upper part, the enrichment is 0.2-0.5% higher and Gd content is lower than in the lower part. The number of Gd-bearing rods is not indicated in Fig. 4.1, but with regard to the data given in Tables III.7 and III.8 (App. III) the average number of Gd-bearing rods for one FA for an 8 x 8 design is equal to ~ 5-6 for Hitachi fuel and ~ 7 for NFI fuel. The AZR fuel itself is able to reduce the axial peaking factor by flattening the axial power distribution. Reactor operation and PCIOMR has consequently improved.

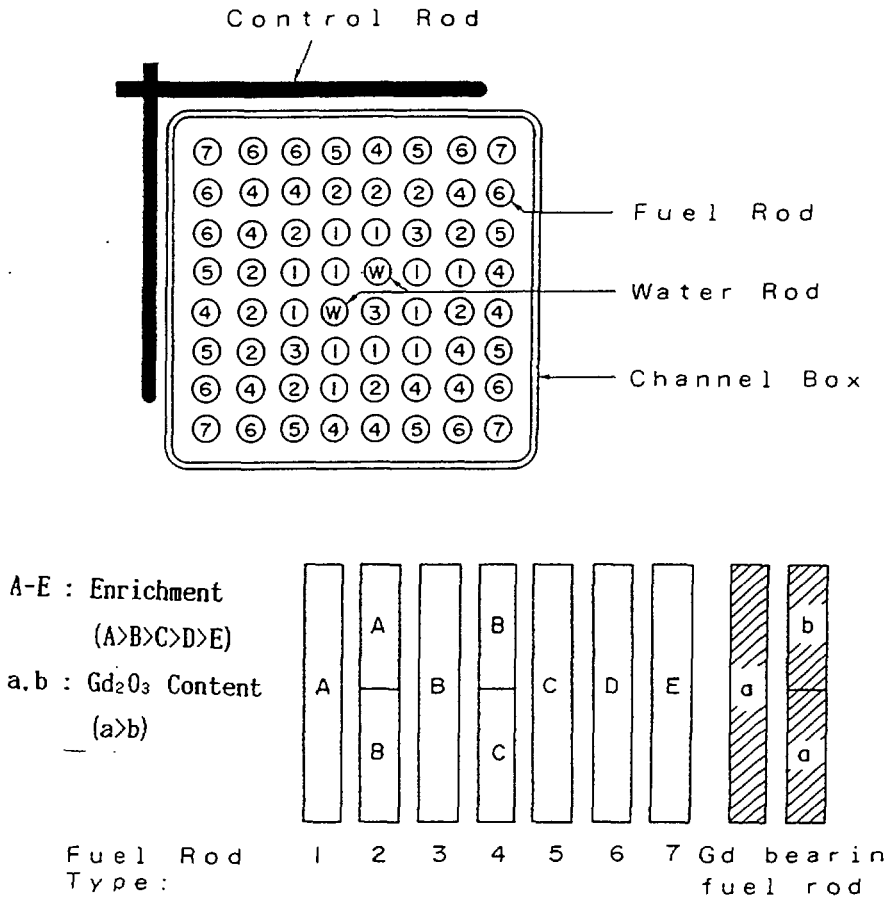

Fig. 4.1. *Typical enrichment and Gd_2O_3 content distribution in a BWR FA (number and position of Gd rods are not indicated)*

Since 1988, zirconium lined Zr-2 cladding tubes have been used and in 1992 a new 8 × 8 - 4 fuel design was adopted as a high burnup fuel. Design parameters of the typical latest Japanese BWR fuel design are shown in Table 4.1. The fuel structure is shown in Fig. III.1 and Fig. III.2 (App. III).

Typical Siemens/KWU FA BWR designs are shown in Fig.4.2.

4.1.3. PWR fuel design

4.1.3.1. Fuel assembly design

France

Until now, the required maximum Gd_2O_3 concentration was 8 w/o Gd for 17 × 17 FAs in 900 MWe PWR plants, due to utility requirements (fuel management schemes and cycle lengths lower than 18 months). It will also be 8 w/o for the future 1300 MWe PWR new strategy (with an increased cycle length).

Concerning the location of the Gd FRs, FRAGEMA proposes two positionings (Fig. 4.3):

- inside the FA
- in the peripheral row of the FA.

TABLE 4.1. LATEST BWR FUEL DESIGN (8 × 8 HIGH BURNUP)

Item	Sub Item	Unit	Parameter
Fuel pellet	Diameter	cm	1.04
	Height	cm	1.0
	Density	%TD	97
	Material		UO_2, UO_2-Gd_2O_3
	Gd_2O_3 content	w/o	6 or less
Cladding	Outer diameter	cm	1.23
	Thickness (total/liner)	mm	0.86/0.1
	Material		Zr lined Zr-2
Fuel rod	Fuel effective length	m	3.71
	Pellet clad gap	mm	0.20
	(Plenum volume/fuel volume) ratio	-	0.1
	Initial He pressure	bar	5
Fuel assembly	Total length	m	4.47
	Fuel rod pitch	cm	1.63
	Rod/rod gap	cm	0.40
	Outer diameter of water rod	cm	3.40
	Number of fuel rods		60
	Number of water rods		1
Burnup	Region average	MWd/t	39 500
	FA	MWd/t	50 000
Max. LHGR		kW/sec	44.0
Max. fuel temperature	UO_2	°C	1 590
	UO_2-4.5wt%Gd_2O_3	°C	1 740
Max. clad temperature	Outer surface	°C	310

The choice depends on the use of the gadolinia rods in the core (boron concentration decrease, power distribution control during the cycle).

With peripheral positioning, the gadolinia efficiency is reduced at beginning of life. However, there is a better distribution of gadolinia effects over the whole core (fresh gadolinia fuel assemblies and surrounding assemblies). So the power peaking factor is decreased at end of cycle (Fig. 4.4), the most critical moment for Fxy control in loading patterns with gadolinia.

The peripheral positioning is chosen in Sweden (annual cycles require gadolinia for power distribution control). The mid-assembly location is chosen in France (longer cycles require gadolinia for boron concentration reduction).

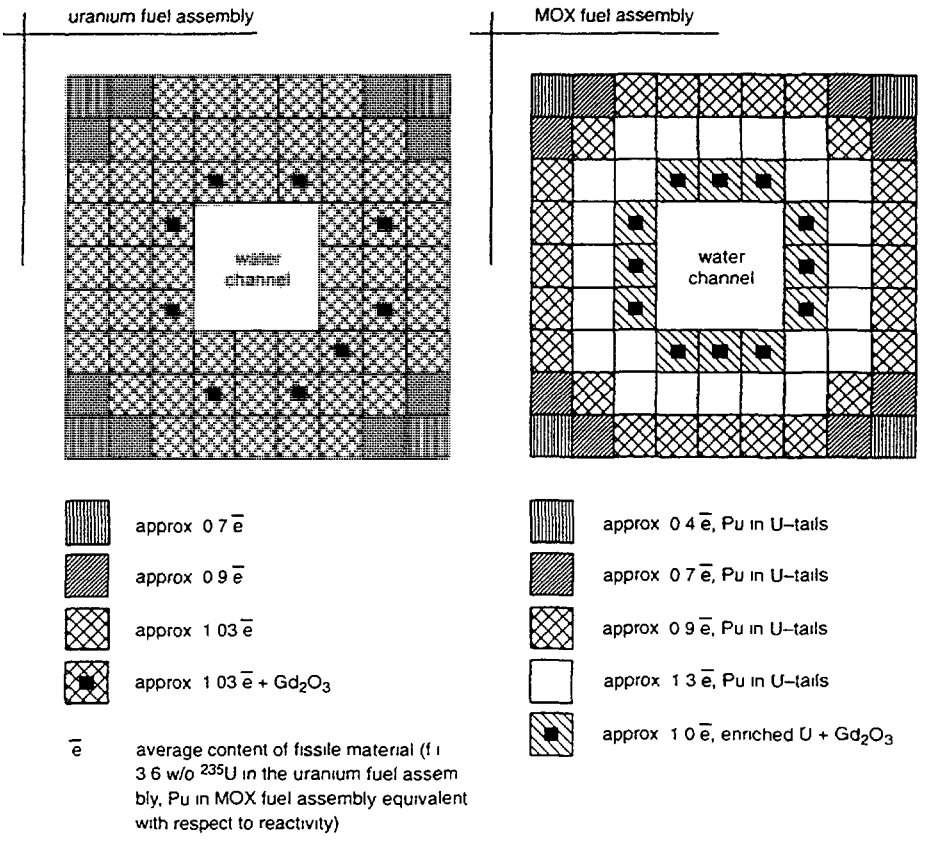

Fig. 4.2. *Typical distribution of fissile material and Gd_2O_3 in ATRIUM™ 9 fuel assemblies for symmetric BWR lattices*

The U^{235} matrix of a UO_2-Gd_2O_3 pellet is mostly depleted uranium. Power peaking is hardly dependent on the U^{235} enrichment of the matrix and, from an economic standpoint, a depleted uranium matrix is little different from an enriched matrix when the number of fresh gadolinia bearing rods per cycle is relatively low.

Axial gadolinia concentration grading is not necessary from a hot spot control point of view , but the use of axially truncated Gd FRs allows a better utilization of gadolinia (lower residual penalty).

In summary, the main features of FRAGEMA's Gd FA (Gd positioning, enriched matrix) are determined on the basis of the fuel management characteristics and its associated gadolinia use.

The Gd FR is usually homogeneous but FRAGEMA has also already designed assemblies with axially truncated Gd FRs.

Japan

Design studies showed that 6 w/o Gd in UO_2 was the optimum in terms of reactivity control capability at the begining of cycle, peaking factors and residual penalties. This was confirmed from usage experience. Therefore, only one content of Gd_2O_3 (6 w/o) is used in Japanese PWRs.

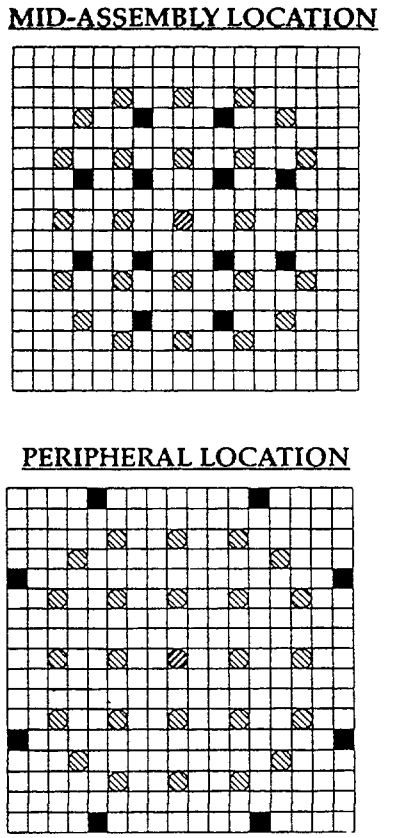

Fig. 4.3. *Positioning of Gd FRs in a FA*

Melting temperature and thermal conductivity of UO_2-Gd_2O_3 both decrease with increasing Gd_2O_3 content. The local power peaking factor (F_q) of a Gd FR therefore must be less than 60-70% of the design F_q of a standard FR. The F_q limitation is achieved by limiting the radial power peaking factor of a Gd rod to less than 80% of the assembly average at the time when the Gd poison disappears. The F_q limitation is determined by evaluating the effect of the melting point reduction (70°C for 6 w/o Gd_2O_3), the thermal conductivity reduction and the required safety margin. In order to satisfy these requirements, the uranium enrichment is reduced by 1.5 w/o for a 6 w/o Gd FR. Recently, out-of-pile experiments and PIE results demonstrated that safety margins are sufficient. Fig. 4.5 shows k_{INF} vs. burnup for 17 x 17 fuel. The k_{INF} of Gd fuel is 1 ~ 2% lower than that of standard fuel when the Gd poison disappears because of the low U^{235} enrichment and residual Gd poisoning. The U^{235} enrichment of standard fuel is designed to be 4.1 w/o for 13 EFPM, 2.5 ~ 3 reload batches, to account for the low k_{inf} of the Gd fuel assembly.

The design parameters for three types of fuels - 14 × 14, 15 × 15, 17 × 17 - are shown in Table 4.2. Basically the fuel design depends on the fuel vendor and consequently there are two types of design for each fuel type as indicated in Table 4.2 and in Fig. III.3 (App. III). Fig. 4.6 shows Gd FR arrays commonly used by fuel vendors in Japan.

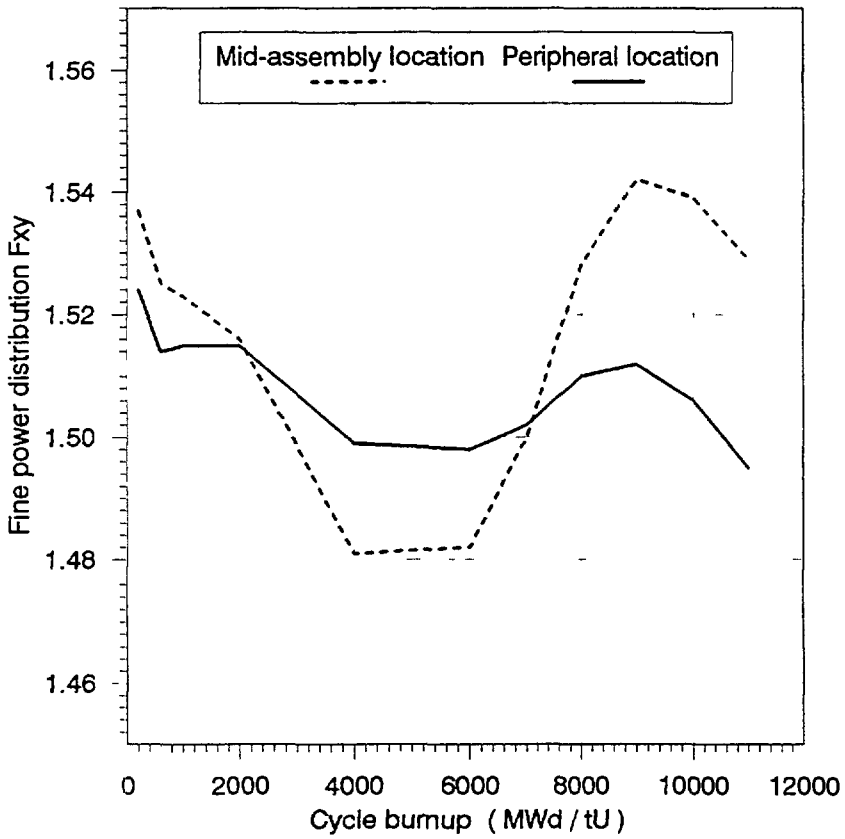

Fig. 4.4. *Comparison between peripheral and mid-assembly locations: Fine power distribution (Fxy)*

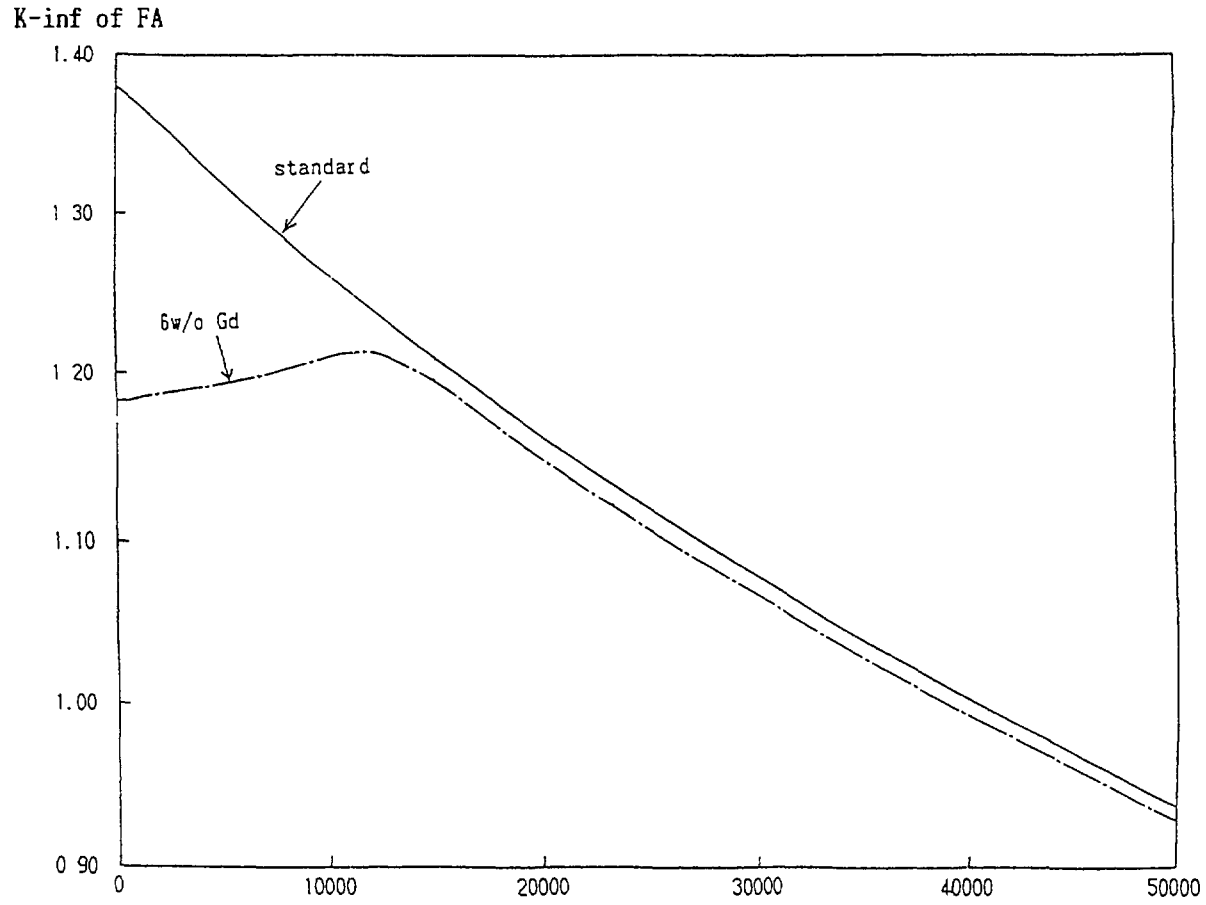

Fig. 4.5. *K-inf vs burnup (17x17, 4.1 w/o)*

TABLE 4.2 JAPANESE PWR FUEL DESIGN

Item	Type			14 x 14	15 x 15	17 x 17
Fuel pellet	Material			UO_2/UO_2-Gd_2O_3	UO_2/UO_2-Gd_2O_3	UO_2/UO_2-Gd_2O_3
	^{235}U enrichment	UO_2 fuel	w/o	4.1-3.4	4.0-3.4	4.1-3.6
		UO_2-Gd_2O_3 fuel	w/o	2.6-1.9	2.5-1.9	2.6-2.1
	Gd_2O_3 content		w/o	6	6	6
	Density		%TD	95	95	95
	Diameter		mm	9.29 or 9.21*	9.29 or 9.21*	8.19 or 8.05*
	Height		mm	11.2 or 10.0*	11.2 or 10.0*	10.0 or 9.0*
Burnup	Region average		MWd/t U	41 000-30 000	43 000-32 000	40 000-33 000
	Maximum FA		MWd/t U	48 000	48 000	48 000
	Maximum pellet		MWd/t U	62 000	62 000	62 000
Max. fuel temp.	at rated power	U fuel	°C	2 000	1 870	1 770
		Gd fuel	°C	1 980	1 840	1 730
	Transient	U fuel	°C	2 350	2 270	2 270
		Gd fuel	°C	2 170	2 170	1 990
Cladding	Material			Zr-4	Zr-4	Zr-4
	Outer diameter		mm	10.72	10.72	9.50
	Thickness		mm	0.62 or 0.66*	0.62 or 0.66*	0.57 or 0.64*
	Pellet cladding gap		mm	0.19	0.19	0.17
	Max. surface temperature		°C	350	350	350

* Two Designs are in use (See Fig. III.3, App.III)

TABLE 4.2 (CONT.)

Item			14 x 14	15 x 15	17 x 17
Fuel assembly	Number of fuel rods		179	204	264
	Fuel rod length	m	3.86	3.86	3.9
	Fuel rod pitch	mm	14.1	14.3	12.6
	Length	m	4.06	4.06	4.1
	Size	mm	200 x 200	214 x 214	214 x 214
	Number of grid spacers		7 or 8	7	9
	Material of grid spacer		Ni-Cr-Fe alloy	Ni-Cr-Fe alloy	Ni-Cr-Fe alloy
	Number of RCCA guide thimble tubes		16	20	24
	Outer diam. of RCCA guide thimble tube	mm	13.69	13.87	12.2
	Thickness of RCCA guide thimble tube	mm	0.43	0.43	0.41
	Material of RCCA guide thimble tube		Zr-4	Zr-4	Zr-4
	Number of instrumentation tubes		1	1	1
	Outer diam. of instrumentation tube	mm	10.72	13.87	12.2
	Material of instrumentation tube		Zr-4	Zr-4	Zr-4

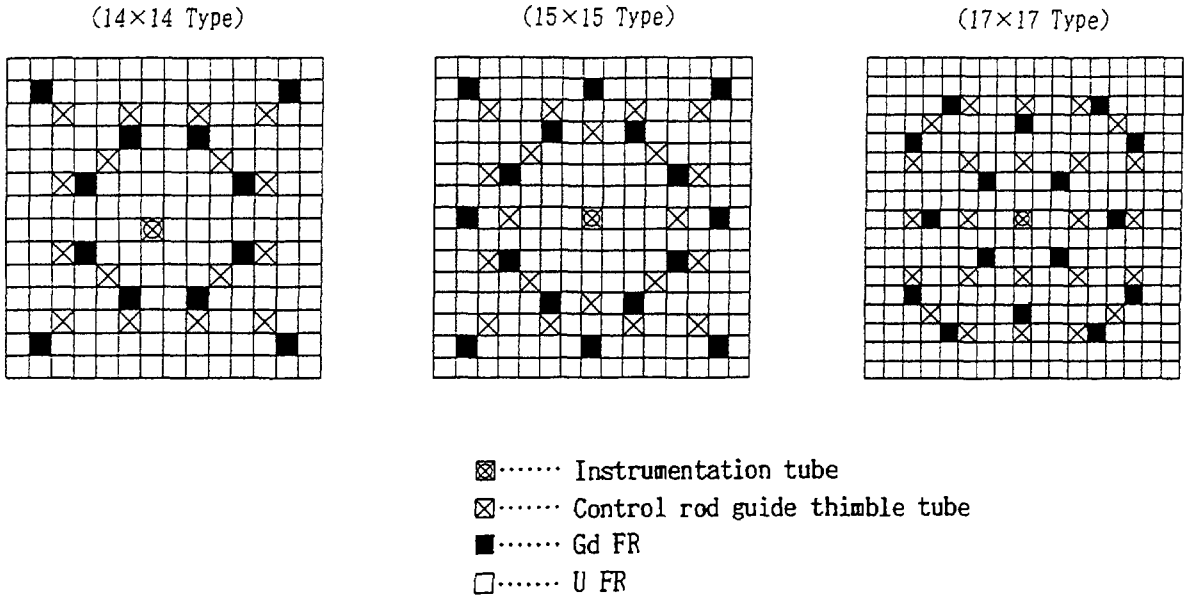

Fig. 4.6. *Positions of Gd FRs in a Japanese assembly*

Korea, Rep. of

As the nuclear programme expanded, Korea was interested in "kuksanwha" (indigenization of foreign technology) of various aspects of commercial nuclear reactor technology. As part of this policy, fuel design and manufacture started in the form of joint projects with foreign vendors. These joint projects included Gd fuel.

In order to keep the moderator temperature coefficient negative by reducing the required soluble boron concentration, gadolinia integrated burnable absorbers have been chosen instead of discrete burnable poison rod assemblies. Some FRs are replaced by Gd FRs with the fuel pellets containing 6 ~ 9 w/o gadolinia in enriched uranium.

In a typical reload core design in Korea four or eight Gd FRs are used in a gadolinia poisoned FA. The position of Gd FRs in a poisoned FA and the position and number of poisoned FAs in the core are optimized for better power peaking control and cycle economy [4.2].

Because the absorber is integral to the fuel, gadolinia integrated burnable absorbers offer a lower residual penalty and thus lower fuel cycle costs than the standard burnable poison rod assembly. Also the poisoned fuel assemblies can be loaded under control assemblies for better design flexibility. Moreover, the separate handling and disposal costs associated with standard burnable poison RCC assemblies are not necessary in a gadolinia integrated burnable absorber design.

Sweden

The use of advanced features, such as LLLP and axial blankets, is readily achievable with ABB PWR Fuel [4.3]. Both improve the fuel cycle cost but normally reduce the available margin for both LOCA and DNB. This has been overcome by the use of axially graded gadolinia integral burnable absorber (BA) [4.4]. This concept, patented by ABB Atom, makes it possible to use both advanced features simultaneously without having to increase safety limits.

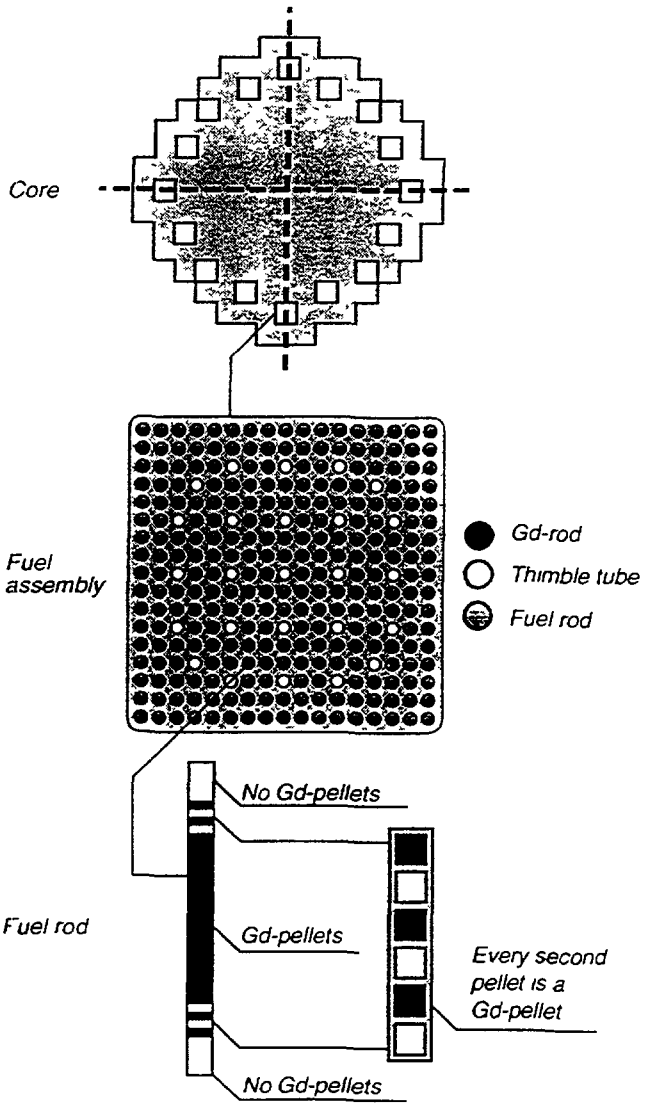

Axially graded burnable absorber, BA

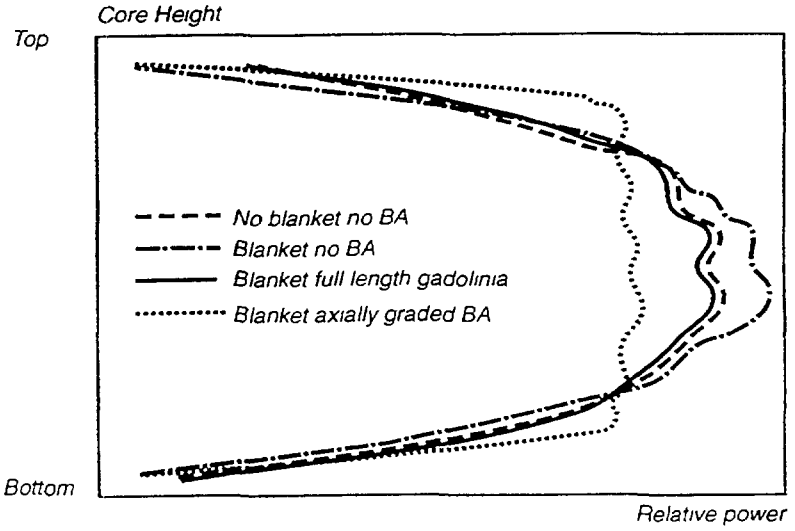

The influence on axial power distribution with axially graded BA

Fig. 4.7. *ABB design of a PWR fuel assembly*

The BA design (Fig. 4.7) controls the power distribution in three ways:

- It reduces the power capability of the fresh fuel.

- It distributes the power more evenly amongst the assemblies and over the cycle length.

- It distributes the power more evenly along the length of the assembly.

The BA concept is based on the long and favourable experience gained in BWRs, but adapted to the specific needs and requirements of PWRs. This means that, for example, the uranium of the BA rods is only slightly enriched (1.38 w/o has been used.) This concept has already been implemented in three consecutive PWR reload designs and has resulted in substantial fuel cycle cost savings.

4.1.3.2. Core design

France

With the continous aim of maximizing core operating margins (DNB, LOCA, etc.) FRAGEMA has developed a wide range of fuel management schemes for 900 MWe reactors (12 feet cores) and 1300 MWe reactors (14 feet cores) for EDF plants and foreign plants, with the following principal characteristics:

- the fresh FA enrichment (U^{235}) varies from 3.25% to 4.00%;

- the composition of the reload varies from 32 assemblies per reload in Ringhals (900 MWe) to 64 assemblies per reload in third core fuel management for long cycles (1300 MWe).

Since 1983, about 5200 Gd FRs have been tested under severe operating conditions (load follow, reduced power operation) and have demonstrated improved PWR operating flexibility.

Japan

Requirements for safety certification of a reload core are specified by the regulatory guide, which is enacted by the Japanese Atomic Energy Safety Commission. The issues to be considered are:

- Stuck rod margin
- Maximum LHGR
- Maximum FA burnup
- Maximum reactivity insertion rate
- F_{XY}^N
- Moderator temperature coefficient
- Doppler coefficient (not required for routine reload core)
- Control rod worth for rod drop incident
- $F_{\Delta H}^N$ for control rod drop incident
- Control rod worth for rod ejection accident
- F_Q for rod ejection accident.

Typical reload core designs of 4, 2, and 3 loop PWRs for 13 EFPM equilibrium cycles are shown in Appendix III. In most cases about 50% of the FAs are Gd FAs. Additionally, a small number of conventional BPRAs may be used to supplement a Gd fuel core to reduce power peaking factor. Most of the core designs are OUT-IN refuelling schemes, but some cases are IN-OUT or hybrid.

Korea, Rep. of

i. Reload core

As an example of a reload core design, Kori-2 cycle 7 is shown in Appendix IV. The core consists of 121 FAs. In refuelling (low leakage loading pattern), 52 standard FAs are currently being replaced by 4 fresh standard fuel assemblies (3.41 w/o U-enrichment) and 48 fresh KOFAs (Korean Fuel Assemblies designed by KAERI and KWU).

Out of these 48 KOFAs, 28 fuel assemblies contain UO_2 fuel rods of 3.5 w/o U-enrichment and 20 fuel assemblies contain UO_2-Gd_2O_3 fuel rods of 1.8 w/o - 6 w/o of Gd_2O_3. The length of cycle 7 is 14,42 GWd/tU (375 EFPD). This compares with the cycle 6 length of 13.1 GWd/tU (348 EFPD).

ii. Initial cores

The initial core of Yonggwang-3/4 is currently under design jointly by KAERI and C-E. It is characterized by a 4 batch low leakage fuel management scheme, enrichment zoning and the use of part-length control rods although the design is not yet finalized. In the current proposed design, the Gd FAs contain Gd FRs of natural uranium and 4 w/o Gd_2O_3. The initial cycle length will be 12 months. The design goal for the average burnup is 55 GWd/tU for later cycles. Fig.4.8. shows the infinite multiplication factors as functions of burnup for the 8 shimmed fuel assemblies. The factors for 12 shimmed FAs are shown in Fig. IV.17 (App. IV).

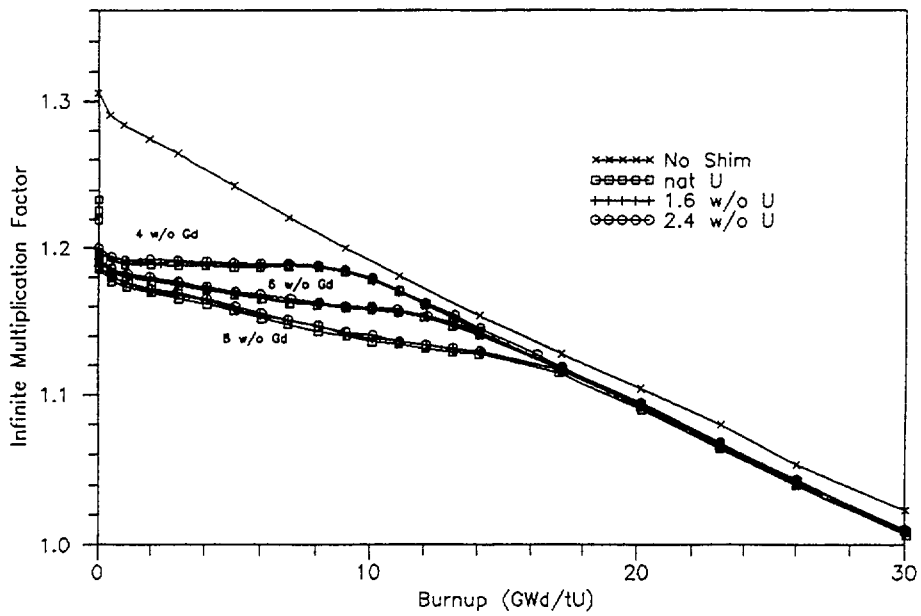

Fig. 4.8. *Infinite multiplication factor for YGN - 3 / 4 initial core: 8 Shim FA*

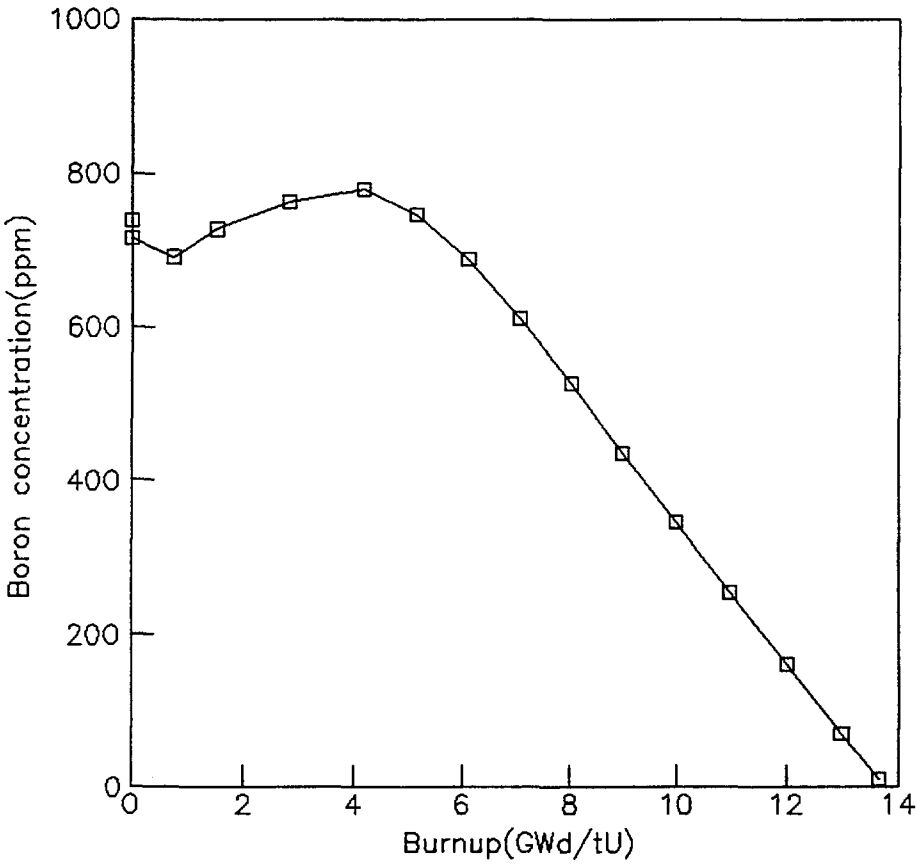

Fig. 4.9. *YGN - 3 / 4 critical boron concentration: 4 w/o Gd_2O_3 - natural uranium*

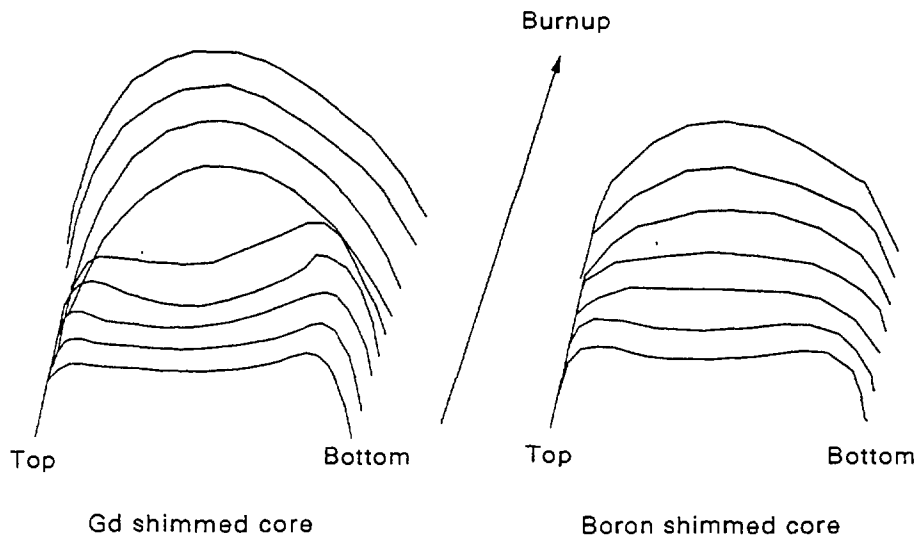

Fig. 4.10. *Axial power distribution vs burnup*

The Gd fractions remaining as functions of burnup are shown in Fig. IV.18 and 19 (App. IV). Fig. 4.9 shows the critical boron concentration as a function of burnup. Fig. 4.10 illustrates the evolution of the axial power shape of the Gd-shimmed core as burnup progresses in comparison with the axial power shape of the conventional boron-shimmed core. It is worth noting that the axial power peak appears late in the cycle of the Gd-shimmed core [4.5].

The following observations and conclusions are noted:

- Occurrence of high peaking factor in mid-cycle due to too rapid depletion of Gd (low Gd content).
- If high Gd content is used, a residual reactivity penalty may occur. This would shorten the cycle length.
- The benefit in fuel cycle cost appears to be minimal, if not negligible.
- More sophisticated analysis is required to optimize:

  number of Gd FRs in an assembly
  location of Gd FRs in an assembly
  position of Gd FAs in the core
  Gd content
  enrichment of U^{235} in Gd FRs.

4.1.4. WWER fuel design

4.1.4.1. Fuel assembly design

Gd FR design is similar to U FR design in terms of pellet size, rod diameter, etc. Uranium enrichment values in Gd FRs are traditionally lower than in a U FR and are defined by thermo-physical characteristics. Gd_2O_3 content is determined by a number of requirements for the core including fuel cycle length, power peaking factors, reactivity coefficients, etc.

For the three-year WWER-1000 fuel cycle, average enrichment is equal to 4.23% (66 fuel rods in the peripheral rows with corner FRs of the next row having an enrichment of 3.6% and all other FRs having an enrichment of 4.4%). In the Gd FRs enrichment was reduced to 3.6% [4.6]. The range of Gd_2O_3 content was chosen to be from 4 to 9 w/o and the number of Gd FRs per FA from 12 to 24. All cases were calculated during 1991-93. A FA design with 18 Gd FRs (8 w/o Gd_2O_3) was selected for the first loading of Gd fuel into WWERs (Fig. 4.11).

In choosing the position of the Gd FRs in the FA, allowance is made for the following effects:

- the non-uniformity of the FR power distribution and the position of the highest-power FR;
- the mutual "shadowing" of the Gd FRs and the reduced depletion rate of Gd in them.
- the control and protection system efficiency.

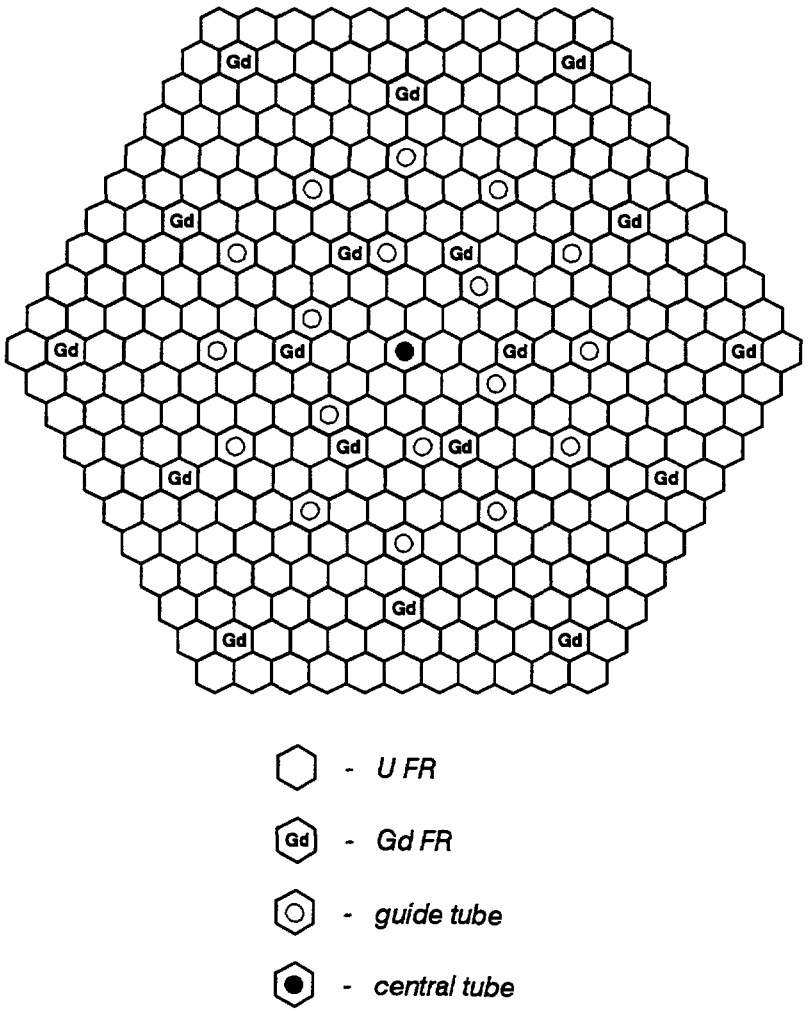

Fig. 4.11. *Fuel rod array of WWER-1000 FA*

A basic loading pattern with 18 Gd FRs in a FA has been chosen; with this the highest rated FR is at the FA periphery up to a burnup of ~ 16 MWd/kgU and then moves to the centre of the FA when the F_{xy} has been reduced to 1.0.

4.1.4.2. Core design

Calculations have shown the acceptability of the basic design with regard to power shaping in the reactor core. The use of a refuelling strategy with a LLLP is complicated for WWER-type reactors due to difficulties with smoothing of radial peaking, i.e. to constrain the FA power peaking factor within $F_Q \leq 1.35$.

The first experience was obtained at Kola NPP Unit 3 with a WWER-440 reactor [4.7] when 36 FAs with an enrichment of 3.6% were moved after the third year to the core periphery. By the end of the fourth year of irradiation, the burnup reached 38 GWd/tU (average burnup for three years fuel cycle around 28 GWd/tU). During this period the relative power of the highest rated FA was maintained within the limits ($F_Q \leq 1.26$). Further reduction of neutron leakage using such a reload scheme could be achieved by full loading of the core periphery with FAs which have already been burned for several years in the inner part of the core. This would complicate the smoothing of F_{xy} but would provide a saving in fresh fuel requirements and also a reduction of radiation damage to the reactor vessel.

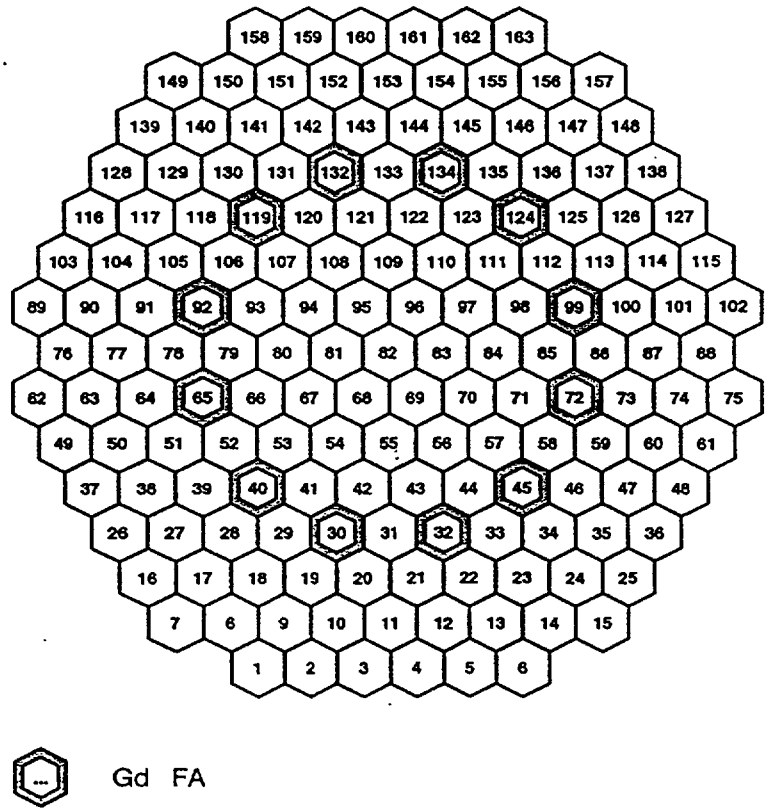

Fig. 4.12. *FA array of WWER-1000 core*

The economic benefit for the transition to a LLLP for a WWER-440 is around 2-3% of the fuel cycle cost for equilibrium fuel cycles, although it is more appreciable for transition fuel cycles (up to 10%).

Design studies for the transition to LLLPs for WWER-1000 plants have also been performed. In some plants, partial LLLPs have already been used whereby some burnt and some fresh FAs are placed on the core periphery. Work is underway to validate the introduction of more complete LLLPs.

In 1993, 12 WWER-1000 FAs with Gd fuel were manufactured. Each FA includes 18 FRs with Gd fuel, as shown in Fig. 4.11. These FAs were loaded in the WWER-1000 of the third unit of Balakovo NPP, as shown in Fig. 4.12.

The fuel enrichment in the Gd FRs was 3.6% and the Gd content was 8 w/o. Enrichment in the other FRs of these FAs was 4.4%. The enrichment in the Gd FRs was set to prevent overheating at the end of the reactor cycle (Table 4.3); $k_{inf.}$ vs burnup for standard FAs and FAs with Gd FRs are shown in Fig. 4.13.

Analysis of the calculations shows that substitution of lumped boron burnable absorber by Gd fuel allows a WWER-1000 core pattern with reduced radial neutron leakage, thus enabling an increase in fuel burnup and a decrease in fast fluence to the pressure vessel compared with the standard three-year fuel campaign. The use of the integral burnable absorber also improves reactor stability (self-regulating properties) due to an increase in negative feedback via coolant temperature resulting from a decrease in the boron content.

TABLE 4.3. TYPICAL WWER FUEL DESIGN

Characteristics	Standard WWER-1000 FA	WWER-1000 FA with Gd fuel
Core average LHGR (kW/m)	16.7	16.7
Number of FRs in FA:		
- U FRs	312	294
- Gd FRs	-	18
Number of guide tubes	18	18
Fuel rod:		
- length (cm)	353	353
- outer diameter (cm)	0.915	0.915
- cladding material	Zr - 1% Nb	Zr - 1% Nb
- maximum LHGR in U FRs (W/cm)	448	448
- maximum LHGR in Gd FRs (W/cm)	-	260
- enrichment of U FRs (w/o U-235)	4.4	4.4
- enrichment of Gd FRs (w/o U-235)	-	3.6
-Gd_2O_3 content (w/o)	-	8
- maximum fuel temperature in U FR (°C)	~1400	~1400
- maximum fuel temperature in Gd FR (°C)	-	~1360
Fuel pellet:		
- outer diameter (cm)	0.753-0.757	0.753-0.757
- central hole diameter (cm)	0.24	0.24

4.2. MODELLING

4.2.1. Thermal and mechanical considerations

Gd content is considered to have four significant effects on fuel performance: it degrades fuel thermal conductivity, it produces a distorted, rapidly changing radial power profile, it reduces the fuel melting point and it slows the fission gas release rate. The codes developed in countries producing and/or using Gd fuel take these effects into account.

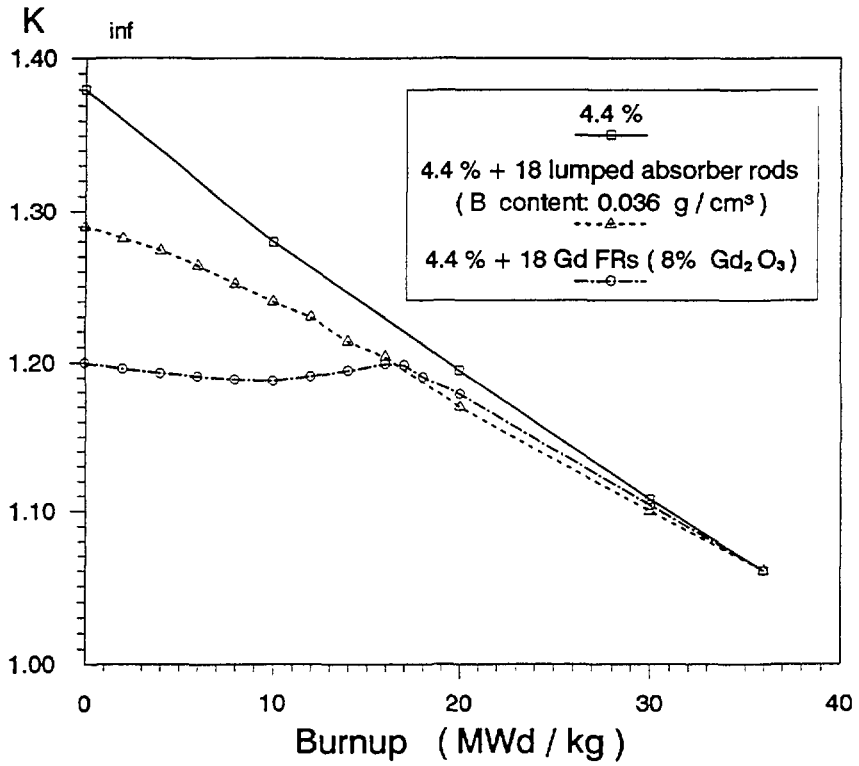

Fig. 4.13. *K_{inf} versus burnup in a WWER-1000*

Belgium

The COMETHE fuel rod performance modelling code developed by BELGONUCLEAIRE contains models for which several options can be selected to fit the specific characteristics of the fuel to be modelled. The user can even input his own model for the fuel rod constituent (e.g. cladding or pellet) which departs from the models contained in the user manual.

For most common fuels, BELGONUCLEAIRE has incorporated adequate models in the basic library and the user manual includes preferred options recommended for each of the commercial fuels used routinely in NPPs. These recommendations are based on benchmarking against a large experimental data base.

For gadolinia fuel, the data base includes, as of December 1992, a total of 31 FRs, made by different fabrication processes and irradiated over a large range of operating conditions. On this basis, two leading phenomena of the fuel behaviour were identified and incorporated in the COMETHE modelling of Gd fuel: the dependence of thermal conductivity upon Gd content and the evolution of radial power profile.

A single conductivity correlation, independent of whether the fuel was made by coprecipitation or mechanical blending, has been found to model the fuel adequately, largely due to the homogeneity achieved by the industrial fuel manufacturers [4.8].

An acceptable model of evolution with burnup of the radial power profiles has also been achieved. Early sensitivity studies [4.8] had indeed demonstrated this to be the major factor influencing the modelling results of gadolinia fuel.

Experience has also shown the importance of adequately modelling the axial evolution of burnup, which depends on good predictions by the nuclear design code of the axial depletion of gadolinium.

Japan

Four fuel vendors in Japan have their own code packages to analyse the thermal and mechanical behaviour of Gd fuel. Details of models of individual code packages vary, but in principle the following are addressed:

- for pellets: densification, swelling, temperature distribution, fission product gas release, thermal expansion, creep
- for cladding: creep (thermal and irradiation), oxidation (inner and outer), hydrogen pick-up, stress, strain, thermal expansion, crud deposit
- for rods: PCI, gap conductance.

The code package analyses these inter-related items step by step. The code packages have been continually revised based on the PIE results to date. Recently, the rim effect has been attracting attention, especially for Gd fuel pellets.

Russia

Three codes for WWER-1000 U and Gd FR performance calculations, namely PIN-mod1, the system RETR and START-3 have been developed respectively by RRC "Kurchatov Institute" and ARSR Institute of Inorganic Materials. In comparison with earlier codes, they have now taken into account the effects of extended burnup, Gd impact on thermal-mechanical properties and radial depression of neutron flux as a function of burnup (calculated with neutron-physics codes).

In the PIN-mod1 code, the increase of gas release from the fuel at extended burnup is taken into account (the gas release model is changed in the region of grain growth during fuel restructuring; the share of FGR due to the recoil mechanism is increased; fast neutron flux from adjacent FRs is also accounted for)

The PIN-mod1, RETR and START-3 codes were tested on the results of post-irradiation examination of WWER-1000 FRs [4.9]. Also, the Gd influence on thermal expansion coefficient, on density of fuel and on power density distribution over the fuel pellet radius was taken into account.

UK

The code adopted in the UK for FR performance calculations by BNFL and Nuclear Electric (NE, formerly CEGB) is ENIGMA [4.10], developed jointly by BNFL and CEGB. The code is constructed in a modular fashion, enabling new models describing specific mechanisms, such as thermal conductivity or gas release, to be incorporated and tested easily, without upsetting the code's overall calculational robustness. Modification of the code to allow modelling of non-standard fuel types, such as gadolinia-doped, niobia-doped or mixed oxide fuels, has consequently proved relatively straightforward. ENIGMA has therefore been extended to include a suitable thermal conductivity formulation, a specific radial power profile model for gadolinia-doped fuel, a modified melting point equation and a modified fission gas diffusion model.

For standard U fuel, the expression used to calculate thermal conductivity at absolute temperature T, is

$$k = (a + b \cdot T)^{-1} + \text{electronic contribution}$$

The expression for k is valid for temperatures above 773 K. For temperatures below 773 K, the value of k at 773 K is taken to apply. "b" is a constant which depends on the host material and "a" depends on impurities. "a" is therefore proportional to burnup (representing the build-up of fission products in the UO_2 lattice), such that

$$a = a_0 \cdot (1 + C \cdot \text{Burnup})$$

The coefficient "C" was fitted to thermocouple data from FRs irradiated to intermediate burnups in the Halden reactor. The same trend was subsequently found to fit high burnup temperature measurements from re-instrumented rods at Risø.

For Gd fuel, "a" is further modified such that the thermal conductivity equation becomes

$$k = [c \cdot (1 + d \cdot G) + e \cdot T]^{-1} + \text{electronic contribution}$$

where G is the weight percentage of gadolinia, d and e are constants and c is again a burnup-dependent term

$$c = c_0 \cdot (1 + C_1 \cdot \text{Burnup})$$

For G = 0, the two expressions for k are equal. The expression is valid for gadolinia weight fractions up to 12 w/o.

Radial power profiles are calculated using a modified version of the RADAR routine, [4.11] widely used in fuel performance codes to calculate radial rating profiles for UO_2 fuel. RADAR is a physically based code that calculates the radial variation of thermal neutron flux in a fuel pellet. The irradiation dependence of the radial power profiles arises through the depletion of U^{235} and the buildup of Pu^{239}, both of which are modelled by RADAR. The modified RADAR models the additional radial rating depression due to gadolinia and the burnup of the principal gadolinium isotopes with irradiation. Since gadolinia is a very strong neutron absorber, radial power profiles are strongly affected.

With these additions, the modified version of ENIGMA (known as ENIGMA-B) has been used to model gadolinia data from the BELGONUCLEAIRE organized international GAIN project, with good agreement.

France

FRAGEMA, FRAMATOME and the CEA have completed an extensive programme of development, based on the CEA test facilities, whose main objectives are to determine:

- Gd fuel physical-chemical characteristics (melting point, thermal conductivity, etc);
- Gd fuel thermal-mechanical characteristics.

4.2.2. Neutronic Considerations

Belgium

BELGONUCLEAIRE utilizes an improved version of LWR-WIMS, modified on the basis of critical experiments conducted in the VENUS facility (on a national and, with the GAP International Programme, international basis) and from lessons learned as a result of Gd fuel utilization in LWRs, including cores containing MOX fuel.

Japan

Four fuel vendors in Japan have their own code package to analyse the nuclear properties of Gd fuel. In addition, some utility customers, including their subsidiary companies, have their own code packages. Analytical models of individual code packages are different from each other. In principle, the models are simplified transport theory and ENDF B-VI/V nuclear data are used. However, based on the results of critical experiments and experience of commercial reactors, the packages have been continually revised to improve the accuracy.

The following is an example of the upgraded methodology of a nuclear code package "HAMMER-AIM" [4.12]: More detailed calculational mesh divisions in a Gd fuel pellet compared with a U pellet are necessary because of the very large neutron capture cross section of Gd. For this reason, the standard nuclear design code could not be used for Gd fuel. The HAMMER-AIM code which is the multi-group space dependent neutron transport evaluation code in the FR cell has now been modified. Various critical experiments containing Gd FRs were evaluated using the modified HAMMER-AIM code which was also used to assess Gd fuel irradiation data in overseas PWRs. Both evaluations show the validity of the analysis method. This modified HAMMER-AIM code was also applied to the evaluation work of the OHI 2 Gd fuel demonstration irradiation, which verified the validity of this analysis method for the operating plant.

During startup physics tests at BOC 5, the measured parameters such as critical boron concentration, MTC, control rod worth and power distribution agreed with the predicted values very well. Also the measured critical boron concentration vs. burnup agreed with the predicted curve. Fig. 4.14 shows the mean power change of a Gd FA vs. burnup, from which it can be seen that the measurements and predictions agree very well.

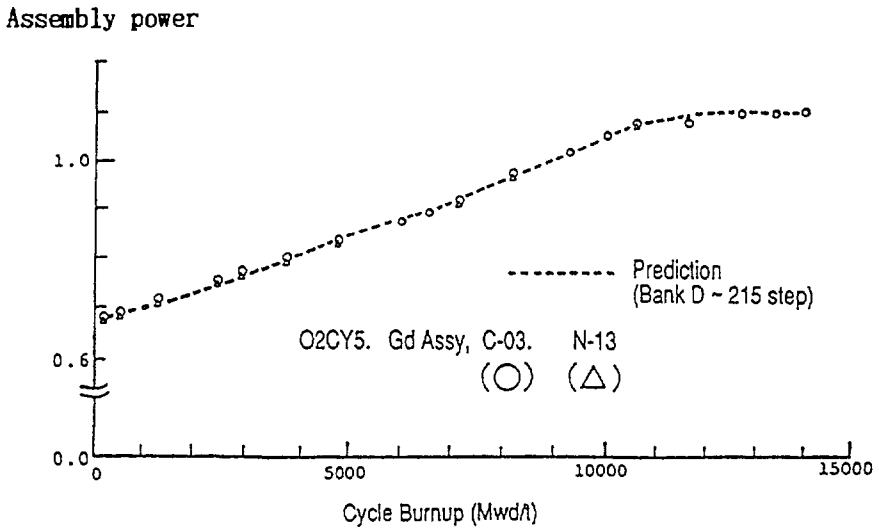

Fig. 4.14. *Gd FA power vs cycle burnup*

France

As for thermal and mechanical modelling FRAGEMA, FRAMATOME and the CEA have completed an extensive programme of development, based on CEA's test facilities. The neutronic methods for cross-sections and fine mesh calculations have been validated. The qualification is based on two types of experiments:

- critical experiments (zero burnup)
- depletion experiments

Korea, Rep. of

The computer codes that are used in Korea by KAERI and CE to perform the neutronic design of the Yonggwang Unit 3 and 4 reactor intial cores containing gadolinia are DIT and ROCS/MC. Fig. IV.20 to IV.23 (App. IV) show the code system for FA and core design of Yonggwang Unit 3 and 4.

The DIT code is a transport theory based code which performs spectrum and spatial calculations in fuel cell and fuel assembly geometries. These DIT calculations provide few group neutron cross sections for the PDQ-7 and ROCS/MC codes, few group spatial calculations in exact fuel assembly calculations, and isotopic depletion calculations for every cell in a fuel assembly including subregions of each cell when necessary. Calculations performed with the ROCS code provide reactor power distributions and effective neutron multiplication factors. The MC code is a module in the ROCS code which provides a two-dimensional fine mesh local flux and power distribution calculation extracted from the global ROCS results. The DIT and ROCS/MC codes and their methodologies have been reviewed and approved by the USNRC.

The use of Gd as a burnable absorber in the neutronic design of a reactor core causes some difficulties in the calculations because of the very large neutron absorption cross sections of the Gd^{155} and Gd^{157} isotopes. These very large neutron absorption cross sections cause significant spatial self-shielding and spectral variation of the thermal neutron flux within a Gd FR. This spatial self-shielding varies strongly with burnup. Modifications have been made by CE to the DIT and ROCS/MC codes to accommodate these neutronic effects in order to maintain accuracy. A discussion of these modifications follows.

One of the changes to DIT is in the mathematical modelling. This change was necessary to maintain accuracy in calculations for Gd FAs. The DIT 41 group neutron cross section library was found to calculate reaction rates and infinite multiplication factors accurately over a normal depletion range for a gadolinium reactivity holdown larger than design values by about a factor of two (with one exception) when compared with calculations with the reference 85 group neutron cross section library. The exception is a non-negligible difference in the rhodium reaction rates. A correction factor has been derived by CE and is used for constructing CECOR coefficient libraries for reactor cores containing Gd FAs. CE determined that from 8 to 10 flat flux regions are necessary to model Gd depletion in a FR. CE also determined that additional thermal groups are necessary to perform the few group DIT fuel assembly calculations with the total number of groups increased from 4 to 7. For the depletion calculations a predictor-corrector method is employed to keep the number of time steps manageable over a depletion range. This predictor-corrector method was checked against calculations with very small time steps and shown to be of acceptable accuracy. The Gd neutron cross sections generated by DIT for the coarse mesh calculations are functions of the initial gadolinia content, the concentration of either Gd^{155} or Gd^{157} and the soluble boron concentration in the coolant. Differential Gd cross section coefficients with respect to changes in moderator density and

fuel temperature are also constructed as a function of either the Gd^{155} or Gd^{157} concentration, and either the moderator density or the square root of the fuel temperature depending on the differential cross section. The table-sets that are constructed result in point reactivity errors, due to linear interpolation and the assumed functional dependencies, of less than 0.1 % in reactivity with a random distribution. The two-dimensional fine mesh MC module of ROCS employs a simpler functional dependency in the Gd table-sets that is used to calculate local powers and burnups within a FA from the results obtained from the global ROCS calculations.

The ROCS code includes a number of provisions to accommodate the burnable absorber gadolinia. It explicitly traces the Gd isotopes Gd^{154}, Gd^{155}, Gd^{156} and Gd^{157}. Other Gd isotopes are treated as a lumped residual. ROCS depletion of Gd has been changed to maintain accuracy for the commonly used burnup step interval of 1000 MWd/t by a computational strategy that permits time step average cross sections to be evaluated as an empirically weighted average of their values at the beginning and end of each time step. This Gd depletion procedure allows CE to calculate Gd reaction rates within 1 % of reaction rates obtained with calculations performed with very small burnup intervals. No changes were required to the MC module of ROCS since this MC module obtains neutron cross section data and calculated results directly from the ROCS code.

The few group structures for the DIT fuel assembly calculations were changed from 4 to 7 groups for Gd FAs. CE determined that a minimum of 8 flat flux regions were required for modelling a Gd-U fuel pellet. Some simplifications were made to the cross section representations of the Gd isotopes. For all of the approximations that were made to the reactor design calculations performed with DIT and ROCS/MC, CE determined that accuracy of computed quantities with respect to more detailed calculations was maintained. The USNRC has reviewed the changes made to the DIT and ROCS/MC codes and their methodologies to accommodate the use of Gd in PWR cores. These changes are typical of those type made by the industry for designing gadolinia cores. The numerical results that were provided show that acceptable agreement has been obtained between detailed calculations and design calculations.

The codes used in Korea by KAERI and Siemens/KWU in nuclear reload fuel designs including using Gd, are described in App.IV.

Russia

Neutron physical properties of the Gd core are calculated using a neutronic code package [4.13] with the following main features:

- three dimensional core power distribution , fuel burnup, reactivity coefficients and effectiveness of reactivity regulation are calculated using the BIPR-7 program;

- a library of small group constants is compiled using the KASSETA-TVEL and KASSETA programs;

- the power distribution for each rod is calculated using the PERMAK program

UK

BNFL utilizes the standard Westinghouse Nuclear Design code package ALPHA/PHOENIX-P/ANC which includes the capability to model Gd fuel and which has been validated against operating plant data. BNFL has further validated this code package against data obtained from the VENUS facility in Belgium.

REFERENCES TO CHAPTER 4

[4.1] ENOMOTO, T., "Present status and future perspectives of BWR core-fuel design" (Journal of the Atomic Energy Society of Japan, Vol. 26. No. 2, 1982)

[4.2] SOHN, D.S., KIM, S.H., YANG, C.K., "Korean nuclear fuels in the nineties", Proceedings of the 6th KAIF/KNS Annual Conference, 529-539, April 1991, Seoul, Korea.

[4.3] LINDELÖW, U. et al., "Asea-Atom Advanced PWR Reload Fuel Assembly Design", Nuclear Europe, May 1985.

[4.4] LINDBERG, M. et al., "Advanced Axial Gradation of the Asea-Atom PAAD Fuel", Proceedings of the ANS Topical Meeting on LWR Fuel Performance, April 17-20 (1988), Williamsburg, Virginia, USA.

[4.5] SONG, J.S., "Analysis of effects of Gd_2O_3 content and UO_2 enrichment in Gd burnable poison rods on nuclear design of fuel assembly", RT-NI-YG8-89006K, Korea Advanced Energy Research Institute, July 1989.

[4.6] ONUFRIEV, V.D., PROSELKOV, V.N., SIMONOV, V.D., "Issues of ensuring safety and increasing the economic indices of water cooled reactors in the USSR in the use of U-Gd fuel", presented at the first BAF RCM, 22-25 October 1990, Vienna, Austria.

[4.7] PROSELKOV, V.N., et al., "Some aspects of fuel cycle efficiency increase for WWER-440", Preprint IAE, No. 5252/4, 1980.

[4.8] BILLAUX, M., BLANPAIN, P., BOULANGER, D., "Evaluation of the thermomechanical properties of high burnup gadolinia fuel", ANS Top. Mtg. on LWR Fuel Performance, Williamsburg, April 1988.

[4.9] BIBILASHVILI, Yu.K., ONUFRIEV, V.D., PROSELKOV, V.N. et al, "Thermo-physical characteristics of WWER-1000 fuel rod in Unit 5 at Novozonezh NPP", Atomnaja Energia, 1993, Vol. 74, Issue 5, 450.

[4.10] KILGOUR, W.J., et al, "Capabilities and validation of the ENIGMA fuel performance code" ANS Topical Meeting, Avignon, April 21-24, 1991, 919-928.

[4.11] PALMER, I.D., et al, "A model for predicting the radial power profile in a fuel pin", Proceedings of IAEA Specialists Meeting, Preston, March 1982.

[4.12] MATSUOKA, Y., et al, "Gadolinia fuel development and plutonium recycle experience in Japanese PWR", Transactions of the Intern. Symp. on Achievement of Good performance in Nuclear Projects, April 17-20, 1989, Tokyo, 77-79.

[4.13] NOVIKOV, A.N., et al., "Code package for WWER cores analysis and some aspects of fuel cycle improvements", VANT, 1992, issue 1, 3-9.

5. EXPERIENCE WITH GADOLINIA FUEL

5.1. UTILIZATION OF GADOLINIA FUEL

This section provides a description of Gd fuel utilization worldwide including representative experiences in test reactors and in power reactors.Table 5.1 shows an overview of the status of Gd fuel utilization which is described hereafter.

5.1.1. Belgium

Between 1973 and 1987, the BR3, an 11 MWe PWR was extensively used to test on a reduced scale FAs containing new or advanced fuel types. In the framework of the Belgian R&D programme, relatively large quantities of Gd fuel with increasing Gd contents

TABLE 5.1. *OVERVIEW OF Gd FUEL UTILIZATION AND/OR DELIVERY*

Country (fuel vendor) section	Status date	Number of Gd FRs Used	Number of Gd FAs	Reactor type	Starting year
Belgium 5.1.1	Oct 93	354 3 144	70 365	BR3 (prototype PWR) PWR	1974 1982
Germany (KWU) 5.1.5	Febr 92	69 524 12 954	12 572 1 396	BWR PWR	1974 1982
France (FRAGEMA) 5.1.2	Dec 1993	5200	600	PWR	1983
Korea 5.1.3	Oct 93	3 728	640	PWR	1990
Japan 5.1.4	mid 91	30 7 092 59 980	- 460 10 228	Test reactor PWR BWR	1984 1984 1976
Russia 5.1.8	Oct 93	34 216	- 12	MIR (test) WWER-1000	1991 1993
Sweden (ABB) 5.1.6	Sept 93 April 94	90 000 5100	na na	BWR PWR	1975 1984
U K (BNFL) 5.1.7	Dec 93	na	400	BWR	1975

were loaded in the reactor (Fig. V.1, App. V) to acquire a database on the thermal-mechanical behaviour of Gd fuel and on the nuclear characteristics of a core heavily loaded with MOX and Gd fuel [5.1 - 5.4]. The main characteristics of the Gd FRs and U reference FRs are summarized in Table V.1 (App. V). The peak burnup ranged from 33 to 70 GWd/tU and the peak LHGR from 100 to 450 W/cm. A typical evolution of the peak power for two reactor cycles as a function of the irradiation time is presented in Fig. V.2 (App. V). The PIE performed on experimental fuel at the request of the licensing authorities has revealed no special features.

Taking advantage of the existing facilities at the Belgian Nuclear Centre (SCK/CEN) in Mol, parallel international programmes such as GAIN and GAP were conducted and various types of Gd FRs were irradiated [5.3].

Gd has also been utilized at the Tihange power plant in all three units as shown in Table V.2 (App. V). The policy of this plant is to go progressively to longer reactor cycles. The Gd FRs represent 0.9-1.9 % of the total FRs loaded as compared with the 7% in the BR3 demonstration cycles. The reloads have been delivered by various fuel vendors (FRAGEMA, KWU, SPC etc.)

5.1.2. France

FRAGEMA, FRAMATOME and CEA have completed an extensive programme of development based on test facilities at CEA. The main objectives have been to investigate physical-chemical characteristics, thermal-mechanical characteristics, neutronic characteristics and qualification of fabrication processes. The neutronic methodology has been qualified on two types of experiments: critical experiments (zero burnup) and depletion experiments. A large amount of measurement data is available to confirm the suitability of the design codes [5.5 - 5.6].

Since 1983, FRAGEMA's Gd fuel with mid-assembly or peripheral [5.7] positioning schemes has been incorporated in:

- 3 reloads with 8 demonstration assemblies
- 30 reloads with from 8 to 36 Gd FAs
- 1 first core with 24 Gd FAs.

The fuel management strategies cover a range of U enrichments up to 3.8%, and a variety of fuel management schemes. A typical hybrid type fuel loading scheme (transition to LLLP) in Ringhals 4 is shown in Fig. II.1 (App. II). Future Ringhals reloads will use Gd FAs in 100% IN-OUT loading schemes.

By the end of 1990, about 5200 FRs had been irradiated, a large proportion of which were under severe operating conditions (load follow, reduced power operation), demonstrating the flexibility of reactor operation with Gd fuel.

5.1.3. Korea, Republic of

In Korea, 9 nuclear reactors are currently in commercial operation: 8 PWRs (2 of 600 MWe and 6 of 900 MWe) and a CANDU (600 MWe). In addition, 2 PWRs of 900 MWe each are under construction. Until recently the vendor for each reactor supplied the fuel. Now, KAERI (Korea Atomic Energy Research Institute) is responsible for the fuel and

TABLE 5.2. *Gd FUEL UTILIZATION STATUS IN KOREA*

Fuel type	Plant name (No. of FAs in core)	No. of Gd FRs per FA/total Gd FRs in core	w/o Gd and % U^{235} in Gd fuel	Reload cycle (year) from which first Gd FAs were introduced
14 x 14	Kori - 1 (121)	4 / 64	6.0 / 1.80	11 ('90)
16 x 16	Kori - 2 (121)	4 / 80	6.0 / 1.80	7 ('90)
17 x 17	Kori - 3/4	4 and 8 / 112	9.0 / 1.80	5 ('90)
	Yonggwang - 1/2			4 ('90)
	Ulchin - 1/2			2 ('90)
	(157)			
(All of the above plants are supplied by Wh)				
16 x 16	Yonggwang - 3/4 (Supplied by KHKAECE)	4 and 8 / 140	4.0 / 0.71	1 ('94)

reactor core design and KNFC (Korea Nuclear Fuel Company) is responsible for the fuel fabrication activities. Three types of Korean Fuel Assembly (KOFA) were developed jointly with Siemens/KWU: 14 × 14 for Kori Unit 1, 16 × 16 for Kori Unit 2 and 17 × 17 for the other six PWRs [5.8].

The KOFA has several significant differences from the Wh and FRAMATOME fuel designs which were used previously in Korean PWRs. The KOFA design includes a thicker cladding, removable top and bottom nozzles, Zircaloy intermediate spacer grids with Inconel corner springs, Gd FRs and hold down springs with an additional leaf.

The KOFAs were loaded firstly into Kori Unit 2 in February 1990 and subsequently into all the other PWRs. Irradiated KOFAs were first inspected in Yonggwang Unit 2 in March 1991. Similar inspections will follow in other units. For the verification of KOFA performance, selected FAs from each type of KOFA were pre-characterized during their fabrication and will be examined in detail during refueling shutdown periods of the relevant units.

Table 5.2 shows the Gd fuel utilization status in Korea.

KAERI has contracts with KWU for reload core fuel design for all operating reactors and with ABB/CE for initial core fuel design for the Yonggwang 3 and 4 units. More details of these and the experience with other reactors are presented in App.IV.

5.1.4. Japan

Gd fuel has been used in Japanese BWRs from the mid-1970s with the adoption of an advanced 7 × 7 type fuel. Since that time the fuel design has changed several times in order to increase burnups and safety margins. The number of Gd FRs in a FA, Gd content, uranium enrichment and FR array in an assembly have all been changed over the years. The design modifications are summarized in Table III.1 (App. III). Recently an 8 × 8 BJ type fuel has been introduced. Nowadays, most of Japan's reload BWR FAs contain Gd FRs. For BWR fuel, lead test assembly irradiation and PIE have been carried out. The results showed the integrity of BWR Gd fuel. Details are given in section 5.3.1 and in [5.9].

Utilization of Gd in PWRs started in the middle of the 1980s. For reload fuel, about half of the assemblies contain Gd. Prior to the commercial use of Gd FRs in PWRs, irradiation experiments and PIE were carried out on some experimental reactors. Lead test FAs were then irradiated in a commercial reactor.

By 1991, more than 7000 Gd FRs had been irradiated in PWRs and more than 60 000 Gd rods in BWRs without failure. Details of the irradiation experience of all the Japanese PWR and BWR Gd FAs are given in App. III, together with typical core loading details for 4-loop, 2-loop and 3-loop PWR plants.

5.1.5. Germany

Test FRs containing 2-4 w/o Gd have been irradiated in the Obrigheim reactor up to maximum burnups of 18 GWd/tU and 33 GWd/tU) [5.10]. LHGRs ranged from 140-180 W/cm to 200-250 W/cm respectively. Gd FRs showed identical dimensional behaviour with regard to cladding creepdown and FR growth as U FRs and fission gas release was low (<4%) which was also in agreement with comparable U FRs. Metallographic examinations revealed the fact that the as-manufactured pellets contained areas of high

gadolinia content and some areas of almost pure UO_2. At burnups above around 25 GWd/tU, large pores appeared to develop at the areas of previously higher gadolinia concentration, accompanied by some grain growth (no information as to the number or frequency of these pores is given). These pores were not prone to densification; the Gd fuel was therefore observed to densify less than the U fuel. However, this pore formation stopped between 25 and 30 GWd/tU, and hence, because of the relative stability of these pores with increasing burnup, it can be assumed that the doped and undoped rods exhibit the same swelling behaviour above around 30 GWd/tU.

A large quantity of Gd fuel (Table 5.1) has been loaded in BWRs since 1970 [5.11] with up to 6.5 w/o Gd; a peak burnup of 52 MWd/kg U has been achieved. Furthermore, Gd fuel with 3 to 7 w/o Gd (and test FRs up to 12 w/o Gd) have been loaded in 7 PWRs to achieve low-leakage core patterns; a peak burnup of 45 MWd/kg U has been achieved.

5.1.6. Finland and Sweden

A Finnish-Swedish high burnup fuel evaluation programme [5.12] was initiated in 1984 to investigate a number of phenomena, included in which were a number of Gd FRs with up to 9 w/o Gd and burnups ranging up to 48 MWd/kgU. The highest gas release seen was 12%. As observed by radial and axial gamma-scanning of the mobile fission nuclide Cs^{137}, Gd pellets do in fact retain mobile fission products better than pure U pellets even though the Gd pellet is apparently operating at a higher temperature. As releases from the central regions of the pellets are known to be equal for volatile fission products such as caesium and for fission gases, fission gas release should also be reduced. Since it is concluded from this study that less fission product migration takes place, this should counteract the increase in gas release expected as a result of higher fuel temperatures.

The global experience of ABB Atom on BWR Gd-fuel extends to 10 w/o Gd and 49 MWd/kg U FR average burnup (Fig. 5.1). The manufacturing and burnup experience of ABB Atom PWR BA fuel is given in Fig. 5.2. The maximum BA assembly burnup is 45 MWd/kgU.

5.1.7. United Kingdom

BNFL's interest in Gd burnable absorber fuel originated around 1970 when laboratory scale work was carried out over a range of concentrations up to 30 w/o gadolinia.

Production-scale work commenced in 1972 when BNFL made Gd fuel for the Dodewaard BWR at up to 250 kg/year over a 16 year period. Initially, the gadolinia addition was at the 1 w/o level but rose to 2 w/o after 1979. In 1984 some 2.7 w/o Gd fuel was made and later a small quantity of 4 w/o Gd duplex fuel for an irradiation experiment was also fabricated. Since 1975, over 2800 kg of BWR Gd fuel has been irradiated in over 400 FAs, each of which has reached its design burnup. The peak assemblies have achieved burnups in excess of 30 GWd/tU with no failures.

5.1.8. Russia

A batch of 34 experimental Gd FRs (enrichment 3.6 w/o U-235, Gd content 4.4 and 5.0 w/o, rod length 250 mm) was fabricated and commenced irradiation in the MIR test reactor in 1991. The maximum burnup reached was 4.6 MWd/kgU (FR average = 2.3 MWd/kgU) and the maximum LHGR was 84 W/cm.

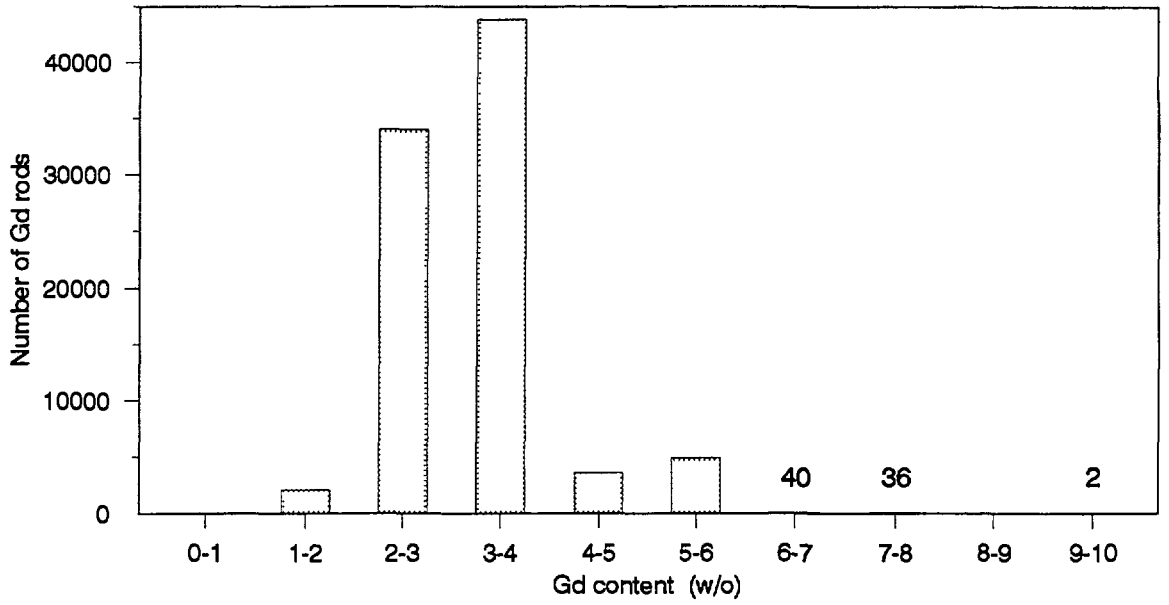

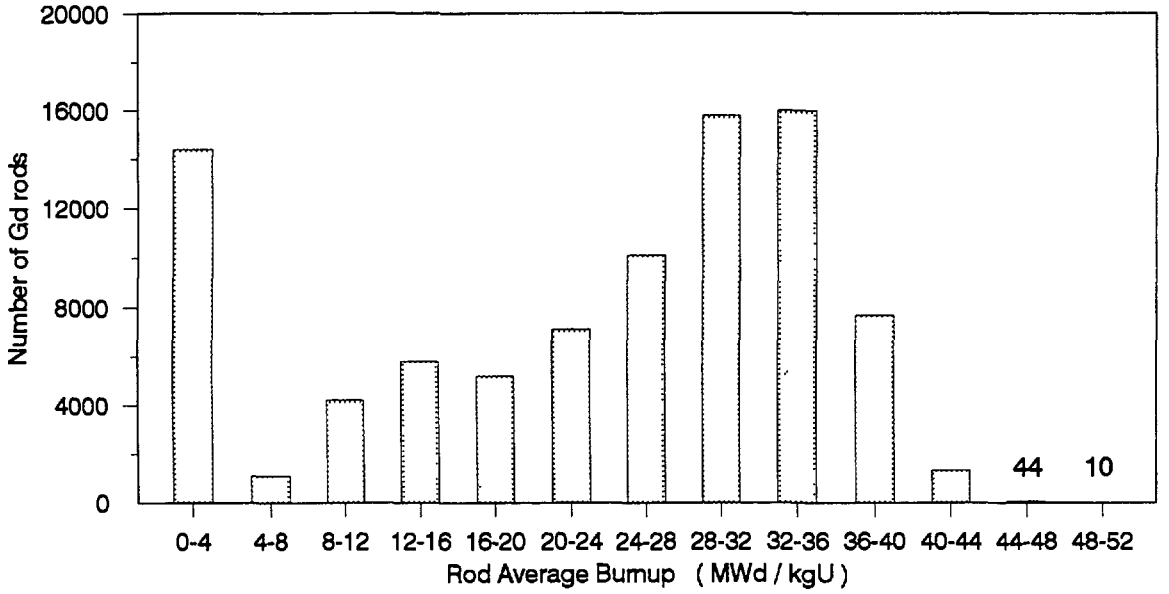

Data valid 1993-09-15

Fig. 5.1. *BWR Gd Experience of ABB Atom*

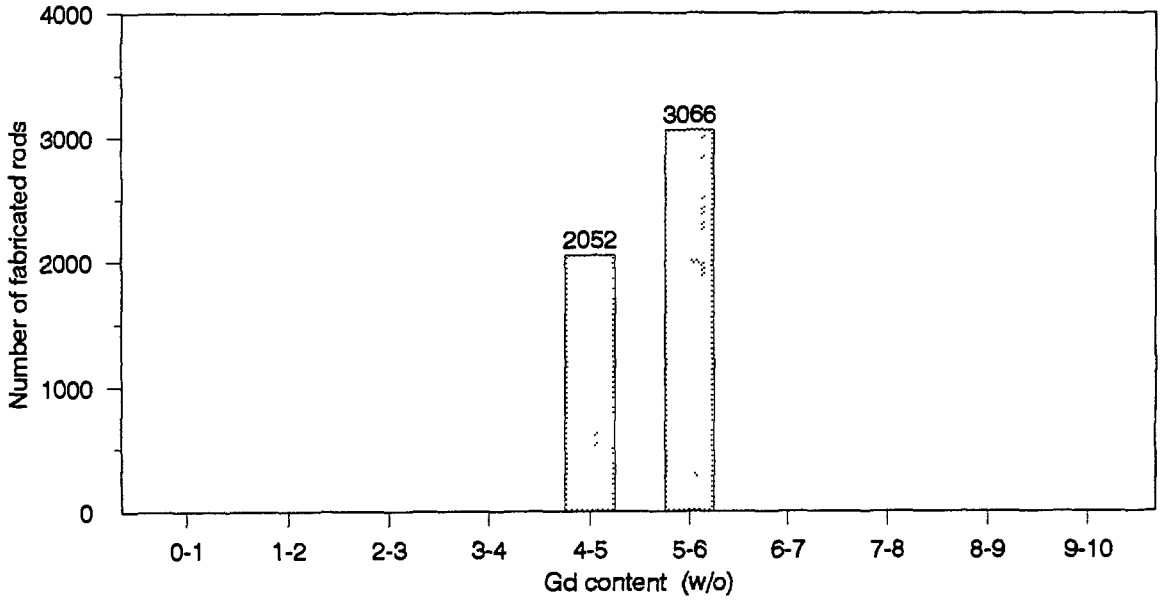

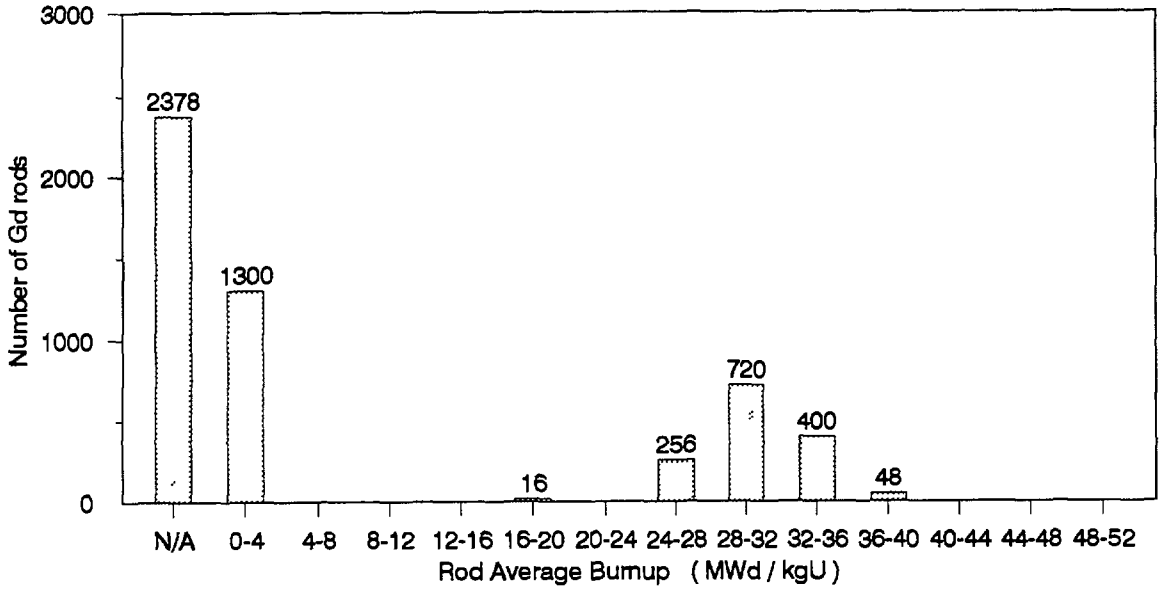

Data valid 1994-04-01

Fig. 5.2. *PWR Gd Experience of ABB Atom*

The first loading of 12 demonstration Gd FAs into Unit 3 Balakovo NPP (WWER-1000) was during the autumn 1993 reload. The set of technical documents for transfer of this unit to full Gd fuel cycle is in preparation.

5.1.9. USA

Exxon, later ANF, now SPC

Over 5300 FRs with gadolinia concentrations ranging from 1 to 10 w/o have been irradiated up to burnups of 50 GWd/tU with no failures or problems [5.13, 5.14]. From examinations performed on some 8 w/o Gd FRs in Tihange 1 after burnups of 13.2 and 37 GWd/tU, no differences in clad integrity were noticeable. The Gd fuel showed less densification, possibly due to the lower operating temperatures on the first cycle of operation. No redistribution of gadolinia within the pellets was observed and the pellet cracking patterns were similar to standard U pellets, as were changes in the pellet density.

BWFC

BWFC have irradiated Gd FAs in the Oconee reactor to a burnup exceeding 58 GWd/tU. PIE was carried out on some FAs and the results confirmed the integrity of the Gd FRs at high burnup. BWFC also supplied Gd FAs for the TMI-1 reactor for the cycle due to start operation in 1993.

5.2. NUCLEAR DATA - NEUTRONIC MEASUREMENTS

The qualification of neutronic codes relies on the interpretation of three types of experiment:

- Critical experiments in test reactors that allow definition of local power distribution inside the FA.
- Startup tests and periodic measurements performed in power reactors (boron concentrations, control rod efficiency, 3D power distributions),
- Hot cell examinations (isotopic concentrations of Gd fuel and of adjacent U fuel, micro gamma-scanning).

Information from these three types of experiments is described below.

5.2.1. Test reactor experiments

Such experiments have been carried out in Japan [5.15, 5.16], in France, where FRAMATOME and CEA have completed a program of qualification based on critical experiments (zero power) and depletions [5.17], in Belgium, where BELGONUCLEAIRE and SCK/CEN have conducted experiments both in the critical facility VENUS at Mol and in the BR3 reactor (e.g. the depletion experiments GAP [5.3], already mentioned) and in Russia [5.18].

5.2.2. Neutronic experience from power reactors

5.2.2.1. France

Core physics tests performed during startups and measured data obtained throughout operating cycles have yielded a large number of data on such parameters as FA powers, 3D power distributions, rod cluster control worths and boron concentrations.

For example, Table II.2. (App. II) presents a comparison between measurements and calculations of the initial start-up tests of RINGHALS 4 cycle 11. It also shows cycle length comparisons for cycles 10 and 11. Fig. II.2 (App. II) compares Gd power trends at hot full power for RINGHALS 4 cycle 9. The analysis of these data and comparisons with predicted design values demonstrates the adequacy of the design models and codes developed by FRAMATOME and used by FRAGEMA for Gd cores.

Operation surveillance of demonstration assemblies has proved the accuracy of power distribution calculations (agreements better than 2 w/o on Gd FA power).

5.2.2.2. Japan

Demonstration FAs

Demonstration irradiation and physics test results from Ohi 2 are reported in [5.16, 5.19, 5.20].

Eight demonstration Gd FAs were loaded into the Ohi 2 reactor cycle 5, in July 1984 in order to confirm the irradiation performance. Each Gd FA contained 16 Gd FRs (see Chapter 4) with 6 w/o Gd and 1.6 w/o U^{235} enrichment, while enrichment of the standard U fuel was 3.2 w/o. The cycle 5 started in July 1984 and ended in September 1985, reaching a cycle burnup of about 15000 MWd/tU.

During the startup physics tests at BOC, the measured parameters such as critical boron concentration, moderator temperature coefficient, control rod worth and power distribution were found to agree very well with the predicted values. Also the measured critical boron concentration and assembly power vs. burnup as shown in Fig. III.16 (App. III) and Fig. III.17 (App. III) respectively agreed well with predictions.

Commercial operation

Commercial use of 6 w/o Gd FAs in PWR plants was started in 1988. Eight FAs were loaded in Mihama 1 (2 loop core with 14 × 14 fuel assemblies) and 32 assemblies were loaded into both Ohi 1 and 2 (4 loop core with 17 × 17 fuel assemblies). The physics parameters measured during the startup physics tests and during commercial operation agreed very well with the predictions.

Tables III.7-8 (App. III) summarize the startup test experience of the commercial use of Gd FAs. They show that there are no nuclear design problems in the large scale commercial use of gadolinia fuel.

5.2.3. Hot cell neutronic examinations

Determination of the isotopic concentration of irradiated Gd fuel has been performed in several countries, e.g. Belgium [5.3], France [5.7] and Japan [5.21].

Hot cell examinations have been performed on Gd fuel irradiated in Ohi 2, including axial gamma-scanning, Fig. III.18 (App. III), and micro-gamma scanning of pellet cross-sections. Micro gamma scanning revealed the effect of a water cell adjacent to a Gd FR. The water cell promoted the depletion of Gd and fission of U. As a result, the burnup profile was asymmetric with respect to the centre axis of the pellet, as shown in Fig. III.19 (App. III).

5.3. THERMAL-MECHANICAL BEHAVIOUR

5.3.1. Overview

Knowledge of the in-pile performance of Gd fuel results from its steadily increasing use over the past ten years in PWR power plants and extensive use in BWR power plants for 30 years.

Several sources of data are available from the open literature and a short summary of the irradiation conditions, reactor type, gadolinia content and gas release is provided in Table 5.3 for PWR conditions. Test fuel rods containing 3 - 10 w/o gadolinia have been, or are being, irradiated in PWR conditions up to 70 GWd/tU peak burnup with LHGRs ranging from 16 to 45 kW/m. Up to now no failure of a Gd FR irradiated in steady conditions has been reported in the open literature with nominal LHGRs and no specific problem has been revealed either in MTRs or in nuclear power plants. The principal post irradiation test results of fuel rods referenced in Table 5.3 are reported below and the main features discussed.

The results of the BWR fuel irradiation tests are presented in [5.9], based on the results of Japanese investigations. The characterized FAs were typical BWR 8 × 8 design. They were designed by Toshiba Corporation as part of the first reload fuel for the Fukushima Daiichi No. 3 Reactor, an 800 MW(e) BWR. The FA consisted of sixty-three FRs and one water rod. Their design specification is as listed in Table 5.4. The ten characterized FAs were irradiated from October 1977 for a maximum of four cycles. A total of seven characterized FAs (two each discharged after 1 cycle, 2 cycles and 4 cycles and one assembly discharged after 3 cycles), were shipped to the hot laboratory of Nippon Nuclear Fuel Development Co., Ltd. (NFD) and examined. The exposure of the assemblies ranged from 6 GWd/tU to 29 GWd/tU which covers almost the entire range over which Japanese BWR fuel assemblies are currently irradiated.

5.3.2. Dimensional changes of the FRs

5.3.2.1. PWR FRs

No significant differences in fuel length changes have been observed between Gd and U FRs irradiated at high [5.2, 5.4] or low [5.9, 5.10] LHGR. The same quasi-linear relationship of rod growth with the fast neutron dose accumulated by both FR types has also been observed [5.4, 5.8, 5.9, 5.15].

In the Belgian experiments at high LHGR, the cladding creep-down due to the coolant pressure was less pronounced in the Gd FRs [5.2]. For Gd and U FRs, the creep-down phenomenon generally stops at around 48 GWd/tU corresponding to the appearance of ridging which is more marked in the Gd FRs [5.2, 5.4].

Japanese investigations, carried out during the the first reloading of the Mihama-3 NPP, showed a continuous cladding tube creep down [5.9].

Demonstration irradiation on Gd FRs extracted from one lead test fuel assembly loaded in the Ohi 2 reactor revealed that the outer diameter of the Gd FRs was slightly smaller than that of the U rods [5.15]. This fact is explained by the difference in the creep down and oxide film thickness caused by the power difference between the two types of FRs (20 kW/m and 16 kW/m for Gd and U FRs respectively).

In conclusion, at low LHGR ($\leq$ 20kW/m) there is no significant difference between Gd and U fuel. More pronounced fuel-clad mechanical interaction and less creep-down is observed in high LHGR fuel rods, due to the increase of the centre temperature induced by the lowering of the thermal conductivity.

5.3.2.2. BWR FRs

Every characterized FR (Table 5.4) irradiated in the FUKUSHIMA reactor [5.9] was measured for length and outer diameter by profilometry. Fig.5.3 shows that the growth of measured FRs was almost in proportion to exposure and reached more than 10 mm after 4 cycles. This growth was within the range of other literature data.

The diameter of the characterized FRs changed very little, however, taking into account slight variations in claddings supplied by different vendors, as shown in Fig. 5.4. The rod diameters with claddings supplied by vendor K increased slightly with exposure. On the other hand, those supplied by vendor S changed only a little. However, when the contributions of oxide and unremovable crud were considered, all the FRs appeared to have decreased slightly in diameter due to creep down, by the order of several tens of μm.

5.3.3. Crud deposition and water side corrosion

Some authors [5.4, 5.15] have reported no enhancement of the crud and/or external cladding oxidation of PWR Gd FRs. However, heavy nodular corrosion and significant oxide layers have been observed in BWRs on some Gd FRs although they have been irradiated in some cases at presumably lower powers than adjacent fuel rods [5.23]. A mechanism to explain this corrosion enhancement based on the ß-radiolysis of the primary water has been proposed [5.24]. In summary, enhanced corrosion due to the neutron absorbing material is explained by pair production from conversion energy capture photons in the cladding giving rise to a strong emission of energetic ß-.

In conclusion, it is necessary to obtain more data on irradiated Gd FRs both in BWR and PWR power plants, relating to the chemistry of the water circuit, temperature of the cladding (i.e. LHGR) and from the direct in-pile environment of these Gd FRs. It is too early at present to conclude that the presence of absorbing material could induce any corrosion enhancement.

5.3.4. Reaction layer between fuel and cladding material

In high LHGR FRs [5.2, 5.4], both Gd and U FRs have shown a pronounced interaction layer between cladding and fuel material. This reaction layer consisted of ZrO_2 (5μm) and caesium uranate (10μm) at 42 MWd/tM. After a second reactor cycle (70 MWd/tM) caesium zirconate was observed. Such fuel cladding bonding appeared more important in the Gd FRs indicating a significant radial caesium and oxygen migration.

TABLE 5.3. *PWR FRs IRRADIATION CONDITIONS*

Programme	MTR and/or power plant	% Gd	Average burnup GWd / tM	Peak burnup GWd / tM	Peak LHGR kW / m	Gas release %	Refe-rences
BN - CEN / SCK	BR3	3		42	45	13.3	[5.1, 5.2] [5.3, 5.4]
		3		71	45	15.6	
CEA	Siloe Gd GRIF	5	1.75		20.5	2	[5.22]
		8	7.4		29.9	12 - 17	
	CAP	3	15 - 16	25	25		
		3	25 - 29	37	25		
		10	12				
	BR3 - R2	10	60				
MHI - NFI - 5 Utilities	Halden (HBWR)	6	7				[5.19]
	BR3	6	8				
		6	26				
		10	13				
	BR3 - R2	10	40				
	DR3	10	3 days				
NUPEC	MIHAMA - 3		8.4		26		[5.9]
			17.6		24		
			31.4		24		
	OHI - 2	6		21 - 24.6	16	< 1	[5.19] [5.20]

TABLE 5.4. *MAIN SPECIFICATION OF LEAD FAs IN FUKUSHIMA DAIICHÎ - 3 (BWR)*

Item			Specification
Fuel assembly	Lattice arrangement		8 x 8 square lattice
	Total length	m	4.47
	Fuel rod pitch	mm	16.3
	Total heat transfer area	m^2	9.06
	UO_2 weight	kg	About 210
	Total weight (including channel box)	kg	About 310
Fuel rod	Number		63
	Effective length	m	3.66
	Plenum length	m	0.4
	Fill gas		He
	Fill gas pressure	$kg / cm^2 a$	1
Pellet	Diameter	mm	10.6
	Height	mm	10.7
	Material		UO_2 (partially UO_2 - 2 w/o Gd_2O_3)
	Density	% TD	95
Cladding & water tube	Number of water rods		1
	Outer diameter	mm	12.5
	Thickness	mm	0.86
	Material		Zircaloy - 2 (recrystalized and annealed)
Spacer	Number		7
	Material		Zircaloy - 4 Inconel X - 750

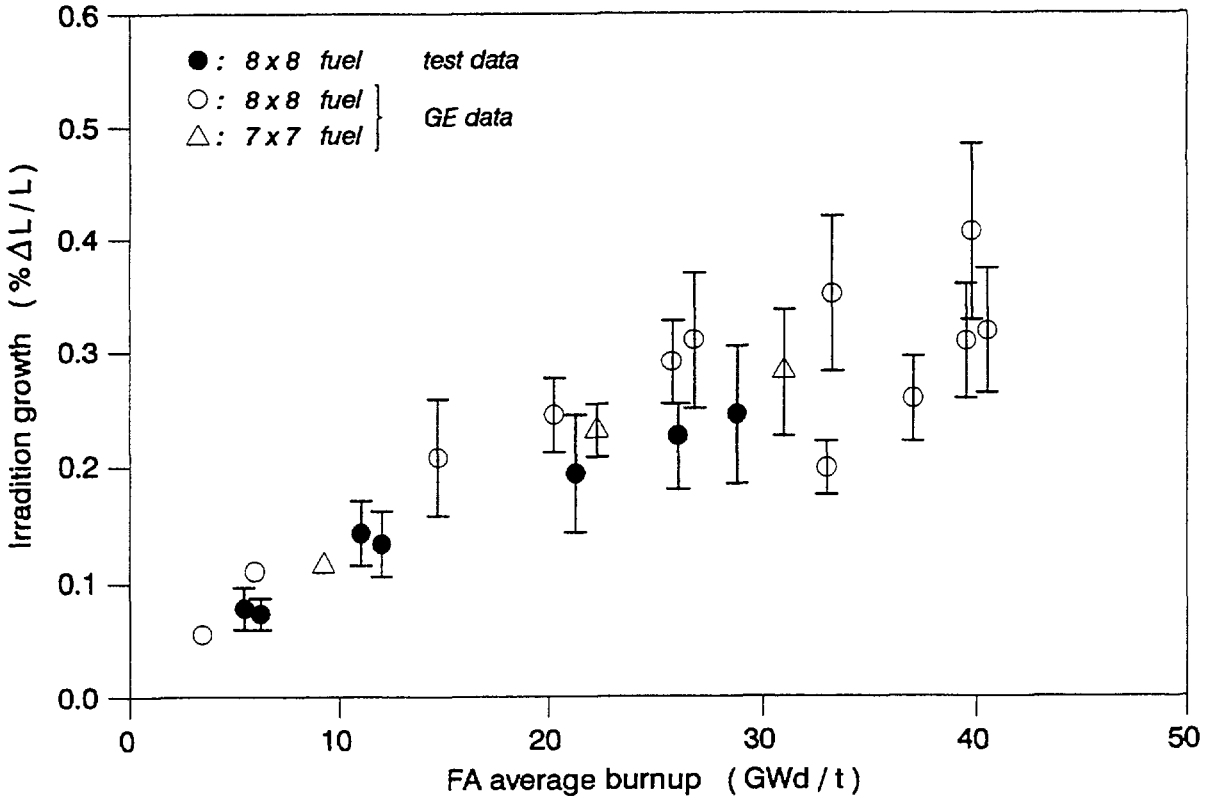

Fig. 5.3. *Irradiation growth of FRs [5.9]*

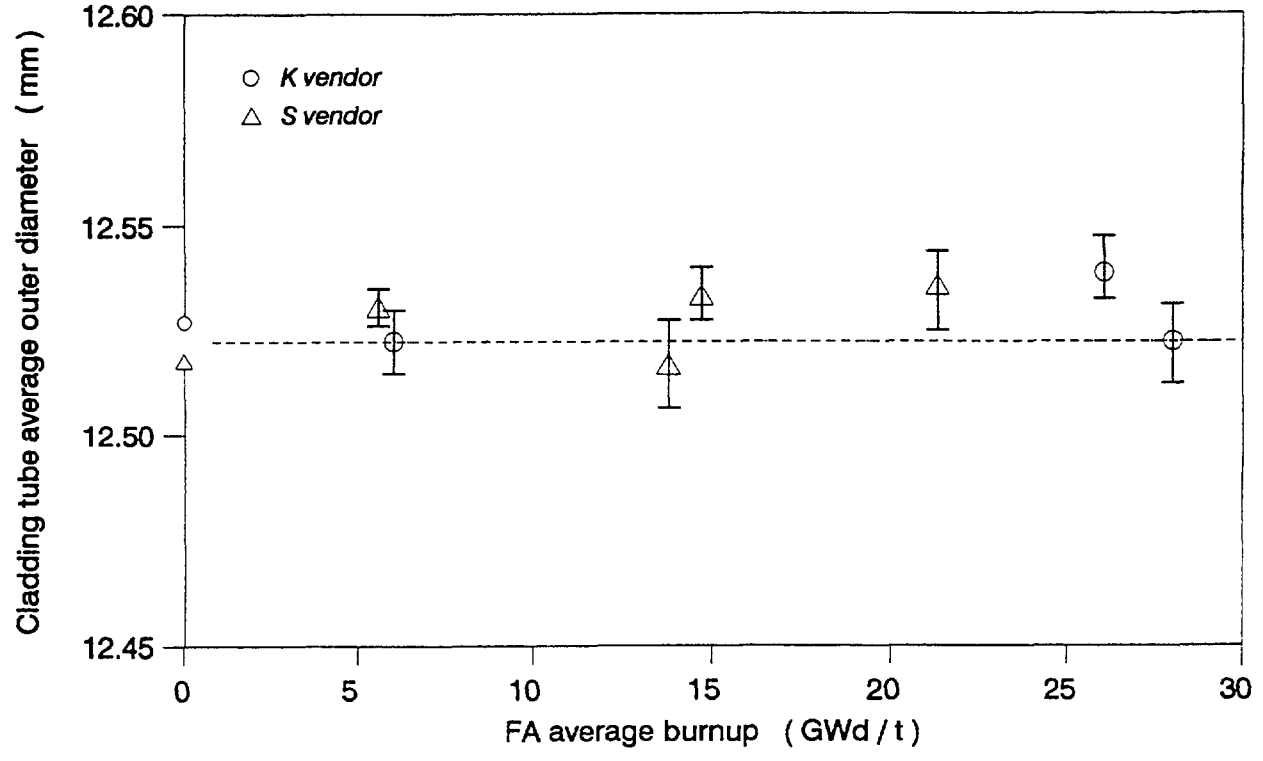

Fig. 5.4. *Change of FR average outer diameter with burnup [5.9]*

At lower LHGR (20 - 30 kW/m), a thin interaction layer has been observed, although a trend towards an enhancement of the inner oxide layer has been reported [5.10] for Gd FRs. The thickness increase of the inner oxide layer is generally well correlated with the higher centre temperature of the Gd FRs resulting from the lowering of the thermal conductivity.

Furthermore, two observations are to be noted:

- the relative mobility of Cs in the Gd FRs which axially migrated into the peak LHGR region (40 kW/m) (see section 5.3.6.2.)

- the formation of an oxidised compound containing Zr and Cs at the internal cladding surface.

These two observations can be explained by a lowering or stabilization of the chemical oxygen activity during the irradiation.

It was observed after the first cycle in Gd FRs irradiated at high burnup and LHGR in BR3 that the compounds present at the fuel-clad interface were ZrO_2, $Cs_2UO_{3.56}$, and Cs_2Te and after the second cycle, ZrO_2, Cs_2ZrO_x, and Cs_2Te. It can be deduced from the thermodynamic stability [5.25, 5.26] and from observations [5.25] that the following reaction occurred:

$$ZrO_2 + Cs_2Te + Cs_2UO_{3.56} \rightarrow Cs_2ZrO_x + ZrTe_m + UO_2$$

$$\Delta G(Cs_2Te) \simeq \Delta G(ZrTe_m)$$

$$\Delta G(Cs_2ZrO_x) << \Delta G(Cs_2UO_{3.56})$$

$$\Delta G(ZrO_2) < \Delta G(UO_2).$$

The chemical oxygen potential ΔGO_2 in the system (ZrO_2, Cs_2ZrO_x, Cs_2Te) is lower than the ΔGO_2 in the system (UO_2, $Cs_2UO_{3.56}$, Cs_2Te).

The axial mobility of Cs in the Gd FRs is another indicator of the lower oxygen activity prevailing in the FR. The volatility of Cs is directly related to its chemical activity, which is high enough to induce axial migration. From a thermodynamic point of view, oxygen activity in the Gd fuel is not drastically modified in comparison with U or MOX fuel.

5.3.5. Microstructural fuel features

5.3.5.1. Pellet density - densification - swelling

No significant difference between Gd and U fuel irradiated in PWRs has been reported as far as geometrical pellet stability is concerned. After a temporary densification during the first cycle, pellet density returns to the as-manufactured value at the end of the irradiation [5.9] when the LHGR is around 20 kW/m. Pellet changes have been observed at higher power ratings [5.2, 5.4] due to the higher centre temperatures of the FRs. After restructuring, stability of the pellet geometry is reached and no creep-down is observed between 48 and 70 GWd/tU.

In BWR FRs [5.9], the fuel density returns almost to the as-manufactured value at burnups of 30 GWd/tU. The densification appears higher for Gd fuel pellets than for U pellets but the swelling rate is similar (Fig.III.20, App. III).

5.3.5.2. Microstructure and gadolinium diffusion

In FRs irradiated in PWRs at low LHGR ($\leq$ 25 kW/m), no gadolinium diffusion has been observed and grain growth is also generally not observed at low burnup. At high burn-up, some incipient growing of the grains is observed in parallel with a small Gd diffusion [5.9, 5.15]. Above 25-30 GWd/tU burnup, large pores appear to develop in the zone where Gd_2O_3 was previously in higher concentration. This phenomenon is accompanied by some grain growth. These pores, due to the difference between the U and Gd interdiffusion coefficient, are very stable and contribute to the density decrease of the gadolinia doped fuel [5.10].

At higher LHGR ($\geq$ 30 kW/m), a central restructured zone is observed in which complete solution of Gd_2O_3 in UO_2 fuel and grain growth are observed. In contrast to the situation with low rated FRs, the grain growth seems to be enhanced. No completely satisfactory explanation has been given up to now [5.2, 5.4].

The grain growth of fuel irradiated in a BWR [5.5, 5.27] was measured at different radii during the PIE. The calculation based on the out-of-pile investigation overestimated the value in some cases. This was attributed to grain boundary bubbles observed in the corresponding specimens which retarded grain growth. The observations reveal that the grains at the centre of the pellet grow slightly during irradiation; the grain size differences between the centre and the periphery of the pellets are shown in Fig. III.21 (App. III).

5.3.5.3. Power to melt

To investigate the combined effect of reduced thermal conductivity and burnup, a power-to-melt experimental determination has been conducted on a PWR Gd FR in the frame of the International Programme HBC (High Burnup Chemistry) organized by BELGONUCLEAIRE. The results are restricted to the participants in the programme.

5.3.5.4. Conclusion on microstructure

When the LHGR is maintained around the nominal design value (15 - 20 kW/m), no significant modification of the initial fuel structure has been observed. Some incipient diffusion of gadolinium into the fuel matrix has been noted in the centre of the hottest fuel rods (20 kW/m < LHGR < 25 kW/m).

At high LHGR, no significant difference between Gd and U FRs has been recorded.

5.3.6. Fission gas release and fission product distribution

5.3.6.1. Fission gas release (FGR)

Both at high and low LHGR, the fission gas release from Gd and U FRs shows the same trend. No significant influence of the Gd presence has been recorded and the phenomenon is believed to be more related to the fuel temperature than to the gadolinia solid solution in the fuel matrix.

Gd fuel irradiated at a peak rating below 20 kW/m releases a small fraction of the total fission gas inventory [5.9, 5.10, 5.15]. Larger fission gas release rates seem to be observed in the high burnup FRs compared with the low burnup FRs [5.1, 5.4].

Fission gas release data of FRs irradiated at high rating reveal similar release rates both for Gd and U fuel [5.2, 5.4, 5.22]. On the basis of the available results, gadolinia addition does not appear to affect the fission gas release rate. The most important factor for the gas release is therefore the centre temperature and its evolution with time [5.1, 5.4].

The puncturing of 44 characterized FRs irradiated in a BWR power plant [5.9] showed the same trends for both Gd and U FRs. In the high burnup range, the FGR principally depends on LHGR (Fig. III.22 (App. III)) but less on burnup (Fig. III.23 (App. III)). The FGR of Gd fuel was found to be similar to that of U fuel.

5.3.6.2. Fission product distribution

In low-rated FRs, Mo, Nd and Cs elements with a high fission yield are almost uniformly distributed within the fuel pellet. Only some deposits containing Cs-U-O have been detected on the inner clad surfaces.

In contrast, high-rated FRs show an important radial Cs migration to the inner clad surface. Compounds containing Cs-U-O and Cs-Zr-O have been observed in the FRs of the Belgian programme [5.1, 5.4]. Furthermore, axial Cs migration was observed in these Gd FRs and not observed in the U or MOX fuel rods irradiated in similar conditions (see section 5.3.4).

5.3.6.3. Conclusion on fission product behaviour

The fission product behaviour in the fuel matrix does not seem to be influenced by the presence of Gd in solid solution in the fuel matrix. The most important parameter is the temperature of the fuel matrix which governs the diffusion and transport processes.

5.4. BEHAVIOUR UNDER REACTIVITY-INITIATED ACCIDENTS

In-reactor experiments were conducted to study the failure behaviour of Gd FRs under reactivity-initiated accidents by using the NSRR. The specific objectives of the study were to determine the thresholds of fuel failure and mechanical energy generation and to identify the fuel rod failure mechanism compared with U fuel.

The work was performed as a joint study between JAERI and MHI [5.28]. Details are given in App. III. It was concluded that:

1. The failure mechanism of Gd FRs is oxygen induced cladding embrittlement accompanied by wall thinning due to local melting of the cladding, which is the same as that of U fuel.

2. The failure threshold of Gd FRs is between 265 and 275 cal/g.UO_2, almost the same as that of U fuel.

3. Both the Gd and U FRs have almost the same mechanical behaviour as a function of energy generation.

4. In consideration of the radial power profile in the fuel and the pulse power shape expected in an LWR, the failure threshold in an LWR is estimated to be at the same level or greater than the presented results. Indeed, in the

FRs of the NSRR experiment, Gd^{160}-enriched Gd was used to provide high reactivity in the test FR; as a result, the power profile within the FR is less depressed than in an LWR. In addition, the ratio of beta/energy release is larger in the NSRR core than in an LWR core and consequently the rates of power change (both power increase before and decrease after the peak) are faster than in LWRs.

REFERENCES TO CHAPTER 5

[5.1] BAIRIOT, H., et al, "Gd fuel behaviour to high burn-up", Performance of fuel and Cladding Material under Reactor Operating Conditions, Proc. KTG Sem. Karlsruhe, 1985, Kerntechnische Gesellschaft Bonn (1985).

[5.2] BLANPAIN, P., HAAS, D., MOTTE, F., "High rated and high Burn-up Gadolinia Fuel irradiated in the BR3 17 x 17 PWR", IAEA-SM-288/40, Proceeding of Int. Symp. on "Improvements in Water Reactor Fuel Technology and Utilisation", Stockholm, 15-19 Sept.1986.

[5.3] HAAS, D., MOTTE, F., "Experimental Programmes on Gadolinium Fuel Utilisation in LWRs in Belgium", Proc. Specialists Mtg Mol, 1984, IWGFPT/20, IAEA, Vienna, pp.171-181.

[5.4] BILLAUX, M., BLANPAIN, P., BOULANGER, D., "Evaluation of the Thermomechanical Properties of High Burn-up Gadolinia Fuel. ANS Topical Meeting on "LWR Fuel Performance" Williamsburg, April 17-20, 1988. pp.356-363.

[5.5] BRUET, M., et al., "Analytical out-of-pile and in-pile experiments on gadolinium-bearing fuels", ENC 86, Geneva, June 1986.

[5.6] BRUNA, G., NOBILE, M. and VALLEE, A., "Transport and diffusion infinite medium assembly calculations of pin power distribution", presented at International Meeting on Advances in Mathematics, computation and reactor physics ANS. Pittsburgh, PA, USA, April 1991.

[5.7] BONNIAUD, M., MAGNIN, D., NORSTROM, G., LARSSON, J., "Advanced Fuel Managements with Gadolinium Peripheral Design", Deutsches Atom Forum, Dusseldorf, May 1989.

[5.8] SOHN, D.S., KIM, S.H., and YANG, C.K., "Korean Nuclear Fuels in the Nineties," Proceedings of the 6th KAIF/KNS Annual Conference, pp.529-539, April 1991, Seoul, Korea.

[5.9] NUPEC, "Proving Test on the Reliability for Nuclear Fuel Assemblies - Irradiation Test on Fuel Assembly", Summary Report Nuclear Power Engineering Test Center - 1987.

[5.10] MANZEL, R. and DOERR, W.O., "Manufacturing and Irradiation Experience With UO_2/Gd_2O_3 Fuel", Ceramic Bulletin Vol. 59, No. 6 (1980), pp.601-616 (paper presented at the Annual ACS meeting, Cincinati, May '1979).

[5.11] SIEMENS - Fuel Assemblies - References '92.

[5.12] ANDERSSON, S.O., PATRAKKA, E., HYDEN, L., PETTERSSON, H. and GRAPENGIESSER, B., "The Finnish-Swedish High Burnup Fuel Evaluation Programme", IAEA-SM-288/45, pp.281-289.

[5.13] SKOGEN, F.B. and KILLGORE, M.R., "Performance of Exxon Nuclear Gadolinia-Bearing Fuel in Pressurized Water Reactors", ANS Topical Meeting on LWR Fuel Performance, Orlando, Florida, April 21-24 1985, pp.5-43 to 5-49.

[5.14] SKOGEN, F.B., O'LEARY, A.H. and KARCHER, K.E., "Performance of Gadolinia Burnable Absorber Assemblies at Burnups up to 50,000 MWD/MTU", ANS Topical Meeting on LWR Fuel Performance, Williamsburg, Virginia, April 17-20 1988, pp.348-355.

[5.15] YOKOTE, M., et al., "A Japanese Gadolinia Fuel Usage and Demonstration Program", (ANS Trans. Oct. 1989).

[5.16] MATSUOKA Y., et al., "Gadolinia Fuel Development in Japanese PWR", Proceedings of an International Symposium in Tokyo by OECD, April 1989.

[5.17] BGUNA, G., NOBILE, M. and VALLEE, A., "Transport and diffusion infinite medium assembly calculations of pin power distribution", International Meeting on Advances in Mathematics, computation and reactor physics ANS. Pittsburgh, USA, April 1991.

[5.18] POLJAKOV, A.A., et al., "Investigation of neutronic parameters of uranium water lattice with Gd absorber" in Modelling and investigation of neutronic processes in nuclear power reactors, Moscow, Energoatomizdat, 1991, pp.118-121.

[5.19] MORI K., et al., "Development of gadolinia Fuel for PWR", IAEA-SM-288/22P.

[5.20] YOKOTE M., et al., "Gadolinia Fuel Usage and Demonstration Program in Japan", ANS/ENS meeting on LWR Fuel Performance, Avignon Meeting, April 1991, p.897-908.

[5.21] DOI, S., "Post Irradiation Examination on the Gadolinia Containing Fuel Irradiation in the Domestic PWR" Mitsubishi Genshiryoku Gihou No. 57 pp. 14, 1990.

[5.22] BRUET, M., PORROT, E., TROTABAS, M., MELIN, P. and BONNAUD, E., "Analysis of Thermomechanical behaviour of UO_2 Gd_2O_3 Fuel Under Irradiation Conditions", ANS Topical Meeting on LWR Fuel Performance, Orlando, Florida, April 21-24 1985, pp.5-51 to 5-63.

[5.23] MARLOWE, M.O., ARMIJO, J.S., CHENG, B., ADAMSON, R.B., "Nuclear Fuel Cladding Localized Corrosion", ANS Topical Meeting on LWR Fuel Performance, Orlando, Florida, April 1985, p.3-73.

[5.24] LEMAIGNAN, C., "Impact of ß-radiolysis and Transient products on irradiation-enhanced corrosion of zirconium alloys", J. Nucl. Mat. 187 (1992) 122-130.

[5.25] DROUWART, J., Personal Communication V.U.B. Free University of Brussels.

[5.26] RAND, M.H. and POTTER, P.E., Personal Communication UKAEA (AEA) HARWELL..

[5.27] KOGAI, T., et al., "In-Pile and Out of Pile Growth Behaviour of sintered UO_2 and (U, Gd) O_2 Pellet", Journal of Nuclear Science and Technology, 26[8] p. 744-751, Aug. 89.

[5.28] SHIOZAWA, S., et al., "Study on the Behaviour of Gd_2O_3 Fuel Rod Failure under a Reactivity Initiated Accident", (JAERI-M 88-084, May, 1988).

6. FUEL CYCLE BACK END

6.1. SPENT FUEL STORAGE

Since the discharge burnup of FAs with burnable absorbers is, in principle, identical to the burnup of standard FAs, no major difference is apparent between the two types of Fas. Amongst the more subtle differences, however, it should be noted that:

- the power rating of Gd FAs at EOL is usually higher than the rating of the standard FAs for a given reload. The residual heat after shutdown is therefore affected during the initial period of spent fuel handling and storage. This difference disappears with time once the residual heat becomes predominantly affected by burnup and not by EOL power rating.

- the relatively high Pu build-up and consumption during the first cycle due to the neutron spectrum hardening results in a slightly higher Pu content in the spent fuel and a shift of the Pu composition towards higher isotopes. This effect, limited to the Gd FRs in the FA, has a negligible impact on the spent FA characteristics.

6.2. TRANSPORTATION

The characteristics mentioned in section 6.1 would also influence spent fuel transportation. However, since transportation will only take place 2 to 10 years after EOL, the impact is negligible.

6.3. REPROCESSING AND WASTES

Gd is frequently added to the dissolver in reprocessing plants to increase the margin to criticality. Gd has been proven not to interfere with the chemistry of the process and to be recovered in the HLW stream to be vitrified.

In the most recent French reprocessing plants, criticality control is achieved principally by implementation of criticality-safe geometry of the equipment. This is not the case for the dissolver in the UK's THORP facility, where monitoring for fissile content can be exploited to reduce the level of Gd addition in the process thereby reducing the volume of vitrified waste.

The main effect of the presence of Gd in irradiated fuel is to increase slightly the volume of vitrified waste and consequently the cost of reprocessing and waste disposal. The total oxide content of the glass is not affected by the presence of Gd since the oxide loading is determined by the incorporation level set by plant operating parameters (although Gd oxide now forms part of the total). The consequence of adding Gd is potentially to reduce the quantity of Initial Heavy Metal whose waste oxides can be accommodated in a single vitrified container.

The quantity of glass is determined by the total mass of waste oxide (including the inactive species) and its incorporation level. So far as activity is concerned, this will decay with time. At the time of vitrification the remaining active species constitute about 25% of the total fission product mass. The principal limitations imposed by activity levels are the secondary effects of heat production and dose rate.

If the quantity of oxides to be incorporated in the glass were to be limiting, the quantity of vitrified waste would only be increased by ≈7% for BWRs, ≈1.5% for PWRs and ≈2.2% for WWERs. Assuming the vitrification to be 30% of the reprocessing cost [6.1] this would then increase the reprocessing cost by ≈2.2% for BWRs, ≈0.5% for PWRs and ≈0.7% for WWERs i.e. small enough not to be reflected in the reprocessing price.

REFERENCE TO CHAPTER 6

[6.1] OECD/NEA, "The economics of the nuclear fuel cycle", 1985.

7. CONCLUSIONS

The use of burnable absorber fuel is a well established technology resulting from over 30 years of commercial utilization in BWRs. Gadolinia has emerged as the most widely used burnable absorber. Application to PWRs, BWRs and WWERs together with the trends toward increase of reactor cycle length and fuel discharge burnup have resulted in higher Gd contents being required, leading to new technical challenges. Experience has shown that these challenges can be and have been met. It has, nevertheless, also fostered the development of two alternative solutions to Gd: zirconium diboride coating and erbium.

For Gd fuel, the fuel properties, manufacturing techniques, design approaches, utilization and performance as well as potential impacts on the backend of the fuel cycle are all illustrated in this report and provide evidence of the success and the maturity of this type of fuel technology.

Gd resources are adequate to meet expanded usage in nuclear fuel. The known geological reserves and the established mining and refining capacity can cope with even huge increases of demand from the nuclear industry, since this will never exceed a few percent of the annual production of Gd for other purposes.

Many of the physical properties of Gd fuel are known with adequate precision. However, a large scatter is observed in reported measurements of thermal conductivity and melting point, two key properties affected by the presence of Gd. This is probably due, in part, to the use of different fuel manufacturing techniques.

The neutronic properties are well known but their incorporation into nuclear design methodology requires further attention, due to overlapping of certain resonances of Gd with those of U and Pu isotopes. The evolution of radial power distribution across the pellet is very different in Gd fuel compared with standard U fuel and requires a specific adaptation of the fuel rod modelling code.

The considerable number of alternatives for positioning the Gd fuel axially in the fuel rod, radially in the fuel assembly and radially in the core has been utilized by fuel vendors to meet various objectives. The flexibility this affords has resulted in quite different approaches, some of which are described in the report.

The performance of Gd fuel has been good and post-irradiation examinations have provided a database to validate the design methodology. This data base is constantly being augmented and updated to provide a better statistical validation and to cover higher performance regimes.

The backend of the fuel cycle is practically unaffected by the addition of Gd to the fuel.

It should be noted that this report represents achievements up to the period 1991-93. After a few more years, it would be useful to update the status and to compare Gd fuel with its alternatives, which by then will have achieved a greater number of reactor-years of operating experience, enabling a more useful statistical comparison to be made.

Appendix I

GADOLINIUM AND ERBIUM — A REVIEW OF RESOURCES AND SUPPLY

E. Müller-Kahle
Division of Nuclear Fuel and Waste Management,
International Atomic Energy Agency,
Vienna

1. Introduction

Gadolinium (Gd) and Erbium (Er) belong to the rare earth elements (REE). The name rare earth reflects the earthy appearance of the discovered oxides and the perception of the early discoverers that these elements were present in the earth's crust only in small quantities.

A number of REEs were discovered in geological material from the town of Ytterby, near Stockholm, Sweden by Karl Axel Arrhenius in 1787 [1]. One year later, Bengt Reinhold Geifer further investigated the rocks of Ytterby, which later were named gadolinite after Johann Gadolin of Finland, who lived between 1760 - 1852. It seems that Gadolin had separated Gd from this material, although he thought that he had found the element yttrium. From the same material that Gadolin had discarded in 1794, G.G. Mosander in 1843 discovered Er together with yttrium and terbium.

Gd and Er belong to the lanthanide series, which together with the elements scandium and yttrium constitute the REEs. Gd and Er have the atomic numbers 64 and 68 respectively. Gd belongs to the REE group with high melting and boiling points, while Er also has a high melting point but a low boiling point. Both elements belong to the "heavy" REEs, also referred to as the yttrium subgroup.

2. Industrial application of REEs

The REEs have a wide range of industrial applications in a number of sectors. An overview is given in the following table [1].

Metallurgy: alloying elements in iron, steel, superalloys, etc., and for corrosion resistant materials,

Glass: polishing compounds, radiation stabilizer, ingredient to increase refraction etc...

Ceramics: high temperature refractories, engines, metal substitutions, coatings,

Electronics: cathodes, electrodes, semiconductors, computer memories and substrates, lasers,

Chemicals: catalysts for oil refineries, chemical processing and analyses, pharmaceuticals,

Magnets: electric motors, alternators, generators, computer disk drive actuators, proton linear accelerators, headphones, speakers,

Nuclear: control rods in nuclear submarines, burnable absorbers, shielding material, reprocessing additive,

TABLE I.1. *WORLD REPORTED RESERVES OF RARE EARTHS (TONNES OF RARE EARTH OXIDE)*

Country	Reserves
North America	
U. S. A.	5 500 000
Canada	164 000
South America	
Brazil	20 000
Europe	
Finland, Norway, Sweden	450 000
Former USSR	50 000
Africa	
Burundi	1 000
Egypt	100 000
Kenya	13 000
Madagascar	50 000
Malawi	297 000
South Africa	357 000
Asia	
China	36 000 000
India	1 800 000
South Korea	45 000
Malaysia	30 000
Sri Lanka	13 000
Thailand	1 000
Oceania	
Australia	345 000
World Total (rounded)	45 236 000

Source: U. S. Bureau of Mines

Other: jewellery, paint and ink dryers, hydrogen fuel storage, refrigerant, lubricants, thermometers.

3. Resources

The available literature refers in general to the whole REE group. If available, special emphasis will be placed on Gd and Er in this paper.

The REEs are widely distributed in a variety of geological environments. The overall abundance of the REEs in the earth's crust is estimated to be of the order of 150 - 200 part per million (ppm).

Gd and Er concentrations in igneous rocks of different chemical compositions show only small variations: the Gd traces in igneous rocks ranging from basaltic to granitic composition vary from 6.2 to 7.4 ppm, with an average of 7.2 ppm. For Er these ranges are 3.6 to 4.2 ppm, with an average of 3.9 ppm [2]. Higher concentrations are found in alkaline rocks e.g. syenites, and carbonatites. For these rock types the Gd contents range from 8.7 to 79 ppm and those for Er from 3.6 to 48 ppm [2].

Mineralogically, there are a large number of minerals containing REEs. However, no mineral could be found in the literature where Gd is included in the chemical formula, while Er is contained in the chemical formula for the mineral fergusonite (Y, Er, U, Th) (Nb, Ta, Ti) O_4.

The economically important REE minerals are:

Mineral	Composition		REE content
bastnaesite:	$CeFCO_3$	max.	75 % REO *
monazite:	(Ce, Y) PO_2		65 % REO
apatite:	$(Ca,Ce)_5/(P,Si)O_4/_3(O,F)$		12 % REO
brannerite:	$(U,Ca,Fe,Y,Th)_3(Ti,Si)_5O_6$		70 % REO
gadolinite:	$(Y,Ce)_2FeBe_2Si_2O_{10}$		48 % REO
xenotime:	YPO_4		62 % REO

*** REO = Rare earth oxides**

It seems that Gd, and probably also Er, is contained in these minerals replacing some of the other REEs in the crystal lattices.

The worldwide resources of REEs, as reported and published [3], are mainly located in China (nearly 80 % of the total) and in the USA (12 %). A summary of the known resources is given in Table I.1.

Of these resources, the vast majority of over 90 % is estimated to be located in carbonatites and associated rocks, and the remainder in placers, beach sands, etc. In addition to these known resources, on which reliable information is available in the literature, there are other REE resources which cannot be classified as known resources, but rather as speculative resources.

These include, for example, a total of 100 million tons REO in China as well as the Mount Weld deposit in Western Australia with resources of 6.2 million tons REO. Also, there are a number of deposits, associated with the East African rift zone, which are not yet fully explored. Furthermore, there is a potential for REE in the large alkaline complex of Ilimaussaq in Greenland.

These examples show that the potential to increase the known resource base listed above, is good.

4. REE Production

The REE production comes essentially from the same countries which host the resources listed in Table I.1.

The latest data [3] refer to the 1989 production of 50 000 t REO, distributed as follows:

Australia:	7 200 t REO
Brazil:	1 100 t REO
Canada:	100 t REO
China:	20 000 t REO
India:	2 200 t REO
Malaysia:	3 300 t REO
Thailand:	800 t REO
USA:	14 000 t REO
former USSR:	1 500 t REO
Others:	100 t REO

Past REE productions are available from two sources for different periods and areas (WOCA /non-WOCA): 1981 and 1982 for WOCA [4], 1983 and 1984 for WOCA + non WOCA = world by the same author, and for 1986 - 1990 for the world in [3]. The respective data for these years and areas are:

1981	28 535 t REO (WOCA only)
1982	28 340 t REO (WOCA only)
1983	36 000 t REO (world)
1984	50 000 t REO (world)
1985	not available
1986	38 750 t REO (world)

1987	44 470 t REO (world)
1988	46 000 t REO (world)
1989	50 000 t REO (world)

The most important REE production centres in hard rock environments are Molycorp's bastnaesite Mountain Pass mine in California, USA and the Baotou mine at Bayan Obo, Inner Mongolia, China. Both producers account for over two thirds of the 1989 world production. A small amount of REE, mostly yttrium is retrieved as a byproduct from U mining in Canada's Elliot Lake district. As U mining in this area is ceasing, it is expected that the yttrium recovery will also be terminated.

The remainder of the REE production is issued from beach placer deposits in Australia (East and West coasts), Brazil, India, and South Africa, although the Palabora mine recovers monazite from carbonatite. The production in Malaysia and Thailand comes from tin mining tailings, and consists mainly of monazite and xenotime.

Specific production data for Gd and Er are not available. In order to provide reasonable estimates, the Gd and Er content of the most important source minerals are given below expressed as % of total REO [5]:

	Gd	Er
bastnaesite	0.35	0.01
monazite	5.00	0.22
xenotime	4.00	5.40

The 1986 production is estimated to include about 22 000 t bastnaesite, 30 000 t monazite and 250 t xenotime. Using the above contents, this production amounts to about 1 300 t Gd and 75 t Er.

Using the average Gd and Er contents of over 3.5 million t REO evaluated in [4] in 1986 and applying them to the total production of 50 000 t REO reported at the beginning of this chapter, the Gd and Er contents are estimated as 500 t and 50 t respectively. Based on these two approaches, it is estimated that the total Gd and Er productions are about 500 - 1 300 t/a and 50 - 75 t/a respectively.

5. Suppliers of REEs

The suppliers of REEs in their different forms i.e. concentrates or REE as metals can be divided into three groups: suppliers of concentrates, vertically integrated concentrate producers with subsequent processing facilities and finally the processors, which process purchased concentrates.

The most important suppliers of concentrates are Allied Eneabba Ltd. and Associated Minerals Consolidated Ltd., which mine beach sand deposits in Australia. Other, less important, producers are located in Thailand, Sri Lanka, South Africa, etc.

The Molycorp., Inc. operator of the mountain Pass mine in California and processing facilities in Washington and York, Pennsylvania, and the Baotou Iron & Steel

Co. in China are the largest integrated REE suppliers. Also in China is the Ganija Rare Earths Corp., a partnership between the Canadian Pacific Rare Earths & Metal Corp. and the Ganzhou Metallurgical Industries Corp., which produces concentrates and processes them to REO. The 1987 production was reported [5] to include nearly 5 t Gd oxides. In Japan, there are two processors with foreign raw material sources: Mitsubishi Chemical Industries Ltd., which has a joint venture with the Malaysian producer Beh Minerals, and Shin-Etsu Chemical Co. Ltd., which participates (or participated) with Denison and Molycorp in the recovery of yttrium from the Elliot Lake uranium mine in Ontario, Canada. Other integrated suppliers are in Brazil (Nuclemon) and India (Indian Rare Earths Ltd.) which recovers Th in addition to the REE, including Gd.

The most significant REE processor is Rhone-Poulenc, France, with worldwide interests. Its main plants are located in La Rochelle, France and Freeport, Texas, USA. In addition there are a number of Japanese processors which import raw material mainly from China.

6. Market

The REE market is experiencing profound changes due to the declining demand in certain "traditional" areas and the demand growth in new fields. The two main areas where the REE demand has decreased are the petroleum and the metallurgical industries. In the petroleum industry, REEs are mainly used as catalysts for the cracking of leaded gasoline, which in many countries is being replaced by unleaded gasoline, while in the steel industry the use of high strength steels for pipelines and oil drilling pipes has decreased over the past years.

In a broad sense, there is a compensation for the above decline, through the increase in REE demand in new fields such as magnets (neodymium, dysprosium), automotive catalysts (yttrium, cerium), additives for phosphors in colour TV and computer screens (yttrium and gadolinium) and superconductors (1-2-3 compounds: 1 atom REE, 2 atoms barium and three atoms of copper).

The main current markets (year was not specified) for REEs are the USA and Japan. As shown below each REE has different uses [3]. As a result the demand differs between REEs:

USA:	Petroleum catalysts	53% of demand
	metallurgical additives	22% "
	ceramics and glass	18% "
	electronics, phosphors, magnets etc.	7% "
Japan:	glass and ceramics	70% of demand
	magnets	19% "
	phosphors	6% "
	petroleum catalyst & metallurgical additives	5% "

These different trends are also reflected in the demand data for the USA and Japan available for the period 1983 - 1987 [5]:

1983	1984	1985	1986	1987
USA[1]				
19 600[2]	21 400	12 100	11 800	9 400
Japan				
3 870	4 840	5 450	5 675	5 710[3]

[1] Estimate
[2] Tonnes REO
[3] Includes an estimated 850 t materials for RE magnets.

Details on the composition of the above demand data are not available. However, judging from the end uses, it can be assumed that the US demand is mainly for the "light" REEs, comprising the first seven elements of the series (lanthanum - europium), while the Japanese demand is mainly for the "heavy" REE (gadolinium - lutetium plus yttrium), whose projected growth rate is estimated at 15 % p/year.

REEs including Gd (no information on Er) have been traded since 1988 on the Industrial Metal Exchange (IME). Recent prices for Gd or Er are not available. An indication of the approximate Gd price is a reference in [5], where the price range for 99.99% pure Gd from Molycorp's refineries is quoted as 65.00 - 70.00 USD/lb.

REFERENCES TO APPENDIX I

[1] MORRAL, F.R., A history of the rare earth elements, CIM Bulletin, November 1990.

[2] WEDEPOHL, H., Handbook of Geochemistry, Springer, Heidelberg, 1978.

[3] SPOONER, J., GRACE, K.A., ROBJOHNS, N., The economics of the rare earth elements, CIM Bulletin, 1991.

[4] ANSTETT, T.F., Availability of rare earth, yttrium, and related thorium oxides - market economy countries, a minerals availability appraisal; U.S. Bureau of Mines, Information Circular 9111, Washington, D.C. 1986.

[5] O'DRISCOLL, M., Rare earth, Enter the dragon, Industrial Minerals, November 1988.

Appendix II

GADOLINIA FUEL UTILIZATION IN FRANCE

This Appendix provides further details of French experience with Gd fuel as summarized in Chapter 5.

Table II.1 gives details of reload characteristics (cycle lengths, numbers of GD FRs etc.) for all plants for which FRAGEMA has supplied Gd fuel, as summarized in Section 5.1.2. Figure II.1 provides details of the core loading patterns for IN-OUT fuel management with Gd FRs in peripheral locations.

Table II.2 provides details of the results of comparisons of predictions with measurements of core physics parameters. These are referred to in Section 5.2.2.1. Figure II.2 provides a graphical representation of measured and predicted FA power evolutions, as also mentioned in Section 5.2.2.1.

TABLE II.1. FRAGEMA'S GADOLINIUM EXPERIENCE IN POWER REACTORS

Date (beginning of cycle) Plant/cycle	Reload's characteristics	Cycle length (MWd/t) stretch included	Positioning scheme of U/Gd rods	Number of U/Gd rods
1983				
Gravelines 2 Cycle 3	52 assemblies (E = 3.25 w/o) (8 Gd-bearing assemblies)	11020	mid-assembly	96
1984				
Gravelines 2 Cycle 4	64 assemblies (E = 3.45 w/o) (36 Gd-bearing assemblies)	13820	mid-assembly	288
Tricastin 3 Cycle 4	64 assemblies (E = 3.45 w/o) (24 Gd-bearing assemblies)	15050	mid-assembly	288
Gravelines 5 Cycle 1	1st core (24 Gd-bearing assemblies)	14925	mid-assembly	352
1985				
Gravelines 2 Cycle 5	64 assemblies (E = 3.45 w/o) (36 Gd-bearing assemblies)	15330	mid-assembly	288
1986				
Tricastin 3 Cycle 5	52 assemblies (E = 3.70 w/o) (16 Gd-bearing assemblies)	12035	mid-assembly	128

TABLE II.1 (cont.)

1986				
Gravelines 1 Cycle 6	52 assemblies (E = 3.70 w/o) (16 Gd-bearing assemblies)	13590	mid-assembly	128
Chinon B1 Cycle 4	52 assemblies (E = 3.70 w/o) (16 Gd-bearing assemblies)	13360	peripheral	128
Ringhals 4 Cycle 4	32 assemblies (E = 3.40 w/o) (8 Gd-bearing assemblies) 8 assemblies (E = 3.10 w/o)	10380	peripheral	96
1987				
Chinon B1 Cycle 5	52 assemblies (E = 3.70 w/o) (16 Gd-bearing assemblies)	14055	mid-assembly	128
Ringhals 4 Cycle 5	48 assemblies (E = 3.40 w/o) (16 Gd-bearing assemblies)	11920	peripheral	128
Tihange 2 Cycle 5	48 assemblies (E = 3.80 w/o) (16 Gd-bearing assemblies)	12390	mid-assembly	128
1988				
Gravelines 1 Cycle 7	52 assemblies (E = 3.70 w/o) (16 Gd-bearing assemblies)	13890	mid-assembly	128
Ringhals 4 Cycle 6	32 assemblies (E = 3.50 w/o) (20 Gd-bearing assemblies) 8 assemblies (E = 3.40 w/o)	9508	peripheral	160
Tihange 2 Cycle 6	52 assemblies (E = 3.80 w/o) (16 Gd-bearing assemblies)	13800	mid-assembly	128
Tihange 3 Cycle 4	52 assemblies (E = 3.80 w/o) (16 Gd-bearing assemblies)	11800	mid-assembly	128

TABLE II.1 (cont.)

1989				
Ringhals 4 Cycle 7	44 assemblies (E = 3.50 w/o) (24 Gd-bearing assemblies)	11700	peripheral	192
Ringhals 3 Cycle 7	32 assemblies (E = 3.50 w/o) (12 Gd-bearing assemblies)	9950	peripheral	96
Tihange 2 Cycle 7	52 assemblies (E = 3.80 w/o) (12 Gd-bearing assemblies)	13510	mid-assembly	128
Tihange 3 Cycle 5	52 assemblies (E = 3.80 w/o) (16 Gd-bearing assemblies)	14190	mid-assembly	128
1990				
Ringhals 4 Cycle 8	37 assemblies (E = 3.50 w/o) (16 Gd-bearing assemblies)	11860	peripheral	128
Ringhals 3 Cycle 8	32 assemblies (E = 3.50 w/o) (8 Gd-bearing assemblies)	10240	peripheral	64
Tihange 2 Cycle 8	52 assemblies (E = 3.50 w/o) (16 Gd-bearing assemblies)	11025*	mid-assembly	128
Tihange 3 Cycle 6	52 assemblies (E = 3.80 w/o) (16 Gd-bearing assemblies)	12500*	mid-assembly	128

* natural cycle length

TABLE II.1 (cont.)

1991				
Ringhals 4 Cycle 9	48 assemblies (E = 3.50 w/o) (28 Gd-bearing assemblies)	11430	peripheral	224
Ringhals 3 Cycle 9	36 assemblies (E = 3.50 w/o) (12 Gd-bearing assemblies)	10310	peripheral	96
Tihange 2 Cycle 9	52 assemblies (E = 3.80 w/o) (16 Gd-bearing assemblies)	15250	mid-assembly	128
Tihange 3 Cycle 7	52 assemblies (E = 3.80 w/o) (16 Gd-bearing assemblies)		mid-assembly	128
1992				
KKP2 Cycle 8	4 demo assemblies (E = 3.48 w/o)	11300	mid-assembly	32
KBR Cycle 6	8 demo assemblies (E = 3.95 w/o) Uranium matrix 2.3 w/o axially truncated Gd rods		mid-assembly	64
Ringhals 3 Cycle 10	32 assemblies (E = 3.60 w/o) (20 Gd-bearing assemblies) 12 assemblies (E = 3.50 w/o) (4 Gd-bearing assemblies)	11372	peripheral	192
Ringhals 4 Cycle 10	28 assemblies (E = 3.60 w/o) (20 Gd-bearing assemblies) 12 assemblies (E = 3.50 w/o)	11122	peripheral	160
Tihange 2 Cycle 10	52 assemblies (E = 3.80 w/o) (16 Gd-bearing assemblies)		peripheral	128
1993				
Ringhals 3 Cycle 11	36 assemblies (E = 3.60 w/o) (16 Gd-bearing assemblies)		peripheral	128
Ringhals 4 Cycle 11	36 assemblies (E = 3.60 w/o) (16 Gd-bearing assemblies)		peripheral	128
KKP Cycle 9	4 assemblies (E = 3.48 w/o) Uranium matrix 2.3 w/o Axially truncated Gd rods		mid-assembly	32

TABLE II.2. RINGHALS 4 — CYCLE 11

CORE PHYSICS TEST RESULTS

PARAMETER	CONTROL ROD CONFIGURATION	RESULTS		DIFFERENCE (C - M)	CRITERIA
		MEASUREMENT	CALCULATION		
Critical boron concentrations (BOL - HZP)	ARO Din D + Cin	1496 ppm 1360 ppm 1188 ppm	1499 ppm 1359 ppm 1191 ppm	+ 3 ppm - 1 ppm + 3 ppm	50 ppm
Isothermal temperature coefficient (BOL - HZP)	ARO	- 10.5 pcm/°C	- 9.5 pcm/°C	+ 1.0 pcm/°C	5.4 pcm/°C

CYCLE LENGTH COMPARISONS

CYCLE		NATURAL CYCLE LENGTH AT 0 PPM (MWd/tU)		DIFFERENCE (C - M) (MWd/tU)
		MEASUREMENT	CALCULATION	
RINGHALS 4	CYCLE 10	9976	10164	+ 188
RINGHALS 3	CYCLE 10	10459	10561	+ 102
	CYCLE 11	9523	9729	+ 206

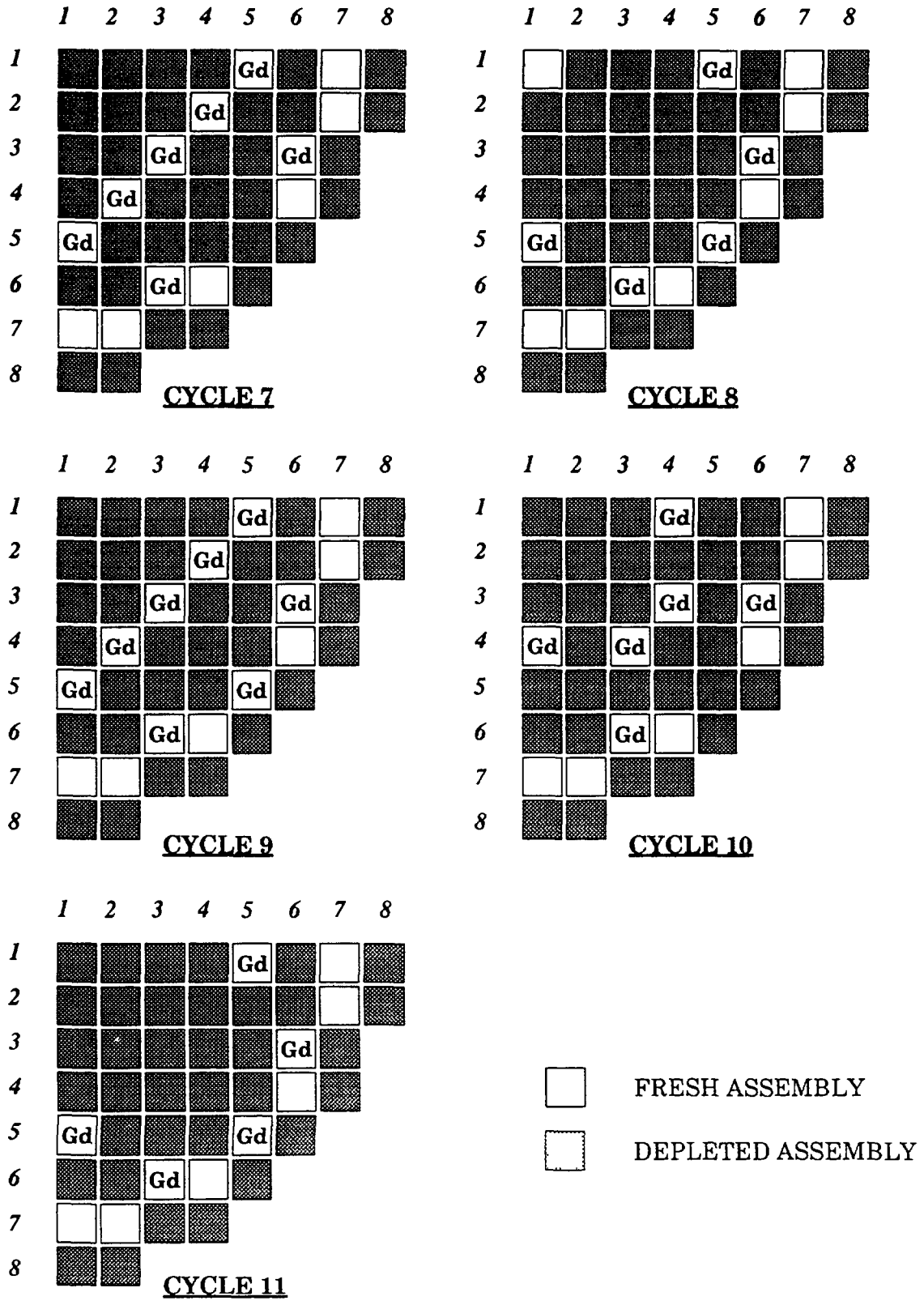

Fig. II.1. *Ringhals 4 — Core loading patterns with fresh assembly locations*

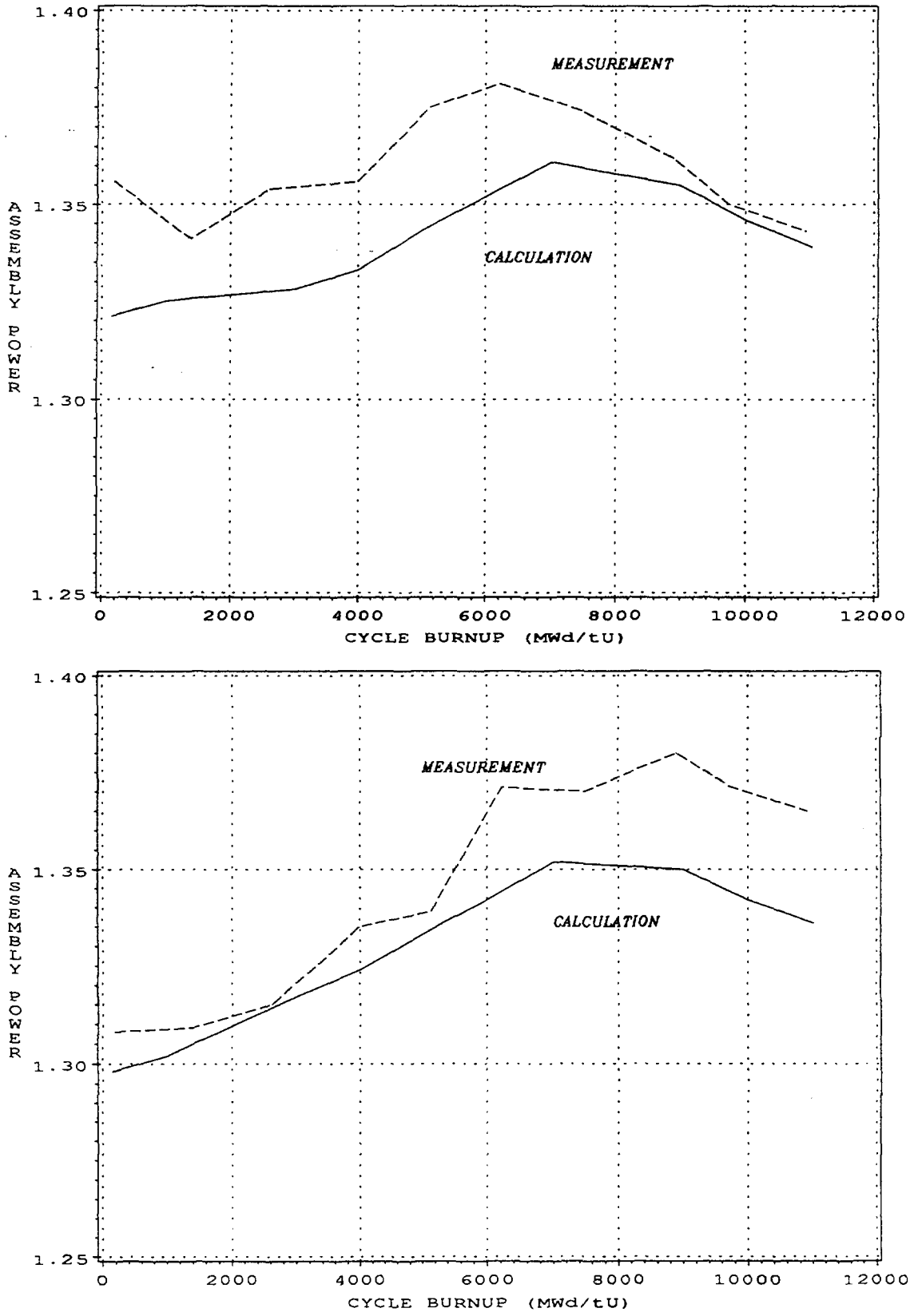

Fig. II.2. *Ringhals 4 – cycle 9. Power evolution of two GD FAs*

Appendix III

GADOLINIA FUEL UTILIZATION IN JAPAN

This Appendix provides further details of the experience with Gd in Japan, as summarized in Chapter 5.

III.1. *Gd fuel development and utilization*

Table III.1 shows the historical development of Japanese BWR design from 7 x 7 to the present day 8 x 8 BJ design, giving key parameters of each design. This is referred to in Section 5.1.4.

Figures III.1-2 show the geometrical arrangement of the latest 8 x 8 BWR assembly design; Figure III.3 shows the geometrical arrangement of a 17 x 17 PWR design.

Table III.2 gives a breakdown of test reactor irradiation details for Japanese PWR Gd FRs. Table III.3 provides corresponding details for the commercial irradiation of Gd FRs and FAs in both PWRs and BWRs. These are referred to in Section 5.1.4.

Tables III.4-6 give typical fuel loading schemes for 4 loop, 2 loop and 3 loop PWRs respectively.

Typical core loading patterns for the equilibrium cycle of a Japanese 4 loop, 2 loop and 3 loop plants are shown in Figures III.4, III.8 and III.12 respectively. Corresponding critical boron curves are shown in Figures III.5, III.9 and III.13 respectively, radial power distributions are shown in Figures III.6, III.10 and III.14 respectively, and corresponding graphs of F_{xy} vs burnup are shown in Figures III.7, III.11 and III.15 respectively. These are referred to in Section 5.1.4.

Startup test measurements, and comparisons with predictions for Gd fuel loaded in Mihama and Ohi (Table III.7)are given in Table III.8. Figures III.16 and III.17 provide a graphical representation of the comparisons of critical boron concentration and assembly power. These are referred to in Section 5.2.2.2.

Figures III.18 and III.19 give axial gamma scanning and radial micro gamma scanning plots respectively, as observed in the hot cell examinations referred to in Section 5.2.3.

PIE results, covered in Section 5.3, are shown in Figures III.20 - III.23.

III.2. Safety tests

The behaviour under reactivity initiated accidents, corresponding to the experimental test matrix carried out in the NSRR and the test results, summarized in Section 5.4, are detailed further below:

Test Fuel

Three types of PWR FRs were used for the experiment as shown in Table III.9 and Fig. III.24. The fuel design is the same as that of commercial PWR fuel except for the length, the fuel enrichment and the Gd isotopic composition.

Irradiation Condition

NSRR is a swimming pool type thermal neutron pulse reactor. The core consists of 149 fuel rods, 3 transient rods, 6 regulating rods and 2 safety rods as shown in Fig. III.25. The pulse power is generated by rapidly withdrawing transient rods. The maximum available reactivity is 4.7$. Fig. III.26 shows a typical shape of pulse power of 4.67$ reactivity, which generates 21100 MW peak power, 117 MWs integrated power and 4.4ms pulse width.

Test Results

Table III.10 summarizes the test results. Typical fuel failures are shown in Fig. III.27. Fuel rod failure thresholds derived from the results are shown in Table III.11. The cladding deformation as a function of energy deposition is given in Fig. III.28.

Table Ⅲ.1 Typical BWR Fuel Design

Fuel Type	7×7	Adv. 7×7	8×8	8×8 RJ	8×8 BJ
Max. linear heat rate (kW/m)	57.4	60.7	44.0	44.0	44.0
Avg. Discharge Burnup (MWd/t)	21,500	27,500	27,500	29,500	33,000
Pellet					
Material	UO_2	UO_2 UO_2-Gd_2O_3	UO_2 UO_2-Gd_2O_3	UO_2 UO_2-Gd_2O_3	UO_2 UO_2-Gd_2O_3
Diameter (mm)	12.4	12.1	10.6	10.3	10.3
Height (mm)	22	12	11	11	11
Stack Length (mm)	3,660	3,660	3,710	3,710	3,710
Cladding					
Material	Zr-2	Zr-2	Zr-2	Zr-2	Zr lined Zr-2
Diam (mm)	14.3	14.3	12.5	12.3	12.3
Thickness (mm)	0.81	0.94	0.86	0.86	0.86
Liner Tickness (mm)	—	—	—	—	~0.1
Fuel Assembly					
Number of Fuel Rods	49	49	63	62	62
Number of Water Rods	0	0	1	2	2
Beginning of Commercial Use	Early 1970's	Mid of 1990's	End of 1970's	Early 1980's	End of 1980's

Table Ⅲ.2 Test Reactor Irradiation (As of mid.'91)

Reactor Name	Type	Gd_2O_3 content (wt%)	Number of Gd Fuel Rods	Irradiation Period	Burn-up (FR av)	Fuel Rod Fabricator	PIE	Power Ramp	Note
HBWR (Halden Reactor)	17×17 short rod	6	1	'84 Feb~'85 Aug	7GWd/t	Mitsubishi	NDT DT	None	
HBWR (Halden Reactor)	17×17 short rod	10	1	90 Jun~	10GWd/t	Mitsubishi	NDT DT	None	
BR-3	17×17 short rod	6	4	'84 Jul~'85 Nov '84 Jul~ 87 Jun	10GWd/t 27GWd/t	Mitsubishi	NDT DT	One rod	GAIN
BR-3	17×17 short rod	10	2	'86 Jul~ 87 Jun	12GWd/t	Mitsubishi	NDT DT	One rod	
BR-3 ↓ R-2	17×17 short rod	10	1	'86 Jul~ 87 Jun '89 Aug~	~60GWd/t	Mitsubishi	(NDT) (DT)	——	
NSRR	17×17 short rod	6	10	'83 Dec~'84 Sep	unirradiated	Mitsubishi	NDT DT	10 rods	
HBWR	17×17 short rod	6	1	'84 Feb~'85 Aug	7GWd/t	NFI	NDT DT	NONE	
BR-3	17×17 short rod	6	4	'84 Jul~ 85 Nov '84 Jul~'87 Jun	8GWd/t 26GWd/t	NFI	NDT DT	ONE ROD	GAIN
BR-3	17×17 short rod	10	4	'86 Jul~'87 Jun	13GWd/t	NFI	NDT DT	ONE ROD	
BR-3 ↓ R-2	17×17 short rod	10	1	'89 Apr~	~40GWd/t	NFI	(NDT) (DT)	——	
BR-3 ↓ DR-3	17×17 short rod	10	1	'90 Sept (3day)	——	NFI	NDT	——	

Table Ⅲ.3 Commercial Reactor Irradiation (As of mid.'91)

Fuel Type	Irradiation	Supplier	Max. Burnup (GWd/t)	Disharged and In Use	
				Number of FAs	Number of Gd Rods
PWR 14×14 10ft	1988-up to date	Mitsubishi	24	16	192
PWR 14×14 12ft	1990-up to date	Mitsubishi	6	8	96
PWR 15×15	1989-up to date	Mitsubishi	17	52	832
PWR 17×17	1984-up to date	Mitsubishi	33	224*	3584
PWR 14×14	1989-up to date	NFI	19	28	336
PWR 15×15	1991-up to date	NFI	3	28	448
PWR 17×17	1984-up to date	NFI	33	100*	1600
PWR 8×8	1978-up to date	NFI	38	2768	19480

* Including 4 LTAs

Fuel Type	Irradiation	Supplier	Max. Burnup (GWd/t)	Discharged and In-Use	
				No. of Assy	No. of Gd Rods
BWR 7×7	1975～1982	Hitachi	28	560	2300
BWR 8×8	1977～	Hitachi	38	6900	38200

Table Ⅲ.4 Typical Fuel Loading Scheme (4 loop PWR)

·Fuel Type ·····17×17
·Cycle Length ·····12months
·Fuel ^{235}U Enrichment ·····3.4wt%

Region	Cycle / Enrichment	N−1 Load	N−1 Discharge	N Load	N Discharge	N+1 Load	N+1 Discharge
N−3	3.4wt%+Gd*	1	1				
	3.4wt%	16	16				
N−2	3.4wt%+Gd*	60	59	1	1		
	3.4wt%	28	12	16	16		
N−1	3.4wt%+Gd*	60	0	60	59	1	1
	3.4wt%	28	0	28	12	16	16
N	3.4wt%+Gd*			60	0	60	59
	3.4wt%			28	0	28	12
N+1	3.4wt%+Gd*					60	0
	3.4wt%					28	0
Cycle Burnup (MWd/t)		14200		14200		14200	
Critical Boron conc at BOC (ppm)		1390		1390		1390	
Number of Fresh Gd Fuel Rods		960		960		960	

*A Fuel Assembly Contains 16 rods of 1.9 wt%U235-6wt%Gd_2O_3

Table Ⅲ.5 Typical Fuel Loading Scheme (2 loop PWR)

·Fuel Type ·····14×14
·Cycle Length ·····12months
·Fuel ^{235}U Enrichment ·····3.5wt%

Region	Cycle / Enrichment	N−1 Load	N−1 Discharge	N Load	N Discharge	N+1 Load	N+1 Discharge
N−4	3.5wt%+Gd*	1	1				
N−3	3.5wt%+Gd*	12	12				
	3.5wt%	28	27	1	1		
N−2	3.5wt%+Gd*	12	0	12	12		
	3.5wt%	28	0	28	27	1	1
N−1	3.5wt%+Gd*	12	0	12	0	12	12
	3.5wt%	28	0	28	0	28	27
N	3.5wt%+Gd*			12	0	12	0
	3.5wt%			28	0	28	0
N+1	3.5wt%+Gd*					12	0
	3.5wt%					28	0
Cycle Burnup (MWd/t)		11100		11100		11100	
Critical Boron conc at BOC (ppm)		1451		1451		1451	
Number of Fresh Gd Fuel Rods		144		144		144	

*A Fuel Assembly Contains 12 rods of 2.0 wt%U235-6wt%Gd_2O_3

Table Ⅲ.6 Typical Fuel Loading Scheme (3 loop PWR)

·Fuel Type ·····15×15
·Cycle Length ·····12months
·Fuel ^{235}U Enrichment ·····3.4wt%

Region	Cycle / Enrichment	N−1 Load	N−1 Discharge	N Load	N Discharge	N+1 Load	N+1 Discharge
N−3	3.4wt%+Gd*	17	17				
	3.4wt%	20	20				
N−2	3.4wt%+Gd*	40	23	17	17		
	3.4wt%	20	0	20	20		
N−1	3.4wt%+Gd*	40	0	40	23	17	17
	3.4wt%	20	0	20	0	20	20
N	3.4wt%+Gd*			40	0	40	23
	3.4wt%			20	0	20	0
N+1	3.4wt%+Gd*					40	0
	3.4wt%					20	0
Cycle Burnup (MWd/t)		12300		12300		12300	
Critical Boron conc at BOC (ppm)		1112		1112		1112	
Number of Fresh Gd Fuel Rods		640		640		640	

*A Fuel Assembly Contains 16 rods of 1.9 wt%U235-6wt%Gd_2O_3

TABLE III.7. EXAMPLE OF COMMERCIAL USE OF GADOLINIA FUEL ASSEMBLY

	MIHAMA Unit 1 Cycle 7	OHI Unit 1 Cycle 8	OHI Unit 2 Cycle 8
No. of Loops	2	4	4
Fuel Assembly			
Total No.	121	193	193
Type	14×14	17×17	17×17
Criticality Date	1988.4.18	1988.6.15	1988.11.30
UO_2 Assembly No.	28	48	72
Enrichment (wt %)	3.2	3.4	3.4
Gadolinia Assembly No.	8	32	32
Gadolinia Rod No./FA	12	16	16
Enrichment (wt %)	1.7	1.9	1.9
MOX Assembly No.	4	—	—
PuO_2 Enrichment (wt %)	3.8	—	—

TABLE III.8. STARTUP PHYSICS TEST RESULTS IN OPERATING PLANT WITH MANY GADOLINIA FUEL ASSEMBLIES

Test Item	MIHAMA Unit 1 Cycle 7	OHI Unit 1 Cycle 8	OHI Unit 2 Cycle 8
Critical Boron Concentration Difference (ppm) (M−P)	ARO −4 Bin −5	ARO −18 Din −18	ARO −11 Din −14
Minimum Shutdown Margin:Boron Concentration Difference (ppm)	4	−10	19
MTC Difference (pcm/°C)	−1.3	−2.8	−0.1
Rod Worth Difference (%) (M-P)/P×100	Bank B −6.8 Bank A −7.5	Bank D 1.5 Bank C −7.1	Bank D 1.1 Bank C −3.8
Boron Worth Difference (%) (M-P)/P×100	ARO ↓ Bin −7.4	ARO ↓ Din 5.3	ARO ↓ Din −1.3
Power Distribution Difference (HZP, ARO)	Max. Error (P>1.0) 6.0 −3.8 1/4 Core Power Tilt 0.7 0.5		6.0 1.0

Table Ⅲ.9 Summary of test fuel rod specifications

Test No.		510	511	512
Item	Fuel Type	U fuel	Gd Fuel	U fuel
		17×17 PWR Type		14×14 PWR Type
Pellet	Diameter (mm)	8.19		9.29
	Length (mm)	13.5		10.0
	U Enrichment (%)	20.0		20.0
	End Shape	dished unchamfered		chamfered
	%Gd	0	~6	0
	Gd^{160} Enrichment (w/o)	———	~98.6	———
Cladding	Material	Zircaloy-4		
	Outer Diameter (mm)	9.50		10.72
	Thickness (mm)	0.572		0.62
Fuel Rod	Fuel Stack Length (mm)	~80		
	Fill Gas	1 atm.He		
	Gap Width (mm)	0.083		0.095

Table Ⅲ.10 Summary of test reslts

Test No.	Fuel Type	Energy Deposition ($cal/g.UO_2$)	Failure or No Failure				Post-test Fuel Rod Appearance
			No Failure	Failure			
				Chack	Fracture	Frag-mentation	
510 −1	17×17	252	○				Uniform oxidation
−3	PWR Type	264		○			Circumferential cracks
−2	UO_2	276		○			Circumferential cracks
511 −1		232	○				Uniform oxidation
−3		265	○				Oxidation, Slight bending
−4	17×17	275		○			Circumferential cracks
−2	PWR Type	293			○		Fracture into three pieces
−7	Gd_2O_3-UO_2	351			○		Fracture into many pieces
−6		386				○	Fragmentation
−5		443				○	Fragmentation
512 −2	14×14	217	○				Uniform oxidation
−3	PWR Type	232	○				Uniform oxidation
−1	UO_2	246		○			Circumferential cracks

Table Ⅲ.11 Fuel rod failure thresholds

Test Series	Fuel Rod Type	Threshold Energy
510	17 ×17 PWR Type UO_2 fuel rod	252 ～264 cal/g.UO_2
511	17 ×17 PWR Type Gd_2O_3-UO_2 fuel rod	265 ～275 cal/g.UO_2
512	14 ×14 PWR Type UO_2 fuel rod	232 ～246 cal/g.UO_2

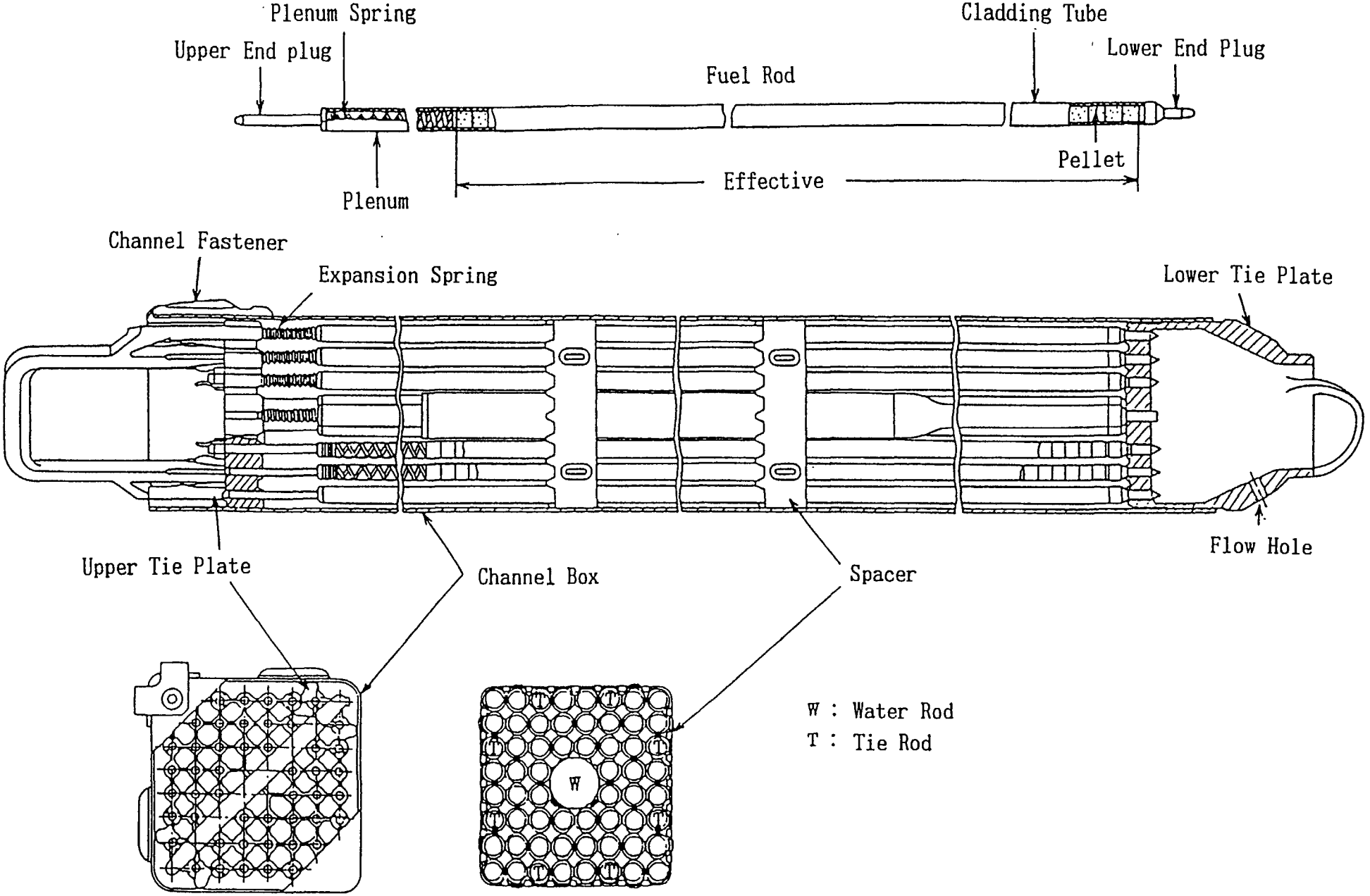

Fig. III.1. *Latest BWR fuel design (high burnup 8 x 8)*

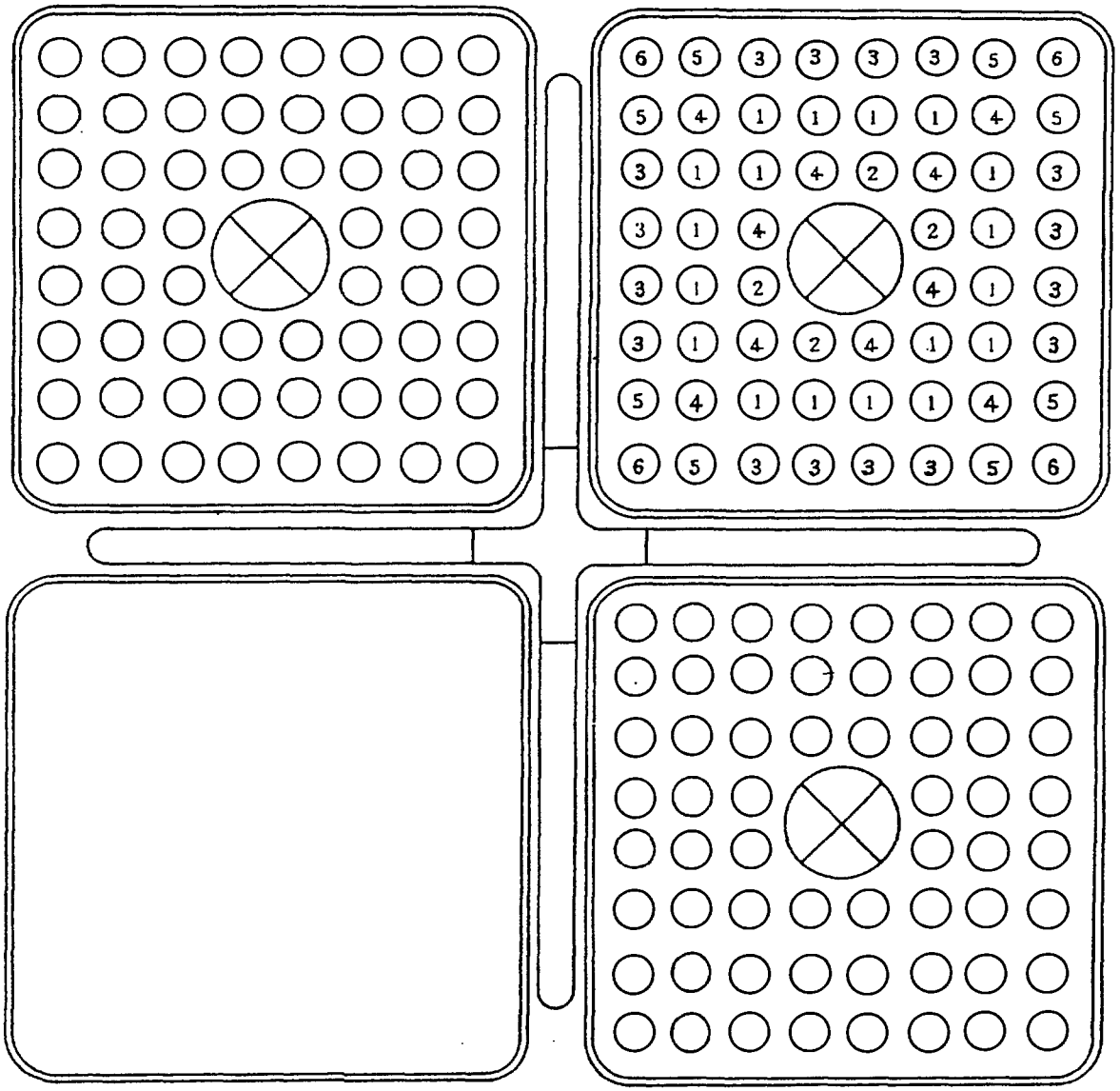

① Highest Enrichment

⑥ Lowest Enrichment

②~⑤ Enrichment decreases as number increases

⊗ Water Rod

Fig. III.2. *Typical rod array of BWR fuel (high burnup 8 x 8)*

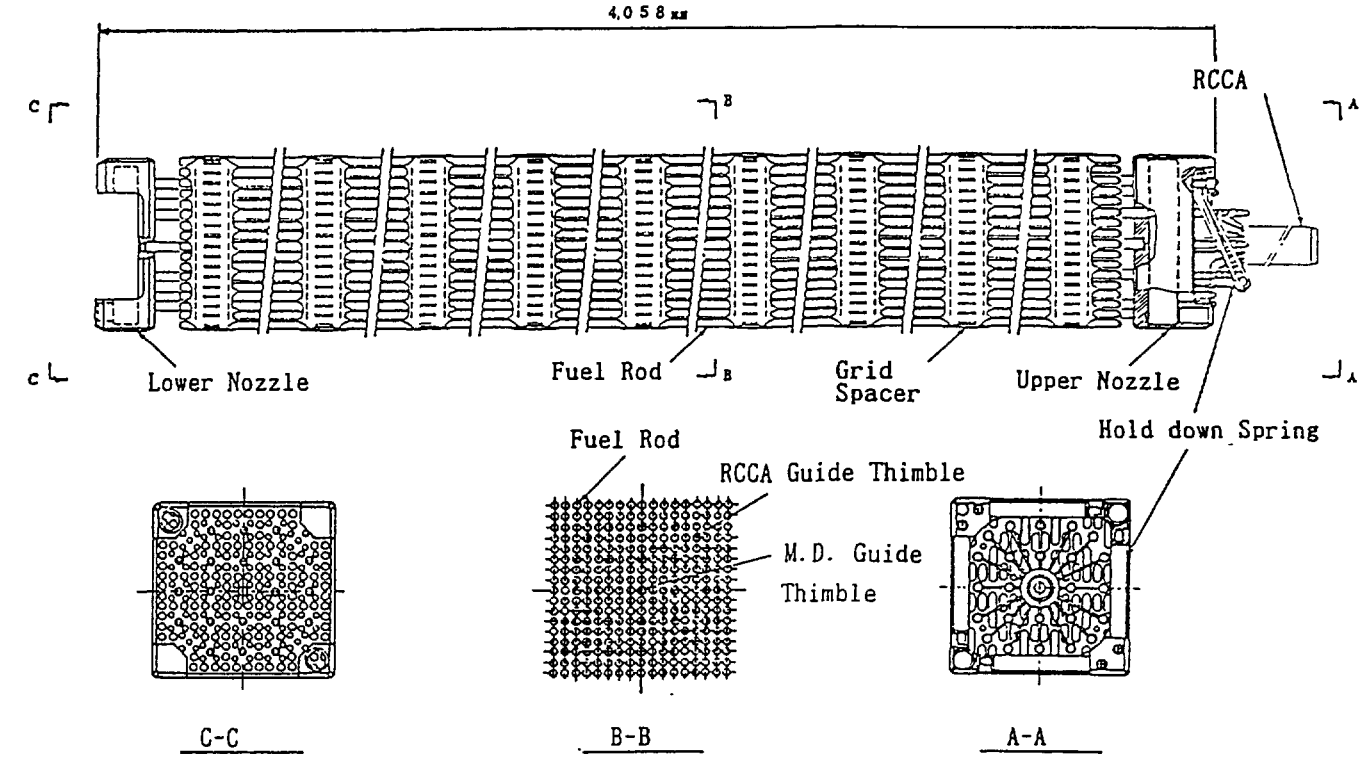

17×17 A-Type Fuel

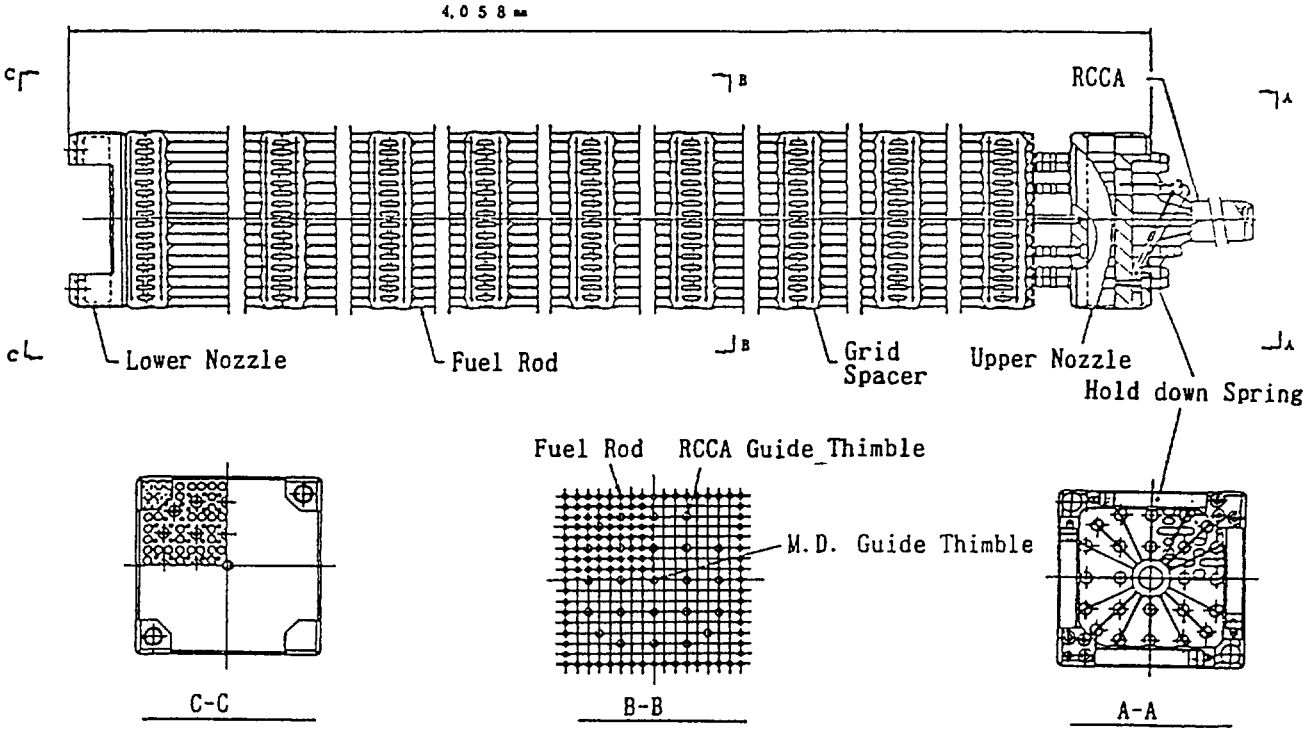

17×17 B-Type Fuel

Fig. III.3. *17 x 17 type PWR fuels*

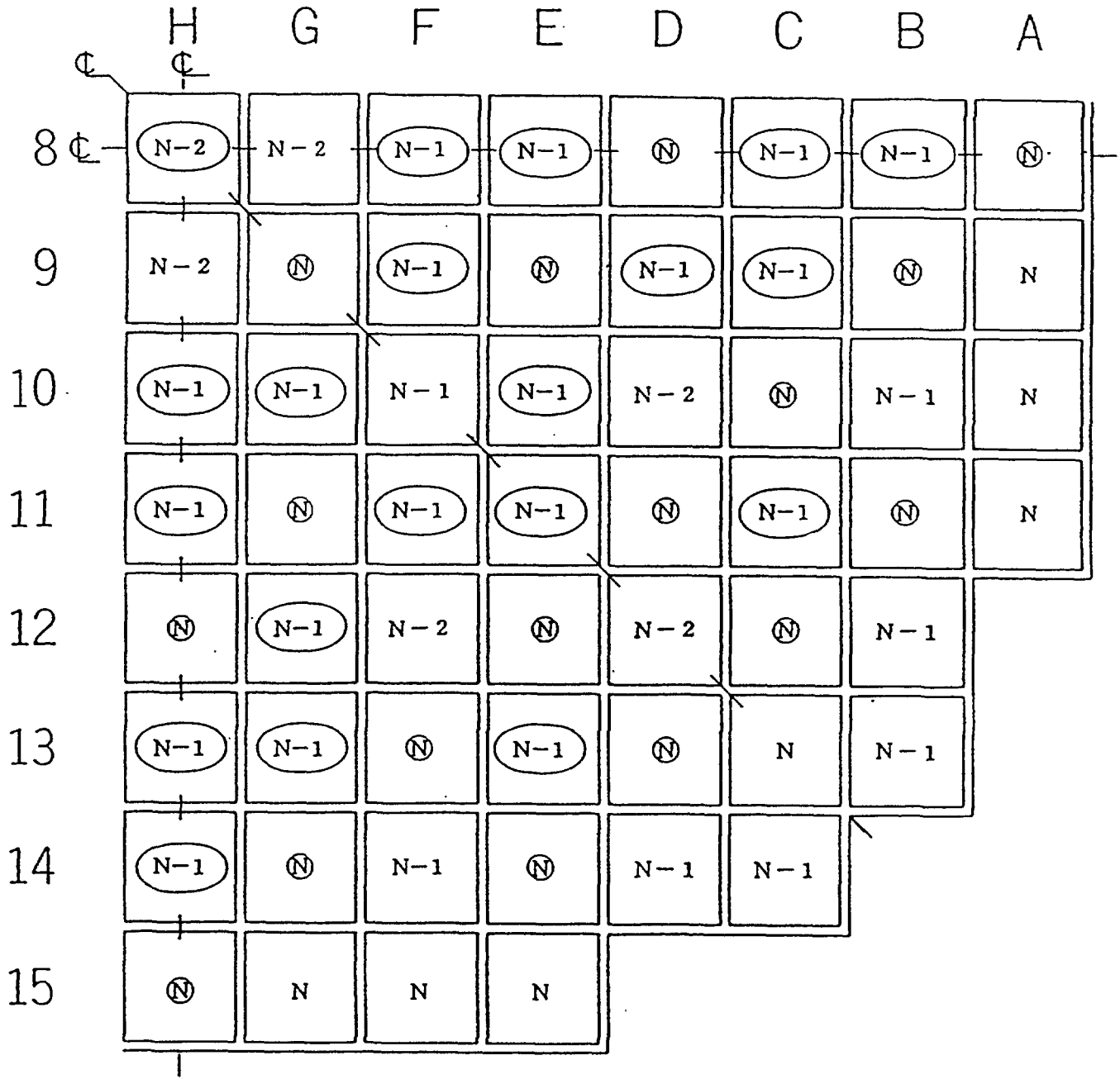

Mark	Region Number	Number of Ass'y
(N-2)	12A (3.4wt%+Gd*)	1 (Twice Burned)
N-2	12B (3.4wt%)	16 (Twice Burned)
(N-1)	13A (3.4wt%+Gd*)	60 (Once Burned)
N-1	13B (3.4wt%)	28 (Once Burned)
N	14A (3.4wt%+Gd*)	60 (Fresh Fuel)
N	14B (3.4wt%)	28 (Fresh Fuel)

*A Fuel Assembly contains 16 FRs of 1.9w/o U235 - 6w/o Gd2O3

Fig. III.4. *Fuel loading pattern*
Equilibrium cycle of 4 loop Gd fuel core

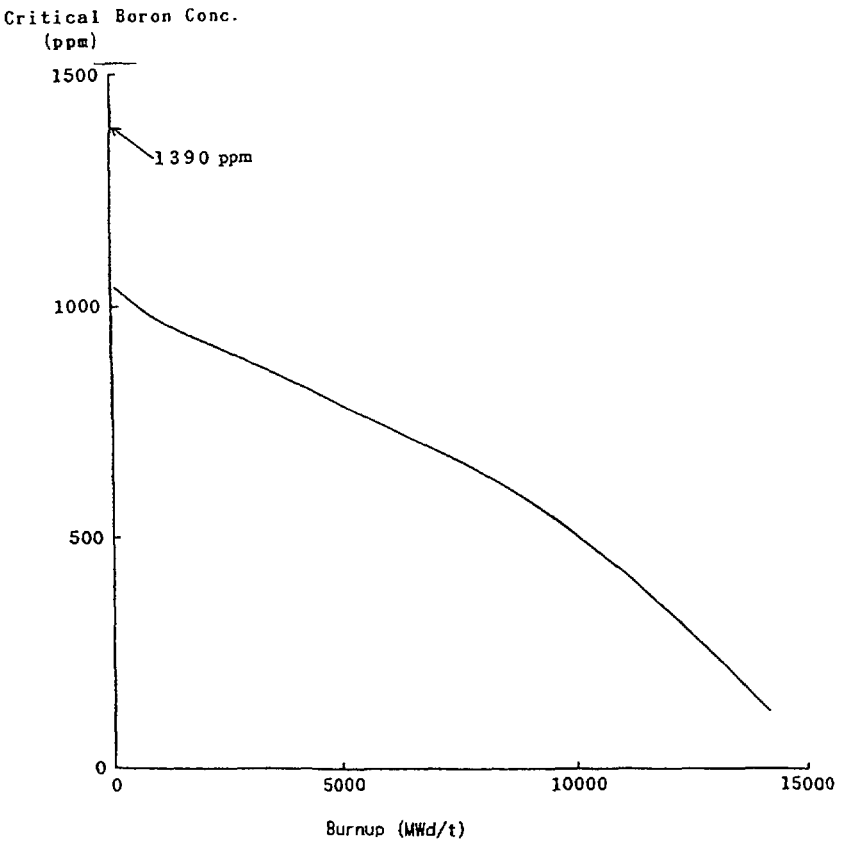

Fig. III.5. *Critical boron concentration vs. burnup Equilibrium cycle of 4 loop Gd fuel core HFP, ARO*

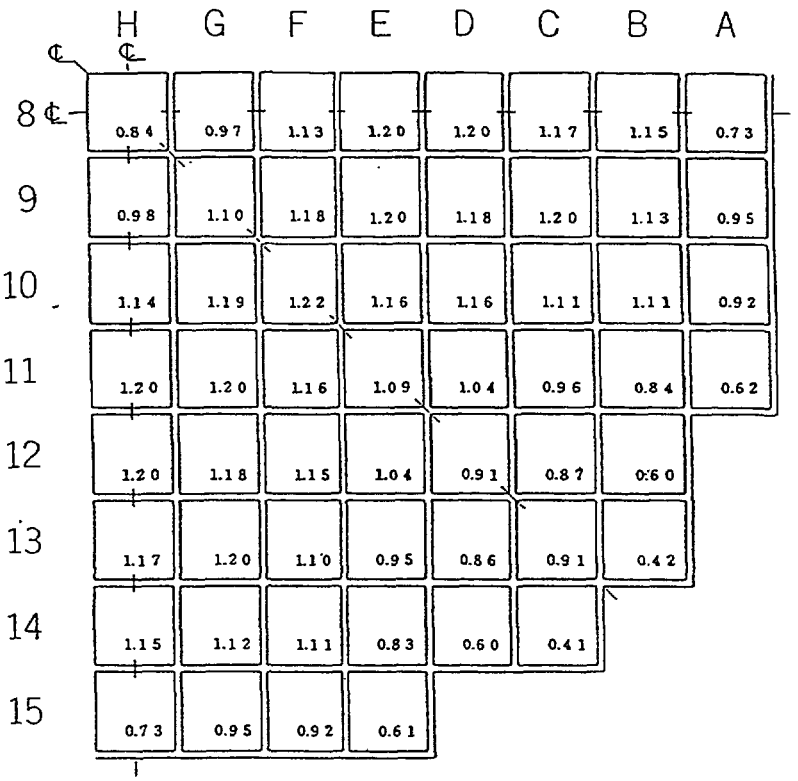

Fig. III.6. *Radial power distribution of 4 loops Gd fuel core BOC, HFP, ARO*

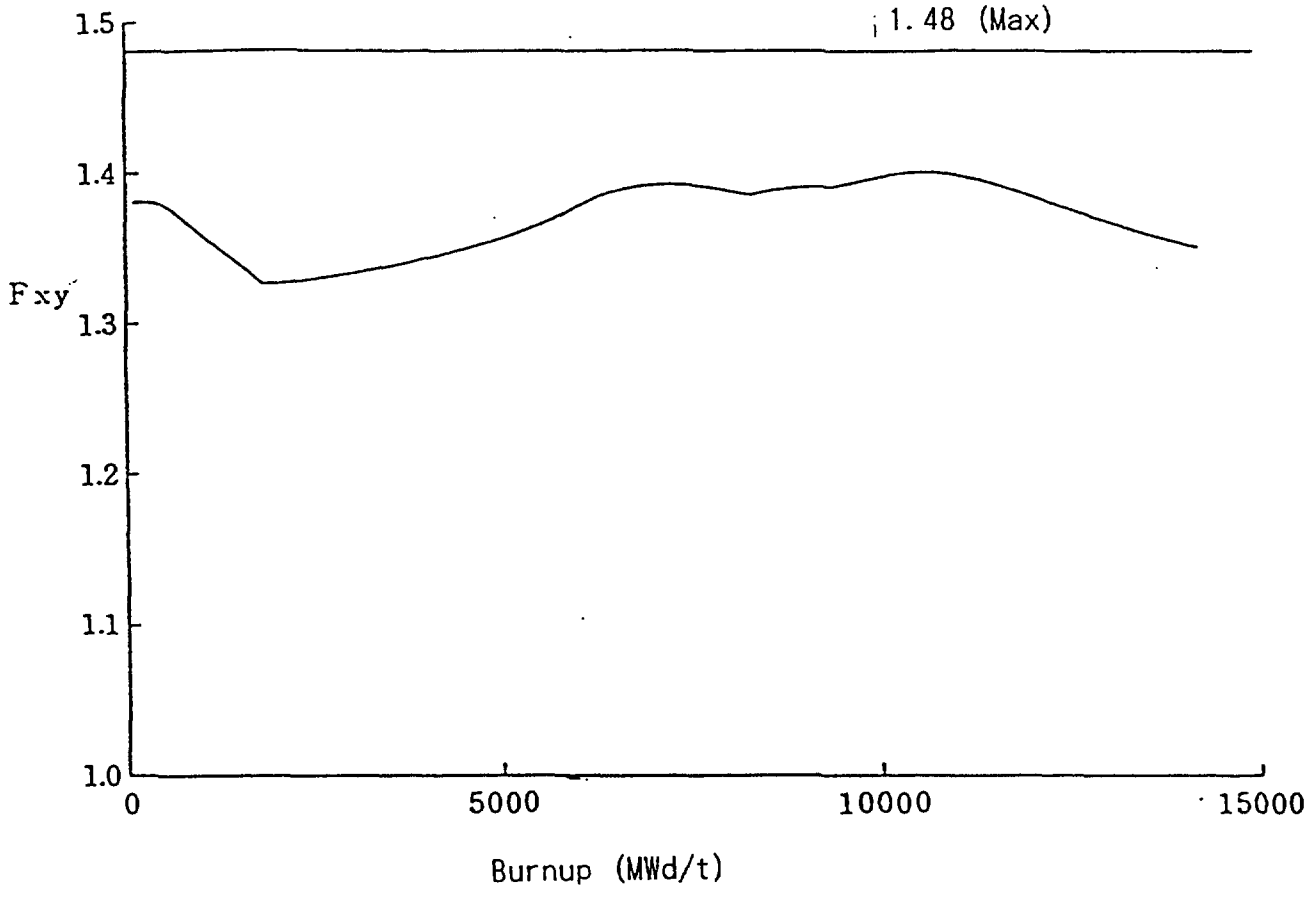

Fig. III.7. *Fxy vs. burnup*
4 loop, equilibrium cycle, Gd fuel core

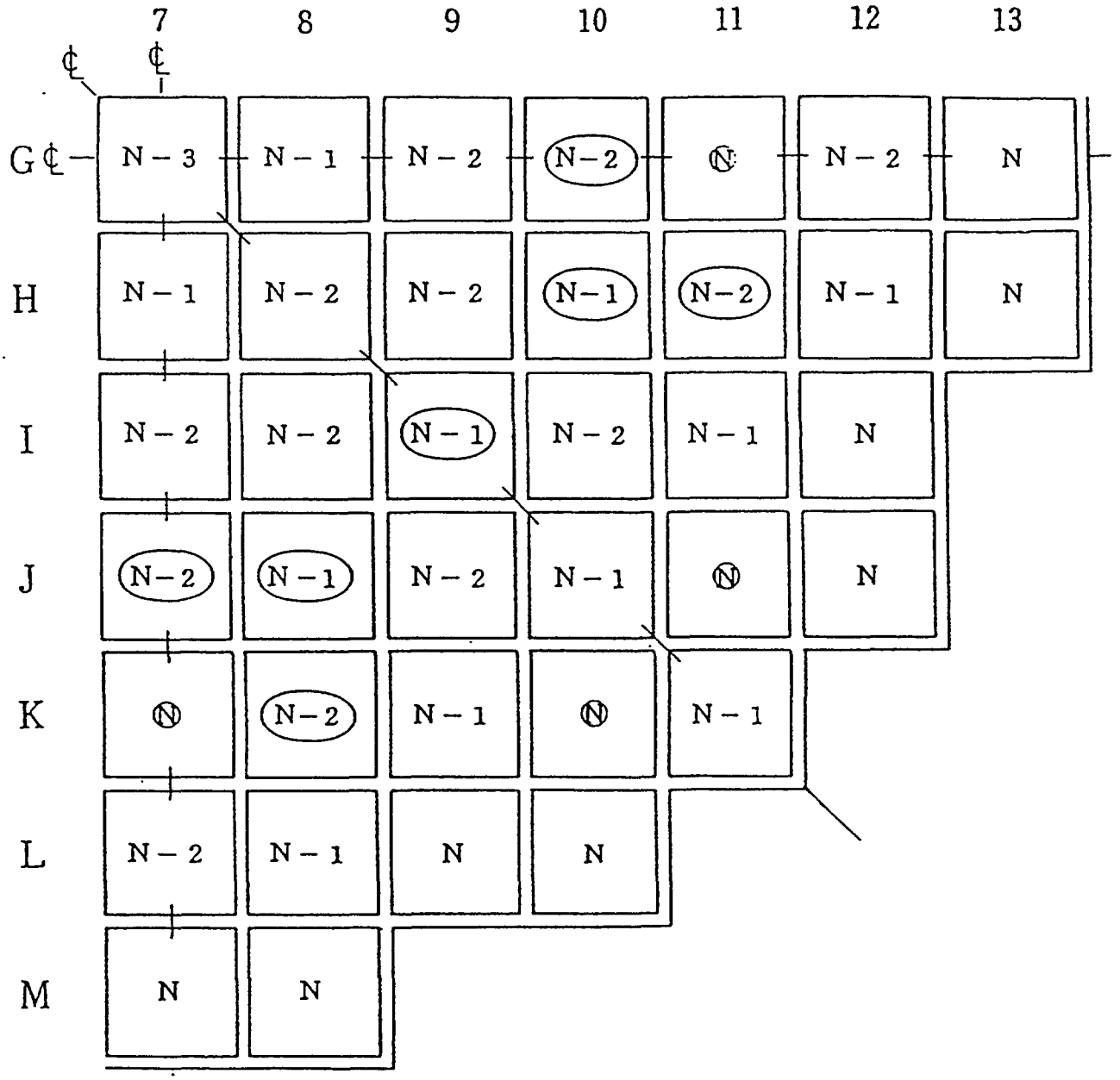

Mark	Region Number	Number of Ass'y
N-3	16 (3.5wt%)	1 (3 Cycle Burned)
(N-2)	17B(3.5wt%+Gd*)	12 (Twice Burned)
N-2	17A(3.5wt%)	28 (Twice Burned)
(N-1)	18B(3.5wt%+Gd*)	12 (Once Burned)
N-1	18A(3.5wt%)	28 (Once Burned)
N	19A(3.5wt%+Gd*)	12 (Fresh Fuel)
N	19B(3.5wt%)	28 (Fresh Fuel)

*A Fuel Assembly contains 12 FRs of 2.0w/o U235 - 6w/o Gd2O3

Fig. III.8. *Fuel loading pattern*
Equilibrium cycle of 2 loop Gd fuel core

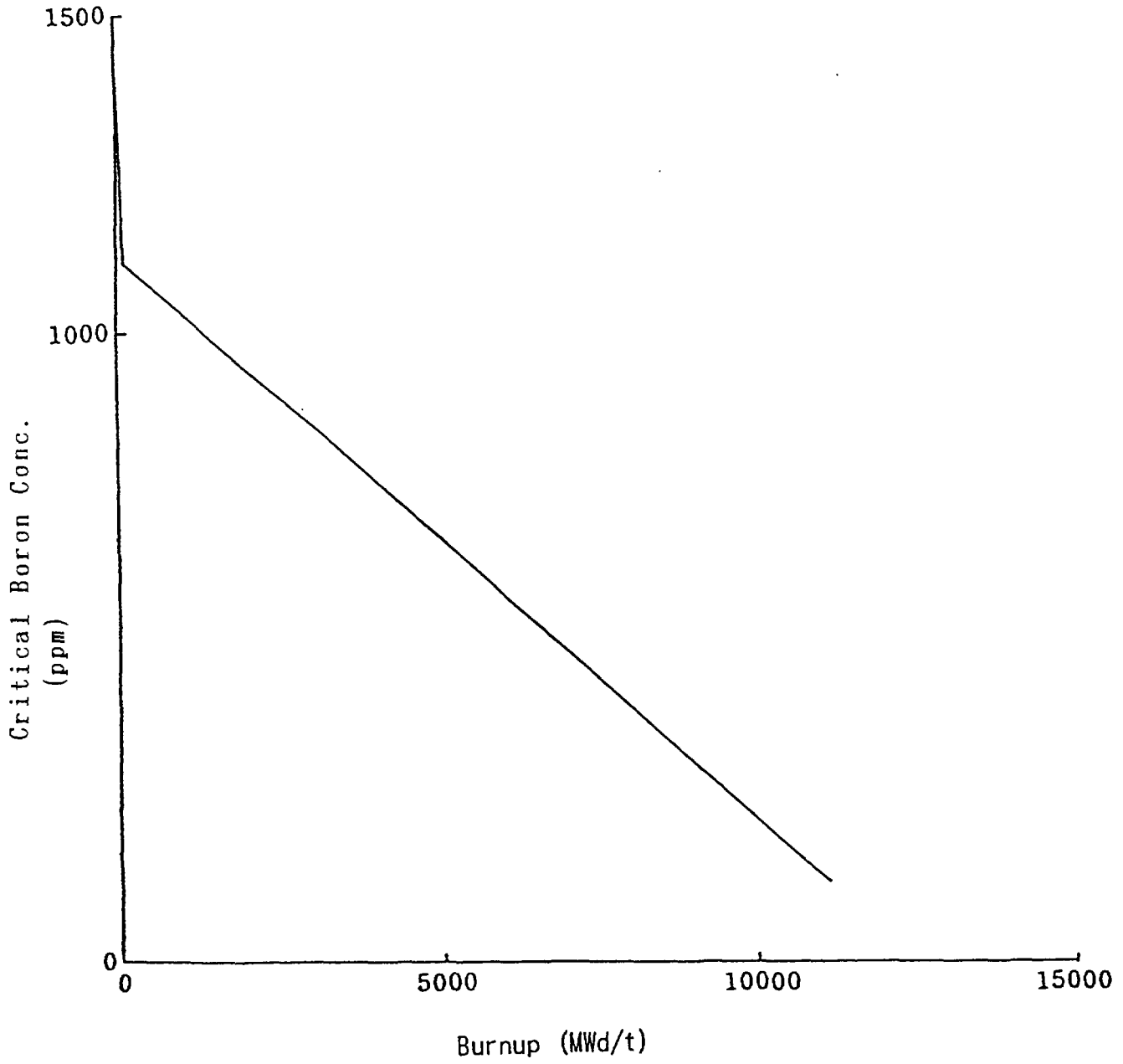

Fig. III.9. *Critical boron concentration vs. burnup*
Equilibrium cycle of 2 loop Gd fuel core HPF, ARO

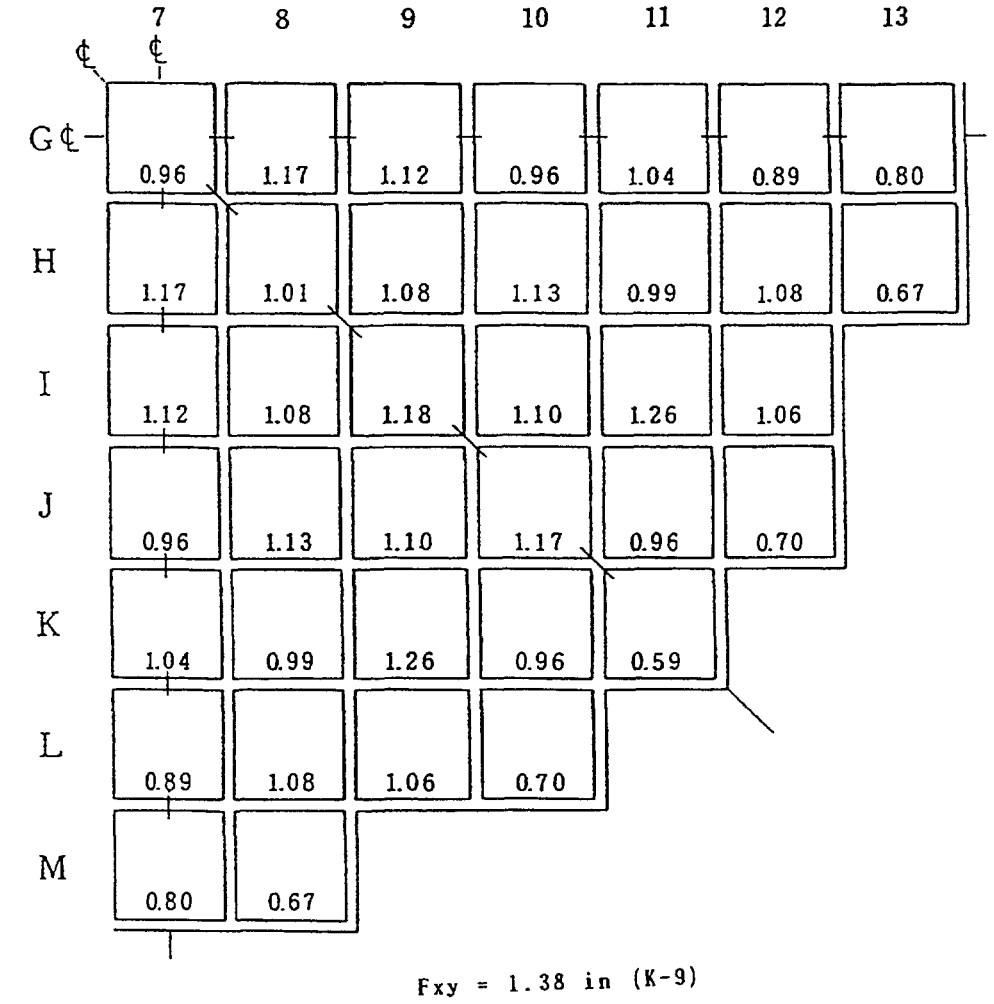

Fig. III.10. *Radial power distribution of 2 loop Gd fuel core BOC, HFP, ARO*

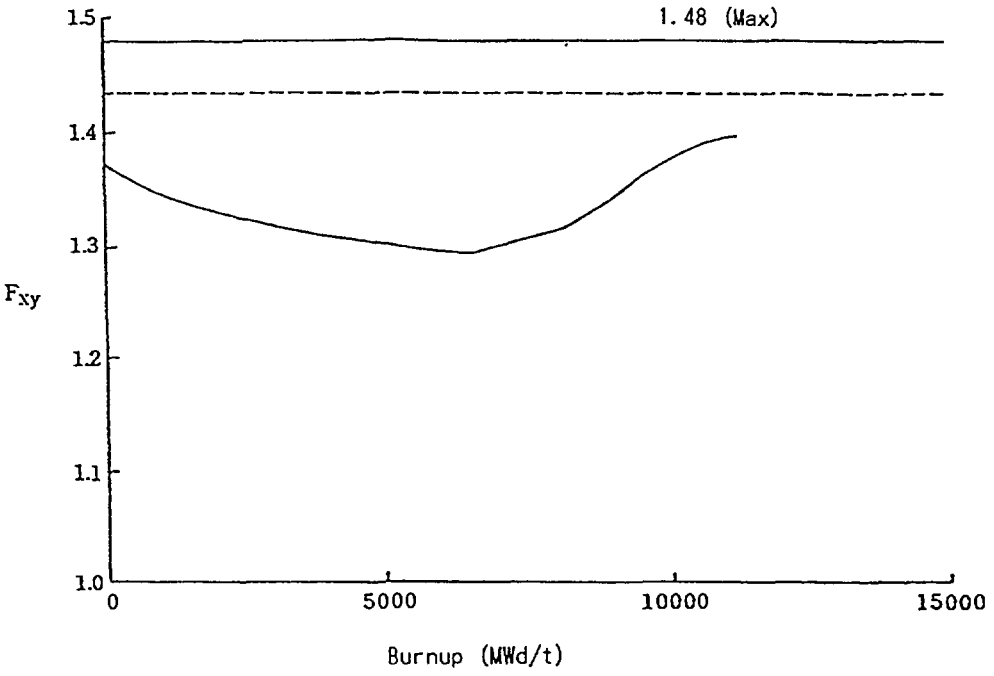

Fig. III.11. *Fxy vs. burnup*
2 loop, equilibrium cycle, Gd fuel core

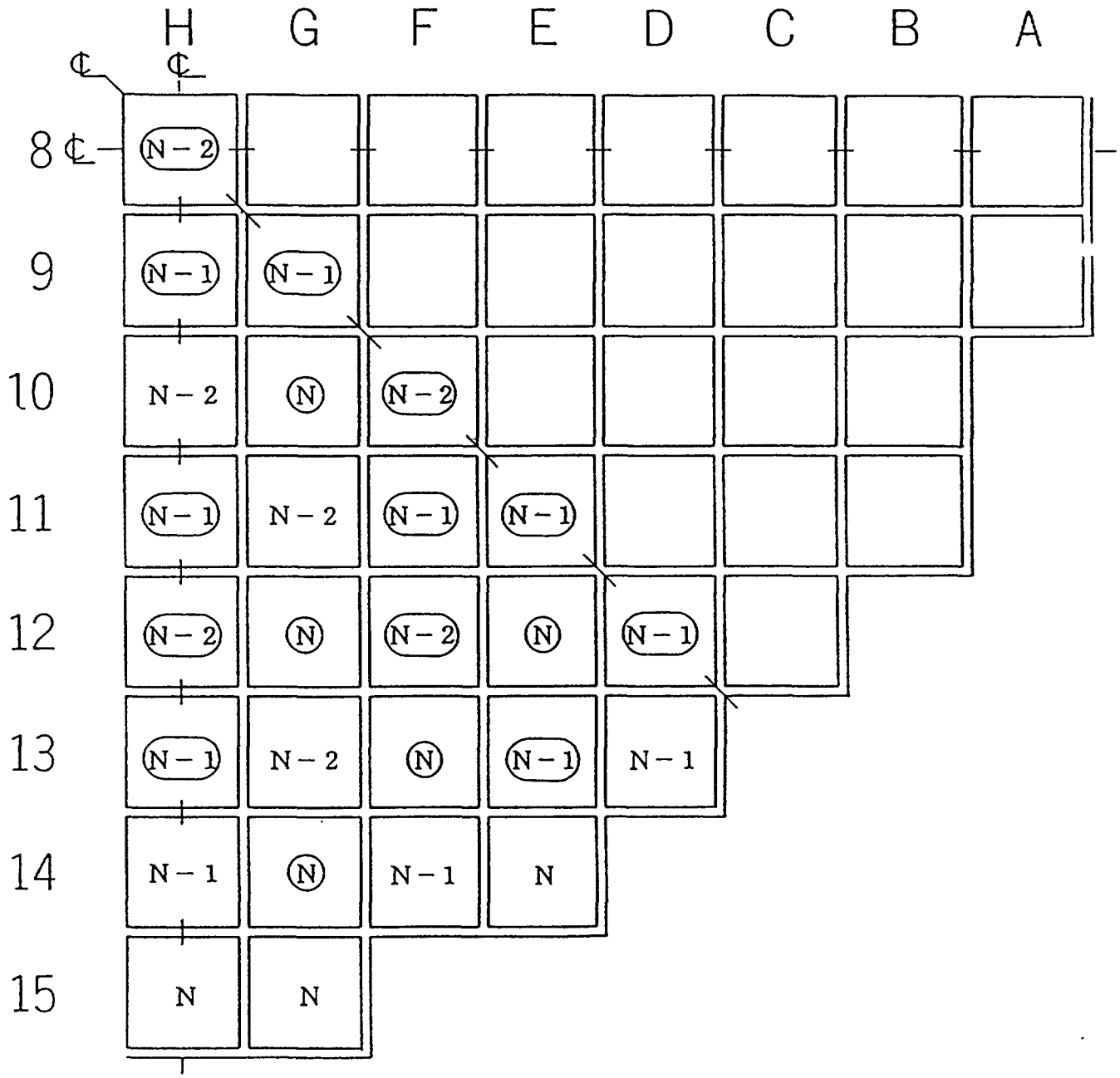

Mark	Region Number	Number of Ass'y
(N-2)	18A(3.4wt%+Gd*)	17 (Twice Burned)
N-2	18B(3.4wt%)	20 (Twice Burned)
(N-1)	19A(3.4wt%+Gd*)'	40 (Once Burned)
N-1	19B(3.4wt%)	20 (Once Burned)
N	20A(3.4wt%+Gd*)	40 (Fresh Fuel)
N	20B(3.4wt%)	20 (Fresh Fuel)

* A Fuel Assembly contains 16 FRs of 1.9w/o U235 - 6w/o Gd203

Fig. III.12. *Fuel loading pattern*
Equilibrium cycle of 3 loop Gd fuel core

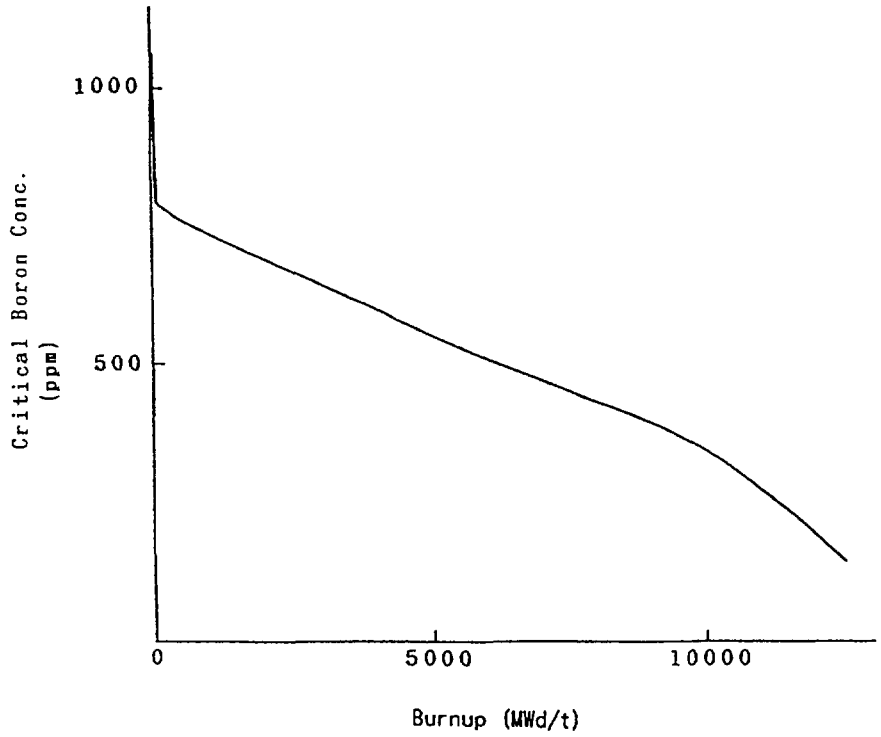

Fig. III.13. *Critical boron concentration vs. burnup*
Equilibrium cycle of 3 loop Gd fuel core HPF, ARO

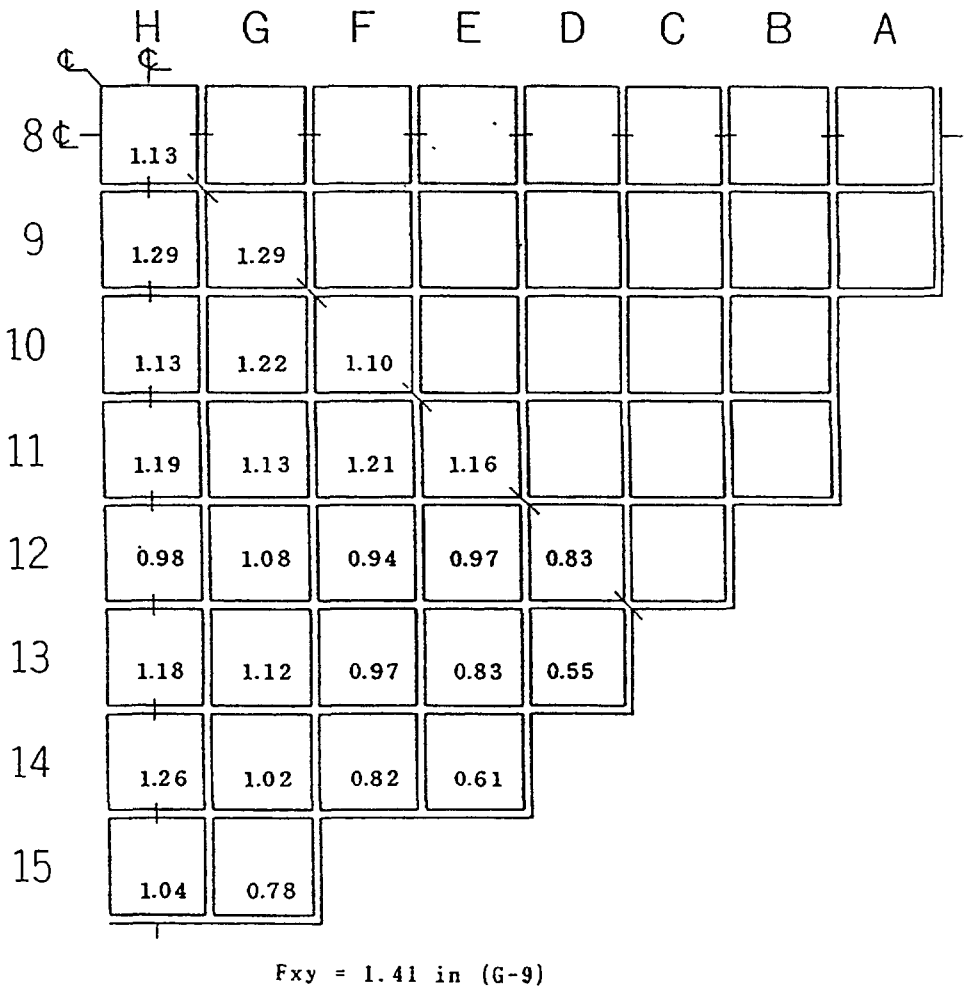

Fig. III.14. *Radial power distribution of 3 loop Gd fuel core*
BOC, HFP, ARO

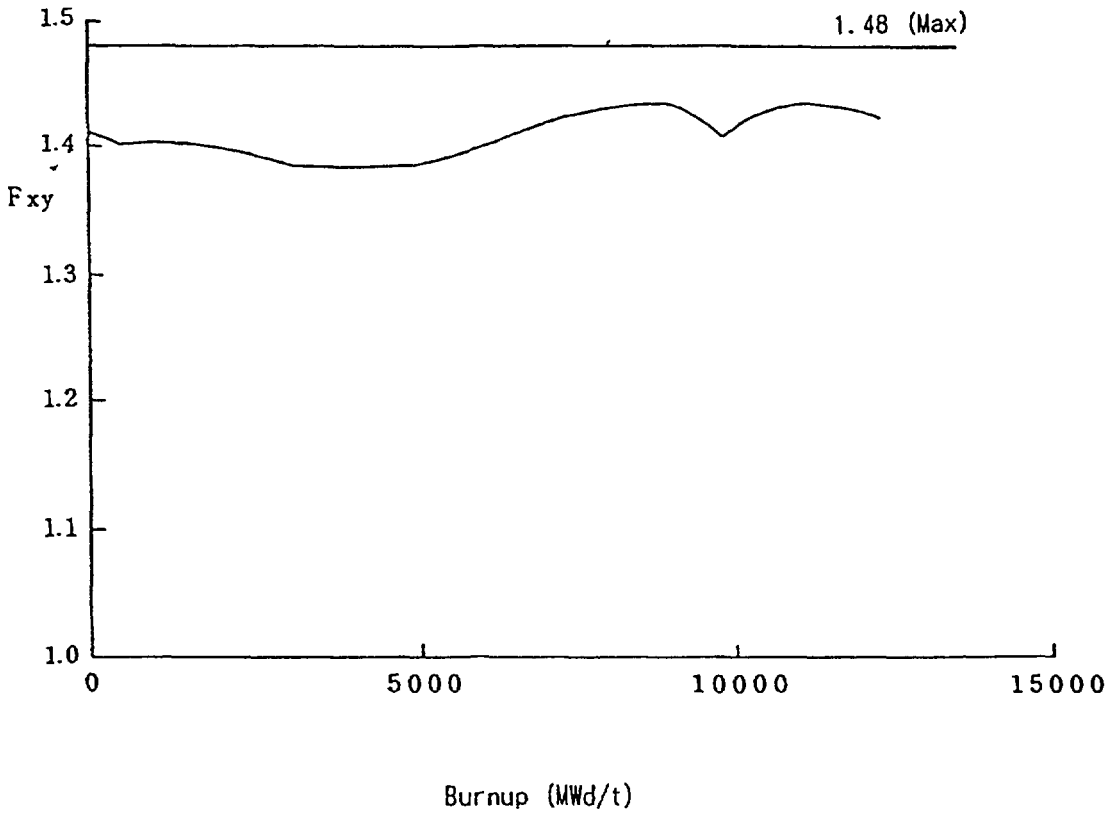

Fig. III.15. *Fxy vs. burnup*
3 loop, equilibrium cycle, Gd fuel core

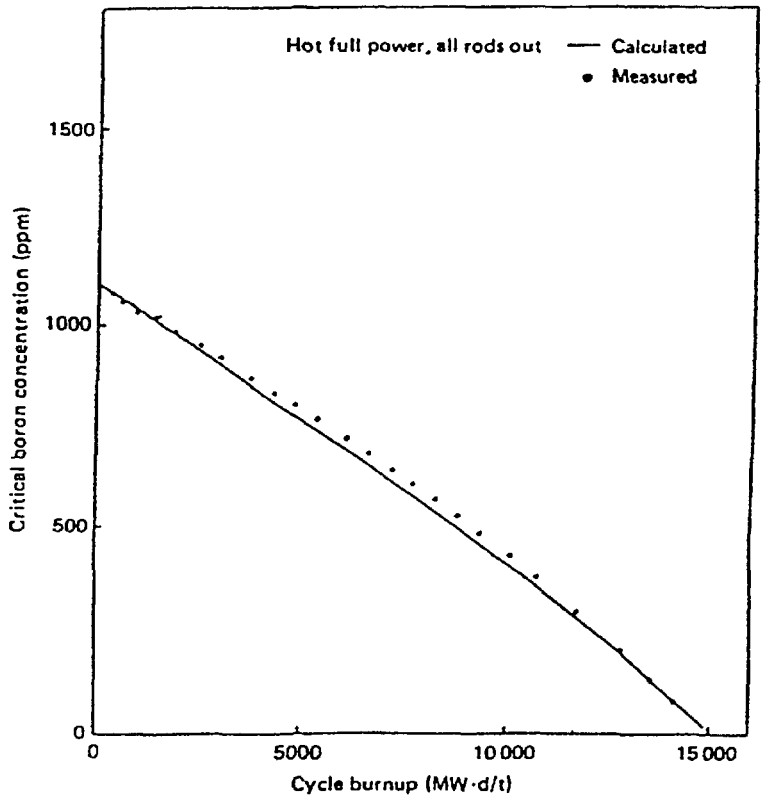

Fig. III.16. *Critical boron concentration*

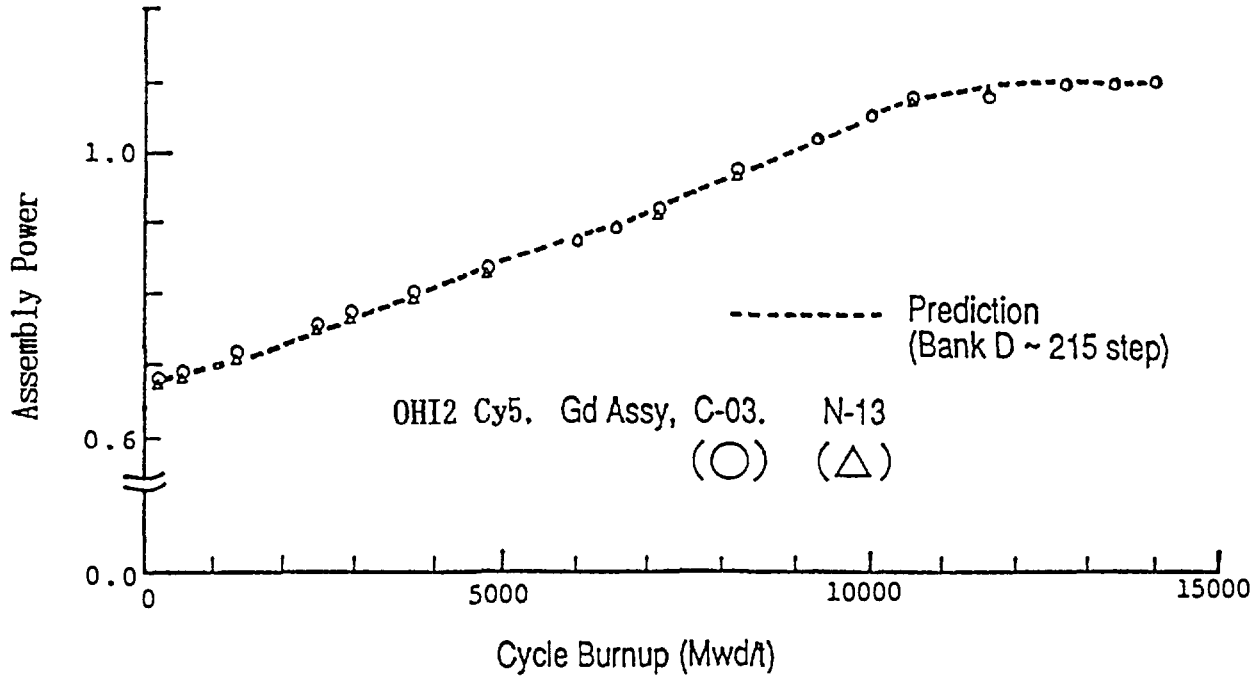

Fig. III.17. *Gd FA power vs. cycle burnup*

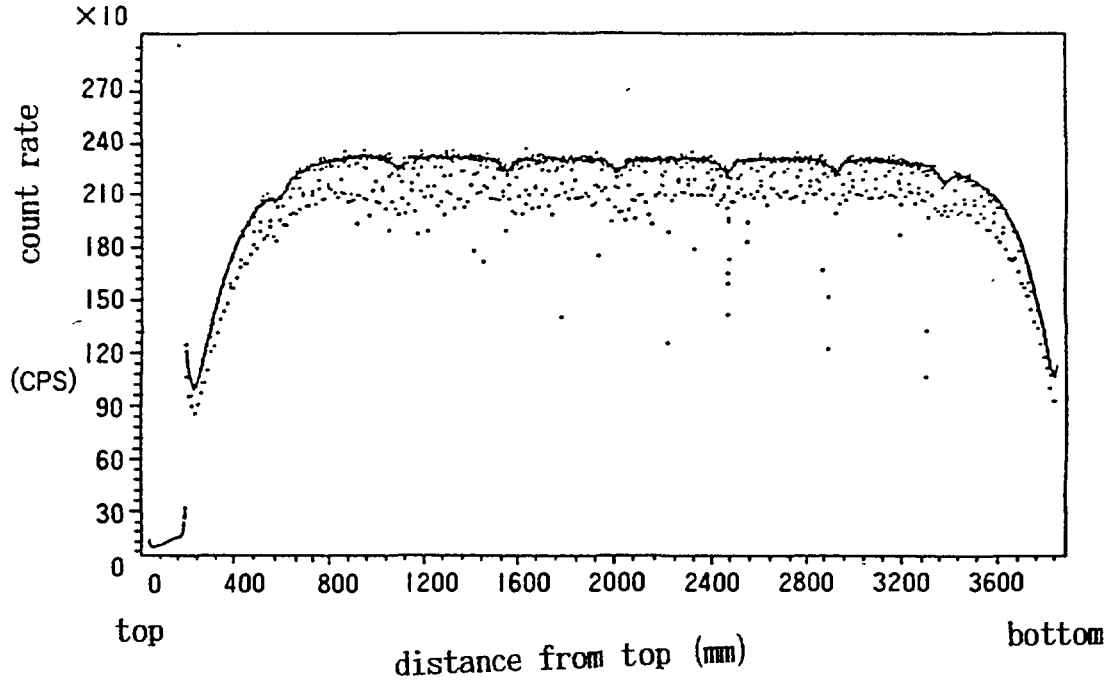

Fig. III.18. *Axial gamma scanning of Gd FR*

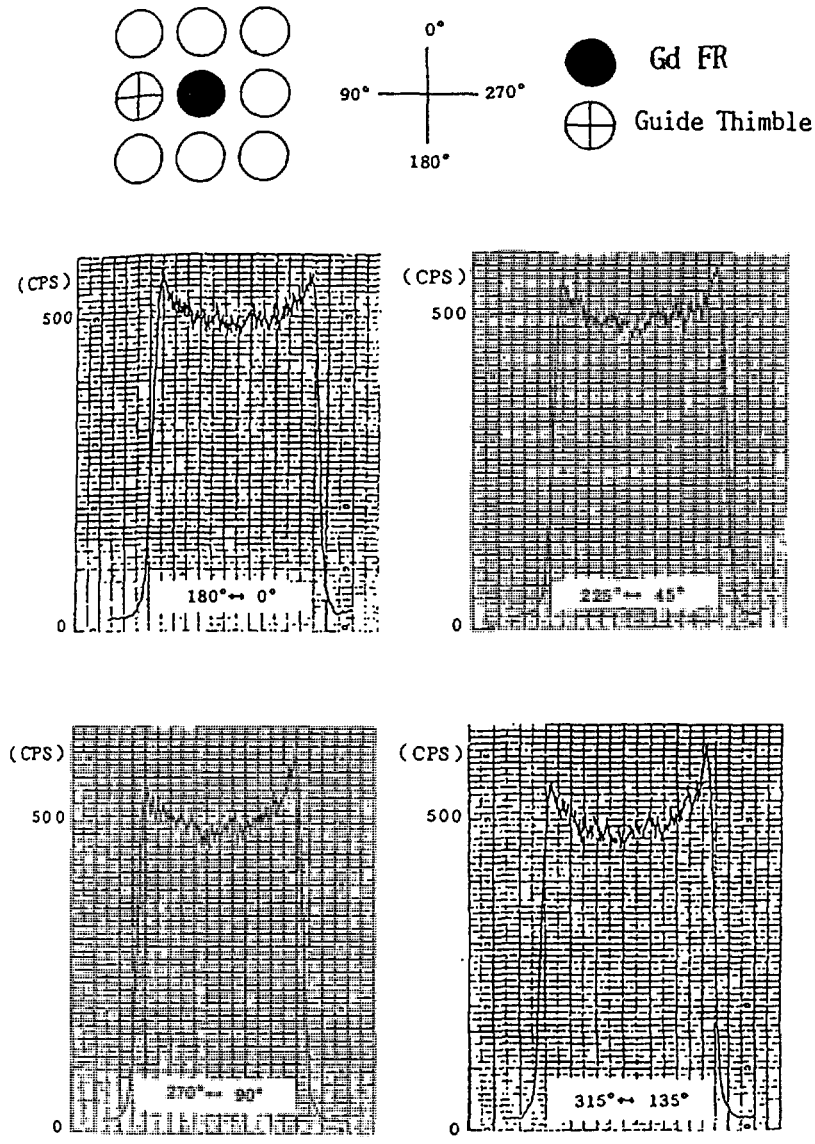

Fig. III.19. *Micro gamma scanning of Gd FR (gross)*

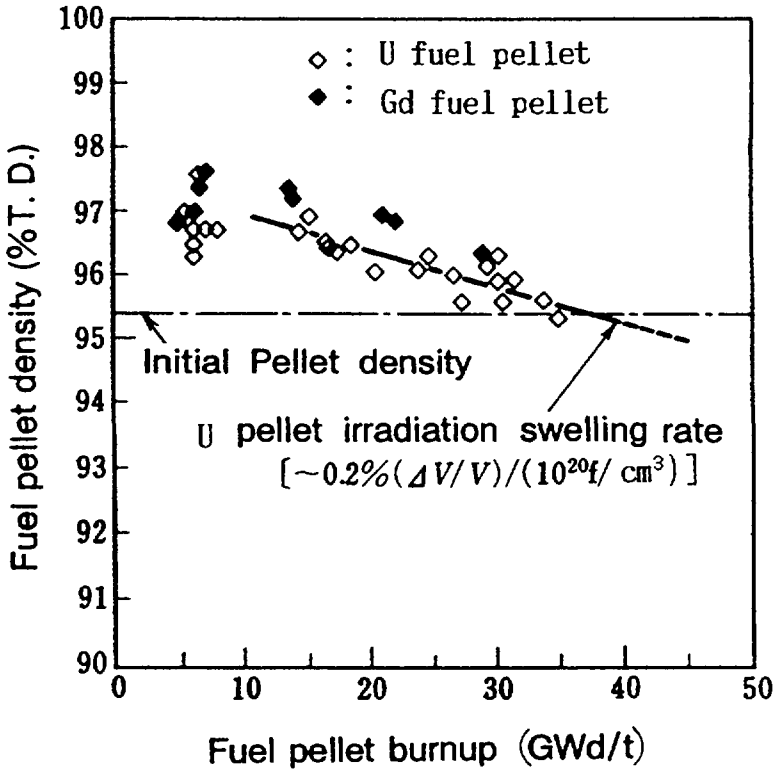

Fig. III.20. *Pellet density change with burnup*

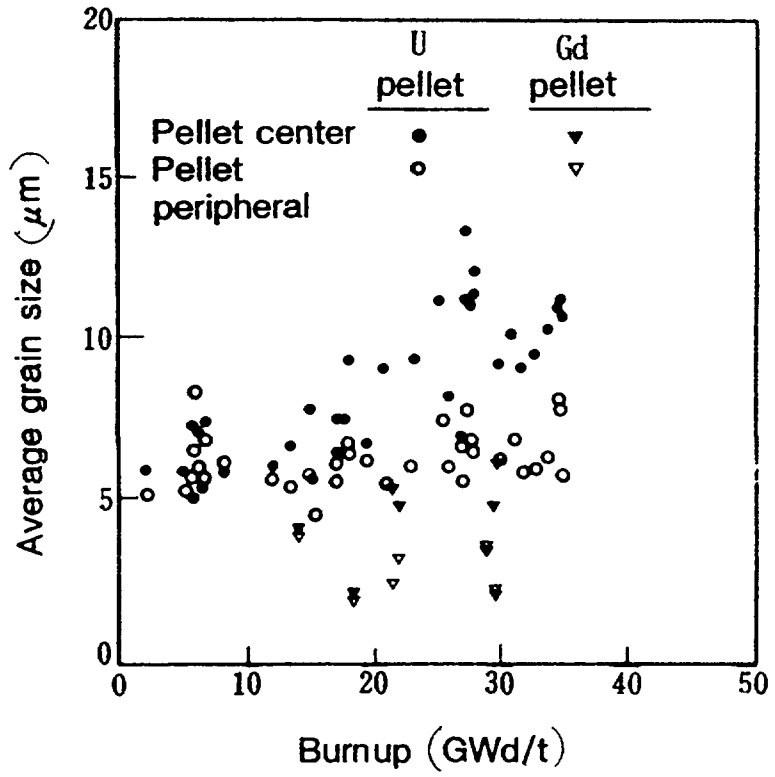

Fig. III.21. *Change of pellet average grain size with burnup*

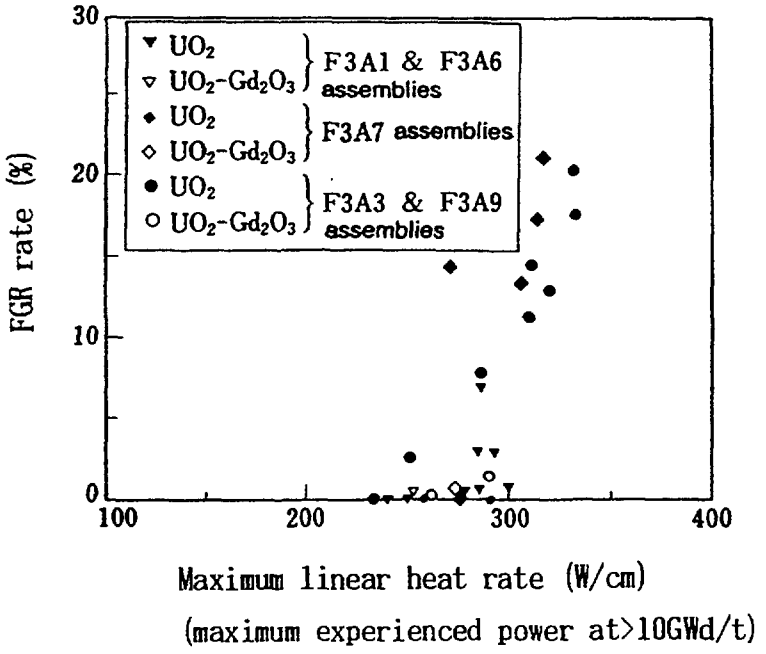

Fig. III.22. *Dependency of fuel rod FGR rate on LHGR*

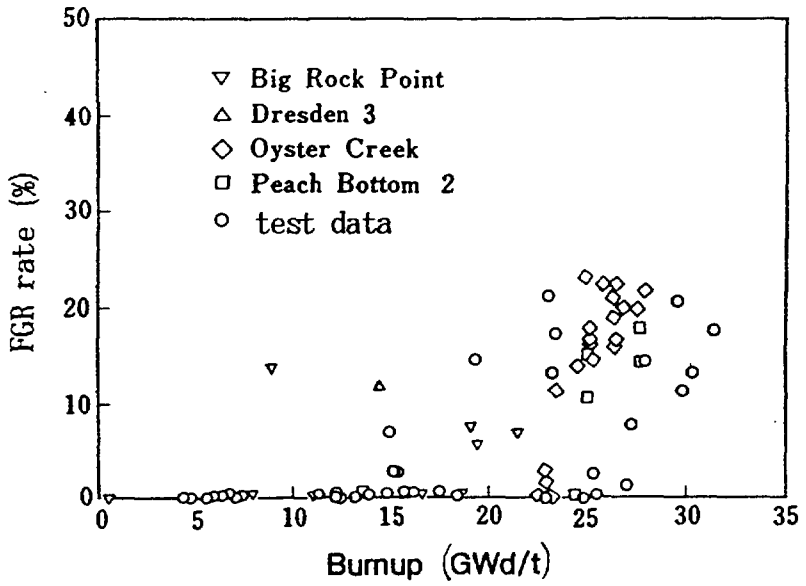

Fig. III.23. *Fuel rod FGR rate vs. burnup*

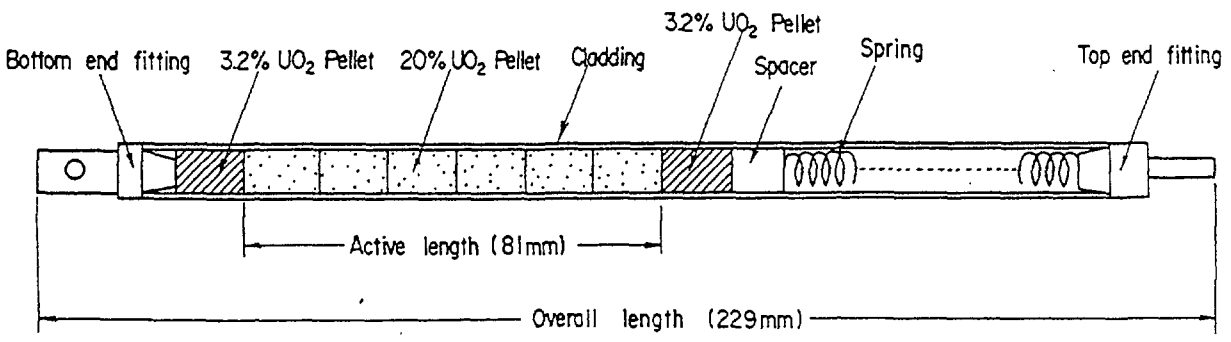

Fig. III.24. *Schematic view of test FR*

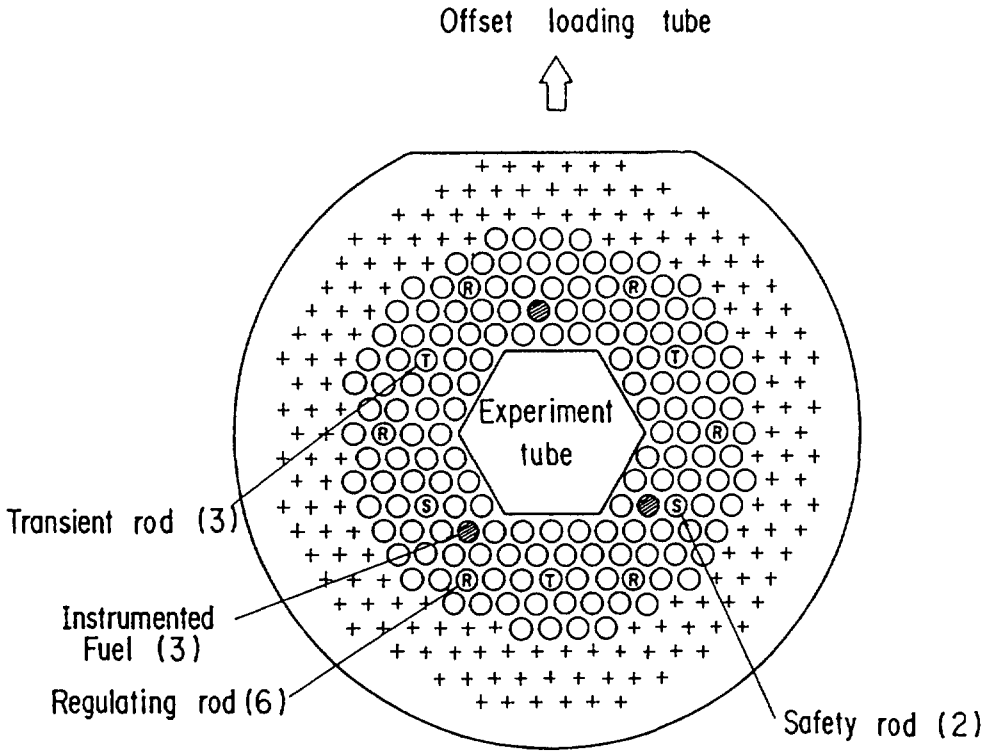

Fig. III.25. *Standard operating core configuration*

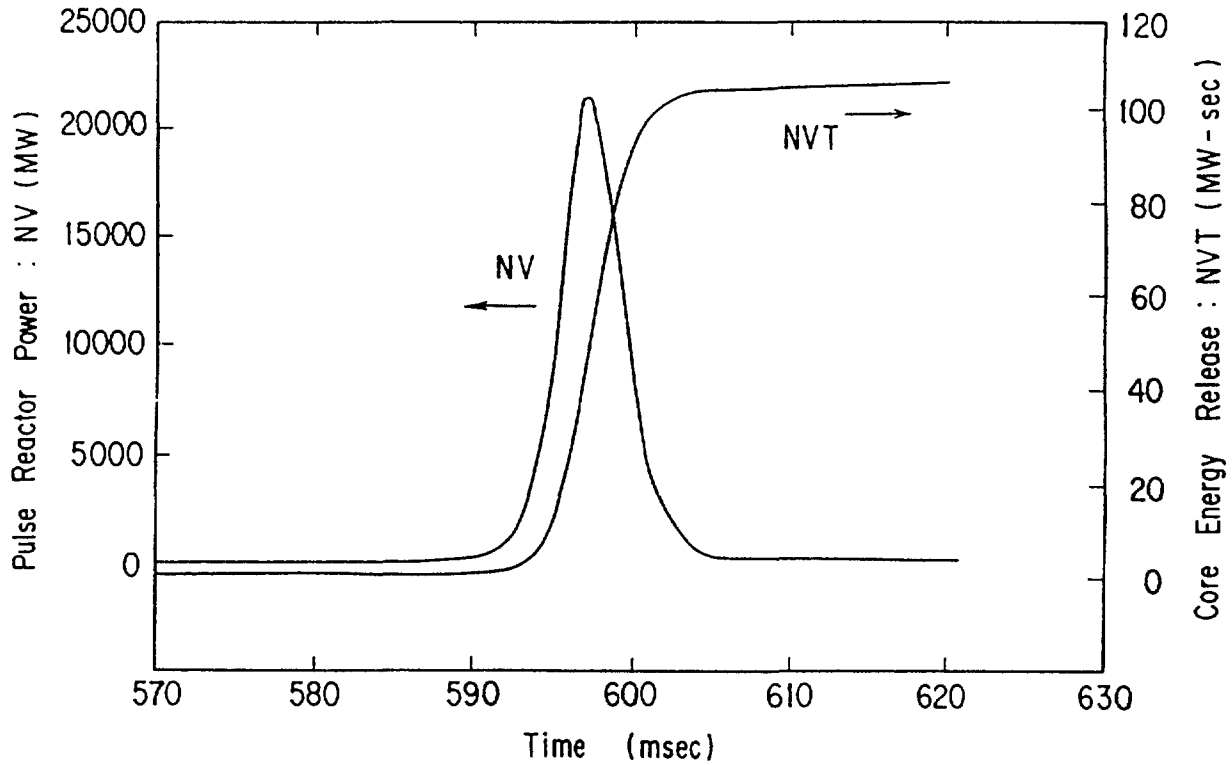

Fig. III.26. *Pulse reactor power and core energy release for 4.67 $ pulse*

Test Series	Fuel Rod Type	Threshold Energy
510	17×17 PWR Type UO_2 fuel rod	252 ~ 264 cal/g.UO_2
511	17×17 PWR Type Gd_2O_3-UO_2 fuel rod	265 ~ 275 cal/g.UO_2
512	14×14 PWR Type UO_2 fuel rod	232 ~ 246 cal/g.UO_2

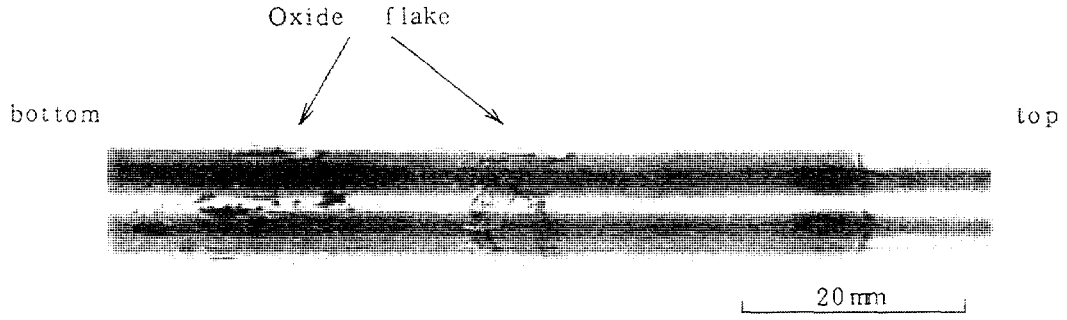

(a) Test No.510-1 (252 cal/g.UO_2)

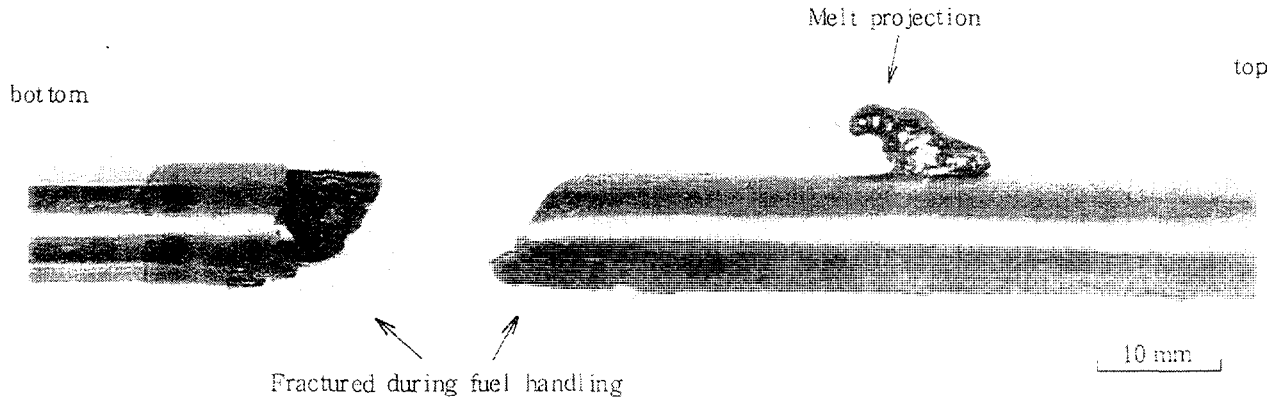

(b) Test No.510-2 (276 cal/g.UO_2)

Fig. III.27. *Representative post-test FR appearances in No.510 test series, showing (a) oxide flake and (b) melt projection*

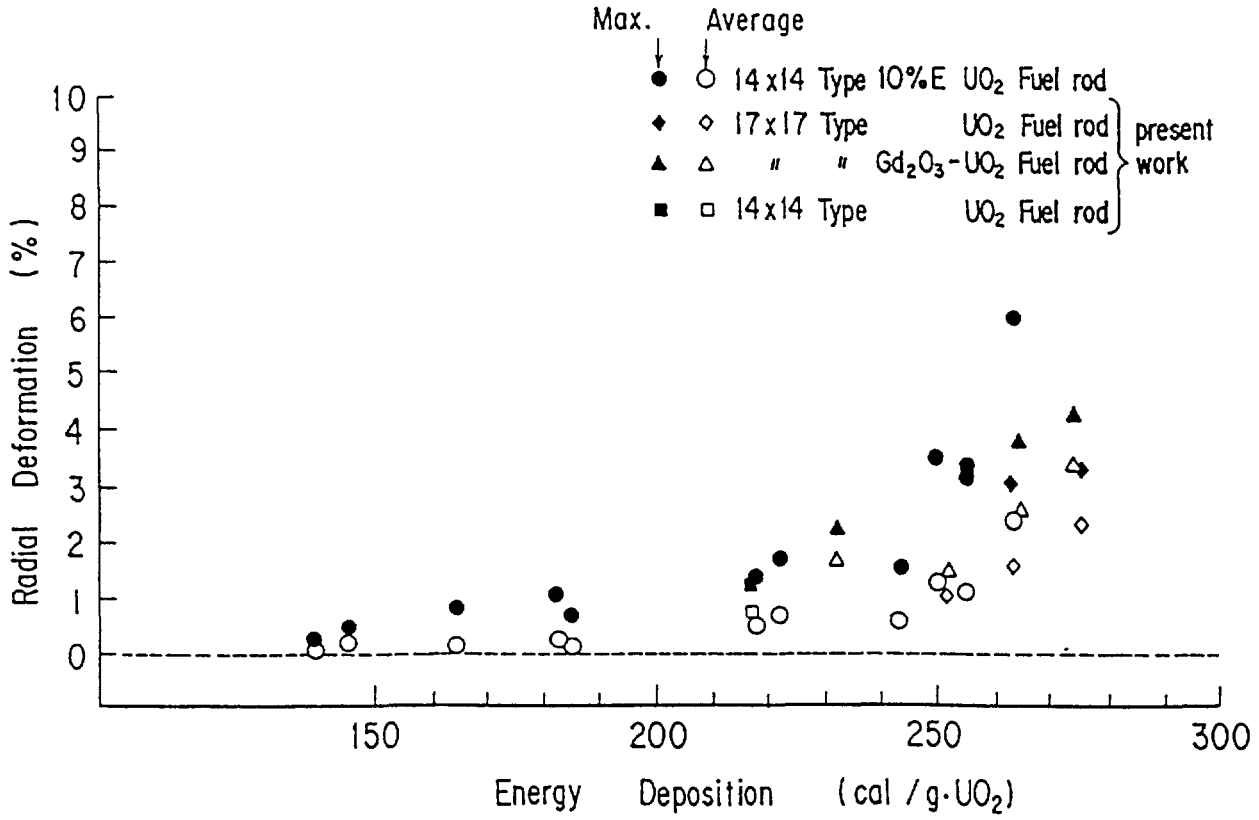

Fig. III.28. *Comparison of radial deformation*

Appendix IV

GADOLINIA FUEL UTILIZATION IN THE REPUBLIC OF KOREA

This Appendix provides additional details on the experience with Gd in Korea, as summarized in Chapter 5.

IV.1. Gd utilization

KAERI has contracts with KWU for reload core fuel design for all operating reactors and with ABB/CE for initial core fuel design for the Yonggwang 3 and 4 units.

Table IV.1 compares various nuclear parameters in reload core design. As an example of a reload core design, in Kori-2 cycle 7 refuelling (low-leakage loading pattern), 52 conventional standard FAs are replaced by 4 fresh standard FAs (3.41 w/o U-enrichment) and 48 fresh KOFAs (designed by KAERI and KWU). Out of these 48 KOFAs, 28 fuel assemblies contain Gd FRs of 1.8 - 6 w/o Gd. The length of cycle 7 is 14,420 MWd/tU (375 EFPD), compared with the cycle 6 length of 13,100 MWd/tU (348 EFPD).

Table IV.2 shows the FA configurations that contain Gd FRs. The design specifications require that Gd FRs not be located directly adjacent to water holes. Table IV.3 shows the FA design parameters. Figures IV.1 through IV.16 present the various burnable absorber patterns in the reload cores.

In Figure 4.8 in Chapter 4, the infinite multiplication factor for the YGN-3/4 initial core is shown for the case of an 8 shimmed fuel assembly. Figure IV.17 shows the same for the case of a 12-shimmed fuel assembly. Figure IV.18 and Figure IV.19 compare the Gd fractions remaining as a function of burnup for the 8 and 12 shimmed fuel assemblies, respectively.

Table IV.4 shows the number of Gd FRs and the number of FAs with Gd FRs, either already loaded in reactors or delivered to the plants as of October 1993. Table IV.5 details the number of Gd FRs and the number of FAs broken down into the number of residence cycles at the various plants. The number of Gd FRs loaded up to October 1993 corresponds to 26 reactor cycles.

Out of the 3728 Gd FRs already loaded, 864 Gd FRs have been discharged from the core and are now stored in the pools as shown in Table IV.6. Some of the Gd FRs completed the third cycle.

Poolside inspections of the Gd FRs showed no noticeable anomalies after the third cycle. These poolside inspections are performed using the equipment developed by KAERI, called "Versatile Fuel Examination Stand" (VFES). The poolside examination with VFES focuses on measuring the difference in dimensions between as-fabricated data and irradiated data, and on verifying the performance of the fuel during irradiation.

IV.2 *Fuel Modelling*

Initial core

The fuel modelling for initial cores of YGN 3 and 4 is described in Chapter 4. Figures IV.20 through IV.23 show the code system used in the initial core design of YGN-3/4.

Reload core

Five main computer codes are used in Korea by KAERI and KWU in nuclear reload fuel design, including Gd FRs. Figure IV.24 shows the calculational flow diagram for fuel assembly design.

FASER is a 1D, 85 group cell-burnup programme for lattice configurations based on a heterogeneous version of the slowing down programme MUFT and a modified version of the thermalization code THERMOS. FASER generates basic nuclear cross section libraries for reactor simulations as functions of nuclide, burnup, soluble boron concentration, coolant density/temperature and fuel rod temperature.

MULTIMEDIUM is a 2-dimensional assembly code for calculation of pinwise flux, power and burnup distributions for PWR fuel assemblies. The maximum number of energy groups is 10. The flux distributions can be determined either by using the nodal expansion method (NEM) for solving the 2D diffusion theory equations, or by applying the nodal discrete ordinate method (NDOM) for the approximated solution of the 2D transport equations with isotropic scattering. The main usage of the programme is to generate heterogeneous fuel assembly form functions and heterogeneity factors for the second homogenization process.

MEDIUM-2 is a two and three dimensional reactor burnup and fuel management code for the prediction of long-term reactivity behaviour, global power distributions, control rod worths, critical boron concentrations, reactivity coefficients and other design parameters. It solves the 2D or 3D multi-group diffusion theory equations in Cartesian geometry by applying a high order coarse-mesh nodal expansion method (NEM) and nonlinear feedback correction (NEMFC) by the second-order representation of macroscopic cross-section variations in a node. MEDIUM-2 also calculates the node-averaged values such as the flux, power, iodine and xenon quantities.

PINPOW is an assembly dehomogenization code for reconstruction of local flux and FR power distribution from the nodal coarse-mesh solution by MEDIUM-2. The programme determines the local continuous flux solution in the X-Y plane of the reactor by a high-order non-separable interpolation method. PINPOW takes into account the node burnup shapes, which are provided by MEDIUM-2, to determine local burnup distributions. The heterogeneous fuel assembly form functions provided by MULTIMEDIUM are used to determine the pinwise flux, power and burnup distributions by using a modulation technique. PINPOW can determine the reaction rates of the incore measurement system and generates all theoretical information needed by the process computer to determine power and burnup distributions.

PANBOX is the reactor dynamics program system used for reload safety analysis and all kinds of transients in which the power distribution is significantly affected. These transients include short term accidents like rod ejection and long term events like xenon redistribution.

The PANBOX program system consists of:

DIEB:	-	input processor for IQSBOX
		data base generator for APCBOX
IQSBOX	-	LWR core transients
APCBOX	-	LWR xenon dynamics

IQSBOX solves the two-group space-time-dependent neutron diffusion equation by the nodal expansion method (NEM) or nodal integration method (NIM) in 3D Cartesian co-ordinates, coupled with an efficient time integration procedure. The program is especially suited for the calculation of steady state and transient power distributions under off-normal core conditions. APCBOX is the 1D version of IQSBOX used for xenon dynamics calculations.

TABLE IV.1. *COMPARISON OF NUCLEAR PARAMETERS IN RELOAD CORE DESIGN*

ITEMS	Kori - 1		Kori - 3 & 4		Yonggwang - 1 & 2		
	W(OFA)	KOFA*	W(OFA)	KOFA	W(OFA)	KOFA	
Fuel enrichment (w / o)	3.2	3.5	3.2	3.7	3.2	3.7	
Region average disch, Bu (MWd / tU)	35 500	35 000	37 000	42 000	37 000	42 000	
Maximum rod average, Bu, (MWd / tU)		47 000		52 000		52 000	
F_q	2.08	2.08	2.30	2.30	2.30	2.32	Limit
F_{xy}	1.55	1.55	1.55	1.55	1.55	1.55	+8% uncertain
Delayed neutron fraction (BOC / EOC)	0.0072 / 0.0043	0.0071 / 0.0049	0.0075 / 0.0044	0.0068 / 0.0049	0.0075 / 0.0044	0.0068 / 0.0049	Limit
Neutron Lifetime (μsec) (BOC / EOC)	26	28	18.1 / 19.4	17 / 28	21.3 / 21.7	17 / 28	Limit
AFD (%)	-5 → +5	-5 → +5	-12 → +3	-12 → +3	-12 → +3	-12 → +3	Limit
BA material (Gd, % / U-235 w/o)	B_4C (13.5)	Gd_2O_3 (8 / 1.8)	B_4C (13.5)	Gd_2O_3 (8 / 1.8)	B_4C (13.5)	Gd_2O_3 (8 / 1.8)	
DTC (pcm / °C)	-5.2 → -1.6	-5.6 → -2.5	-5.2 → -1.6	-6.0 → -2.8	-5.2 → -1.6	-6.0 → -2.8	Limit
MTC (pcm / °C)	+9.0 → -59.4	+10.0 → -64.1	+9.0 → -72.0	+10.0 → -71.3	< +9.0	+10.0 → -71.6	Limit
Doppler-only PC (pcm / % power)	U: -19.4 / -12.6 L: -9.6 / -6.1	U: -16.4 / -14.0 L: -11.2 / -9.0	U: -19.4 / -12.6 L: -9.6 / -6.1	U: -14.3 / -12.5 L: -9.8 / -8.2	U: -19.4 / -12.6 L: -9.5 / -6.0	U: -14.3 / -12.5 L: -9.8 / -8.2	Limit
Boron coefficient (pcm / ppm)	-16 → -7	-14 → -6	-16 → -7	-14 → -6	-17 → -7	-13 → -6	Limit
< Control Rods >							EOC
Total-stuck rod worth (%)	5.75	5.99	9.01	7.55	8.37	7.48	
Control Reactivity (%)	3.09	3.35	3.26	3.55	3.49	3.58	
SDM (%)	2.09	2.04	4.85	3.24	4.04	3.15	

* *KOFA: Korean Fuel Assembly*

TABLE IV.2. *Gd FR DESIGN DATA*

	14 x 14 type	16 x 16 type	17 x 17 type
Active length (mm)	3658	3658	3658
Rod length (mm)	3852	3847	3847
Cladding O.D. (mm)	10.75	9.5	9.5
Rod pitch (mm)	14.12	12.32	12.6
Assembly width (mm)	1972	1972	2140
Gd_2O_3 content (w / o)	6.0	6.0	9.0
U^{235} enrichment (w / o)	1.8	1.8	1.8
UO_2- Gd_2O_3 density (g / cm^3)	10.08	10.08	10.08

Table IV.3. Fuel assembly design parameters

Kori 2 —— Cycle 7

Region	6s	7A-S	7B	8A	8A-S	8B	9	9G
Enrichment (w/o U235)	3.40	3.40	3.61	3.41	3.41	3.62	3.50	3.47
Number of Assemblies	4	4	13	32	4	16	28	20
Approximate Burnup at BOC 7 (GWd/tU)	17.9	14.9	25.5	15.1	0.0	15.0	0.0	0.0

All regions contain as-built data except region 9 and 9G.

Burnable Absorber Rods

	Cycle 6	Cycle 7
Absorber Material	Pyrex (B_2O_3)	Gd fuel
Content, w/o	12.5	6.0
Number in Core	176	80

Table IV.4. Number of Gd FRs and Number of FAs with Gd FRs up to October 1993

Loaded		Delivered But not yet loaded	
Gd FRs	Gd FAs	Gd FRs	Gd FAs
3728	640	784	104

Table IV.5. Number of Residence Cycles of Gd FRs Currently in Operation (October 1993)

Plant			Kori		Kori		YongGwang		Ulchin		Total
Unit			1	2	3	4	1	2	1	2	
Cycle length(month)			18	18	12	12	12	12	12	12	
# of residence cycles	1	Gd Rods	64	0	336	384	256	288	112	112	1552
		FAs	16	0	52	48	36	40	20	20	232
	2	Gd Rods	64	0	128	288	112	112	112	112	928
		FAs	16	0	24	36	20	20	20	20	156
	3	Gd Rods			84		84	104	112		384
		FAs			13		13	21	20		67

Table IV.6. Number of Gd FRs Stored in Pool (October 1993)

Plant			Kori		Kori		YongGwang		Ulchin		Total
Unit			1	2	3	4	1	2	1	2	
# of residence cycles	1	Gd Rods		112							112
		FAs		28							28
	2	Gd Rods	64	192	28	188	28	24			524
		FAs	16	48	7	35	7	3			116
	3	Gd Rods				4		112		112	228
		FAs				1		20		20	41

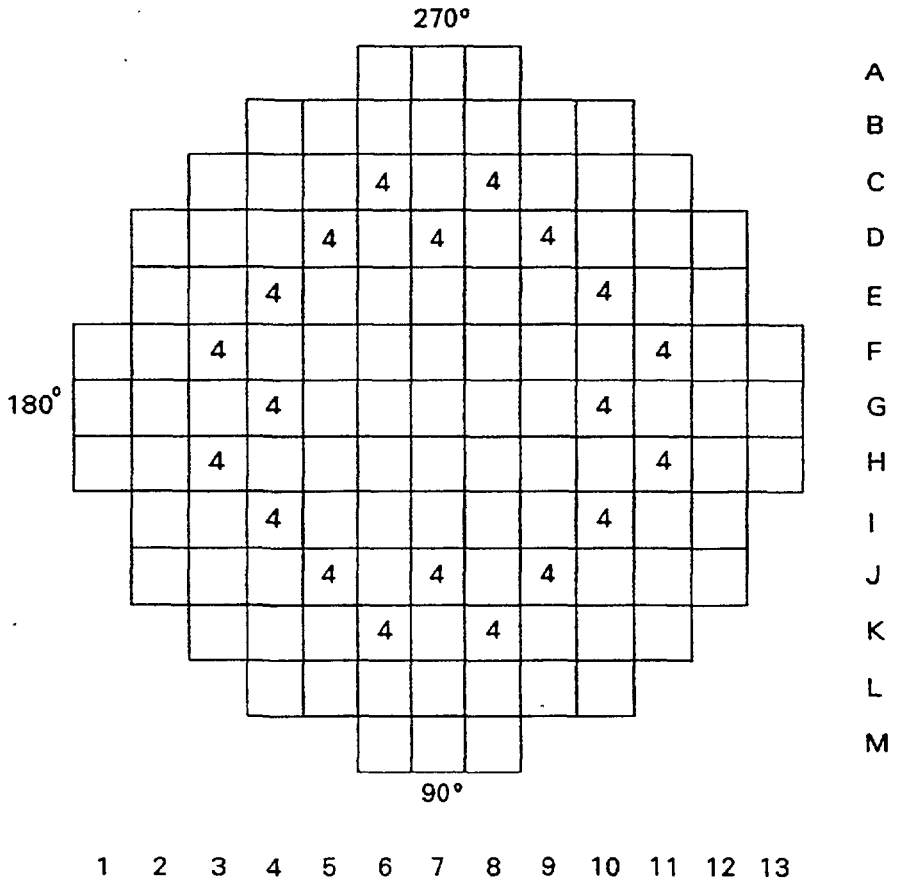

Figure IV.1. Burnable Absorber Pattern (Region 9G):Kori-2 Cycle 7

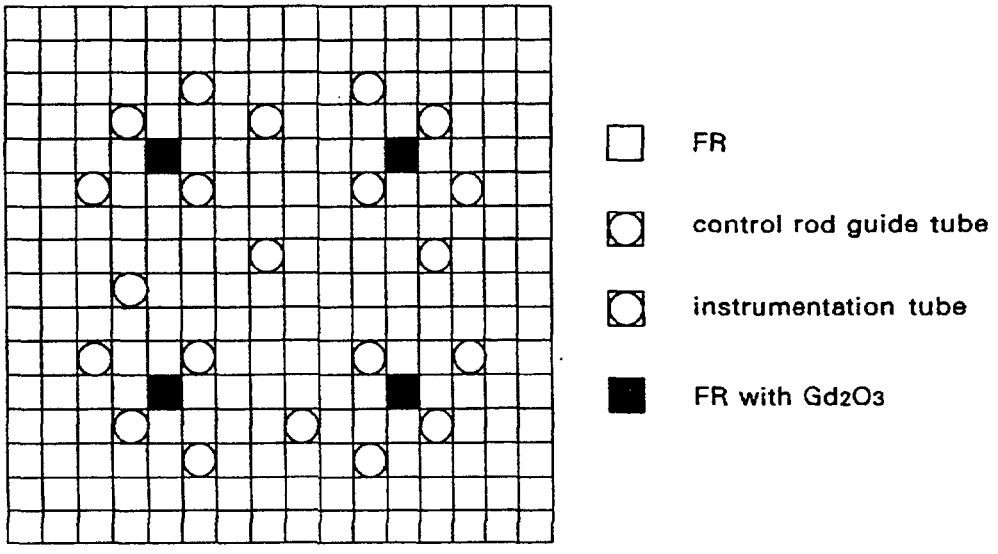

Figure IV.2. Burnable Absorber Configuration Within FA : Kori-2 Cycle 7

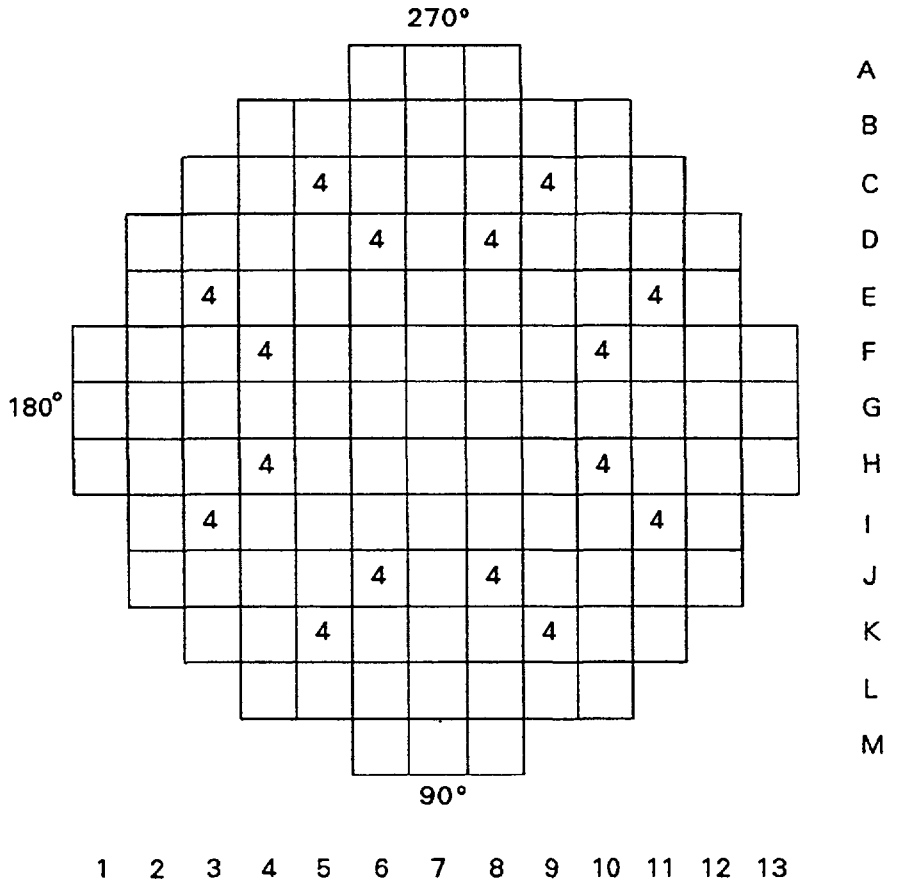

Figure IV.3. Burnable Absorber Pattern (Region 13G):Kori-1 Cycle 11

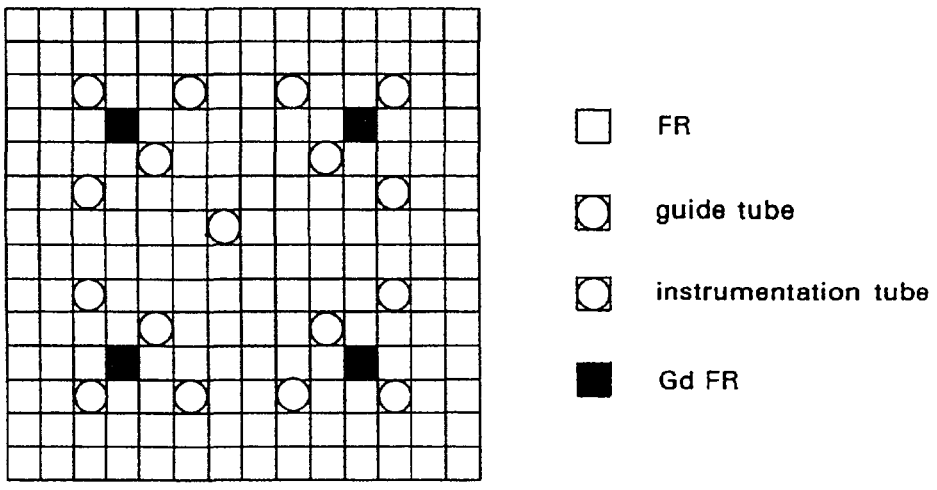

Figure IV.4. Burnable Absorber Configuration Within FA : Kori-1 Cycle 11

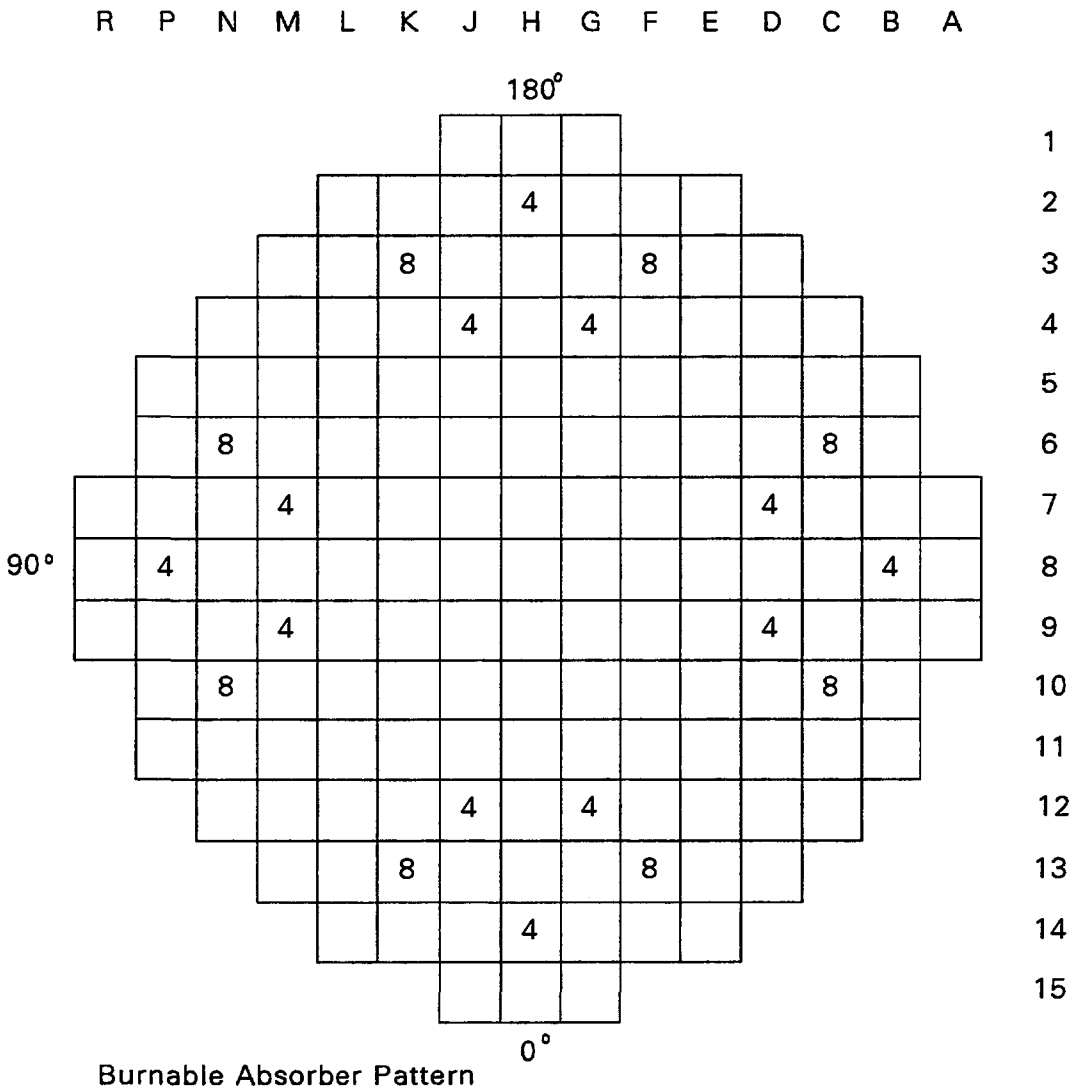

Figure IV.5. Burnable Absorber Pattern (Region 8G-4,8G-8):Kori-3 Cycle 6

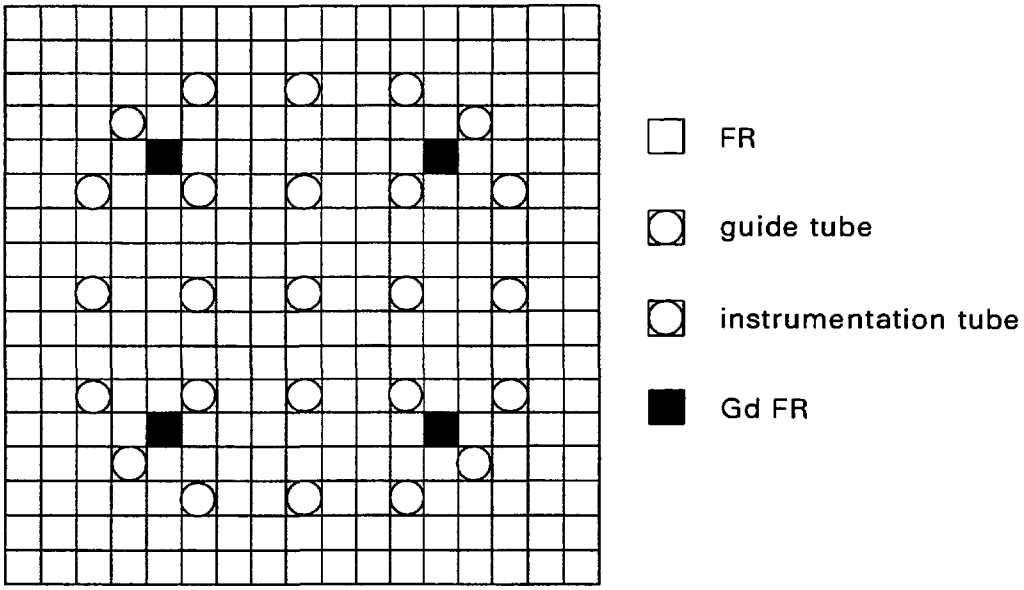

(4 Gd Assembly)

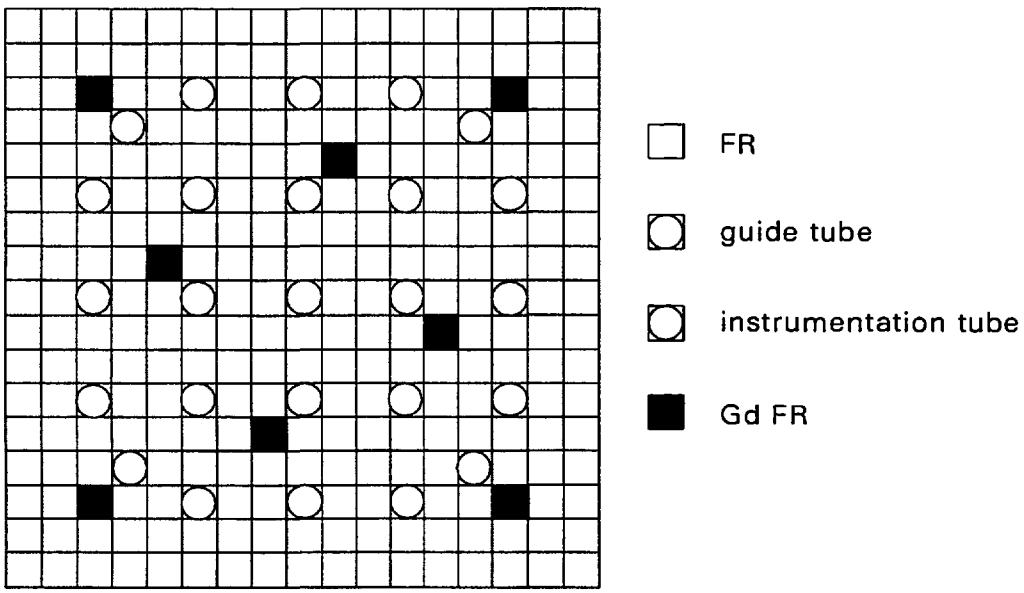

(8 Gd Assembly)

Figure IV.6. Burnable Absorber Configurations Within FA : Kori-3 Cycle 6

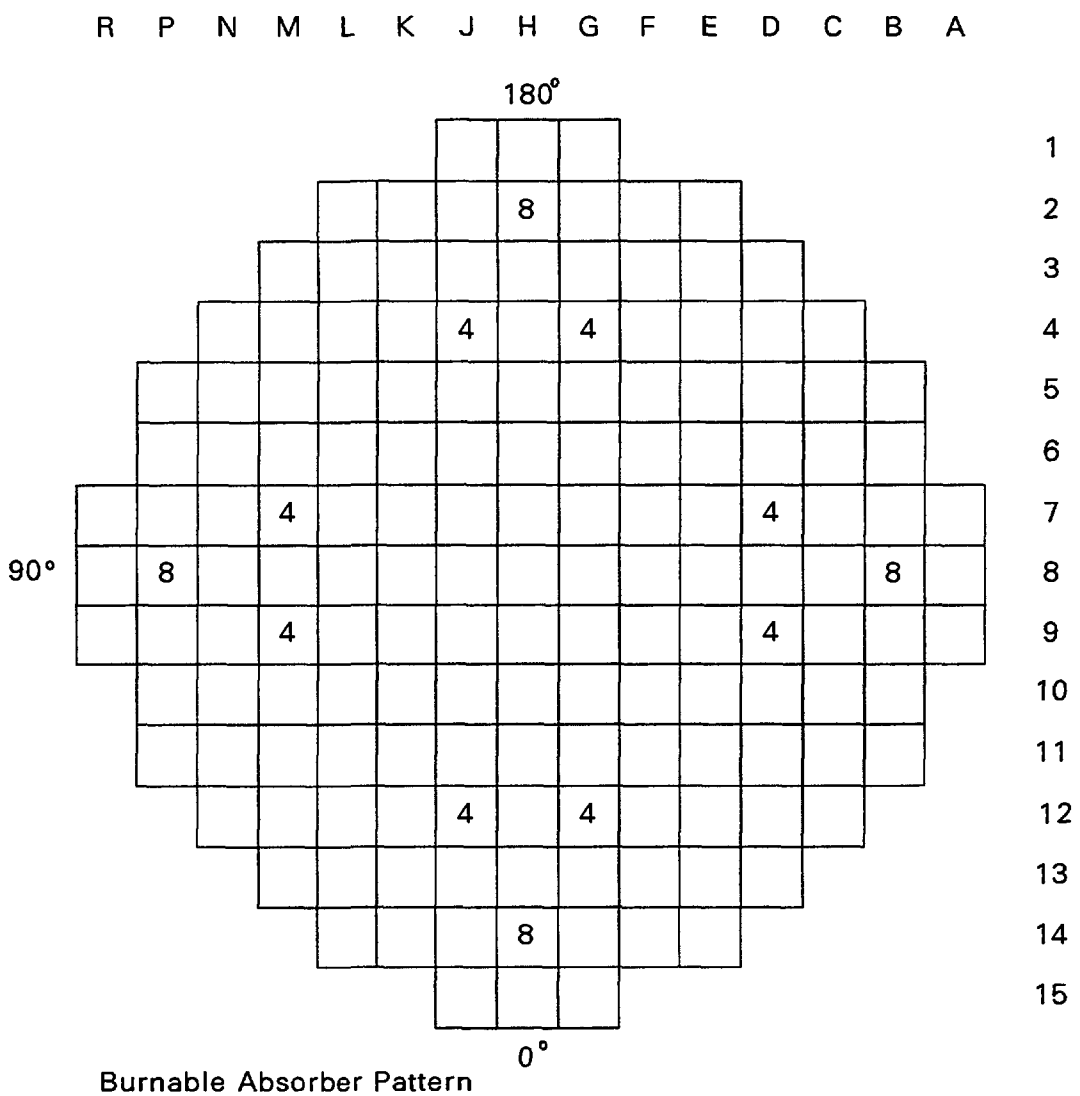

Figure IV.7. Burnable Absorber Pattern (Regions 7G-4,7G-8):Kori-4 Cycle 5

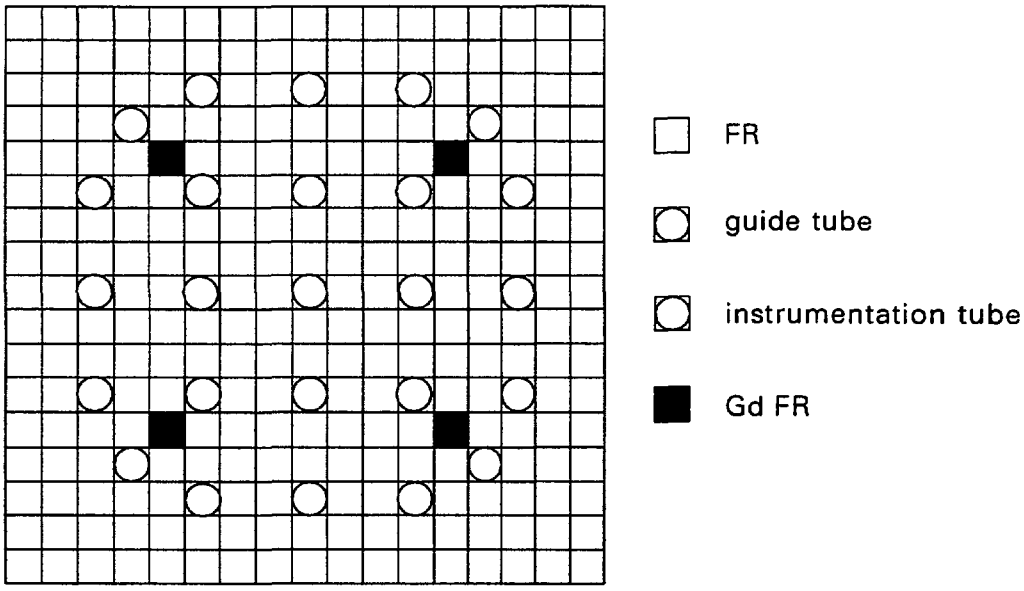

(4 Gd Assembly)

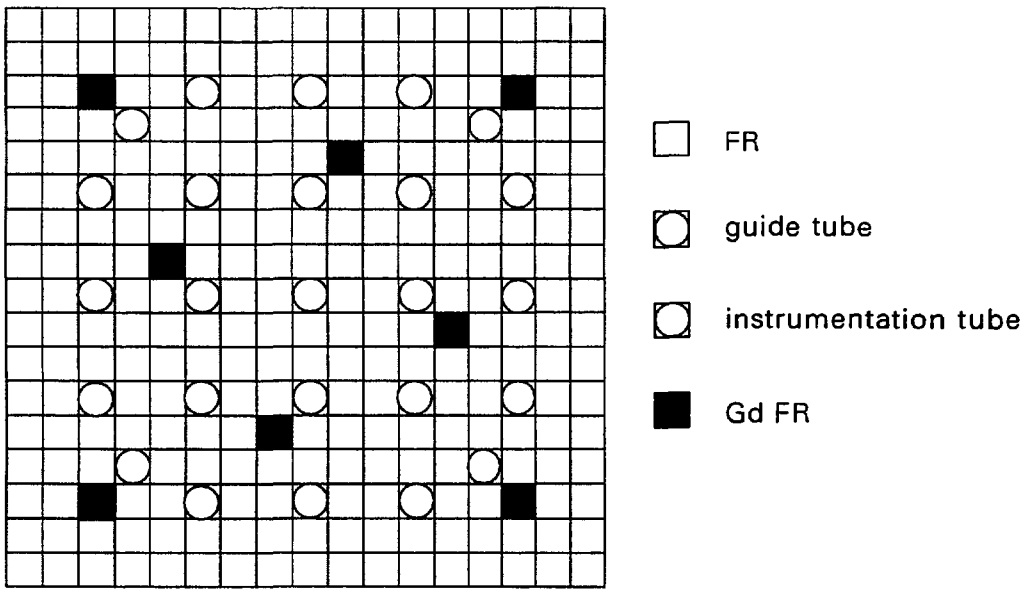

(8 Gd Assembly)

Figure IV.8. Burnable Absorber Configurations Within FA : Kori-4 Cycle 5

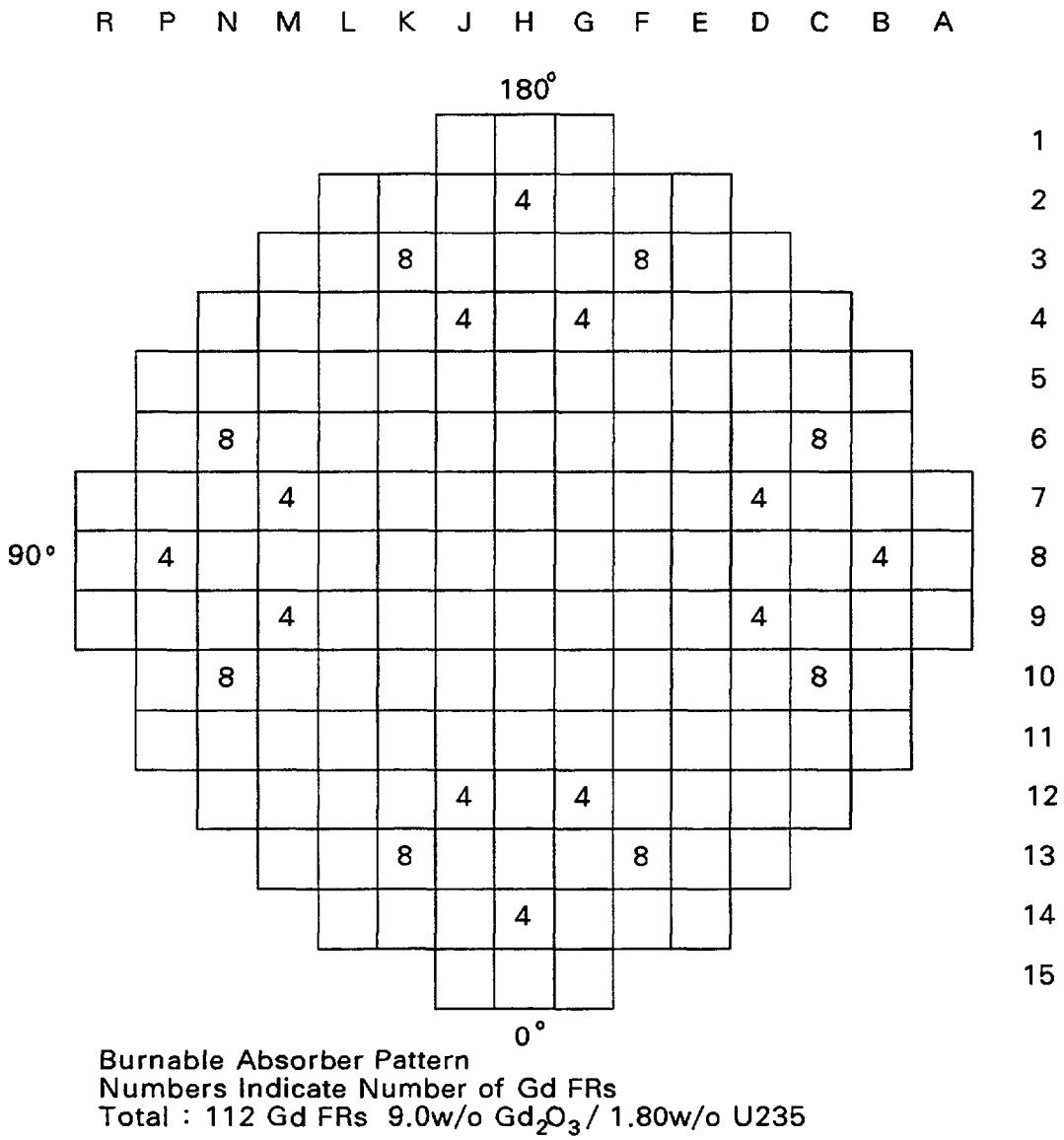

Figure IV.9. Burnable Absorber Pattern (Regions 7G-4,7G-8):Yonggwang-1 Cycle 5

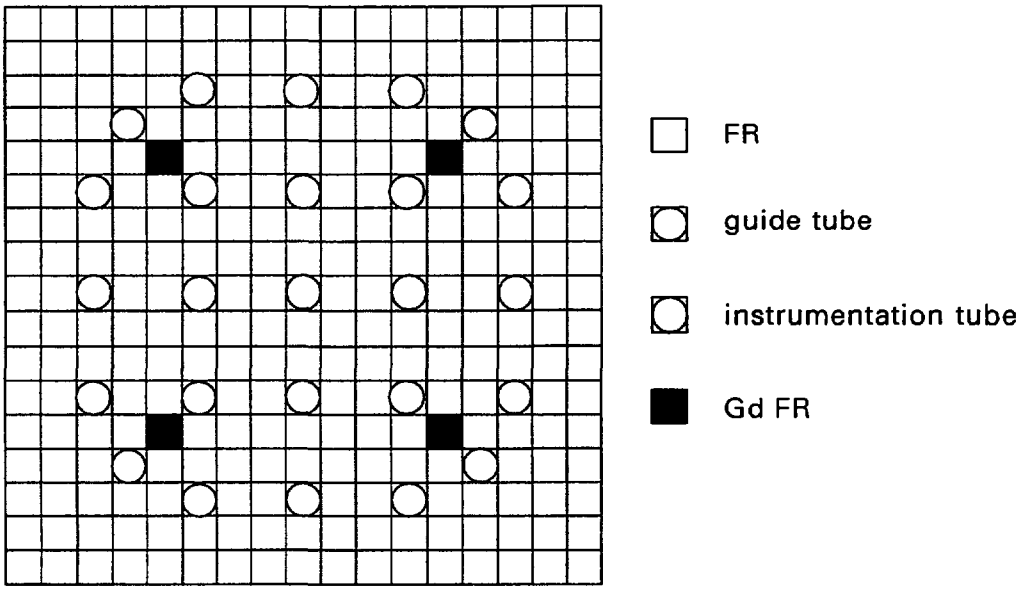

(4 Gd Assembly)

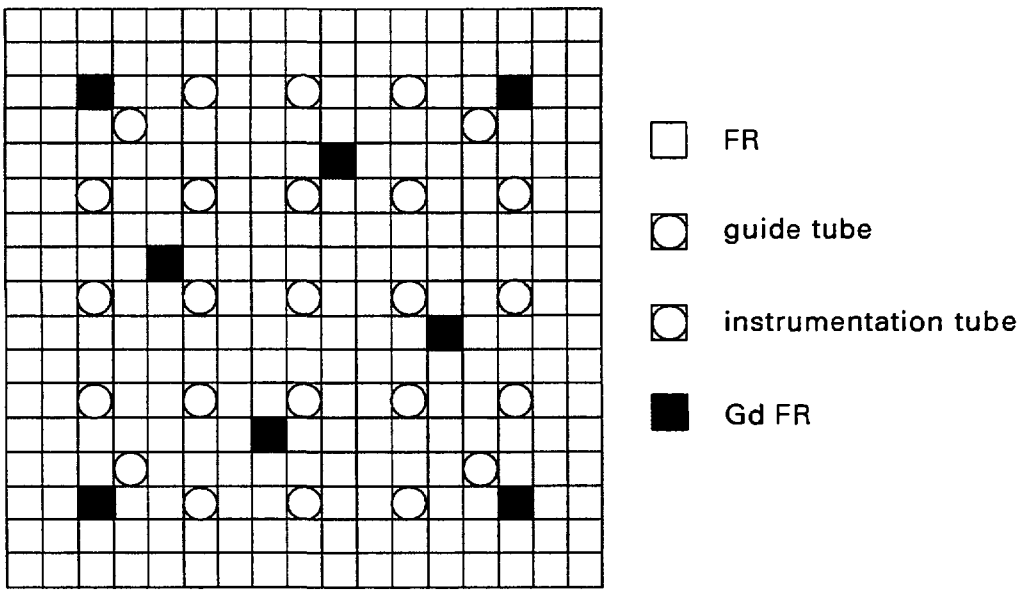

(8 Gd Assembly)

Figure IV.10. Burnable Absorber Configurations Within FA : Yonggwang-1 Cycle 5

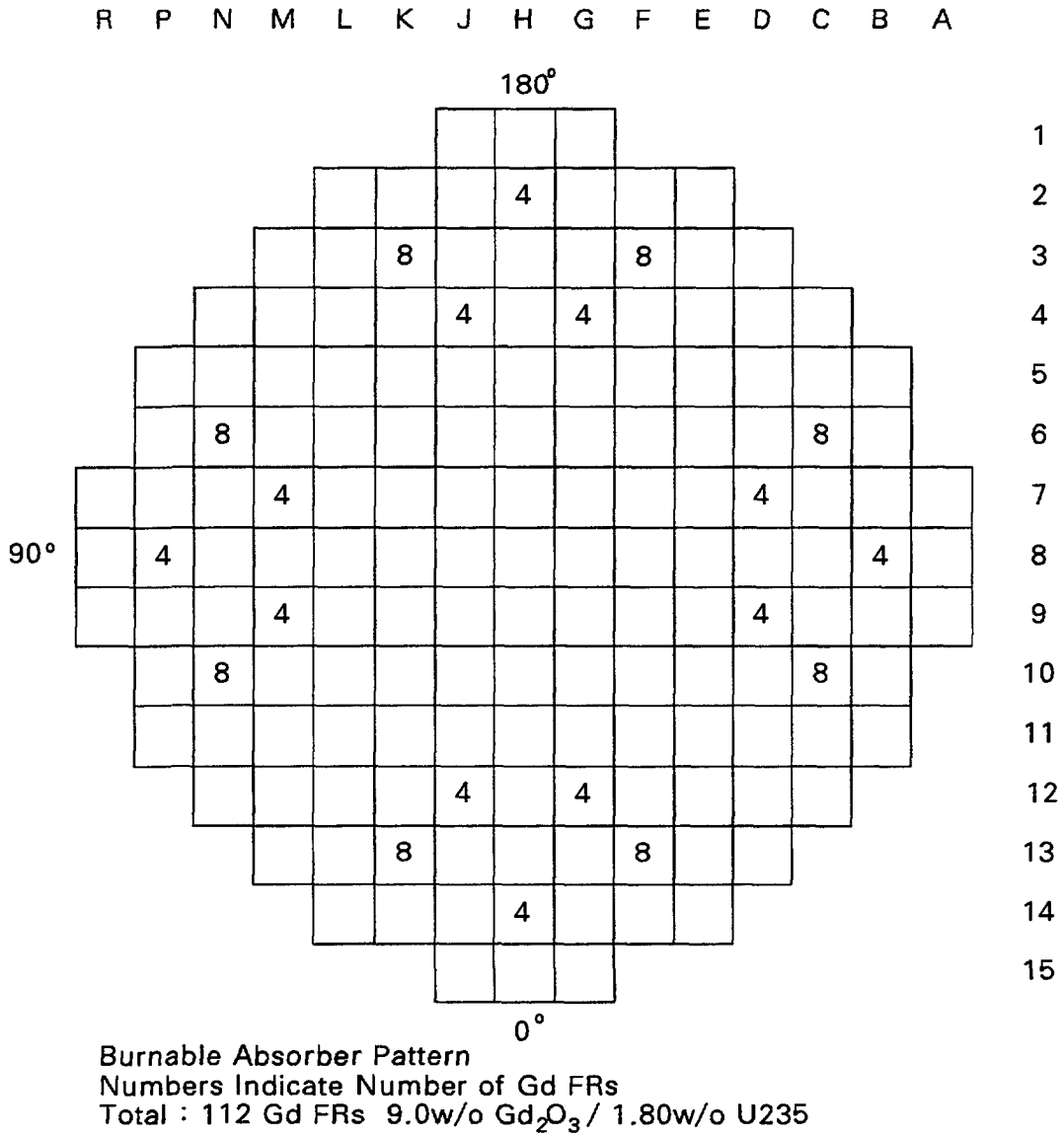

Figure IV.11. Burnable Absorber Pattern (Regions 6G-4,6G-8):Yonggwang-2 Cycle 4

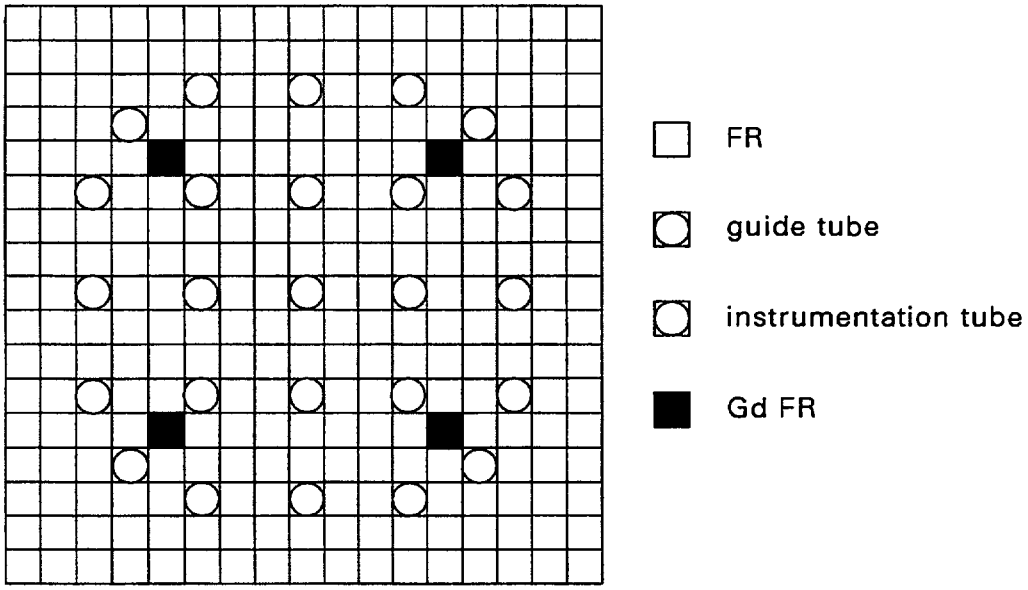

(4 Gd Assembly)

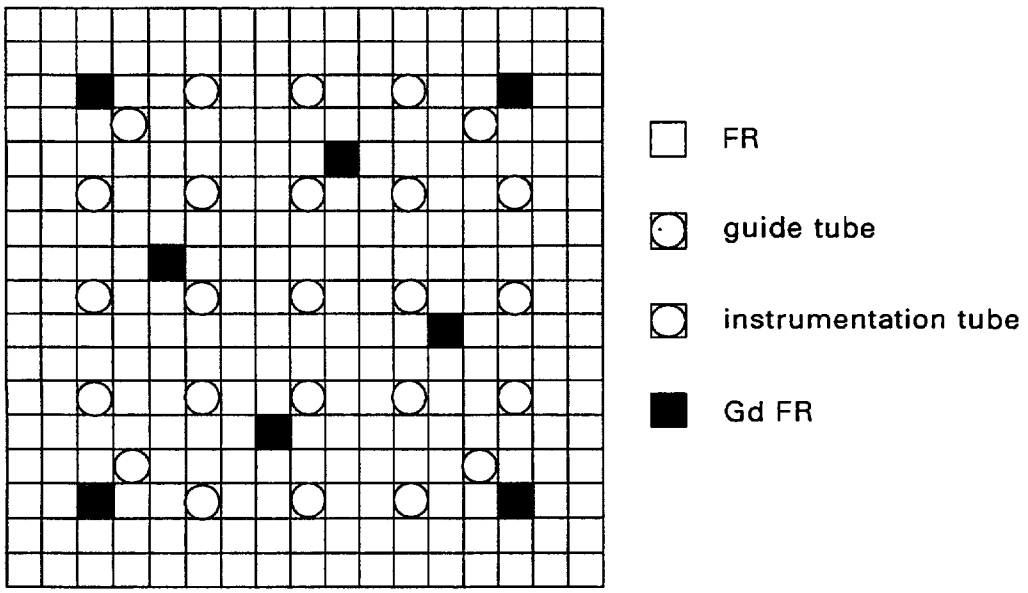

(8 Gd Assembly)

Figure IV.12. Burnable Absorber Configurations Within FA : Yonggwang-2 Cycle 4

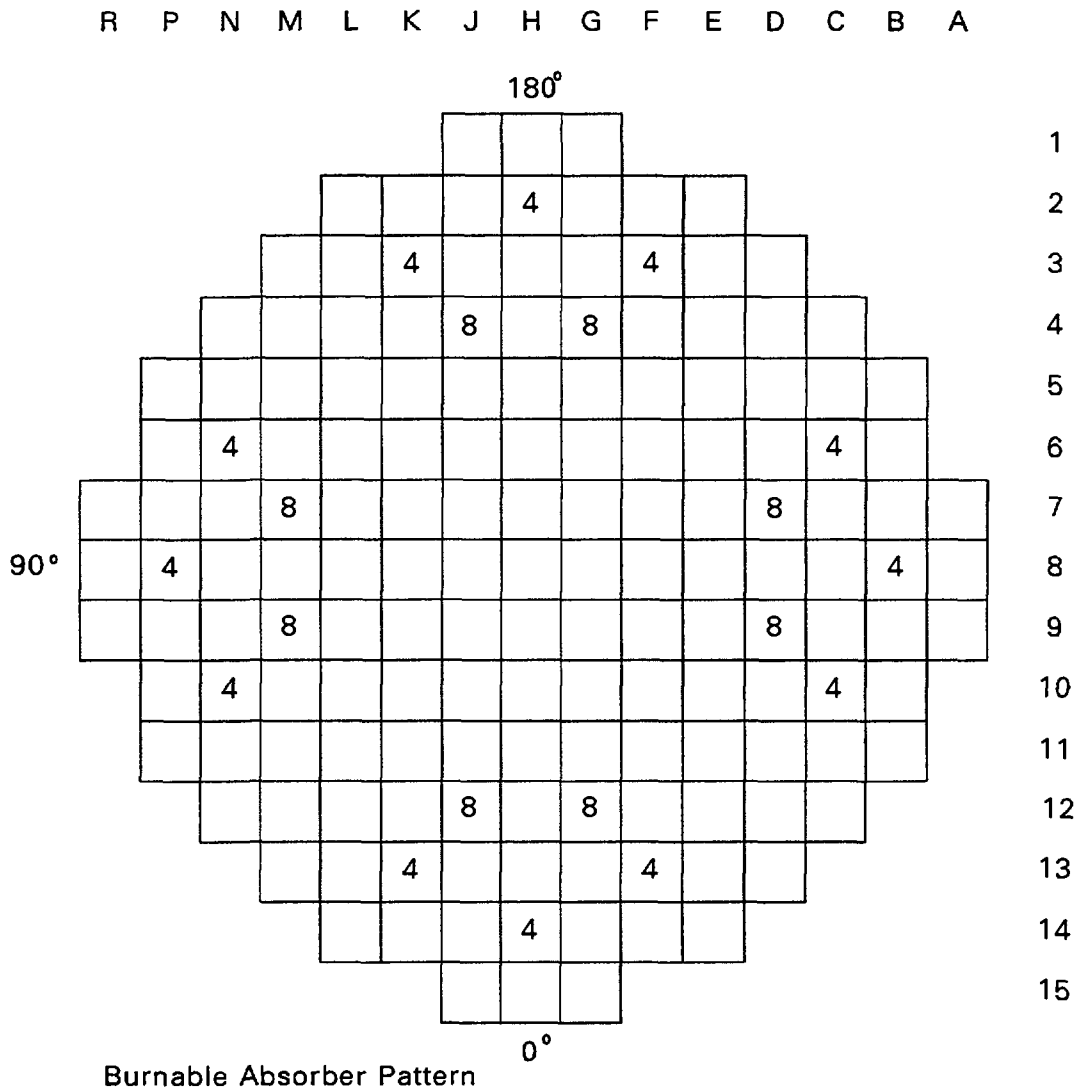

Figure IV.13. Burnable Absorber Pattern (Regions 5G-4,5G-8):Ulchin-1 Cycle 3

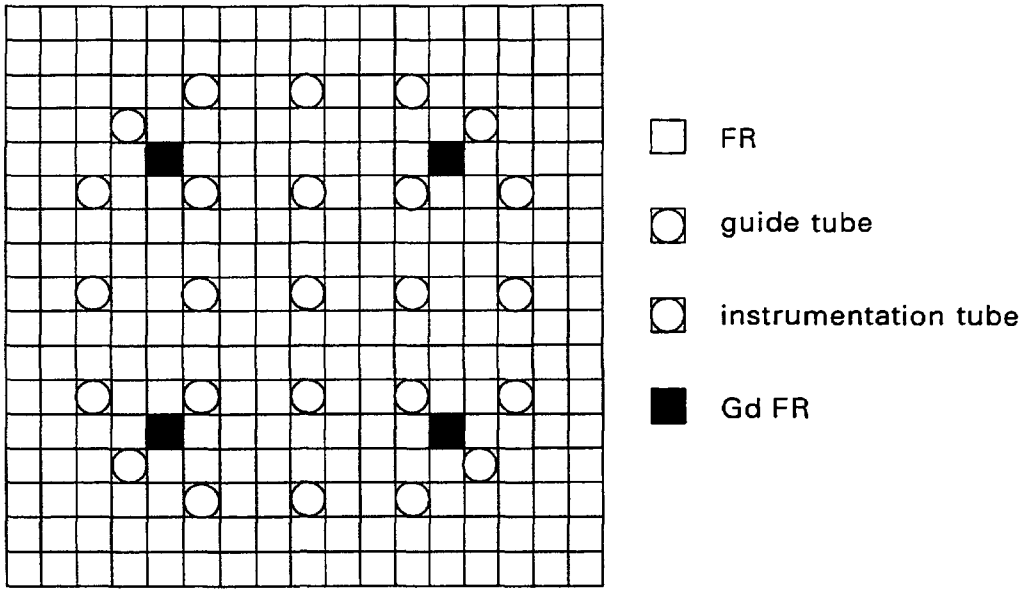

(4 Gd Assembly)

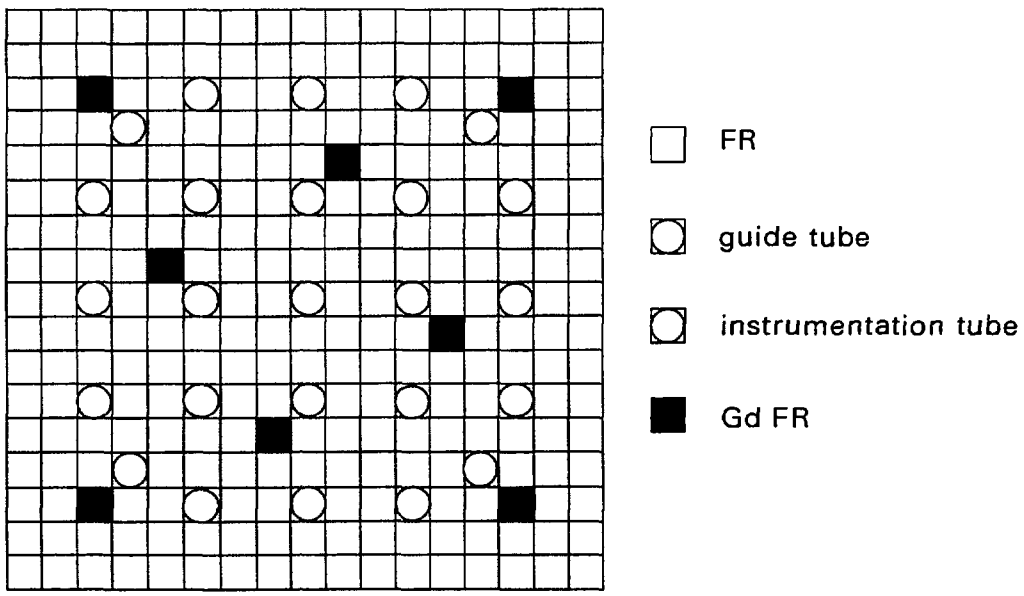

(8 Gd Assembly)

Figure IV.14. Burnable Absorber Configurations Within FA : Ulchin-1 Cycle 3

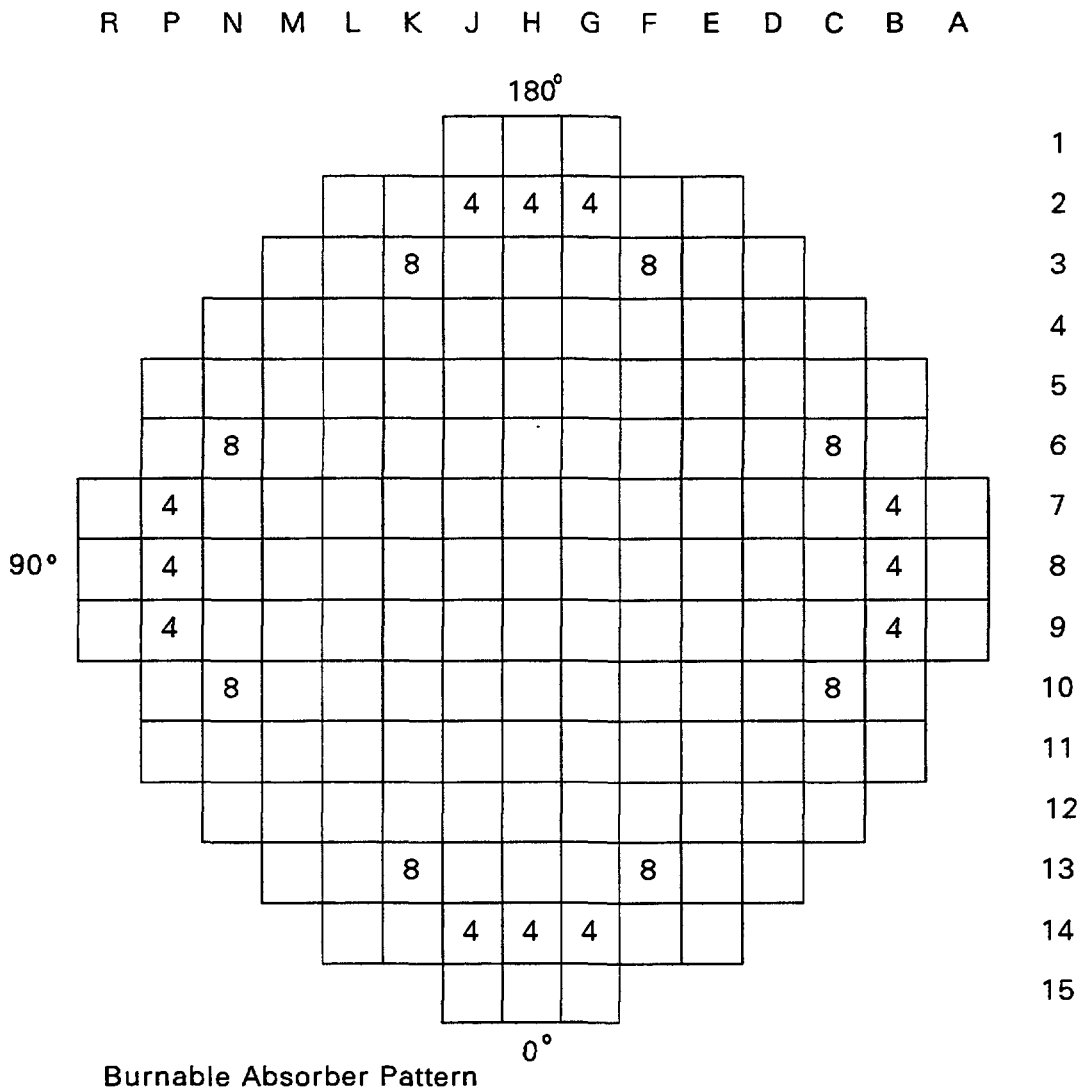

Figure IV.15. Burnable Absorber Pattern (Regions 4G-4,4G-8):Ulchin-2 Cycle 2

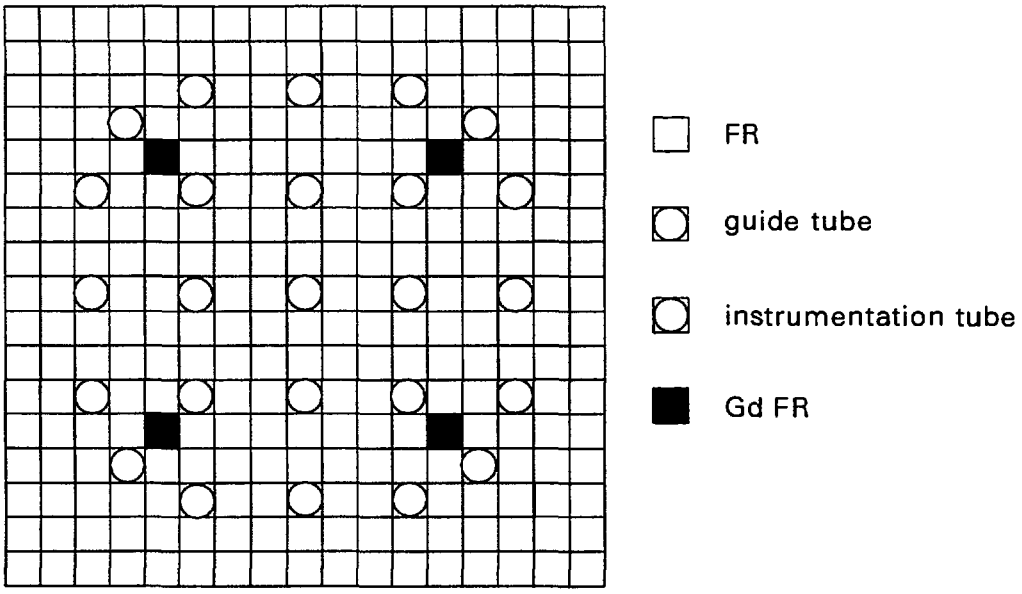

(4 Gd Assembly)

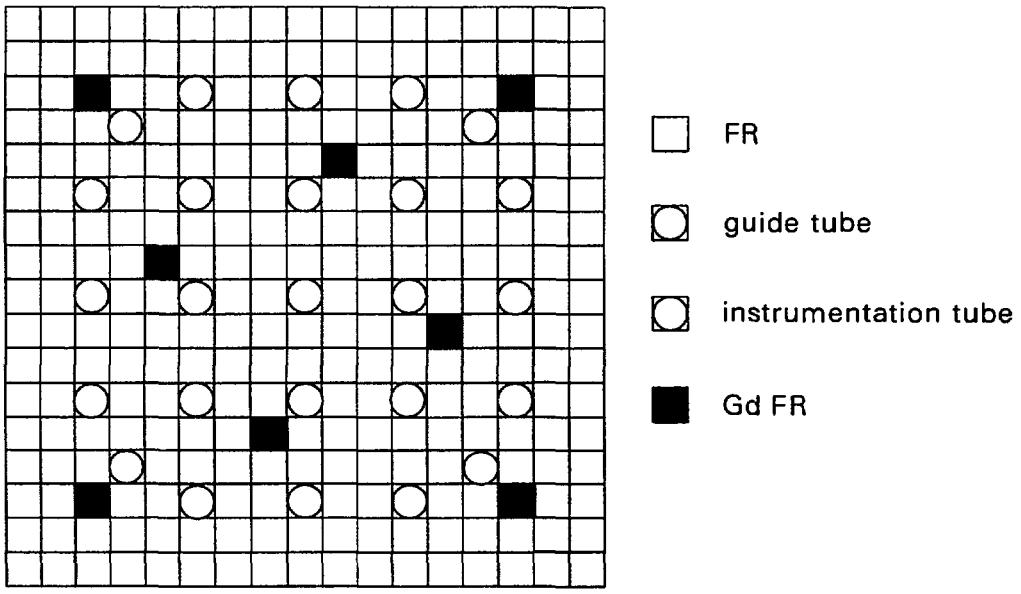

(8 Gd Assembly)

Figure IV.16. Burnable Absorber Configurations Within FA : Ulchin-2 Cycle 2

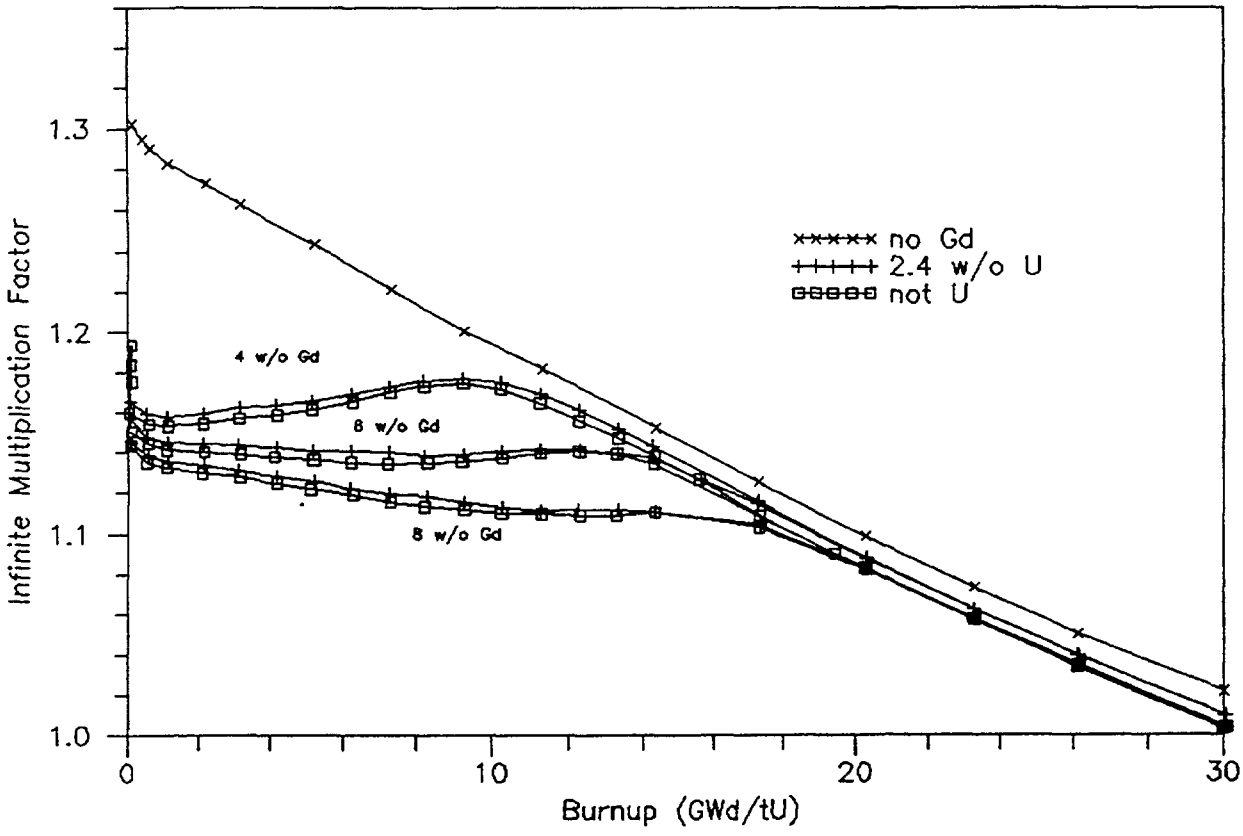

Figure IV.17. Infinite multiplication factor for YGN-3/4 initial core: 12 Gd FRs per FA

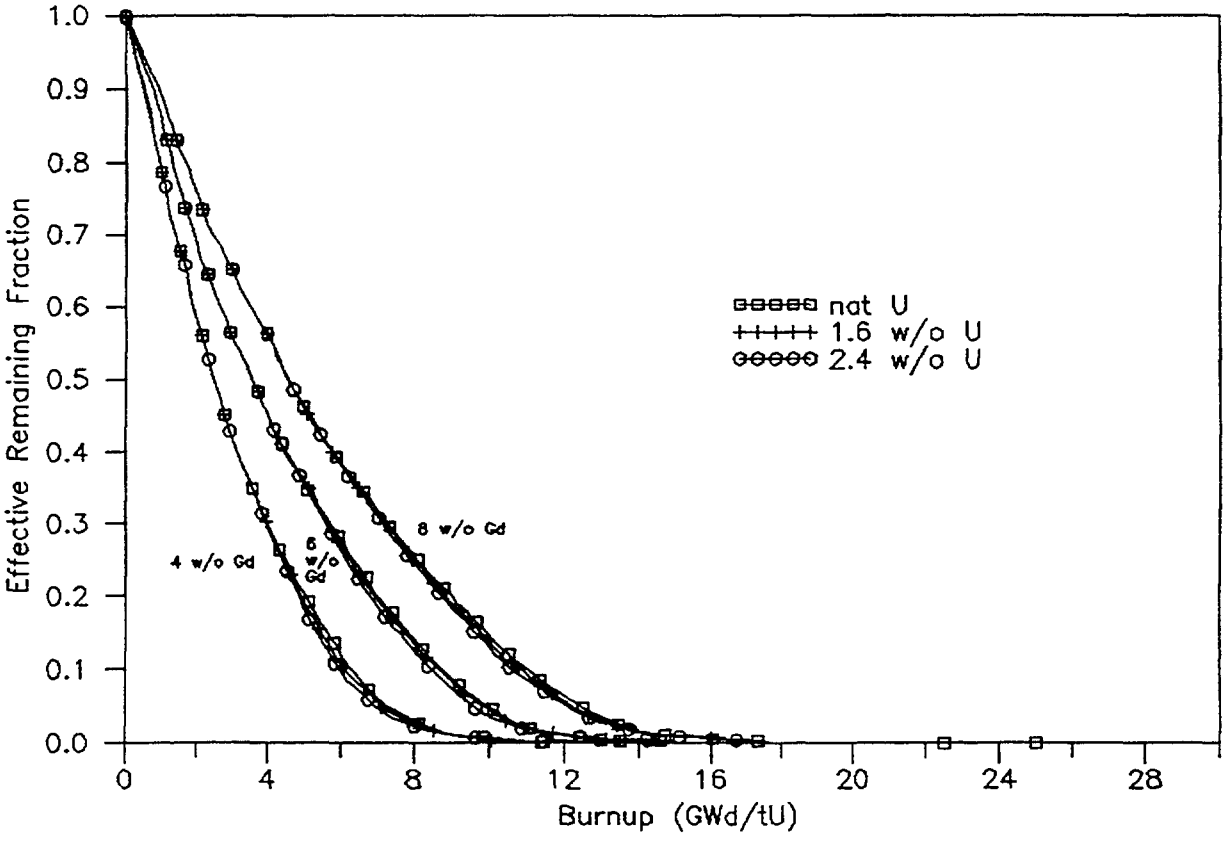

Figure IV.18. Residual Gd Fractions for YGN-3/4 initial core: 8 Gd FRs per FA

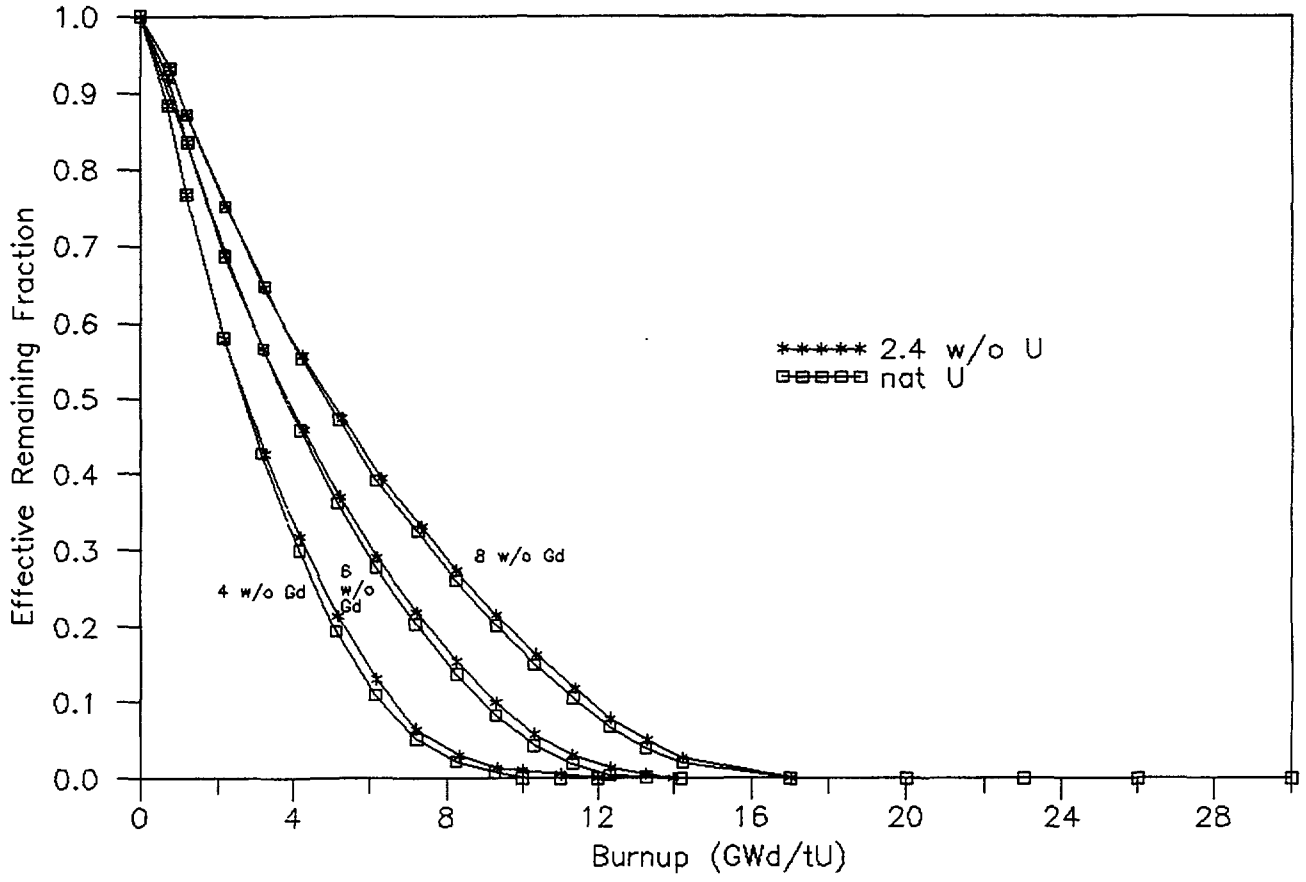

Figure IV.19. Residual Gd Fractions for YGN-3/4 initial core: 12 Gd FRs per FA

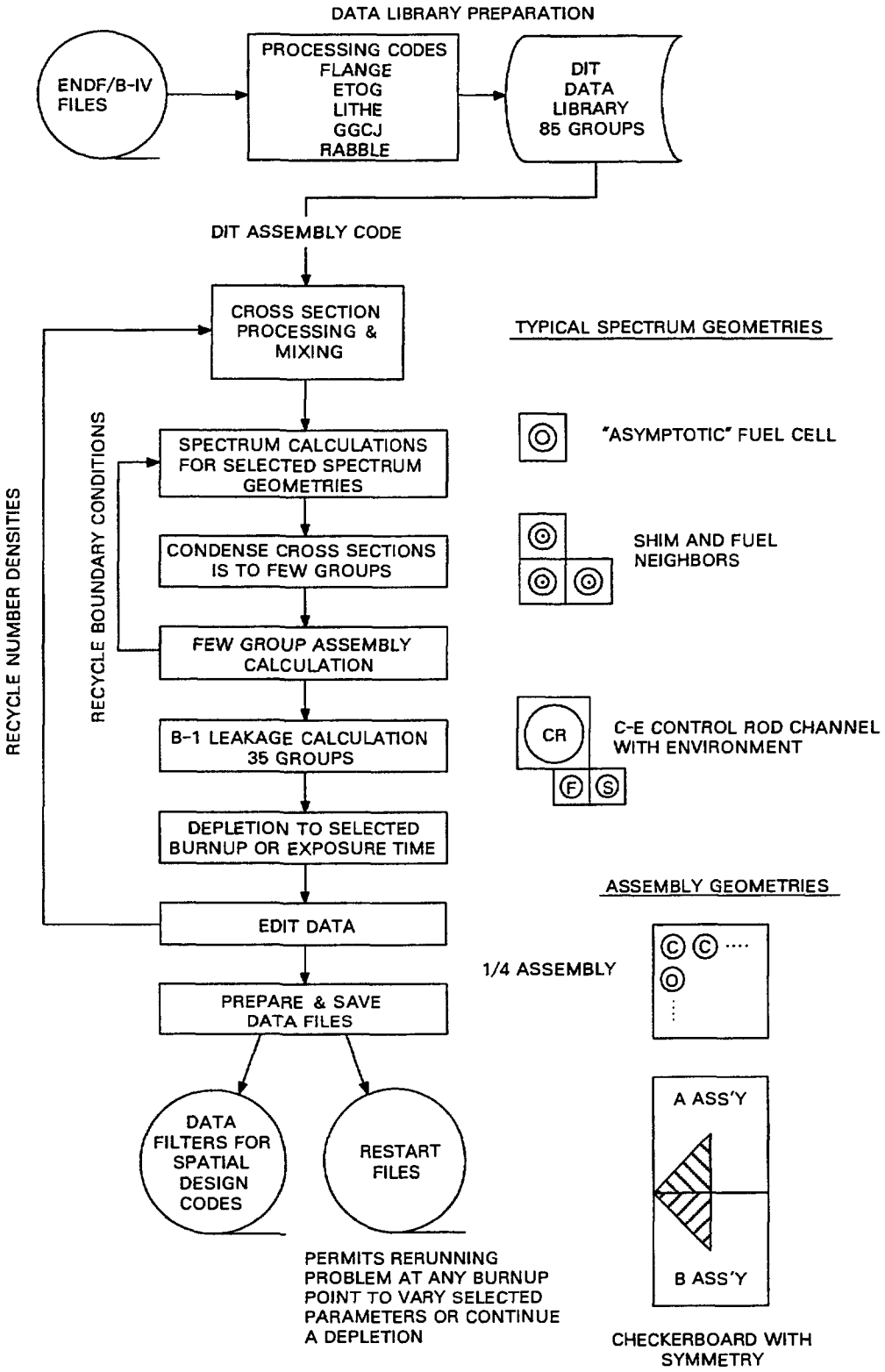

Figure IV.20. The DIT assembly code

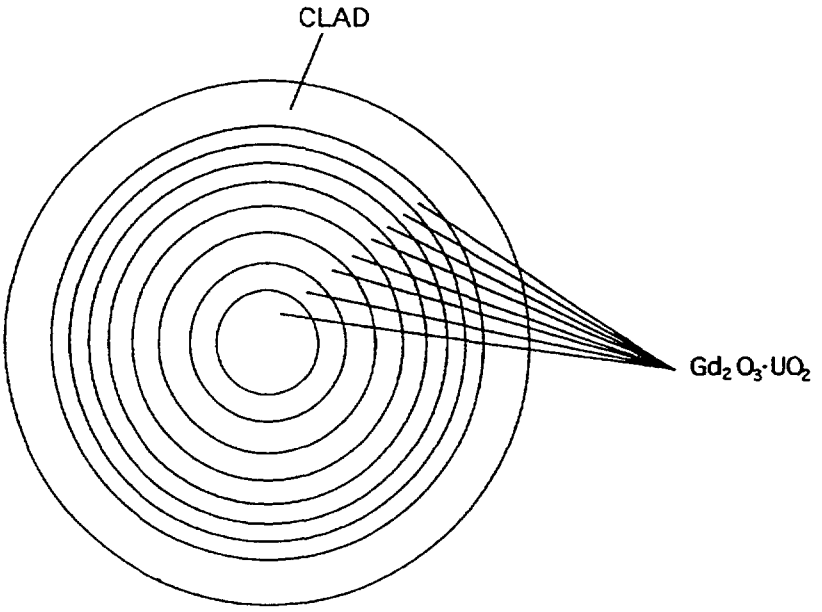

Figure IV.21. Typical DIT cell geometry for Gd fuel

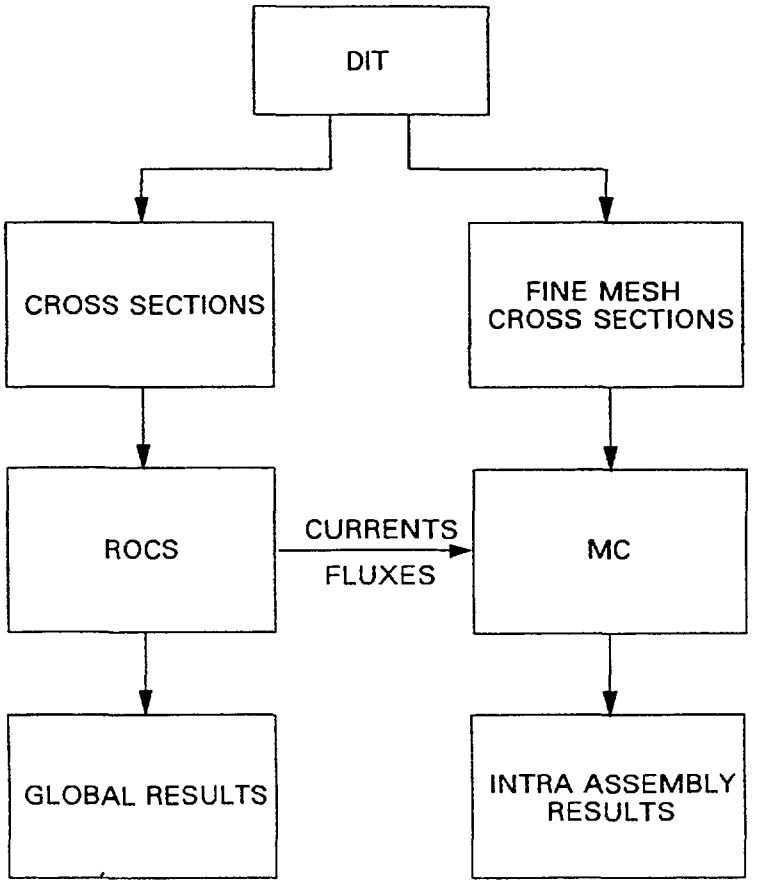

Figure IV.22. FR peaking calculations in coarse-mesh

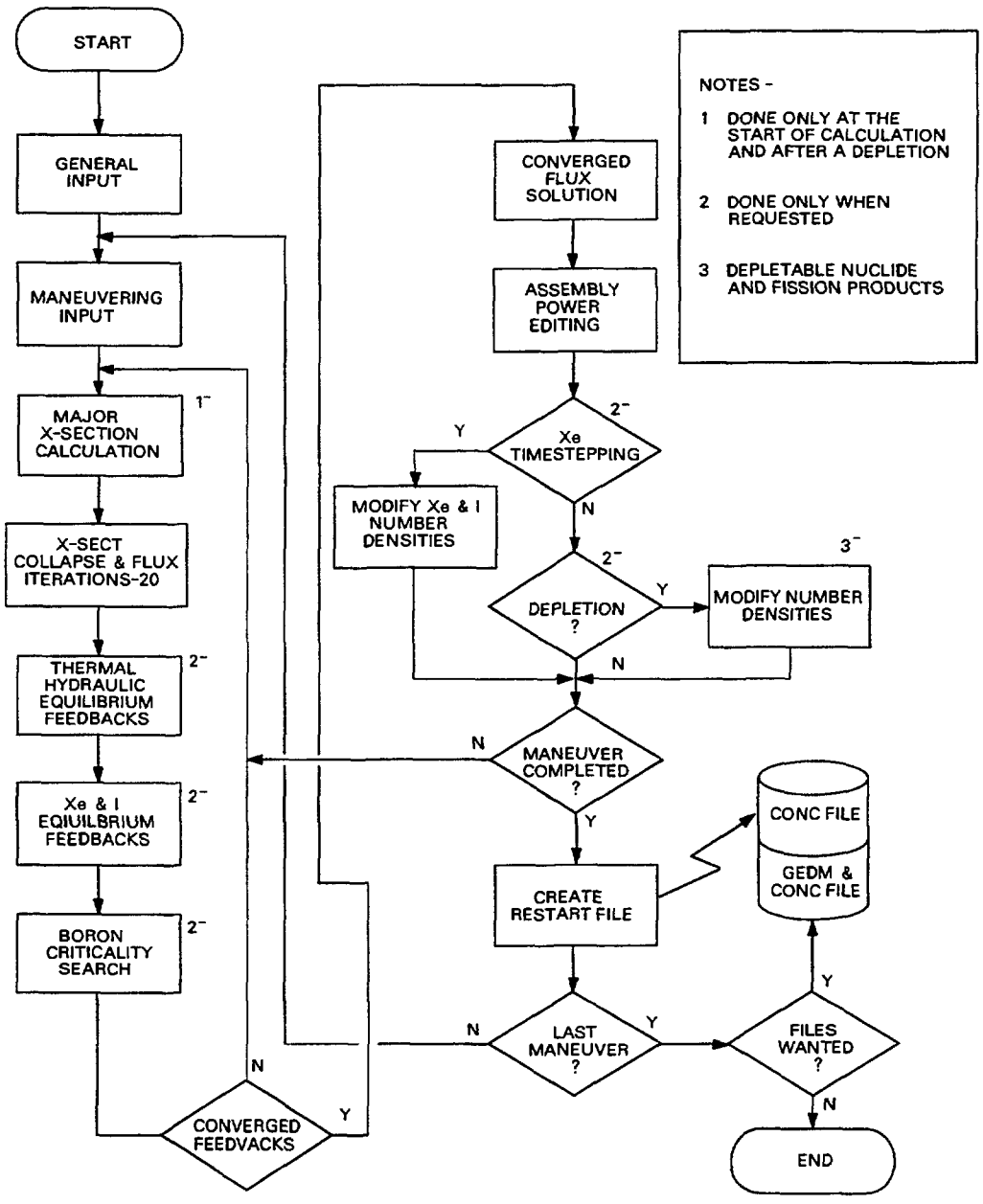

Figure IV.23. ROCS logic flow

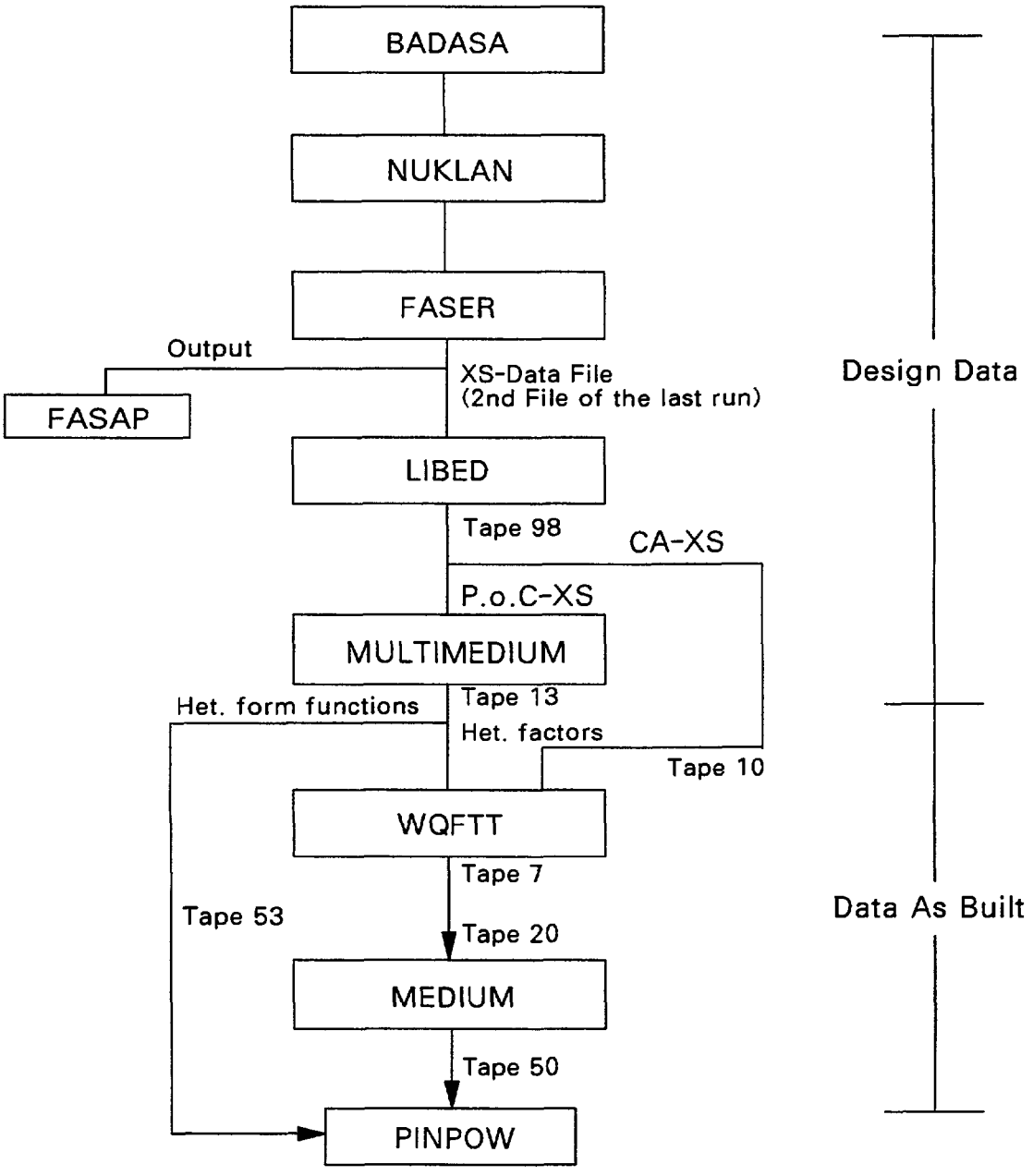

Figure IV.24. Calculation flow of fuel assembly design used by KAERI and KWU

Appendix V

GADOLINIA FUEL UTILIZATION IN BELGIUM

This Appendix provides further details of the experience obtained in Belgium with Gd FAs, as referred to in Chapter 5.

Table V.1 summarizes the main characteristics of both the U FRs and Gd FRs irradiated in the BR3 reactor, as referred to in Section 5.1.1.

Figure V.1 shows the total number of Gd FRs irradiated in the BR3 reactor between 1974 and 1987. Figure V.2 shows a typical evolution of power for two reactor cycles in BR3.

Table V.2 provides details of the commercial irradiations of Gd FAs in Belgian reactors, as also described in Section 5.1.1.

TABLE V.1. MAIN CHARACTERISTICS OF U AND Gd FRs IRRADIATED IN THE BR3 PLANT

	U FRs	Gd FRs
U^{235} enrichment (wt %)	8.25	
Gd_2O_3 content (wt %)	---	1.35 - 10
Pellet density (% theoretical density TD)	94 - 96	
UO_2 grain size (μm)	5 - 15	
Gd_2O_3 maximum particle size (μm)	---	< 100
Pellet geometry	Dished	
L / D ratio	1.5	
Densification after resintering test	< 1 % TD	
Cladding		
Material	Zr4 stress-relieved or fully annealed	
Outer diameter (mm)	9.5	
Fuel Rod		
Active fuel length (mm)	1000	
Diameter gap (μm)	200	
Helium pressure (kg / cm^2)	11 - 20	

TABLE V.2. Gd UTILIZATION IN BELGIAN POWER PLANTS

Tihange 1: 900 MWe PWR 15 x 15 fuel

Cycle	Loading	Cycle length (MWd/t)	Reload FAs x enrichment	Number of Gd FAs	Number of Gd FRs [2]	% Gd	Total Number of Gd FRs
7	1982	11945	8x3.20% 48x3.30%	4	8	8	32
8	1983	11619	8x3.30% 44x3.25%	16	8	8	128
9	1984	12510	52x3.25%	4	8	10	32
10	1985	16745	12x3.25% 60x3.45%	12 24	8 12	8 8	384
11	1986	14847	12x3.25% 56x3.45%	24	8	8	192
12	1988	12768	12x3.45% 40x3.90%	8	8	8	64
13	1989	15710	56x3.90%	20	8	8	160
14	1990	17075	60x3.90%	24	8	8	192
15	1991	13550	52x3.90%	16	8	8	128
16	1992	17400 [1]	63x3.90%	25	8	8	200

(1) Planned

(2) All schemes have Gd FRs at mid assembly positions.

TABLE V.2. (cont.)

Tihange 2: 900 MWe PWR 17 x 17 fuel

Cycle	Year	Reload	Cycle length (MWd/t)	Number of Gd FRs
5	1987		12390	128
6	1988	52 FAs 3.8% 16 Gd FAs	13800	128
7	1989	52 FAs 3.8% 16 Gd FAs	13500	128
8	1990	52 FAs 3.85% 16 Gd FAs	12350	128
9	1991	52 FAs 3.8% 16 Gd FAs	15250	128
10	1992	52 FAs 3.8% 16 Gd FAs	14000	128
11	1993	60 FAs 3.8% 28 Gd FAs	14750 (estimate)	224

In all Gd FAs, 8 Gd FRs per FA and positioning at mid-assembly sites

TABLE V.2. (cont.)

Tihange 3: 1050 MWe PWR 17 x 17 fuel

Cycle	Year	Reload	Cycle length (including stretch) (MWd/t)	Number of Gd FRs
4	1988	52 FAs 3.8% 16 Gd FAs	12000	128
5	1989	52 FAs 3.8% 16 Gd FAs	14190	128
6	1990	52 FAs 3.8% 16 Gd FAs	13500	128
7	1991	52 FAs 3.8% 16 Gd FAs	14500	128
8	1992	52 FAs 3.8% 16 Gd FAs	13800 (estimate)	128

In all Gd FAs, 8 Gd FRs per FA and positioning at mid-assembly sites

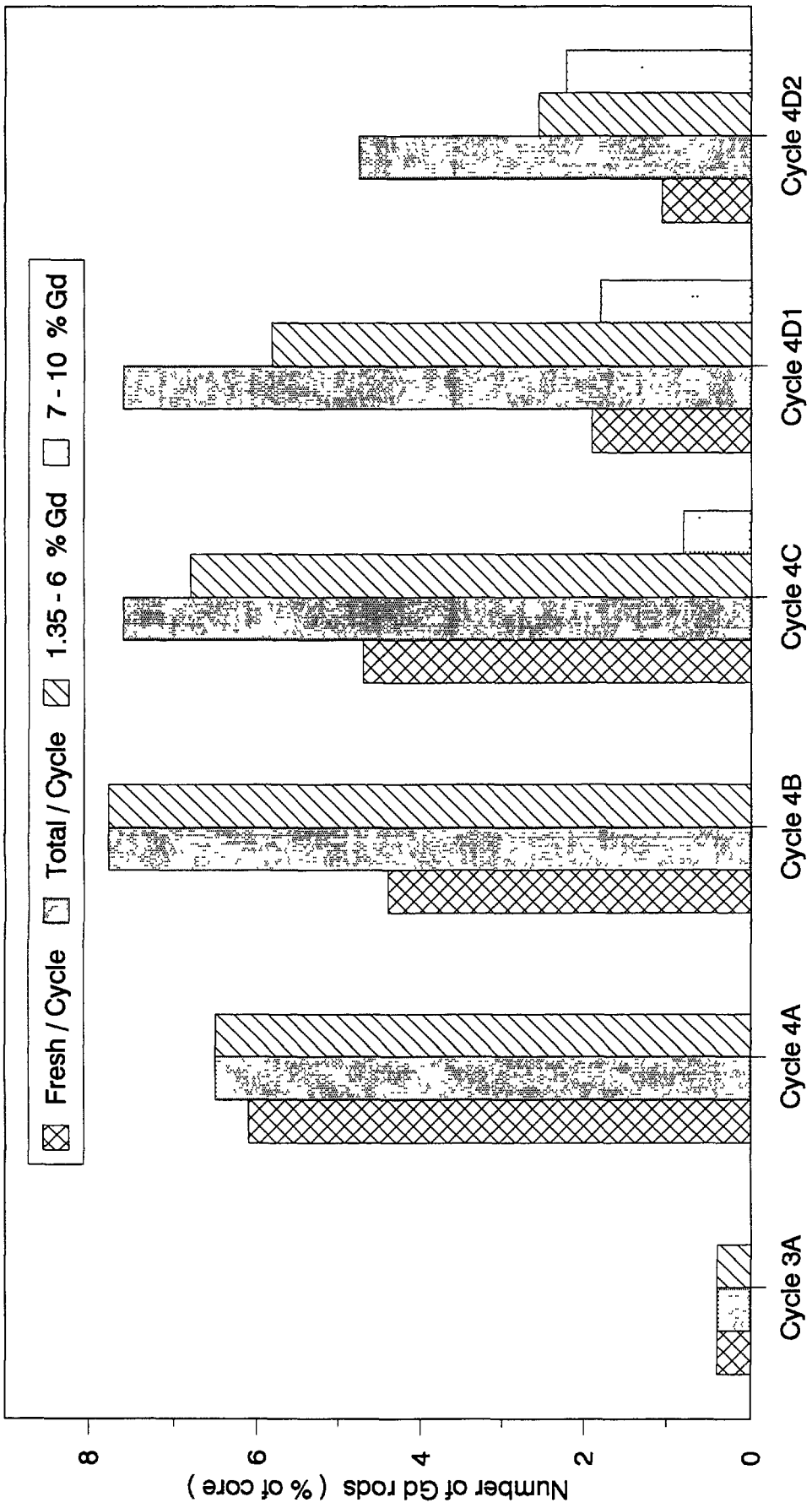

Fig. V.1. *Number of Gd rods loaded in BR3*

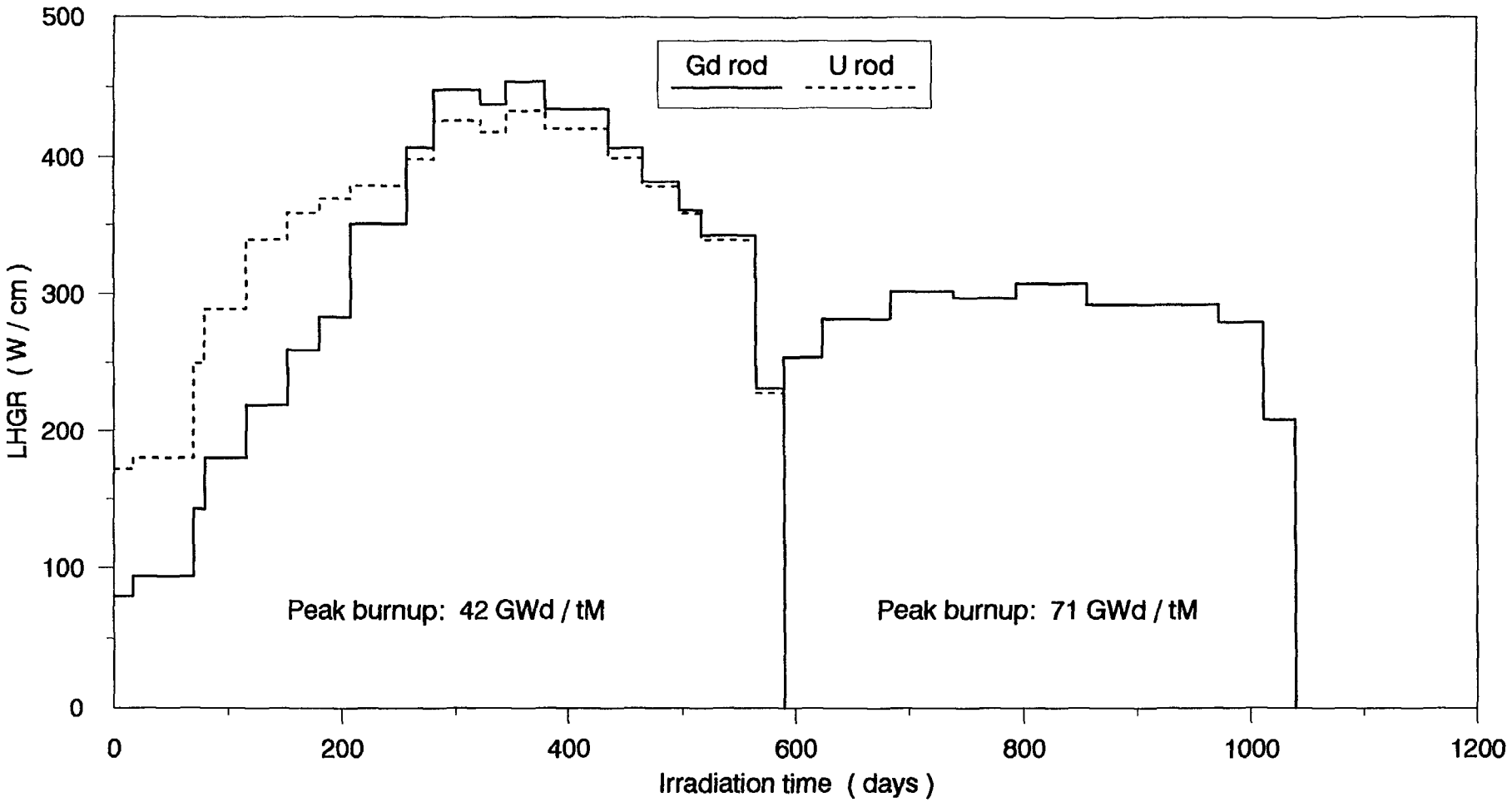

Fig. V.2. *Power & burnup of Gd & U rods irradiated in BR3*

ABBREVIATIONS

1. Technical terms

a	thermal expansion coefficient (unless otherwise mentioned) or annum, for year (used in units)
AO	axial offset
ARO	all control rods out
AZR	axially zoned reactivity (fuel)
BA	burnable absorber
BAF	burnable absorber fuel
bcc	body-centred cubic
BOC	beginning of cycle
BPRA	burnable poison rod assembly
C	bank of control rods operating simultaneously or calculated (hen used in conjunction with M)
Cp	specific heat capacity
CPS	control and protection system
D	bank of control rods operating simultaneously
$	a measure of reactivity (x 500 pcm for U fuel in a PWR)
DC	direct current
DNB	departure from nucleate boiling
DTC	Doppler temperature coefficient
E	Young's modulus
$\dot{\epsilon}$	creep rate
EDTA	ethylene diamine tetraacetic acid
EFPD	equivalent full power days
EDX	energy dispersive X-ray
EFPM	equivalent full power months
EOC	end of cycle

EOL	end of life
FA	fuel assembly
FGR	fission gas release
FP	fission product
F_Q	total peaking factor (sometimes called hot channel factor)
FR	fuel rod
F_{XY}	radial FR peaking factor at average elevation (mid-core usually)
F_{XY}^N	nuclear contribution to F_{XY}
G	shear modulus
GAIN	international data acquisition programme on the thermal-mechanical behaviour of Gd fuel to high burnups
GAP	international data acquisition programme on the kinetics of Gd depletion in a Gd FR
Gd FR	gadolinia-urania fuel rods
GW(e)	electrical power expressed in gigawatts
HBWR	Halden boiling water reactor
HFP	hot full power
HLW	high level waste
HZP	hot zero power
IDR	integrated dry route (UO_2 conversion process)
k	thermal conductivity
keff	effective multiplication factor
IFBA	integral fuel burnable absorber
KOFA	Korean Fuel Assembly
LHGR	linear heat generation rate, expressed in kW/m or W/cm
LLLP	low leakage loading pattern
LOCA	loss of coolant accident
LTA	lead test fuel assembly (demonstration FA)

M	measured
MOX	mixed oxide UO_2-PuO_2
MTC	moderator temperature coefficient
MTR	material testing reactor
MWd/tU	burnup expressed as MW x d per t U initially contained in the fuel
ν	Poisson's ratio
NPP	nuclear power plant
NSRR	Nuclear Safety Research Reactor
OD	outer diameter
o/m	oxygen to heavy metal ratio
PC	power coefficient
PCI	pellet-cladding interaction
PIE	post-irradiation examination
PCIOMR	Pre-conditioning Interim Operating Management Recommendations
pcm	reactivity expressed in 10^5 ($k_{eff\ 1}/k_{eff\ 0}$)
ppm	parts per million
QC	quality control
ρ	density (g/cm^3)
RCCA	rod cluster control assembly
R&D	research and development
REE	rare earth element
RIA	reactivity initiated accident
σ	neutron cross-section
SEM	scanning electron microscopy
SDM	shut-down margin
UFR	UO_2 fuel rod
UGF	urania-gadolinia fuel (Russia)
TD	theoretical density (g/cm^3)

TGA	thermogravimetric analysis
U fuel	UO_2 fuel
WOCA	world outside centrally planned economy area
w/o Gd	weight percent Gd_2O_3 in UO_2 - Gd_2O_3
WWER	water water energy reactor (Russian PWR type reactor)
Zry	Zircaloy
YGN	Yonggwang NPP

2. Organizations

ABB	ABB Atom AB (SWE)
ARSRIIM	All-Russian Scientific Research Institute of Inorganic Materials (RUS)
BN	BELGONUCLEAIRE (BEL)
BNFL	British Nuclear Fuels, plc (UK)
BWFC	Babcock and Wilcox Fuel Cy (USA)
CE	Combustion Engineering, now ABB/CE (USA)
CEA	Commissariat à l'Energie Atomique (FRA)
EDF	Electricité de France (FRA)
ENUSA	Empresa Nacional del Uranio SA (SPA)
FBFC	Franco-Belge de Fabrication du Combustible (FRA & BEL)
FRAGEMA	GIE Framatome-Cogema (FRA)
GE	General Electric (USA)
JAERI	Japan Atomic Energy Research Institute (JPN)
JNF	Japan Nuclear Fuel (JPN)
KAERI	Korea Atomic Energy Research Institute (ROK)
KNFC	Korean Nuclear Fuel Company (ROK)
KWU	Kraftwerk Union, a group within SIEMENS AG (GFR)
MNF	Mitsubishi Nuclear Fuel (JPN)
NE	Nuclear Electric (UK)

NFI	Nuclear Fuel Industries (JPN)
PNC	Power Reactor & Nuclear Fuel Development Corporation (JPN)
RRC/KI	Russian Research Center, Kurchatov Institute (RUS)
SCK/CEN	Stuiencentrum voor Kernenergie/Centre d'Etude Nucléaire (BEL)
SPC	Siemens Power Cy, previously ANF (USA)
USNRC	US Nuclear Regulatory Commission (USA)
Wh	Westinghouse (USA)

PARTICIPANTS IN THE CO-ORDINATED RESEARCH PROGRAMME

Bairiot, H.	FEX, Belgium
Chantoin, P.	International Atomic Energy Agency
Cho, N.Z.	Korea Advanced Institute of Science and Technology, Republic of Korea
Delbrassine, A.	Centre d'Etudes de l'Energie Nucléaire, Belgium
Farrant, D.	British Nuclear Fuels, United Kingdom
Gündüz, G.	Middle East Technical University, Turkey
Hron, M.	Nuclear Research Institute, Czech Republic
Onufriev, V.D.	Scientific and Research Institute of Inorganic Materials, Russian Federation
Proselkov V.	Kurchatov Institute of Atomic Energy, Russian Federation
Roulier, B.	EDF/SEPTEN, France
Sukhanov, G.	International Atomic Energy Agency
Toba, M.	Nuclear Fuel Industries Ltd, Japan

QUESTIONNAIRE ON IAEA-TECDOCs

It would greatly assist the International Atomic Energy Agency in its analysis of the effectiveness of its Technical Document programme if you could kindly answer the following questions and return the form to the address shown below. Your co-operation is greatly appreciated.

Title: **Characteristics and use of urania-gadolinia fuels**
Number: **IAEA-TECDOC-844**

1. How did you obtain this TECDOC?

[ ] From the IAEA:
  [ ] At own request
  [ ] Without request
  [ ] As participant at an IAEA meeting
[ ] From a professional colleague
[ ] From library

2. How do you rate the content of the TECDOC?

[ ] Useful, includes information not found elsewhere
[ ] Useful as a survey of the subject area
[ ] Useful for reference
[ ] Useful because of its international character
[ ] Useful for training or study purposes
[ ] Not very useful. If not, why not?

3. How do you become aware of the TECDOCs available from the IAEA?

[ ] From references in:
  [ ] IAEA publications
  [ ] Other publications
[ ] From IAEA meetings
[ ] From IAEA newsletters
[ ] By other means (please specify)
[ ] If you find it difficult to obtain information on TECDOCs please tick this box

4. Do you make use of IAEA-TECDOCs?

[ ] Frequently
[ ] Occasionally
[ ] Rarely

5. Please state the institute (or country) in which you are working:

Please return to:
R.F. Kelleher
Head, Publishing Section
International Atomic Energy Agency
P.O. Box 100
Wagramerstrasse 5
A-1400 Vienna, Austria